



TESIS DOCTORAL

**DESARROLLO DE NUEVOS MÉTODOS Y ALGORITMOS
DE ANÁLISIS Y CLASIFICACIÓN DE IMÁGENES
MULTIESPECTRALES ORIENTADAS A LA GESTIÓN Y
MONITORIZACIÓN DE PLANTAS ACUÁTICAS INVASORAS**

Elena Cristina Rodríguez Garlito

Programa de Doctorado en Tecnologías Informáticas (TIN)

Conformidad de los directores:

Dr. Abel Francisco Paz Gallardo

Dr. Antonio Plaza Miguel

Esta tesis cuenta con la autorización de los directores de la misma y de la Comisión Académica del programa. Dichas autorizaciones constan en el Servicio de la Escuela Internacional de Doctorado de la Universidad de Extremadura.

2023

A mi familia.

Agradecimientos personales

Agradezco a todas las personas que me han animado y ayudado, de una u otra forma, durante todo este viaje lleno de retos y aprendizaje.

Gracias a mis directores Abel y Antonio por acceder a mi propuesta de ser vuestra pupila de Tesis, darme total flexibilidad y permitirme aprender de vosotros.

También doy las gracias a los que han colaborado resolviendo dudas de trámites y otros asuntos como a los doctorandos de la asociación ADUEx y en especial a Luisa, a la que he mareado bastante con tantas preguntas acerca de “los papeleos”.

Gracias a toda mi familia (la de sangre y la elegida), que me ha cuidado y mimado cuando más lo necesitaba. Gracias a mis padres, Tomás y Merche, por inculcarme la cultura del esfuerzo y contribuir en mi crecimiento personal y académico. Gracias papá por ser el fotógrafo de esta Tesis y gracias mamá por estar ahí siempre.

Doy las gracias a mis chiquitinos Daniel y Miguel. Ellos han respetado tener como “hermana” esta Tesis y que a veces haya tenido que prescindir de momentos de juego para avanzar con ella. Os ha quedado claro que en ocasiones “hay plantas que son muy malas” y que la inteligencia artificial y los satélites nos ayudan. Habéis aprendido mucha jerga científica, a ser unas hormiguitas y a que hay que esforzarse para conseguir vuestros propósitos, pero sobretodo espero haberos enseñado a restar importancia a los obstáculos que hayan por el camino y a ser felices siempre.

Gracias Abel por ser mi guía, ayuda, referente y compañero en esta montaña rusa de emociones en la que hemos estado montados todos estos años, durante el desarrollo de este trabajo. ¡Sigamos sumando muchas más etapas que superar!

Por último, gracias a la vida y a la ciencia, que me ha concedido seguir disfrutando de los míos y, entre otras cosas, terminar esta Tesis Doctoral.

Otros Agradecimientos

La presente Tesis Doctoral ha sido patrocinada por la Consejería de Economía, Ciencia y Agenda Digital de la Junta de Extremadura (antigua Consejería de Economía e Infraestructuras) a través de una ayuda otorgada por resolución de 10 de mayo de 2017 (DOE núm 95, de 19 de mayo), cofinanciada por Fondo Social Europeo: Una manera de hacer Europa, a través de la Ayuda para la Financiación de Contratos Predoctorales para la Formación de Doctores en los Centros Públicos de I+D pertenecientes al Sistema Extremeño de Ciencia, Tecnología e Innovación (Expediente PD16001)

La difusión de esta investigación en revistas internacionales también ha sido financiada en parte por la Consejería de Economía, Ciencia y Agenda Digital de la Junta de Extremadura y por el Fondo Europeo de Desarrollo Regional (FEDER) a través de una ayuda con referencia GR21040. Este trabajo también ha sido financiado en parte por el Ministerio de Ciencia e Innovación bajo el proyecto PID2019-110315RB-I00 (APRISA); en parte por European Union's Horizon 2020 Research and Innovation Program bajo la ayuda número 734541 (EOXPOSURE). Agradecemos también a la Confederación Hidrográfica del Guadiana O.A la información proporcionada acerca de las especies exóticas invasoras presentes en las imágenes analizadas, así como a Greenfield Technologies S.L. por facilitar el conjunto de datos de drones utilizado en los experimentos.



Resumen

La presencia de especies exóticas invasoras en cuerpos de agua dulce supone una preocupación en varias zonas de la geografía mundial. En concreto, en el río Guadiana a su paso por Extremadura (suroeste de España), desde comienzos del año 2000, se encuentran el jacinto de agua (conocido como camalote) y el nenúfar mexicano, entre otras plantas acuáticas invasoras. La rápida propagación de estas plantas provoca impactos medioambientales desfavorables en los ecosistemas invadidos. Además, generan gastos derivados de su gestión, control y erradicación, así como efectos negativos para infraestructuras hidráulicas y para la sociedad. Tras varios años de lucha, las administraciones competentes (como Confederación Hidrográfica del Guadiana (CHG)) han realizado grandes inversiones económicas para evaluar, planificar y ejecutar estrategias para combatir esta problemática. Actualmente, los trabajos están centrados en la detección y alerta temprana para gestionar las actuaciones de control y poder alcanzar su erradicación.

Los recientes avances en las técnicas de la teledetección, u observación remota de la tierra, han propiciado el desarrollo de espectrómetros, instalados en plataformas aéreas (como aviones o drones), o en plataformas satelitales (como la familia de satélites de Sentinel-2), permitiendo capturar grandes volúmenes de datos multiespectrales. Estos datos registran información de la radiación solar emitida o absorbida de los distintos tipos de cobertura terrestre, medidas a distintas longitudes de onda. Por tanto, estas imágenes recogen datos en tres dimensiones en los que cada píxel está definido en el dominio espacial y espectral, facilitando la caracterización de la superficie terrestre. Como resultado, las imágenes multiespectrales han desempeñado un papel fundamental en varios campos de aplicación, como en la agricultura y en la gestión de recursos naturales.

La explotación de la información contenida en las imágenes multiespectrales me-

diante los sistemas de información geográfica mejora su comprensión, edición, análisis y representación de los datos en distintas capas de información georreferenciada y permite la generación de mapas. Por otro lado, las técnicas de inteligencia artificial basadas en algoritmos de aprendizaje automático y profundo (o *machine/deep learning*) se han empleado en tareas de clasificación de la superficie terrestre. Han resultado eficaces en la detección automática de vegetación y cuerpos de agua, evitando tareas de campo.

El principal propósito de esta Tesis Doctoral es facilitar la detección y monitorización de las plantas acuáticas invasoras, extrayendo información clave de imágenes multiespectrales de libre acceso. Por lo tanto, se aplican técnicas de teledetección, sistemas de información geográfica, y técnicas de aprendizaje automático y aprendizaje profundo, proponiendo nuevas metodologías de análisis, agilizando y automatizando procesos.

Palabras clave: plantas invasoras, teledetección, monitorización, aprendizaje automático, aprendizaje profundo, sistemas de información geográfica.

Abstract

The presence of invasive exotic species in freshwater bodies represents a concern in various areas of the world's geography. Specifically, in the Guadiana river basin (southwest Spain), water hyacinth and mexican water lily (among other aquatic invasive plants) are found. Distributed in a worrying manner since the beginning of 2000s, the rapid spread of these plants causes unfavorable environmental impacts on the invaded ecosystems. Moreover, they generate expenses derived from their management, control, and eradication, as well as negative effects on hydraulic infrastructure and society. After several years of struggle, competent administrations such as the *Confederación Hidrográfica del Guadiana* (CHG) have made significant economic investments to evaluate, plan and execute strategies to combat this problem. Currently, efforts are focused on early detection and warning to manage control measures and achieve their eradication.

Recent advances in remote sensing techniques have led to the development of spectrometers installed on airborne platforms (such as airplanes or drones) or satellite platforms (such as the Sentinel-2 satellite family), allowing for the capture of large volumes of multispectral data. These data record information on the radiation emitted or absorbed by different land covers, measured at different wavelengths. Therefore, these images collect data in three dimensions in which each pixel is defined in the spatial and spectral domain, facilitating the characterization of the land surface. As a result, multispectral images have played a fundamental role in various fields of application, such as agriculture and natural resource management.

The exploitation of the information contained in multispectral images through geographic information systems improves their understanding, editing, analysis, and representation of data in different layers of georeferenced information, enabling the generation of maps. On the other hand, artificial intelligence techniques based on machine/deep learning algorithms have been used in land cover classification tasks. They

have been effective in the automatic detection of vegetation and water bodies, avoiding field tasks.

The main purpose of this Ph.D. is to facilitate the detection and monitoring of aquatic invasive plants. For that purpose, the work is focused on extracting key information from freely available multispectral images. Remote sensing techniques, geographic information systems, and machine/deep learning techniques are applied, proposing new methodologies, streamlining and automating processes, avoiding field tasks, reducing costs, thus contributing to the improvement of aquatic invasive plant detection and monitoring tasks, accurately.

Keywords: Invasive plants, remote sensing, monitoring, machine learning, deep learning, geographic information systems.

Contenidos

Agradecimientos personales	v
Otros Agradecimientos	vi
Resumen	ix
Abstract	xi
1 Compendio de publicaciones	1
1.1 Normativa aplicada para la presentación por compendio de publicaciones	1
1.2 Compendio de publicaciones en esta Tesis Doctoral	3
2 Justificación unitaria de la Tesis Doctoral	5
2.1 Objetivos de esta Tesis Doctoral	5
2.2 Consecución de los objetivos de esta Tesis mediante las publicaciones que forman parte del compendio	6
3 Contexto	9
3.1 Plantas acuáticas invasoras	9
3.1.1 Problemática de plantas invasoras en el río Guadiana	10
3.2 Contextualización de técnicas para la detección de plantas invasoras acuáticas en imágenes teledetectadas	14
3.2.1 Detección de plantas invasoras con índices espectrales	14
3.2.2 Detección de especies invasoras mediante inteligencia artificial . .	16
4 Aplicación de técnicas de teledetección	19
4.1 Teledetección e imágenes multiespectrales	19
4.2 Conjunto de datos multiespectrales considerados en esta Tesis Doctoral .	21

4.2.1	Imágenes multiespectrales Sentinel-2	21
4.2.2	Imágenes multiespectrales aéreas PNOA	23
4.2.3	Imágenes multiespectrales UAV	24
4.3	Composición de bandas espectrales e índices espectrales considerados en esta Tesis Doctoral	24
4.4	Áreas de interés en las investigaciones de esta Tesis Doctoral	26
5	Aplicación de técnicas de sistemas de información geográfica	29
5.1	Explotación de imágenes obtenidas de forma remota mediante sistemas de información geográfica	29
5.2	Operaciones SIG desarrolladas en esta Tesis Doctoral	30
6	Aplicación de inteligencia artificial para la detección automática de plantas acuáticas invasoras	33
6.1	Clasificación de datos multiespectrales	33
6.2	Algoritmos de clasificación de aprendizaje automático	34
6.2.1	k-Means	35
6.2.2	Random forest	35
6.2.3	Support Vector Machine	36
6.2.4	K-Nearest Neighbors	36
6.2.5	Multilayer Perceptron	37
6.3	Algoritmos de Aprendizaje profundo	39
6.3.1	Redes neuronales convolucionales	39
6.3.2	Modelos de CNN propuestos	40
6.4	Métricas de evaluación de algoritmos	44
7	Contribuciones de esta Tesis Doctoral	47
7.1	Resumen global de resultados y discusión	47
7.2	Mapeado eficiente de grandes áreas en imágenes de alta resolución mediante estrategia de procesamiento en ventana	51
7.2.1	Resumen	51
7.2.2	Contribuciones de este artículo	51
7.2.3	Esquema metodológico de estrategia de procesamiento en ventana	52
7.2.4	Mapeo de olivar	53
7.3	Detección automática de plantas acuáticas invasoras mediante algoritmos de aprendizaje automático y aprendizaje profundo	56
7.3.1	Resumen	57
7.3.2	Contribuciones de este artículo	58

7.3.3	Estrategia en el preprocesado de imágenes multiespectrales para el tratamiento de los píxeles con valores nulos	58
7.3.4	Estrategia para generación de imágenes verdad-terreno propuesta	60
7.3.5	Mapeo de plantas acuáticas invasoras	60
7.4	Monitoreo de la distribución espacio- temporal de plantas acuáticas invasoras en una serie temporal mediante un modelo de aprendizaje profundo entrenado con escasas muestras de entrenamiento	67
7.4.1	Resumen	67
7.4.2	Contribuciones de este artículo	67
7.4.3	Metodología propuesta para evaluar la evolución temporal	68
7.4.4	Selección de un conjunto de entrenamiento adecuado para predecir la geolocalización del jacinto de agua en toda la serie temporal .	68
7.4.5	Resultados de monitorización del jacinto de agua en el río Guadiana en un periodo de dos años	70
7.5	Reducción del número de bandas espectrales del satélite Sentinel-2 necesarias para el mapeo de plantas acuáticas invasoras mediante modelos de aprendizaje profundo, entrenados con índices espectrales	73
7.5.1	Resumen	74
7.5.2	Contribuciones de este artículo	74
7.5.3	Metodología para detectar plantas invasoras acuáticas entrenando un modelo CNN con un número reducido de bandas espectrales .	75
7.5.4	Mapeado de plantas invasoras acuáticas en el río Guadiana con el modelo CNN	76
7.5.5	Mapeado de plantas invasoras acuáticas en el río Guadiana con el algoritmo RF	77
7.6	Mapeo de las áreas de acumulación de plantas acuáticas invasoras en una serie temporal de imágenes multiespectrales mediante modelo de aprendizaje profundo y SIG	79
7.6.1	Resumen	79
7.6.2	Contribuciones de este artículo	79
7.6.3	Metodología para detectar las áreas de acumulación de plantas invasoras acuáticas en una serie temporal de imágenes de satélite .	80
7.6.4	Análisis de los mapas de acumulación para diferentes periodos temporales	80
7.7	Comprobación del impacto de añadir la componente espacial en el modelo CNN	84
7.7.1	Resumen	84

7.7.2	Contribuciones de este artículo	84
7.7.3	Estrategia metodológica propuesta	85
7.7.4	Mapeo de plantas acuáticas invasoras con CNN2D en dos ROI . . .	85
7.7.5	Comparación de las actuaciones del modelo CNN2D con el modelo CNN1D para mapear plantas acuáticas invasoras	87
8	Conclusiones finales	89
	Bibliografía	91
	Resultados de esta Tesis Doctoral	101
	Publicaciones en el compendio	101
	Otros resultados pendientes de publicar	102
	Capítulo de libro	102
	Comunicaciones	102
	Premios	103
	Otra divulgación	103
	Participación en proyectos de I+D+I regionales	103
	Publicaciones	105
	Efficiently Mapping Large Areas of Olive Trees Using Drones in Extremadura, Spain	106
	Automatic Detection of Aquatic Weeds: A Case Study in the Guadiana River, Spain	116
	Monitoring the Spatiotemporal Distribution of Invasive Aquatic Plants in the Guadiana River, Spain	136
	Mapping Invasive Aquatic Plants in Sentinel-2 Images Using Convolutional Neural Networks Trained With Spectral Indices	151
	Mapping the Accumulation of Invasive Aquatic Plants in the Guadiana River, Spain, Using Multitemporal Remote Sensing	163

Lista de figuras

3.1	Jacinto de agua (<i>Eichornia crassipes</i>), siendo retirada de la superficie del río Guadiana (España) por maquinaria, fotografiada por Tomás Rodríguez	11
3.2	Nenúfar mexicano (<i>Nymphaea mexicana</i>) en el río Guadiana, fotografiada por Tomás Rodríguez.	12
4.1	Algunos tipos de cobertura terrestre presentes en los píxeles de la imagen multiespectral de estudio y sus firmas espectrales.	20
4.2	Esquema general de instrumentos de teledetección (los utilizados en esta Tesis) que captan la radiación solar reflejada por los materiales de la superficie terrestre, a lo largo de diferentes longitudes de onda del espectro electromagnético. Se han utilizado imágenes multiespectrales adquiridas por el satélite Sentinel-2, en los vuelos del PNOA e imagen capturada por un dron.	22
4.3	(a) Localización geográfica de España. (b) Localización geográfica de la región de Extremadura, el río Guadiana y la cuenca del Guadiana. (c) Zoom de una imagen de alta resolución que incluye una zona afectada por nenúfar mexicano en la ciudad de Badajoz. (d) Zoom de una imagen de alta resolución que incluye una zona afectada por el jacinto de agua, próxima a la ciudad de Mérida.	27
4.4	Localización de la superficie dedicada a olivar en Extremadura (España). . . .	28
5.1	Concepto de capas SIG. Como ejemplo, se muestran fragmentos de algunas capas usadas y generadas en SIG en esta Tesis Doctoral.	31

6.1	Arquitectura de la red neuronal convolucional de una dimensión (CNN1D) desarrollada. Los bloques tridimensionales dibujados sobre la imagen multi-espectral representan los píxeles de la imagen. Los datos de entrada de este modelo se corresponden con la información espectral de cada pixel.	41
6.2	Arquitectura de la red neuronal convolucional de dos dimensiones (CNN2D) desarrollada. Los datos de entrada del modelo corresponden con la información espacial y espectral de cada bloque de píxeles (o <i>patch</i>).	43
7.1	Flujo de de trabajo para la detección de olivar.	52
7.2	Estrategia de partición de ventanas en un ejemplo con cuatro ventanas.	54
7.3	Mapa de clasificación del área total obtenido mediante partición de ventanas y RF (a) y mapa de clasificación de una escena ampliada (b).	55
7.4	(a) Imagen RGB del conjunto de datos. Mapas de clasificación obtenidos por diferentes clasificadores: (b) RF, (c) SVM, (d) KNN y (e) MLP.	56
7.5	Métricas de precisión para evaluar los resultados de la clasificación (<i>average precision, accuracy score y balanced acuracy score</i>) para cada clasificador en: (a) Experimento 1, (b) Experimento 2 y (c) Experimento 3	57
7.6	a) Imagen completa de Sentinel-2 para ROI-BA, b) ROI-ME recortado y valores <i>NoData</i> presentes en la imagen debido a su geometría.	59
7.7	Principales pasos en la generación de la imagen verdad-terreno sintética (GT).	61
7.8	Algunas imágenes GT sintéticas generadas para cada región de interés considerada.	62
7.9	Mapas de clasificación de tres escenas representativas en ROI-BA (Badajoz).	63
7.10	Mapas de clasificación en ROI-BA con diferentes clasificadores: a) K-means, b) RF y c) CNN.	64
7.11	Mapas de clasificación de tres escenas representativas de ROI-ME (Mérida).	65
7.12	Mapas de clasificación en ROI-ME con diferentes clasificadores: a) K-means, b) RF y c) CNN.	66
7.13	Flujo de trabajo del procedimiento de monitorización de la distribución espacio-temporal del jacinto de agua en el río Guadiana mediante tres experimentos diferentes. También se muestra la arquitectura de la CNN utilizada para el mapeo.	69
7.14	Firmas espectrales de las muestras de entrenamiento de jacinto de agua extraídas de imágenes Sentinel-2 (adquiridas en 4 fechas diferentes).	70

7.15	Justificación visual de la necesidad de recoger diferentes muestras de entrenamiento de imágenes de Sentinel-2 en 4 fechas diferentes. Se muestran los resultados obtenidos tras procesar con el modelo CNN las imágenes de Sentinel-2 adquiridas en las fechas: (a) 2019-07-11, (b) 2019-02-06, (c) 2019-03-28 y (d) 2019-12-28. Los píxeles que contienen jacinto de agua en la superficie del río están marcados en rojo. Para cada imagen, mostramos los resultados de detección obtenidos utilizando diferentes conjuntos de entrenamiento: muestras recogidas el 2019-07-11 (Conjunto 1), 2019-02-06 (Conjunto 2), 2019-03-28 (Conjunto 3) y 2019-12-28 (Conjunto 4). Las imágenes se visualizan en color verdadero (RGB).	71
7.16	Porcentaje de píxeles de jacinto de agua en la ROI (excluidos los valores sin datos) obtenidos para la serie temporal completa (2019-2021) en cada experimento considerado.	72
7.17	Resultados de la detección del jacinto de agua en algunas fechas de adquisición incluidas en la serie temporal estudiada: (a) 2019-02-06, (b) 2019-03-28, (c) 2019-05-02, (d) 2019-08-05, (e) 2019-12-03, (f) 2019-12-28, (g) 2020-02-16, (h) 2020-06-10, (i) 2020-09-28, y (j) 2020-01-16).	73
7.18	Flujo de trabajo del procedimiento de mapeado de plantas acuáticas invasoras en el río Guadiana utilizando un número reducido de las bandas espectrales ofrecidas por el satélite Sentinel-2. También se muestra la arquitectura de la CNN utilizada.	75
7.19	Resultados de la detección de plantas acuáticas invasoras utilizando diferentes índices para el modelo CNN: (a) Caso Badajoz. (b) Caso Mérida	76
7.20	Resultados de la detección de plantas acuáticas invasoras utilizando diferentes índices con el algoritmo RF: (a) Caso Mérida. (b) Caso Badajoz.	78
7.21	Flujo de trabajo del procedimiento de generación de mapas de acumulación de jacinto de agua en el río Guadiana.	81
7.22	Mapas de acumulación de jacinto de agua para distintos periodos: (a) Serie temporal completa. (b) Desde 2019-04-12 hasta 2019-05-27. (c) Desde 2020-06-05 hasta 2020-08-29.	83
7.23	Histograma que muestra el número de píxeles detectados como jacinto de agua para la serie temporal completa.	83
7.24	Flujo de trabajo del procedimiento de mapeado de plantas acuáticas invasoras en el río Guadiana utilizando el modelo CNN2D.	85
7.25	Resultados de detección de plantas acuáticas invasoras usando los modelos CNN2D y CNN1D para: (a) Caso Mérida. (b) Caso Badajoz.	86

Lista de tablas

4.1	Descripción de las bandas espectrales de Sentinel-2.	23
7.1	Métricas de precisión para el caso de Badajoz y el caso de Mérida	61
7.2	Número de muestras de extremamiento (píxeles) usados en nuestros experimentos	70
7.3	Evaluación del rendimiento para el caso de Mérida y el caso de Badajoz (los mejores resultados en negrita) utilizando el algoritmo CNN.	77
7.4	Evaluación del rendimiento para los casos de Mérida y Badajoz (los mejores resultados en negrita) utilizando el algoritmo RF.	78
7.5	Evaluación del rendimiento para el caso de Mérida y el caso de Badajoz utilizando la CNN1D y la CNN2D	87

Acrónimos y abreviaturas

AI	Artificial Intelligence
ANN	Artificial Neural Networks
AVIRIS	Airborne Visible/Infrared Imaging Spectrometer
AWEI	Automated Water Extraction Index
BSI	Bare Soil Index
CDB	Convenio de Naciones Unidas sobre la Diversidad Biológica
CHG	Confederación Hidrográfica del Guadiana
CNEAI	Comisión Nacional Evaluadora de la Actividad Investigadora
CNN	Convolutional Neural Network
CNN1D	One-Dimensional Convolutional Neural Network
CNN2D	Two-Dimensional Convolutional Neural Network
CNN3D	Three-Dimensional Convolutional Neural Network
DEM	Digital Elevation Model
DL	Deep Learning
DOI	Digital Object Identifier
EEI	Especies Exóticas Invasoras
ENDVI	Enhanced Normalized Difference Vegetation Index
ESA	European Space Agency
ETRS89	European Terrestrial Reference System 1989
EVI	Enhanced Vegetation Index
FAI	Floating Algae Index
FN	False Negative
FP	False Positive

FVC Fractional Vegetation Cover
GDAL Geospatial Data Abstraction Library
GF2 Gaofen 2
GIS Geographic Information System
GNDVI Green Normalized Difference Vegetation Index
GT Ground Truth
INSPIRE Infrastructure for Spatial Information in Europe
KDE Kernel Density estimation
KNN K-Nearest Neighbors
LiDAR Light Detection and Ranging
LSWI Land Surface Water Index
ML Machine Learning
MLP Multilayer Perceptron
MNDWI Modified Normalized Difference Water Index
NDAVI Normalized Difference Aquatic Vegetation Index
NDII Normalized Difference Infrared Index
NDREI Normalized Difference Red Edge Index
NDVI Normalized Difference Vegetation Index
NDVIRE2 Normalized Difference Vegetation Red Edge Index 2
NDVIRE3 Normalized Difference Vegetation Red Edge Index 3
NDWI Normalized Difference Water Index
NGRDI Normalized Green-Red Difference Index
NIR Near-infrared spectroscopy
PNOA Plan Nacional de Ortofotografía Aérea
RAM Random Access Memory
RBF Radial Basis Function
RF Random Forest
RGB Red Green Blue
ROI-BA Region Of Interest Of Badajoz
ROI-ME Region Of Interest Of Mérida
ROI Region Of Interest
S2 Sentinel-2
SAR Synthetic Aperture Radar
SAVI Soil-Adjusted Vegetation Index

- SIG** Sistemas de Información Geográfica
- SVM** Support Vector Machine
- SWIR** Short-wave Infrared
- TN** True Negative
- TOA** Top-Of-Atmosphere
- TP** True Positive
- UAV** Unmanned Aerial Vehicle
- UTM** Universal Transverse Mercator
- VNIR** Visible and Near-Infrared
- WAVI** Water Adjusted Vegetation Index
- WGS84** World Geodetic System 1984
- RNN** Recurrent Neural Network
- ReLU** Rectified Linear Unit

Compendio de publicaciones

Esta Tesis Doctoral es un compendio de las publicaciones que se enumeran en este capítulo, ajustándose a los requisitos establecidos en la normativa que se describe a continuación.

1.1 | Normativa aplicada para la presentación por compendio de publicaciones

La Tesis Doctoral se presenta como compendio de publicaciones ajustándose a los requisitos establecidos en el artículo 33 de la Normativa de Doctorado, según la RESOLUCIÓN de 14 de diciembre de 2021 (DOE núm 248 de 28 de diciembre), del Rector, por la que se ejecuta el acuerdo adoptado por el Consejo de Gobierno por el que se aprueba la Normativa de Doctorado de la Universidad de Extremadura. Dichos requisitos del “Artículo 33. Tesis doctorales presentadas como compendio de publicaciones.” son:

1. La Comisión Académica del Programa podrá autorizar el depósito de Tesis doctorales como compendio de publicaciones, siempre que se reúnan los siguientes requisitos:
 - a) Una introducción general, en la que se presenten temáticamente las publicaciones y se justifique la coherencia e importancia unitaria de la Tesis.
 - b) Un resumen global estructurado de los resultados y de la discusión de los mismos, así como las conclusiones finales.
 - c) Una copia completa de los trabajos publicados, haciendo constar claramente el nombre y la filiación de todas las coautorías de los trabajos y la referencia

completa de las revistas en la que se han publicado o aceptado para su publicación. En este último caso se deberá aportar la documentación justificativa de la aceptación, así como la referencia completa de la revista a la que se ha enviado el trabajo para su publicación. En caso de que se presente algún trabajo realizado en coautoría, hay que incluir también el informe a que hace referencia el apartado 2 de este artículo.

- d) En caso de que alguno de los trabajos presentados se haya publicado en una lengua distinta de las especificadas en el Programa de Doctorado, debe adjuntar un resumen del trabajo en cuestión redactado en alguna de las lenguas del Programa.
- e) De estas aportaciones al menos dos tendrán que estar publicadas en revistas indexadas en el ISI-JCR o tratarse de alguna contribución relevante en su campo científico según los criterios de la Comisión Nacional Evaluadora de la Actividad Investigadora (Comisión Nacional Evaluadora de la Actividad Investigadora (CNEAI)). Al menos en una de ellas el estudiante de doctorado deberá ocupar una posición relevante, entendiendo como tales, la primera, la última o la autoría de correspondencia.
- f) Cualquier otro requisito que pueda establecer la Comisión Académica del Programa de Doctorado.

Por acuerdo del Consejo Permanente de la EDUEx de fecha 3 de marzo de 2022, se mantiene el acuerdo de la Comisión de Doctorado de fecha 30 de noviembre de 2020:

“En el caso de que para algún artículo se haya cedido a la revista el copyright y no se mantengan los derechos para su reproducción sin ánimo de lucro, deberá obtenerse autorización de la revista para reproducir dicho artículo en la tesis. En caso de que la revista no conceda dicha autorización, se sustituirá el artículo por la versión *preprint* y se añadirá una página en la que conste su referencia: título, autores, revista donde fue publicado el trabajo, volumen, página inicial y final, año de publicación, resumen de la publicación y su Digital Object Identifier (DOI).

Se adjuntará obligatoriamente un informe del director de la Tesis Doctoral sobre el factor de impacto o la categorización de las publicaciones incluidas en la Tesis Doctoral y sobre los trabajos realizados en coautoría, especificando exhaustivamente cuál ha sido la participación del doctorando en cada artículo y, si procede, la utilización, implícita o explícita, por parte de los

coautores de los trabajos presentados para la elaboración de una Tesis Doctoral.”

1.2 | Compendio de publicaciones en esta Tesis Doctoral

La presente Tesis Doctoral es un compendio de las siguientes publicaciones, ordenadas en orden cronológico de publicación:

1. Publicación [1]: **E. C. Rodríguez-Garlito** and A. Paz-Gallardo, “Efficiently Mapping Large Areas of Olive Trees Using Drones in Extremadura, Spain”, in IEEE Journal on Miniaturization for Air and Space Systems, vol. 2, no. 3, pp. 148-156, Sept. 2021. DOI: 10.1109/JMASS.2021.3067102.
2. Publicación [2]: **E. C. Rodríguez-Garlito**, A. Paz-Gallardo and A. Plaza, “Automatic Detection of Aquatic Weeds: A Case Study in the Guadiana River, Spain”, in IEEE Journal of Selected Topics in Applied Earth Observations and Remote Sensing, vol. 15, pp. 8567-8585, 2022. DOI: 10.1109/JSTARS.2022.3210373. [IF(2022)=5.5].
3. Publicación [3]: **E. C. Rodríguez-Garlito**, A. Paz-Gallardo and A. Plaza, “Monitoring the Spatiotemporal Distribution of Invasive Aquatic Plants in the Guadiana River, Spain”, in IEEE Journal of Selected Topics in Applied Earth Observations and Remote Sensing, vol. 16, pp. 228-241, 2023. DOI: 10.1109/JSTARS.2022.3225201. [IF(2022)=5.5].
4. Publicación [4]: **E. C. Rodríguez-Garlito**, A. Paz-Gallardo and A. Plaza, “Mapping Invasive Aquatic Plants in Sentinel-2 Images Using Convolutional Neural Networks Trained with Spectral Indices”, in IEEE Journal of Selected Topics in Applied Earth Observations and Remote Sensing, vol. 16, pp.2889-2899, 2023. DOI: 10.1109/JSTARS.2023.3257142. [IF(2022)=5.5].
5. Publicación [5]: **E. C. Rodríguez-Garlito**, A. Paz-Gallardo and A. Plaza, “Mapping the Accumulation of Invasive Aquatic Plants in the Guadiana River, Spain, Using Multitemporal Remote Sensing”, in IEEE Geoscience and Remote Sensing Letters, vol. 20, pp. 1-5, 2023. DOI: 10.1109/LGRS.2023.3277366. [IF(2022)=4.8].

Además está pendiente de aceptación los resultados recogidos en el siguiente trabajo:

1. Publicación [6]: **E. C. Rodríguez-Garlito**, A. Paz-Gallardo and A. Plaza, "Spectral-Spatial Mapping of Invasive Aquatic Plants in the Guadiana River, Spain, Using Convolutional Neural Networks"

Justificación unitaria de la Tesis Doctoral

Las plantas acuáticas invasoras como el jacinto de agua (el conocido camalote) o el nenúfar mexicano producen efectos negativos socioeconómicos y para la biodiversidad, en los ecosistemas invadidos. Conocer su distribución espacio temporal contribuye en las tareas de gestión de esta problemática presente en varias zonas de la geografía mundial. Esta Tesis Doctoral inicia una línea de investigación en la que se explotan imágenes multiespectrales adquiridas por el satélite Sentinel-2 para detectar y monitorizar automáticamente plantas acuáticas invasoras en el río Guadiana (suroeste de la península ibérica). Para este propósito, en las publicaciones resultantes de esta investigación, se proponen y desarrollan nuevas metodologías en la que se utilizan técnicas de teledetección, Sistemas de Información Geográfica (SIG), técnicas de aprendizaje automático y aprendizaje profundo.

2.1 | Objetivos de esta Tesis Doctoral

El **objetivo principal** de la presente Tesis Doctoral es el desarrollo de nuevos métodos y algoritmos de análisis y clasificación de imágenes multiespectrales que se han obtenido de forma remota, orientados a la detección y monitorización de plantas acuáticas invasoras, como el jacinto de agua y el nenúfar mexicano. Para ello se aplican técnicas de teledetección, SIG y técnicas de aprendizaje automático y aprendizaje profundo.

Para la consecución de este objetivo principal, en las contribuciones científicas desarrolladas, se logran los siguientes **objetivos específicos**:

1. Desarrollar una estrategia de mapeado eficiente en imágenes de alta resolución espacial obtenidas de forma remota cuyo procesamiento requiere grandes candi-

- dades de memoria de acceso aleatorio (del inglés *Random Access Memory (RAM)*).
2. Diseñar una metodología para la generación de imágenes verdad-terreno a partir de imágenes de alta resolución espacial que implica técnicas de teledetección y SIG.
 3. Explorar algoritmos de aprendizaje automático y desarrollar modelos de aprendizaje profundo para detectar plantas acuáticas invasoras en cuerpos de agua dulce en imágenes de satélite de media resolución y de libre acceso.
 4. Generar una metodología para el monitoreo a lo largo del tiempo, de plantas acuáticas invasoras independientemente de su estado fenológico, mediante imágenes de satélite de media resolución de libre acceso, a partir de la generación de un modelo de aprendizaje profundo.
 5. Explorar la simplificación del número de bandas espectrales a través de combinaciones o índices espectrales, de las imágenes recogidas por el satélite Sentinel-2 de la Agencia Espacial Europea (del inglés *European Space Agency (ESA)*) para su uso en modelos de aprendizaje profundo.
 6. Proponer una metodología para mapear las áreas de acumulación de plantas acuáticas invasoras, a partir de la monitorización del río en una serie temporal, mediante un modelo de aprendizaje profundo.
 7. Diseñar nuevos modelos de aprendizaje profundo que tengan en cuenta la componente espacial y espectral de las imágenes multiespectrales para la detección de plantas acuáticas invasoras.

2.2 | Consecución de los objetivos de esta Tesis mediante las publicaciones que forman parte del compendio

Los objetivos específicos descritos anteriormente se han cumplido en cada uno de los artículos de esta Tesis Doctoral por compendio de publicaciones científicas en revistas internacionales y con índice de impacto. A continuación, se describen brevemente el contenido de cada uno de ellos.

En la publicación [1] se ha propuesto una estrategia para procesar imágenes multiespectrales de alta resolución espacial, con altos requerimientos de memoria RAM para

su procesamiento. En este caso se ha desarrollado una estrategia que aplica un particionamiento espacial, consistente en dividir la imagen en ventanas, previamente a su procesamiento. Se ha experimentado con una imagen de alta resolución (3 cm por pixel) adquirida por un dron, sobre una superficie dedicada al cultivo de olivos. Mediante algoritmos de aprendizaje automático como *k-means*, *random forest*, *support vector machine*, *multilayer perceptron* y *k-nearest neighbors* se ha clasificado la imagen para detectar los olivos entre otras clases de cobertura terrestre presentes en dicha imagen.

Esta estrategia de procesamiento en ventana descrita en [1] se ha puesto en práctica en la publicación [2], en la que se ha propuesto una metodología para la generación de imágenes verdad-terreno sintéticas a partir de otras imágenes multiespectrales de alta resolución como son las adquiridas por los vuelos del PNOA. En [2] también se ha explorado la detección automática de plantas acuáticas invasoras en imágenes multiespectrales de media resolución espacial (de 10 m a 60 m dependiendo de la banda espectral), adquiridas por el satélite Sentinel-2 de la ESA. Se han evaluado diferentes algoritmos de clasificación de aprendizaje automático (*k-means* y *random forest*) y de aprendizaje profundo (red neuronal convolucional). Las actuaciones de detección de estos algoritmos se han evaluado, mediante métricas de precisión, comparando los resultados de clasificación con la imágenes verdad-terreno generadas.

Partiendo del algoritmo de clasificación que mejor resultados de precisión ha obtenido para la detección de plantas invasoras en [2] (la red neuronal convolucional), en [3] se ha llevado a cabo un estudio de monitorización de plantas invasoras para una serie temporal de 2 años. Se ha generado un modelo de red neuronal convolucional que se ha entrenado con escasas muestras de entrenamiento; únicamente con muestras recogidas de 4 de las 62 imágenes multiespectrales recogidas por el satélite Sentinel-2 en ese periodo temporal. Esto ha permitido el monitoreo de la distribución espacio-temporal de plantas acuáticas invasoras (en este caso el jacinto de agua), permitiendo detectar estas plantas independientemente de su estado fenológico.

En las publicaciones previas, se han explotado las 12 bandas espectrales de las imágenes recogidas por el producto con la corrección atmosférica Sentinel-2 L2A. En la publicación [4], se experimenta con una simplificación del número de bandas espectrales necesarias para entrenar el modelo de red neuronal convolucional propuesto y desarrollado en las publicaciones anteriores. En este caso, se utilizan combinaciones de bandas o índices espectrales en las que únicamente se están explotando dos bandas (en el caso de los índices NDVI o NDII) o tres bandas espectrales (como con RGB, FAI o BSI). Esta simplificación de bandas permite la detección de plantas acuáticas invasoras teniendo como imagen de entrada en el modelo de aprendizaje profundo pocas bandas espectrales de las obtenidas con el satélite Sentinel-2. Además, sus resultados son

comparables a los obtenidos cuando se emplea la totalidad de sus bandas ofrecidas.

La metodología propuesta en [3] para la monitorización de la distribución espacio-temporal de las plantas acuáticas invasoras sirve de base para estudios como el desarrollado en [5]. En él se desarrolla una metodología que engloba técnicas de teledetección, técnicas SIG y modelos de aprendizaje profundo, para analizar y mapear las áreas de acumulación de plantas invasoras en un periodo temporal.

En los modelos de aprendizaje profundo que se han propuesto y aplicado en las publicaciones anteriores, únicamente se ha tenido en cuenta la componente espectral (mediante un red neuronal convolucional de una dimensión) para realizar la predicción de los píxeles contenedores de plantas acuáticas invasoras, en las imágenes multiespectrales de Sentinel-2. En los resultados pendientes de publicación [6], se explora la adición de la componente espacial para dicha predicción. De esta forma, se desarrollan y exploran nuevos métodos de clasificación de píxeles en los que se utilizan capas convolucionales de dos dimensiones para tener en cuenta los píxeles cercanos al píxel del que se está prediciendo su tipo de cobertura terrestre.

Contexto

En este capítulo se contextualiza el problema generado en las zonas afectadas por la existencia de plantas exóticas invasoras en cuerpos de agua dulce, así como la problemática que existe en la actualidad en el río Guadiana. También se hace una revisión de la literatura relacionada con la detección de plantas exóticas invasoras en imágenes obtenidas de forma remota.

3.1 | Plantas acuáticas invasoras

Especies Exóticas Invasoras (EEI) es la terminología empleada para referirse a las especies introducidas fuera de su ecosistema natural y cuya introducción y/o difusión conlleva riesgos para la biodiversidad, según el tratado internacional Convenio de Naciones Unidas sobre la Diversidad Biológica (CDB) que entró en vigor el 29 de diciembre de 1993, del que forma parte España. La ley 42/2007, trata esta problemática para que las Administraciones competentes garanticen la conservación del patrimonio natural y biodiversidad. Como se mostrarán en la sección 4.4, en esta Tesis Doctoral se investiga en regiones de interés afectadas por especies vegetales exóticas invasoras que se encuentran en la superficie de los ríos. Por lo tanto, también se ha utilizado la terminología “**plantas acuáticas invasoras**” para referirse a ellas.

La gestión ineficaz de los residuos domésticos, agrícolas o industriales contribuye al exceso de nutrientes en los ecosistemas acuáticos (por ejemplo, fósforo y nitrógeno), que contaminan el agua mediante un proceso denominado eutrofización [7]. El enriquecimiento de nutrientes en el agua tiene importantes repercusiones ecológicas, como la pérdida de calidad del agua. Este enriquecimiento también provoca un crecimiento excesivo de determinadas especies vegetales también conocidas como malas hierbas acuáticas [8]. Una presencia excesiva de dicha vegetación podría provocar que duran-

te su crecimiento y putrefacción se consume una gran cantidad de oxígeno disuelto en el agua, introduciendo una gran cantidad de materia orgánica en ella [9]. Más notablemente, las plantas acuáticas flotantes tienden a crear un manto en la superficie del agua que absorbe la luz, reduciendo la cantidad de iluminación en los hábitats bentónicos y, por lo tanto, reduciendo la biodiversidad [10].¹

El reto de prevenir y controlar la existencia y propagación de plantas acuáticas invasoras se extiende por gran parte de la geografía mundial. A modo de ejemplo, el jacinto de agua (*Eichhornia crassipes*) es una de las especies más invasoras del planeta. Su distribución geográfica alcanza casi todos los continentes [11]. En África, está presente en muchos lugares como el lago Victoria o el río Níger. En Asia, se encuentra en el río Al Kabir. En Australia, cubre el río Burdeki. Y en América del Norte y del Sur, está presente en el Río Grande y en varias lagunas fuera del Amazonas, entre otros. En Europa, esta maleza acuática también habita en Francia, Italia, Portugal, Alemania y España, donde uno de sus ríos más largos (el río Guadiana) está muy afectado.

3.1.1 | Problemática de plantas invasoras en el río Guadiana

El jacinto de agua (*Eichhornia crassipes* o también conocido como camalote) es un macrófito acuático perenne nativo de hábitats brasileños [12]. Esta planta acuática (que flota libremente en la superficie del agua dulce) se ha extendido a diferentes partes del mundo [13], estando distribuida en más de 50 países de los cinco continentes. Estas especies, en algunos lugares pueden ser consideradas como un recurso valioso con diversas cualidades [14] dado que presentan propiedades únicas. Algunos autores han destacado la aplicación ecológica y socioeconómica del jacinto de agua [15]. Absorbe metales pesados y contaminantes orgánicos, lo que permite su utilización en tratamientos de aguas residuales [16; 17; 18] y para la eliminación de metales pesados [19; 20]. También tiene un uso potencial como biomasa de jacinto de agua en biocarbón [21], bioaceite y gas de síntesis [22]. Su uso también es habitual en la producción de energía, el tratamiento de aguas, la agricultura (como recurso químico y biológico) y como alternativa a los materiales de construcción convencionales [23]. Sin embargo, su presencia amenaza el medio ambiente y produce un impacto socioeconómico negativo en las zonas invadidas [24].

Con una gran tolerancia en condiciones ambientales extremas [25], supera a la vegetación autóctona, lo que afecta a la biodiversidad. Además, el cambio climático hace más vulnerables a las especies vegetales autóctonas, favoreciendo también a las especies vegetales invasoras que se adaptan mejor a los cambios. Como resultado, el jacinto de agua está considerado como una de las peores especies exóticas invasoras, y está in-

¹ Adaptado del artículo [2]

cluida en la Base de Datos Mundial sobre Especies Invasoras [26]. El carácter altamente invasor de esta planta se debe, en parte, a su rápida capacidad reproductiva (puede duplicar su biomasa en 6-12 días [27]). La planta se distribuye generalmente en masas o parches flotantes en la superficie de los ríos. Estos parches densos afectan negativamente a parámetros fisicoquímicos importantes de la calidad del agua. La concentración de oxígeno disuelto (la variable más importante para la fauna acuática) se reduce con el crecimiento de las plantas invasoras [28; 29]. Las masas que cubren el agua bloquean la luz necesaria para la fotosíntesis de otra vegetación sumergida. Estas masas también absorben nutrientes del agua (lo que también afecta a las comunidades ecológicas), disminuyendo la distribución del fitoplancton y modificando la abundancia y diversidad del zooplancton [30].

La Fig. 3.1 muestra la retirada de camalote en zonas invadidas por camalote en Badajoz.



Figura 3.1: Jacinto de agua (*Eichhornia crassipes*), siendo retirada de la superficie del río Guadiana (España) por maquinaria, fotografiada por Tomás Rodríguez

El jacinto de agua apareció por primera vez (siguiendo una distribución en forma de tapiz) en la cuenca del río Guadiana en 2004, causando impactos negativos como los comentados anteriormente. La biología reproductiva del jacinto de agua permite la reproducción sexual y asexual [31; 32]. La reproducción asexual, mediante la formación de estolones, es la principal causa de la rápida propagación del jacinto de agua [33]. Por otro lado, también es posible la reproducción sexual a partir de un banco de semillas [34; 35]. Según informes de la CHG (organismo público español encargado de la gestión de la cuenca del Guadiana), la eliminación total del jacinto de agua de la superficie del río Guadiana se realizó en diciembre de 2020 [36]. Sin embargo, las semillas aún permanecen en el fondo del río y pueden germinar al cabo de unos años [34].

Además de *Eichhornia crassipes*, en el río Guadiana se han extendido otras especies exóticas invasoras como el nenúfar mexicano (*Nymphaea mexicana*, también conocida co-

mo nenúfar amarillo mexicano). Se trata de otra planta flotadora y sus semillas crecen bajo el agua. A diferencia del jacinto de agua (cuyas flores son azules o lilas) tiene flores de pétalos amarillos. En la actualidad, esta planta, a pesar de introducirse durante los años 80, ha proliferado en los últimos años, estando muy presente en la superficie del río a su paso por la ciudad de Badajoz. La Fig. 3.2 muestra imágenes del río Guadiana invadido donde se aprecia su disposición en la superficie. Como se muestra, su distribución en forma de tapiz sobre la superficie del agua impide el paso de la luz y afecta a la vegetación autóctona, así como a los invertebrados acuáticos [37], [38], [39].



Figura 3.2: Nenúfar mexicano (*Nymphaea mexicana*) en el río Guadiana, fotografiada por Tomás Rodríguez.

Las invasiones del jacinto de agua y del nenúfar mexicano también crean impactos negativos en diferentes actividades humanas y recreativas en el río Guadiana, como el piragüismo, ya que invade completamente tramos del río. Su acumulación en los embarcaderos afecta el acceso a la navegación y a la navegabilidad [40]. Desde una perspectiva económica, la invasión del jacinto supone elevados costes en gestión [41], equipamiento, tratamiento y personal cualificado para las tareas de control, retirada y eliminación en las masas de agua afectadas [42; 43; 44].²

3.1.1.1 | Formas de combatirlas

Los negativos impactos ecológicos y socioeconómicos causados por estas plantas invasoras han motivado diferentes mecanismos de control, así como intentos de erradicación por parte de las instituciones públicas. Un aspecto importante para controlar su repro-

²Adaptado del artículo [3]

ducción es la detección precoz, que permite tomar medidas de eliminación. Las especies acuáticas invasoras tienen una gran capacidad para reproducirse y adaptarse al medio en el que se desarrollan. Por ello, es necesario un seguimiento y control continuo de las zonas afectadas.

En Europa existe un marco legal que desincentiva una economía lucrativa en torno a este tipo de especies invasoras, prohibiendo la posesión, el comercio y el tráfico de ejemplares vivos. En la cuenca del río Guadiana, se han adoptado varias estrategias para mitigar el impacto negativo de las plantas invasoras, con grandes inversiones económicas. En ese sentido, se han llevado a cabo diversas acciones de extracción y vigilancia. Algunas de estas actuaciones se han enmarcado en proyectos internacionales [45],[46], entre los que destacan LIFE+ INVASEP "Lucha contra las especies invasoras en las cuencas hidrográficas del Tajo y Guadiana en la Península Ibérica", Interreg España-Portugal LIFE10/NAT/ES 000582 y Proyecto ACECA, cofinanciado por el Fondo Europeo de Desarrollo Regional (FEDER), con presupuestos de 2 895 267 y 5 560 221,66 euros, en los periodos (2012-2016) y (2014-2020), respectivamente. Algunas acciones incluidas en estas estrategias de lucha contra estas plantas, se han centrado en la eliminación manual y mecanizada. Dada la dificultad de erradicar las plantas invasoras en los cursos de agua afectados, los esfuerzos de gestión se dirigen a reducir su biomasa mediante diversas estrategias. Para ello, se ha utilizado el control mecánico o la eliminación manual [47], junto con el control químico [48; 49] o biológico [50; 51]. Se han creado infraestructuras de control (como barreras de contención y eliminación). Sin embargo, la legislación española no permite el uso de herbicidas en cauces naturales. En 2021, se informó de que se había extraído un total de 1 507 830,92 toneladas de jacinto de agua desde 2005 [36]. También se han llevado a cabo actividades de vigilancia para evitar su proliferación y expansión. En la actualidad, la atención se centra en el control y la detección precoz. Se han realizado análisis económicos para demostrar los beneficios para el ecosistema de la gestión de especies invasoras [52]. Así, por ejemplo, se ha previsto una inversión de 27 800 000 euros para medidas de control y erradicación del jacinto de agua para el periodo 2021-2027. ³

³Adaptado del artículo [2] y [3]

3.2 | Contextualización de técnicas para la detección de plantas invasoras acuáticas en imágenes tele-detectadas

Para vigilar y controlar las plantas acuáticas invasoras es fundamental cartografiar su distribución espacio-temporal. La teledetección o *remote sensing* desempeña un papel importante en esta tarea, ya que las imágenes obtenidas de forma remota proporcionan una rica información espectral, espacial y temporal. En las últimas décadas, hemos asistido a un enorme crecimiento de los estudios de teledetección en los que se han explotado el análisis de imágenes y las diferentes especificaciones de los sensores para cartografiar y detectar plantas acuáticas invasoras. A continuación, se citan y resumen técnicas utilizadas en la literatura para tal propósito y que están relacionadas con los métodos utilizados en la presente Tesis Doctoral.

3.2.1 | Detección de plantas invasoras con índices espectrales

Varios autores han explotado el potencial de la utilización de los índices espectrales para cartografiar eficazmente los ecosistemas afectados por plantas acuáticas invasoras [11]. Estas medidas cuantitativas, calculadas mediante combinaciones y relaciones de diferentes bandas espectrales, permiten resaltar alguna característica de la cobertura terrestre. El trabajo en [53] combinó índices de vegetación (por ejemplo, el índice de vegetación de diferencia normalizada *Normalized Difference Vegetation Index (NDVI)*) e índices de agua como el índice de diferencia de agua normalizado (*Normalized Difference Water Index (NDWI)*) para detectar *Eichhornia crassipes* (jacinto de agua) en imágenes Sentinel-2. El trabajo de [54] también se centra en la detección del jacinto de agua mediante el cálculo de la cubierta vegetal fraccional (*Fractional Vegetation Cover (FVC)*) en imágenes Sentinel-2 utilizando el Índice de vegetación ajustado al suelo (*Soil-Adjusted Vegetation Index (SAVI)*).

En [55] se utilizaron imágenes multispectrales adquiridas por vehículos aéreos no tripulados para determinar el NDVI, el índice de vegetación de diferencia normalizada mejorada (*Enhanced Normalized Difference Vegetation Index (ENDVI)*), el índice de borde rojo de diferencia normalizada (*Normalized Difference Red Edge Index (NDREI)*), el índice de diferencia normalizada verde-rojo (*Normalized Green-Red Difference Index (NGRDI)*) y el índice de vegetación de diferencia normalizada verde (*Green Normalized Difference Vegetation Index (GNDVI)*). En [56] se utilizaron imágenes Landsat para calcular el NDVI para la detección del jacinto de agua. Otros trabajos utilizaron índices espectrales

y análisis de autocorrelación espacial para detectar floraciones de algas en imágenes Sentinel-2 y Landsat [57], y también utilizaron imágenes MODIS para calcular el índice de algas flotantes (*Floating Algae Index (FAI)*).

Con el fin de explotar la información proporcionada por los índices espectrales y aprovechar las ventajas del estado del arte de los clasificadores de aprendizaje automático de última generación, varios autores han combinado ambas técnicas en sus estudios. Por ejemplo, los autores de [58] utilizaron datos de Landsat-8 y Sentinel-2 para desarrollar un clasificador jerárquico basado en tres pasos para la detección del jacinto de agua. Los pasos consistían en: 1) detección de agua con un índice de diferencia de agua normalizado modificado (*Modified Normalized Difference Water Index (MNDWI)*), 2) detección de vegetación con NDVI, y 3) detección de jacinto de agua con un clasificador (*Random Forest (RF)*). Los autores de [59] discriminaron entre jacinto de agua y prímula de agua en imágenes Sentinel-2 utilizando RF y nueve índices espectrales de vegetación y agua (NDVI, índice de diferencia normalizada de vegetación acuática (*Normalized Difference Aquatic Vegetation Index (NDAVI)*), índice de vegetación ajustado al agua (*Water Adjusted Vegetation Index (WAVI)*), SAVI, índice de borde rojo de vegetación de diferencia normalizada 2 (*Normalized Difference Vegetation Red Edge Index 2 (NDVIRE2)*), índice de borde rojo de vegetación de diferencia normalizada 3 (*Normalized Difference Vegetation Red Edge Index 3 (NDVIRE3)*), (NDWI), índice infrarrojo de diferencia normalizada (*Normalized Difference Infrared Index (NDII)*) y (*MNDWI*)). Los autores de [60] cartografiaron *Spartina alterniflora* utilizando datos de Sentinel-2 y Sentinel-1, índices de vegetación SAR y siete índices espectrales: NDVI, índice de vegetación mejorado (*Enhanced Vegetation Index (EVI)*), NDWI, índice de agua en la superficie terrestre (*Land Surface Water Index (LSWI)*) e índice de extracción de agua automatizada (*Automated Water Extraction Index (AWEI)*). Hasta donde sabemos, ningún estudio ha combinado clasificadores de aprendizaje profundo e índices espectrales para el entrenamiento de modelos para la detección y el mapeo de plantas acuáticas invasoras.⁴

Estos métodos basados en índices espectrales pueden presentar ciertas dificultades para discriminar plantas acuáticas invasoras del resto de cobertura terrestre. Las plantas invasoras y otros tipos de vegetación pueden coincidir en los mismos umbrales de los índices considerados, como en el caso de las áreas analizadas en los experimentos realizados en esta Tesis. Este hecho implica tareas de segmentación manual para diferenciar entre plantas invasoras y las que no lo son, lo que se traduce en un proceso más costoso y menos automático. Por ello, en este trabajo, la detección de plantas acuáticas invasoras consiste en un proceso automático mediante el uso de técnicas de inteligencia artificial.

⁴Adaptado del artículo [4]

Además, en parte de las investigaciones de esta Tesis, se aprovechan las combinaciones de bandas que son propicias para resaltar la vegetación en el agua, extrayendo muestras de entrenamiento para el modelo de inteligencia artificial desarrollado.

3.2.2 | Detección de especies invasoras mediante inteligencia artificial

Las imágenes obtenidas de forma remota se han procesado con métodos de clasificación para interpretar los datos espectrales y detectar los píxeles de las imágenes que contienen especies exóticas invasoras. [55; 56; 61; 62; 63]. Para tal fin, además de la utilización de técnicas matemáticas y de análisis de datos, mediante el empleo de técnicas de inteligencia artificial (*Artificial Intelligence (AI)*) se pueden desarrollar programas o algoritmos capaces de llevar a cabo la tarea de detección aprendiendo y razonando como los humanos. Mediante el empleo de aprendizaje automático (*Machine Learning (ML)*), una de las ramas de la AI, se permite la interacción con los datos proporcionados por las imágenes teledetectadas, para aprender automáticamente de ellos y realizar predicciones basadas en ellos. Sin embargo, en la literatura hay pocos estudios dirigidos a la vigilancia y el control de las plantas acuáticas invasoras utilizando técnicas de inteligencia artificial [64], [65], [66].⁵ El aprendizaje automático o *Deep Learning (DL)*, es otra rama de la AI, basada en redes neuronales con estructuras más complejas que permiten aprender de los datos extrayendo automáticamente características de alto nivel.

Las redes neuronales convolucionales (*Convolutional Neural Network (CNN)*) son modelos de DL que han demostrado ser adecuados para explotar patrones espaciales, espectrales o temporales de imágenes de teledetectadas en numerosas aplicaciones (clasificación de la cobertura terrestre, detección de anomalías, gestión de recursos naturales, entre otras). Estos modelos predictivos se caracterizan por constar de al menos una capa convolucional, que opera como un filtro o kernel sobre la imagen. Los modelos CNN han sido ampliamente utilizados para la clasificación de la cobertura terrestre [67]. Ante la demanda de métodos analíticos precisos, flexibles y eficientes para la explotación de datos teledetectados de vegetación, se han implementado las CNN con diferentes dimensiones del kernel de las capas convolucionales, en una amplia gama de estudios [68]. Por ejemplo, modelos CNN unidimensionales (CNN1D) para la clasificación de cultivos [69], la cartografía de cultivos en un área agrícola [70] o para la clasificación temprana de cultivos [71] en imágenes de radar de apertura sintética (*Synthetic Aperture Radar (SAR)*). En [72] también se utilizó la arquitectura CNN1D para cartografiar zonas

⁵Adaptado del artículo [2]

agrícolas sobre datos SAR y multiespectrales. Esta arquitectura también ha resultado beneficiosa para extraer información de imágenes multiespectrales, de series temporales Sentinel-2 (S2), en [73] para cartografiar tipos de cultivos, por ejemplo, o del producto MODIS MOD13A2 para clasificar tipos de cultivos en [74]. Las imágenes hiperespectrales también se han utilizado para cartografiar los tipos de cultivos, como en [75], donde se explotan las imágenes hiperespectrales PRISMA. El espectrómetro de imágenes infrarrojas visibles aerotransportado (*Airborne Visible/Infrared Imaging Spectrometer (AVIRIS)*) de la NASA se empleó para la cartografía de la cubierta terrestre en [76].

Por otro lado, las imágenes recogidas por una cámara hiperespectral instalada en un vehículo aéreo no tripulado (*Unmanned Aerial Vehicle (UAV)*) se utilizaron para estimar el rendimiento de las hojas de maíz [77]. En este último trabajo, los autores demostraron una mayor precisión de clasificación con el modelo CNN integrado de CNN1D y CNN bidimensional (CNN2D) (mediante la exploración conjunta de características espectrales y espaciales) en comparación con CNN1D (explotando únicamente características espectrales) o CNN2D (explotando únicamente características espaciales). Las arquitecturas CNN2D y CNN tridimensional (CNN3D) también se han aplicado en el campo de la vegetación. Por ejemplo, [78] utilizó CNN2D para la clasificación espacio-temporal de píxeles de vegetación en imágenes de alta resolución, consistentes en datos adquiridos por una cámara RGB (*Red Green Blue (RGB)*) a bordo de un UAV de ala fija. CNN2D (modelo U-Net) se utilizó en [79] para cartografiar tipos de bosque en imágenes multiespectrales WorldView-3. En [80] se utilizó un modelo CNN2D para predecir fracciones de cobertura de especies vegetales en Modelos Digitales de Elevación (*Digital Elevation Model (DEM)*) y datos RGB recogidos por UAV. En [81] se utilizaron imágenes RGB y *Light Detection and Ranging (LiDAR)* para la detección individual de copas de árboles aplicando la arquitectura CNN2D.

En cambio, se exploraron arquitecturas CNN3D para identificar y contar objetos terrestres indicadores de degradación de pastizales y para estimar las regiones vegetativas en un área en [82] y en [83] respectivamente, recopilando datos hiperespectrales y multiespectrales mediante el uso de UAV. En [84], se propuso un modelo CNN3D para mejorar los datos de Sentinel-3 para índices de vegetación con resolución temporal, superando los resultados de un modelo CNN2D. En otro trabajo [85] se probó la ventaja de CNN3D en comparación con CNN2D para la clasificación de cultivos en imágenes multiespectrales multitemporales Gaofen 2 (GF2). [86] compararon los modelos CNN3D, CNN2D y CNN1D para la clasificación de tres especies sobre datos hiperespectrales, obteniéndose mayores precisiones en ese orden. ⁶

⁶Adaptado del artículo pendiente de aceptación [6]

Aplicación de técnicas de teledetección

En este capítulo se introducen los conceptos de teledetección y se describen los conjuntos de datos multiespectrales considerados en las publicaciones de esta Tesis. Posteriormente, se describen las combinaciones de bandas empleadas así como las regiones de interés de los experimentos.

4.1 | Teledetección e imágenes multiespectrales

En esta Tesis Doctoral se analizan y procesan imágenes que recogen información de la radiación electromagnética reflejada por los materiales de la superficie terrestre y que se han obtenido de forma remota (observación de la Tierra mediante procedimientos sin contacto). Basados en la tecnología aplicada a la teledetección, los sensores multiespectrales o hiperespectrales instalados en plataformas aerotransportadas (aviones /drones) o espaciales (satélites) miden la energía que refleja y absorbe un objeto en la superficie terrestre. De este modo, las imágenes multiespectrales o hiperespectrales registran mediciones en porciones discretas o discontinuas del rango espectral, con decenas o cientos de bandas espectrales. Este tipo de imágenes están dotadas con diferentes números de canales o bandas que cubren una diversidad de rangos espectrales. Por un lado, los sensores hiperespectrales recogen datos en cientos de bandas espectrales casi contiguas. Por otro lado, las imágenes multiespectrales suelen tener un menor número de bandas discretas. Hay sensores de teledetección que pueden participar en diferentes misiones espaciales y otros que forman parte de planes nacionales proporcionando cobertura en todo el territorio internacional o nacional. Por lo tanto se ofrecen imágenes multiespectrales en varios formatos y resolución en los dominios espacial, espectral y temporal.

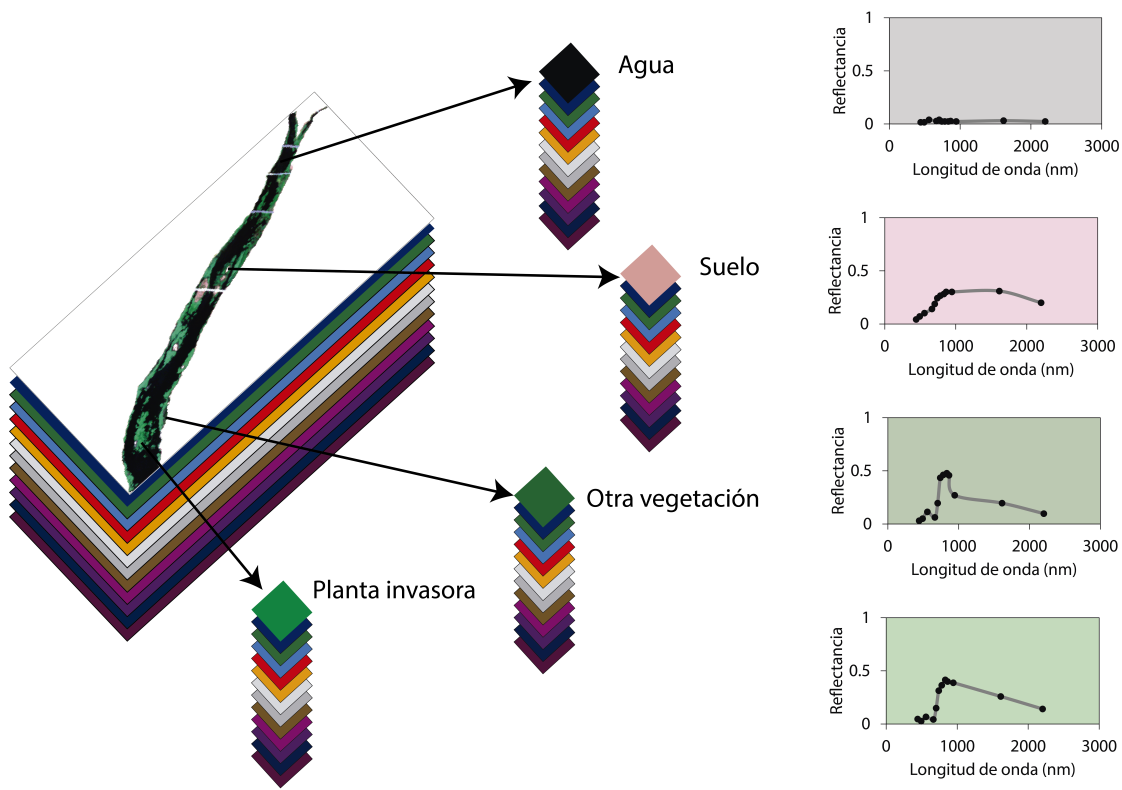


Figura 4.1: Algunos tipos de cobertura terrestre presentes en los píxeles de la imagen multiespectral de estudio y sus firmas espectrales.

Este tipo de imágenes obtenidas de forma remota pueden estar disponibles de manera gratuita o bajo petición. Como resultado, los datos teledetectados contienen una gran cantidad de información en los dominios espacial y espectral, y pueden representarse como cubos de datos, dado que comprenden datos en tres dimensiones [87]. En otras palabras, cada píxel de la imagen se compone de decenas o cientos de mediciones en diferentes longitudes de onda. Representando gráficamente dichos valores de reflectancia en función de la longitud de onda, se obtiene la firma espectral de cada píxel.¹

La Fig. 4.1 muestra el concepto de imagen multiespectral sobre una de las regiones de interés de esta Tesis Doctoral. Como se ilustra, distintos tipos de cobertura terrestre presentes en cada píxel de la imagen (agua, suelo, planta invasora u otra vegetación), tienen diferentes firmas espectrales.

¹Traducido y adaptado del artículo [2]

4.2 | Conjunto de datos multiespectrales considerados en esta Tesis Doctoral

Existen una gran variedad de instrumentos multiespectrales capaces de captar la radiancia o la reflectancia espectral de los distintos tipos de cobertura de la superficie terrestre a diferentes longitudes de onda. Para esta Tesis Doctoral, con el propósito de monitorizar la propagación de plantas acuáticas invasoras con el menor coste económico posible, se han elegido bases de datos de libre acceso. En este sentido, se han seleccionado conjuntos de datos obtenidos de forma remota proporcionados por el satélite Sentinel-2 de la ESA (por sus siglas en inglés *European Space Agency*). Se tratan de imágenes multiespectrales de resolución espacial media, adquiridas con tiempos de revisita frecuentes. También para la evaluación y consecución de las investigaciones englobadas en esta Tesis, ha sido necesaria la utilización de las imágenes multiespectrales obtenidas por los vuelos del Plan Nacional de Ortofotografía Aérea (PNOA). Además, se ha utilizado una imagen multiespectral adquirida por un dron para definir una estrategia de procesamiento eficiente necesaria para el desarrollo de las investigaciones realizadas en este trabajo. La Fig. 4.2 muestra una visión general de espectrómetros de imagen que captan la radiación solar reflejada por los materiales de la superficie terrestre implicados en esta Tesis Doctoral. Los tipos de datos mencionados previamente se describen a continuación.

4.2.1 | Imágenes multiespectrales Sentinel-2

La Agencia Espacial Europea (ESA) desarrolló, como parte del programa Copernicus, una familia de misiones de observación de la Tierra denominadas Sentinel. En este trabajo, dado su éxito en la clasificación de la cobertura terrestre [88], [89], se consideran las imágenes ópticas de media resolución proporcionadas por la misión Sentinel-2 (centrada en la vigilancia terrestre [90]). Sentinel-2 proporciona cobertura sobre todas las áreas terrestres excepto la Antártida, a través de dos satélites idénticos que están compuestos por un instrumento multiespectral, cuyas características técnicas permiten un tiempo de revisita de 5 días. Sentinel-2 ofrece dos tipos de productos: Nivel-1C (S2L1C) y Nivel-2A (S2L2A). Ambos están disponibles gratuitamente y se componen de mosaicos de $100 \times 100 \text{ km}^2$ que son ortoimágenes en proyección UTM/WGS84 (*Universal Transverse Mercator (UTM)/World Geodetic System 1984 (WGS84)*). S2L1C es un producto de reflectancia *Top-Of-Atmosphere (TOA)* y S2L2A un producto de reflectancia *Bottom-Of-Atmosphere (BOA)*. S2L2A es el resultado de aplicar técnicas de corrección atmosférica a las imágenes S2L1C (gracias a un algoritmo de procesamiento llamado Sen2Cor, desa-

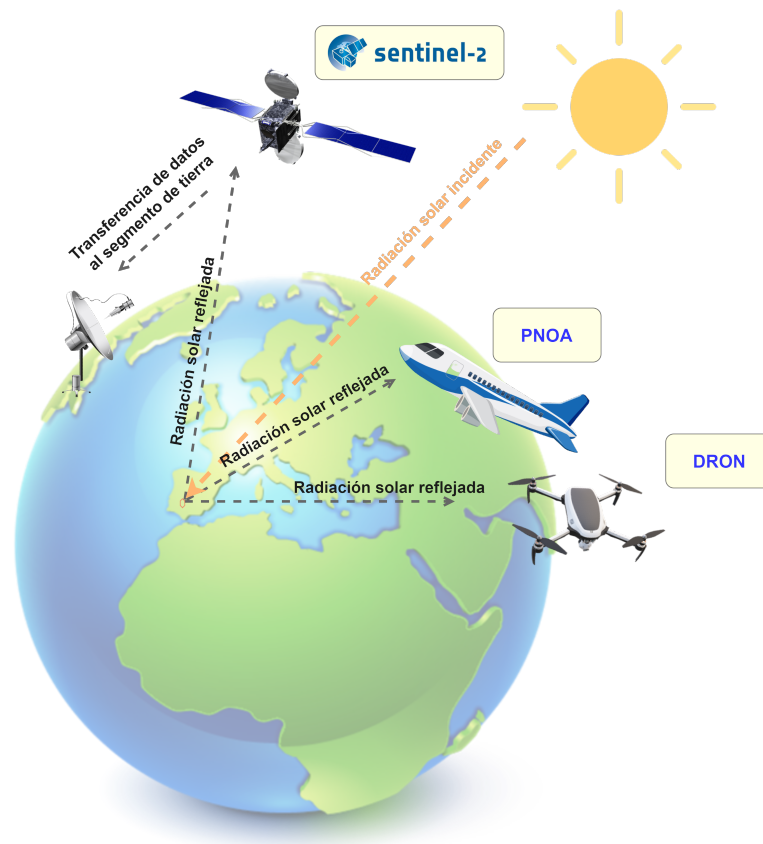


Figura 4.2: Esquema general de instrumentos de teledetección (los utilizados en esta Tesis) que captan la radiación solar reflejada por los materiales de la superficie terrestre, a lo largo de diferentes longitudes de onda del espectro electromagnético. Se han utilizado imágenes multispectrales adquiridas por el satélite Sentinel-2, en los vuelos del PNOA e imagen capturada por un dron.

rollado por la ESA). Como resultado, se corrige la reflexión y dispersión de la luz por la atmósfera antes de llegar al suelo. Cada imagen S2L1C se compone de 13 bandas espectrales, que contienen valores de reflectancia desde el visible y el infrarrojo cercano hasta el infrarrojo de onda corta, con resoluciones espaciales de 10 m, 20 m y 60 m por píxel (dependiendo de la longitud de onda). De este modo, 4 bandas espectrales tienen una resolución espacial de 10 m por píxel (incluyendo las bandas visibles RGB y una infrarrojo cercano (*Near-infrared spectroscopy (NIR)*)), 6 bandas tienen una resolución espacial de 20 m (incluyendo las tres bandas estrechas en el dominio espectral del borde rojo de la vegetación (*Visible and Near-Infrared (VNIR)*)), la del infrarrojo cercano y 2 bandas *Short-wave Infrared (SWIR)* y otras bandas centradas en la detección de nubes, corrección atmosférica y la detección de cirros, tienen una resolución espacial de 60 m. En el caso

del S2L2A, se excluye la banda B10 (utilizada para la detección de cirros) porque no contiene ninguna información en las capas bajas de la atmósfera (véase la Tabla 4.1).²

Tabla 4.1: Descripción de las bandas espectrales de Sentinel-2.

Nombre de la banda	B01	B02	B03	B04	B05	B06	B07	B08	B8A	B09	B10	B11	B12
Resolución (m)	60	10	10	10	20	20	20	10	20	60	60	20	20
Longitud de onda central (nanómetros)	442.7	492.4	559.8	664.6	704.1	740.5	782.8	832.8	864.7	945.1	1373.5	1613.7	2202.4
Aplicación	Aerosol costero	Azul	Verde	Rojo	Vegetación borde rojo ₁	Vegetación borde rojo ₂	Vegetación borde rojo ₃	NIR	Narrow NIR	Vapor de agua	Cirros	SWIR ₁	SWIR ₂

4.2.2 | Imágenes multiespectrales aéreas PNOA

Varios trabajos de investigación han considerado las ortofotografías aéreas digitales recogidas por el PNOA para tareas de fotointerpretación, debido a su alta resolución espacial [91], [92], [93]. Algunos proyectos gestionados por el Ministerio de Fomento (España) siguen la Directiva *Infrastructure for Spatial Information in Europe (INSPIRE)* [94], que establece una infraestructura de datos espaciales para datos geográficos en Europa con el fin de proporcionar coherencia geométrica y temporal de la cartografía y bases de datos geográficos. De este modo, la fotografía aérea constituye una base para la realización de información sobre urbanismo, ocupación del suelo, hidrografía, gestión forestal y cartografía para los territorios pertenecientes a la Comunidad Europea. En el marco del PNOA, es posible realizar vuelos fotogramétricos utilizando aviones equipados con una cámara digital de alta resolución, cuatro sensores multiespectrales y un sensor pancromático, recogiendo imágenes de alta resolución espacial (25 ó 50 cm) de todo el territorio español en un plazo de dos o tres años (dependiendo de la zona) [95]. Entre los productos ofrecidos, el PNOA proporciona gratuitamente imágenes multiespectrales con alta resolución espacial y tres bandas espectrales RGB en el sistema geodésico del Sistema de Referencia Terrestre Europeo (*European Terrestrial Reference System 1989 (ETRS89)*). Además, previa solicitud, pueden adquirirse fotogramas digitales de los vuelos de PNOA. Estas imágenes comprenden cuatro bandas: tres para la parte visible (RGB) del espectro y una para el infrarrojo cercano (NIR), todas georreferenciadas en el marco de referencia cartesiano geodésico ETRS89, con imágenes de alta resolución espacial (0,22 o 0,45 m).³

²Traducido y adaptado del artículo [2]

³Traducido y adaptado del artículo [2]

4.2.3 | Imágenes multispectrales UAV

A continuación se describen las especificaciones del vehículo aéreo no tripulado (UAV, comunmente conocido como dron) y del sensor instalado que recoge la imagen multi-espectral utilizada en un trabajo de investigación que forma parte de esta Tesis Doctoral. Los datos fueron adquiridos usando un dron senseFly eBee Plus que portaba una cámara senseFly S.O.D.A. Las características técnicas de senseFly eBee Plus UAV [96] incluyen una envergadura de 110 cm, un peso (incluida la cámara y la batería) de 1,1 kg, un alcance de enlace de radio de 3 km nominales (hasta 8 km) / 1,86 mi (hasta 4,97 mi), planificación automática de vuelo en 3D, velocidad de crucero de 40-110 km/h (11-30 m/s o 25-68 mph), resistencia al viento de hasta 45 km/h (12 m/s o 28 mph), tiempo máximo de vuelo de 59 minutos y alcance máximo de vuelo de 45 km (28 mi). Las características técnicas de la cámara senseFly S.O.D.A [97] incluyen un objetivo RGB de F/2,8-11, 10,6 mm (equivalente a 35 mm: 29 mm), resolución RGB de 5.472 x 3.648 píxeles (3:2), compensación de exposición de $\pm 2,0$ (incrementos de 1/3), obturador RGB es obturador global 1/30 - 1/2000s, diferentes modos de balance de blancos, rango ISO de 25-6400, soporte RTK/PPK y formatos de imagen en JPEG y DNG+JPEG. ⁴

4.3 | Composición de bandas espectrales e índices espectrales considerados en esta Tesis Doctoral

En esta Tesis Doctoral también se han utilizado imágenes raster cuyos pixeles muestran los valores de algunas combinaciones de bandas o índices espectrales, calculados a partir de las imágenes recogidas por el satélite Sentinel-2. Estas imágenes se han utilizado como datos de entrada en los modelos de redes neuronales convolucionales. A continuación se describen las combinaciones de bandas espectrales y los índices espectrales utilizados en este trabajo. También se especifican los nombres de las bandas de Sentinel-2 conforme a la tabla 4.1. ⁵

4.3.0.1 | RGB

Composición de tres bandas: rojo (B04), verde (B03) y azul (B02), también llamado combinación de bandas de color natural o verdadero. Permite mostrar las cubiertas terrestres en color real. Los valores van de 0 a 255 y se normalizan en este estudio a un rango de 0 a 1.

⁴Traducido y adaptado del artículo [1]

⁵Traducido y adaptado del artículo [4]

4.3.0.2 | NDVI

Un índice bien conocido [98] utilizado habitualmente para la cuantificación de la densidad de la vegetación verde. La Ec. 4.1 define este índice que se calcula considerando dos bandas: rojo (B04) y NIR (B08). Los valores se normalizan en un rango de -1 a 1.

$$NDVI = \frac{NIR - Red}{NIR + Red} \quad (4.1)$$

4.3.0.3 | FAI

Introducido en [99] para detectar vegetación en la superficie de los océanos. Es menos sensible a los efectos atmosféricos que el NDVI y el EVI. La Ec. (4.2) muestra la definición del índice para imágenes Sentinel-2, donde se consideran tres bandas: rojo (B04), NIR (B08), y SWIR₁ (B11). Sus valores están normalizados en un rango de 0 a 1.

$$FAI = (NIR - (Red + (SWIR_1 - Red) \times (\frac{\lambda_{NIR} - \lambda_{Red}}{\lambda_{SWIR_1} - \lambda_{Red}}))) \quad (4.2)$$

donde $\lambda_{NIR} = 832,8$, $\lambda_{Red} = 664,6$ y $\lambda_{SWIR_1} = 1613,7$

4.3.0.4 | NDWI

Combina dos bandas: verde (B03) y NIR (B08). Se propuso en [100] para determinar el estado hídrico de la vegetación. El índice se define en la Ec. (4.3) y sus valores se normalizan en un rango de -1 a 1:

$$NDWI = \frac{Green - NIR}{Green + NIR} \quad (4.3)$$

4.3.0.5 | Bare Soil Index (BSI)

Fue introducido en [101] para discriminar el suelo desnudo y las tierras en barbecho de la vegetación y otras clases de cobertura del suelo mediante la combinación de cuatro bandas: Las bandas SWIR₁ (B11) y roja (B04) (que determinan la composición mineral del suelo), mientras que las bandas NIR (B08) y azul (B02) determinan la presencia de vegetación. Sus valores se normalizan para que oscilen entre -1 y 1. Este índice se define del siguiente modo:

$$BSI = \frac{(SWIR_1 + Red) - (NIR + Blue)}{(SWIR_1 + Red) + (NIR + Blue)} \quad (4.4)$$

4.3.0.6 | NDII

Desarrollado por [102] como índice infrarrojo y posteriormente utilizado en [103] como NDII. Utiliza dos bandas espectrales: NIR (B08) y SWIR (B11). Este índice también puede verse como una versión normalizada de NDMI cuando se utilizan las bandas B08 (o B8A) y B11 de Sentinel-2 [104]. El NDII (o NDMI) proporciona información sobre los cambios en el contenido de agua de la vegetación. La estructura interna de la hoja y el contenido de materia seca de la hoja afectan a la reflectancia NIR, mientras que la banda SWIR da información sobre los cambios en el contenido de agua de la vegetación, así como sobre la estructura del mesófilo esponjoso en los doseles vegetales. Sus valores se escalan en un intervalo de -1 a 1. El índice se define del siguiente modo:

$$NDII = \frac{NIR - SWIR_1}{NIR + SWIR_1} \quad (4.5)$$

4.4 | Áreas de interés en las investigaciones de esta Tesis Doctoral

Las imágenes obtenidas de forma remota utilizadas en esta Tesis Doctoral muestran las regiones de interés (*Region Of Interest (ROI)*) de los experimentos desarrollados en las publicaciones. En las publicaciones [2], [3], [4], [5] y [6] las ROI de estudio son las que muestra la Fig. 4.3. Para la publicación [1] la zona de interés de la superficie dedicada a olivar se muestra en la Fig. 4.3.

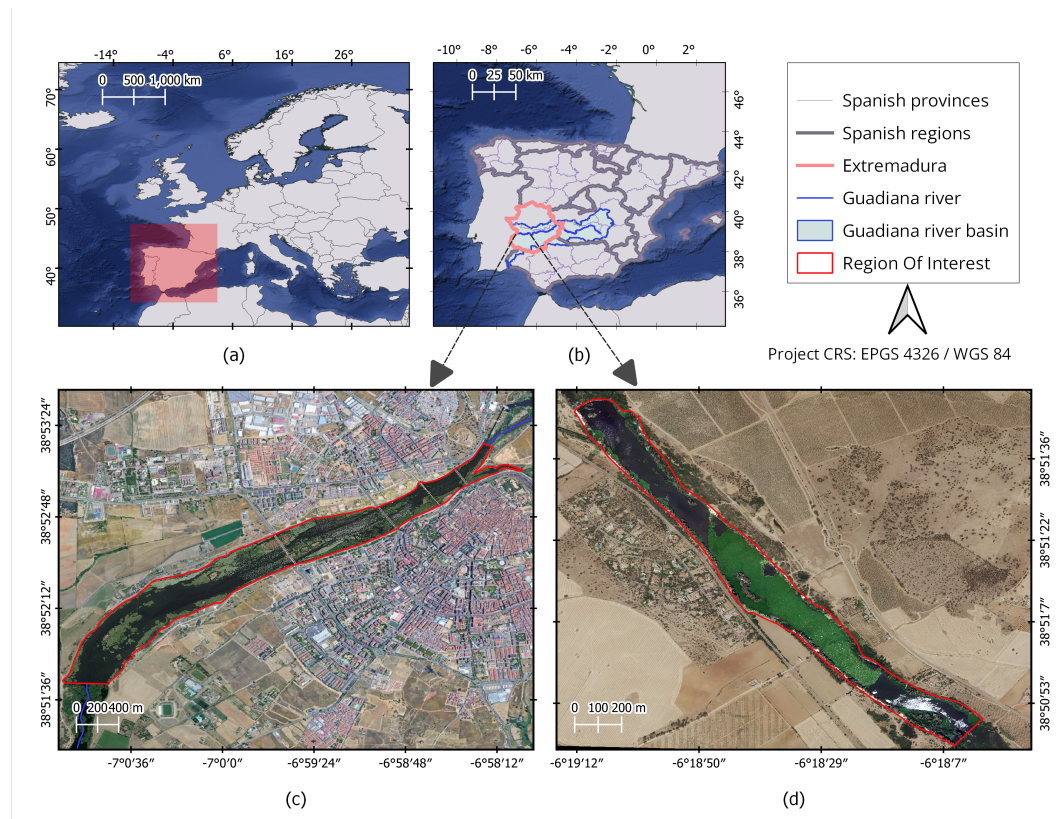


Figura 4.3: (a) Localización geográfica de España. (b) Localización geográfica de la región de Extremadura, el río Guadiana y la cuenca del Guadiana. (c) Zoom de una imagen de alta resolución que incluye una zona afectada por nenúfar mexicano en la ciudad de Badajoz. (d) Zoom de una imagen de alta resolución que incluye una zona afectada por el jacinto de agua, próxima a la ciudad de Mérida.

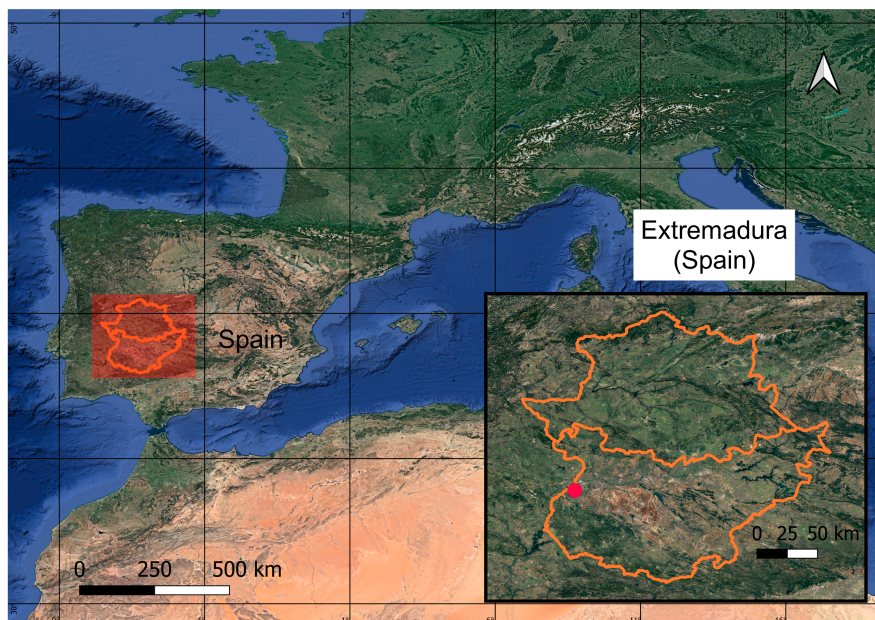


Figura 4.4: Localización de la superficie dedicada a olivar en Extremadura (España).

Aplicación de técnicas de sistemas de información geográfica

En este capítulo se contextualiza la explotación de las imágenes teledetectadas mediante los sistemas de información geográfica. Además se describe su uso en los experimentos de esta Tesis.

5.1 | Explotación de imágenes obtenidas de forma remota mediante sistemas de información geográfica

La teledetección y los SIG (o *Geographic Information System (GIS)*) son dos disciplinas en auge en las últimas décadas. Juntas proporcionan un marco de análisis ideal en muchas disciplinas [105]. La explotación de las técnicas de teledetección junto con los SIG exhibe el potencial de mejorar la comprensión de la superficie terrestre, gracias a la información detallada que proporcionan las imágenes obtenidas de forma remota, permitiendo en consecuencia un análisis preciso y una interpretación basada en SIG aplicable a diversos campos, como la planificación urbana [106], la biodiversidad [107], la gestión de catástrofes [108], la agricultura de precisión [108], la cartografía de la cubierta terrestre [109], la monitorización de vertidos de petróleo y otros eventos [110] o para la publicación de datos en geoportales [111], entre muchas otras aplicaciones. En particular, las técnicas de clasificación de imágenes permiten asignar etiquetas a cada uno de sus píxeles pudiendo, por ejemplo, distinguir las masas de agua de otras superficies impermeables (como entornos urbanos), incluidos el suelo y la vegetación. Esto permite abordar

problemas relacionados (por ejemplo) con el crecimiento excesivo de vegetación en el agua (el recurso más importante del planeta).

La tecnología SIG facilita la comprensión de la información contenida en los píxeles que componen las imágenes multiespectrales aprovechando la información disponible en el ámbito espacial. Las técnicas SIG también facilitan la edición y análisis de los cubos de datos multiespectrales, dado que permiten la disposición de diferentes capas de información georreferenciada para una mejor evaluación de los datos. De este modo, se pueden representar los datos creando mapas que muestren las observaciones espectrales de forma georreferenciada. En la Fig. 5.1 se muestra una representación de fragmentos de capas SIG utilizadas en esta Tesis. Como puede verse, se han empleado capas ráster (en las que cada píxel o celda es el elemento mínimo de la imagen) como las obtenidas de forma remota capturadas por el satélite Sentinel-2 o los vuelos del PNOA. También se han utilizado capas vectoriales de puntos, líneas o polígonos como por ejemplo, las correspondientes a los centroides de los píxeles de las capas ráster o a los polígonos ROI o la de polígonos de la imagen GT.

5.2 | Operaciones SIG desarrolladas en esta Tesis Doctoral

En esta Tesis Doctoral la mayoría de operaciones de preprocesado de imágenes se han realizado utilizando técnicas SIG, desarrolladas mediante el software QGIS [112] o mediante operaciones implementadas en código de programación Python. En términos generales, las técnicas SIG se han empleado para:

- Visualización de imágenes: para las imágenes obtenidas de forma remota como las adquiridas por plataformas aéreas (UAV y los vuelos del PNOA) o satelitales (como las recogidas por Sentinel-2). También para visualizar las imágenes resultantes de aplicar algoritmos de clasificación sobre las imágenes anteriores.
- Tratamiento de valores NoData: para consultar valores de píxeles, analizar histogramas, firmas espectrales, etc.
- Recogida de muestras de entrenamiento: se ha realizado mediante el dibujo de vectores (polígonos) sobre las imágenes que posteriormente se iban a procesar con algoritmos de clasificación. En el caso de la recogida de muestras de entrenamiento de las imágenes de Sentinel-2, se utilizó como capa de referencia la imagen de alta resolución PNOA.

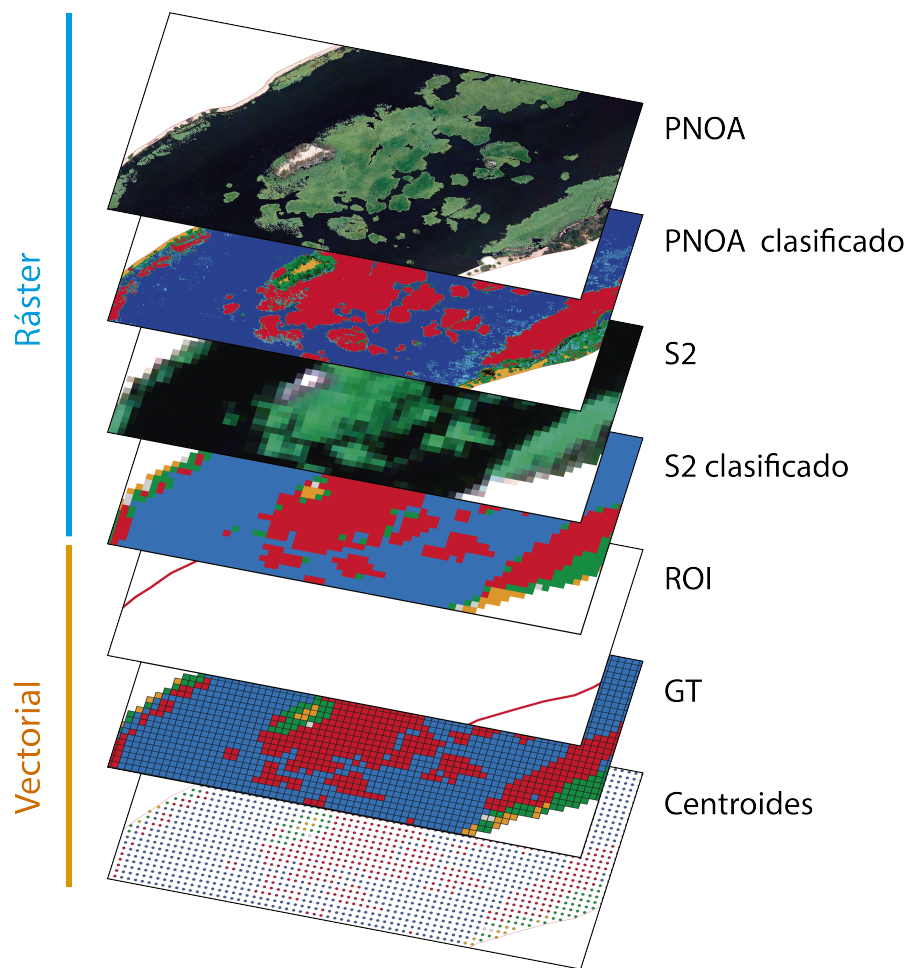


Figura 5.1: Concepto de capas SIG. Como ejemplo, se muestran fragmentos de algunas capas usadas y generadas en SIG en esta Tesis Doctoral.

- Diseño de mapas y composiciones de impresión. Para una mejor comprensión de los resultados relativos a la detección de diferentes tipos de cobertura terrestre, en los experimentos llevados a cabo en las publicaciones científicas, se han representado gráficamente mediante herramientas SIG.
- Operaciones con herramientas SIG también se han empleado para la transformación de datos raster a vectorial en la estrategia propuesta en el artículo [5]) para el mapeado de las áreas de acumulación de plantas acuáticas invasoras en una serie temporal analizada.
- Pre y post-procesado de datos: todas las operaciones anteriores se realizaron directamente sobre QGIS. Otras operaciones SIG se han llevado a cabo sobre los datos multiespectrales implementándolas mediante código de programación Python pa-

ra automatizar los procesos. Utilizando librerías como *Geospatial Data Abstraction Library (GDAL)* [113] y *Rasterio* [114] se han procesado datos geospaciales ráster y vectoriales para, por ejemplo, generar capas vectoriales de puntos contenedores de la información asociada a cada pixel. Del mismo modo, se han desarrollado técnicas SIG para la generación de capas raster que contienen las muestras de entrenamiento de los algoritmos de clasificación supervisados. Para ello, las imágenes multiespectrales se han recortado con polígonos trazados en capas vectoriales, extrayendo la información perteneciente a las muestras de entrenamiento.

- La generación de las imágenes sintéticas verdad-terreno (descrita en [2]) también se realizó mediante un script en Python para automatizar todos los procesos SIG necesarios (geolocalización de cultivos o plantas acuáticas invasoras, generación de centroides, cálculos de datos vectoriales, etc.).

1

¹Adaptado de la contribución [2]

Aplicación de inteligencia artificial para la detección automática de plantas acuáticas invasoras

En esta Tesis Doctoral se llevan a cabo técnicas englobadas en el campo de la inteligencia artificial, como el aprendizaje automático y aprendizaje profundo, para analizar y aprender de la información contenida en las imágenes multiespectrales. Para tal fin, se emplean algoritmos de clasificación para asignar etiquetas a sus píxeles y así detectar los píxeles que contienen diferentes tipos (o clases) de cobertura terrestre como: tipos de suelo, agua, materiales construidos por el hombre, vegetación, entre los que se encontrarán plantas exóticas invasoras. Estos métodos pueden analizar tanto la información espectral como la espacial o las características espectrales-espaciales que son propias de cada clase. En este capítulo se contextualizan las técnicas de aprendizaje automático y aprendizaje profundo para clasificar los píxeles de las imágenes obtenidas de forma remota empleadas en las contribuciones de esta Tesis Doctoral.

6.1 | Clasificación de datos multiespectrales

Dada una imagen multiespectral definida por $X \in \mathbb{R}^{H \times W \times B}$, H y W denotan la altura y la anchura del cubo de datos, respectivamente y B es el número de bandas espectrales. Por lo tanto, dicho cubo de datos multiespectrales estará formado por $H \times W$ número de píxeles que contendrán la información de la reflectancia medida en cada longitud de onda de cada banda espectral. El objetivo de la aplicación de los métodos de clasificación de datos multiespectrales es encontrar una función de mapeo $\mathcal{M}_\theta : X \rightarrow Y$ que asigna a cada píxel x_i una etiqueta correspondiente y_i produciendo un mapa de clasificación $Y \in \mathbb{R}^{H \times W}$. Debido a sus propiedades físico-químicas, cada tipo de material presen-

te en la imagen absorbe y refleja la radiación solar a longitudes de ondas específicas, permitiendo obtener firmas espectrales únicas.

En esta Tesis se procesan las imágenes multiespectrales con métodos de clasificación para detectar los píxeles que contienen las plantas exóticas invasoras, de forma automática. Por lo que sabemos, aún no se han explorado a fondo los métodos de AI para tal fin. En este sentido, los algoritmos de aprendizaje automático (ML, de sus siglas en inglés *Machine Learning*) y los algoritmos de aprendizaje profundo (DL, de sus siglas en inglés *Deep Learning*) construyen un modelo basado en el aprendizaje para realizar predicciones.

En los enfoques supervisados, se recogen muestras de entrenamiento y se dispone de etiquetas para algunos píxeles (por ejemplo, mediante un proceso de anotación basado en humanos). Por el contrario, los enfoques no supervisados agrupan píxeles similares descubriendo patrones de similitud. Por último, los métodos semisupervisados combinan datos etiquetados y no etiquetados durante el proceso de entrenamiento.

Los recientes avances en algoritmos de ML/DL, en computación de alto rendimiento y en accesibilidad de *big data* han llevado a la adopción de redes neuronales artificiales (*Artificial Neural Networks (ANN)*) para tareas de clasificación [115]. DL, que puede considerarse un subcampo de ML [116], se caracteriza por tener arquitecturas más complejas, profundas y explota muchas capas de ANN que son pilas de funciones capaces de extraer características a diferentes niveles [117]. Su estructura presenta grandes ventajas sobre los algoritmos tradicionales de ML. En concreto, los modelos DL pueden adaptarse a tareas de clasificación supervisadas y no supervisadas; su procedimiento de aprendizaje permite extraer características lineales y no lineales, y presentan una gran flexibilidad en sus arquitecturas gracias a su diversidad tanto en términos de los tipos de capas que pueden disponerse, como de su número (profundidad) [118].¹

En las siguientes secciones se revisan brevemente algunos algoritmos de AI empleados en las contribuciones de esta Tesis Doctoral.

6.2 | Algoritmos de clasificación de aprendizaje automático

A continuación, se describen los algoritmos utilizados de ML centrados en extraer patrones o relaciones internas de los datos para aprender de ellos y realizar predicciones.

¹Adaptado del artículo [2]

Se han implementado, utilizando la biblioteca *scikit-learn* [119], los algoritmos: *K-Means*, *K-Nearest Neighbour*, *Support Vector Machine* y *Multi-Layer Perceptron*.

6.2.1 | k-Means

K-Means es un método no supervisado muy popular entre las técnicas de agrupación o *clustering*, en el que los datos se agrupan en clústeres de tal forma que las muestras del mismo grupo (o clúster) son más similares entre sí que las de otros grupos. El objetivo de este algoritmo es elegir centroides dentro de un criterio de suma de cuadrados de cluster dado por la Ec. (6.1):

$$\sum_{i=1}^n \min_{j \in C} \|x_i - \mu_j\|^2 \quad (6.1)$$

donde n es el número de grupos de igual varianza en los que se separan las muestras, x_i son las muestras (divididas en k clusters disjuntos C descritos por la media μ_j). El funcionamiento de este algoritmo puede describirse en varios pasos. En el primer paso, se establece el parámetro k (correspondiente al número de conglomerados que deben identificarse en los datos). A continuación, se eligen los centroides de los conglomerados y cada muestra se asigna a su centroide más cercano. En una segunda etapa, se crean nuevos centroides tomando el valor medio de todas las muestras asignadas a cada centroide anterior. Se calcula la diferencia entre los nuevos centroides y los anteriores, y este proceso se repite hasta que no haya más cambios en la ubicación de los centroides.²

6.2.2 | Random forest

Random Forest (RF) es un método de aprendizaje por conjuntos introducido por primera vez en [120]. En concreto, este método clasifica píxeles creando una multitud de árboles de decisión aleatorios (clasificadores supervisados y no paramétricos), donde la predicción final es una media de los probabilísticos de cada árbol de decisión. Mediante la estrategia de *bagging*, combina múltiples modelos independientes, construyendo los árboles de arriba a abajo basándose en el concepto "*divide y vencerás*"[121], consiguiendo compensaciones de errores. En primer lugar, para realizar la clasificación (supervisada), se define un conjunto de entrenamiento. RF funciona mediante el procedimiento de *bagging* en el que las muestras de entrenamiento se seleccionan aleatoriamente del conjunto de entrenamiento original. Como resultado, algunas muestras pueden no utilizarse y otras pueden elegirse más de una vez. A continuación, cada árbol de decisión se construye con diferentes conjuntos de entrenamiento utilizando un conjunto de datos

²Adaptado del artículo [2]

"*bootstrapped*". Esta técnica mejora la generalización del proceso de aprendizaje al evitar la tendencia al sobreajuste de los árboles de decisión. Resulta ventajosa para reducir la varianza del modelo sin aumentar el sesgo. Otros métodos basados en "*boosting*" son más sensibles al sobreentrenamiento y al ruido [122].³

6.2.3 | Support Vector Machine

El método *Support Vector Machine (SVM)* fue desarrollado en [123] y ha sido ampliamente utilizado para problemas de clasificación y regresión de imágenes hiperespectrales y multispectrales. Se utiliza un kernel para resolver problemas lineales y no lineales proyectando los vectores de píxeles en un espacio de mayor dimensión [124]. En concreto, SVM encuentra el hiperplano óptimo que separa dos clases, maximizando la distancia entre el hiperplano de separación y la muestra de entrenamiento más cercana. Los vectores soporte son estas muestras de entrenamiento más cercanas al hiperplano. Este hiperplano tiene diferentes formulaciones matemáticas dependiendo de cómo se separen los datos. Por ello, se utilizan diferentes funciones kernel (lineal, polinómica, función de base radial (*Radial Basis Function (RBF)*), sigmoidea, entre otras) [125].

El método SVM es capaz de realizar una clasificación binaria y multiclase. Además, SVM puede manejar la clasificación de datos de alta dimensión con un número limitado de muestras de entrenamiento debido al hecho de que sólo las muestras que están más cerca de los límites de clase son realmente necesarias para localizar el hiperplano de separación óptimo [126].⁴

6.2.4 | K-Nearest Neighbors

El algoritmo *K-Nearest Neighbors (KNN)* fue propuesto en [127] para asignar a cada muestra sin clasificar la etiqueta de la más cercana de un conjunto de muestras previamente clasificadas. A pesar de considerarse un método relativamente sencillo, se ha aplicado en numerosos problemas de clasificación y regresión. Además, es un método no paramétrico que puede obtener resultados satisfactorios en problemas en los que los límites de decisión son irregulares.

La clasificación de cada muestra de consulta se calcula por mayoría simple de votos de los vecinos más próximos. En otras palabras, a una muestra desconocida se le asigna la etiqueta que tiene más representantes entre los vecinos más próximos de la muestra.

³Adaptado del artículo [2]

⁴Adaptado del artículo [1]

Cada muestra desconocida se compara con los datos de entrenamiento originales y no se entrena para producir un modelo, a diferencia de otros clasificadores [128].

El clasificador KNN predice la etiqueta de una muestra a través de una constante k (valor entero) que es definida por el usuario y representa el número de muestras de entrenamiento que más se aproximan a ella. Hay que tener en cuenta que la elección de k depende de los datos [129], debido a que se puede producir un límite de decisión complejo para valores muy bajos de k , mientras que valores muy grandes de k reducen el ruido pero introducen una mayor generalización.⁵

6.2.5 | Multilayer Perceptron

Multilayer Perceptron (MLP) es un algoritmo supervisado que se ha utilizado ampliamente en problemas de clasificación y regresión. El funcionamiento de este tipo de ANN se asemeja al del cerebro biológico, ya que trasladan la información desde los nodos (o neuronas) de la capa de entrada hasta las neuronas de la capa de salida, utilizando una o varias capas ocultas, formando una red interconectada. El clasificador MLP utiliza para entrenar esta red el mecanismo de propagación hacia delante (*feedforward*), mediante el que se propaga la instancia de entrenamiento desde la capa de entrada a la capa de salida. En cada capa, cada neurona calcula las salidas mediante la operación descrita en la Ec. (6.2):

$$y = f \left(\sum_{i=1}^n w_i x_i + b \right) \quad (6.2)$$

donde:

y es el valor de salida de la neurona,

f es la función de activación,

w_i son los pesos de la neurona,

x_i son los valores de entrada (que a su vez son los valores de salida de la neurona de la capa previa, y

b es el sesgo (o *bias*).

Para introducir la no linealidad en la red, a la salida de la neurona, se aplica la función de activación f . Algunos ejemplos de función de activación son la función sigmoide, la función tangente hiperbólica o la función Unidad Lineal Rectificada (*Rectified Linear Unit (ReLU)*). A continuación, se compara la salida predicha por la red con la

⁵Adaptado del artículo [1]

muestra de entrenamiento y se calcula el error. Entra en juego el algoritmo de retropropagación (*backpropagation*) introducido en [130] para calcular el descenso del gradiente, mediante el que se propaga el error hacia atrás en la red, desde la capa de salida a la de entrada. El error de cada neurona se calcula en cada capa oculta, teniendo en cuenta lo que contribuye esa neurona al error. De esta forma, se multiplica el error de cada neurona por los pesos correspondientes. El error anterior retropropagado se utiliza para el ajuste de pesos de las conexiones, en sentido contrario a la propagación del error. Por otro lado, para mejorar las predicciones, se hace uso de una función objetivo (o función de pérdida o de costo), como error cuadrático medio (*mean squared error*), entropía cruzada (*Cross-Entropy*), entre otros, con el que se actualizan los pesos, minimizando la función de costo. Este ajuste, mediante un proceso iterativo para varias instancias de entrenamiento, facilita el aprendizaje de la ANN, adaptándose a los patrones presentes en los datos de entrenamiento, mejorando gradualmente la precisión en la predicción. Estos pasos se repetirían para múltiples iteraciones completas (o *epochs*) hasta alcanzar un criterio de convergencia.

Entre las principales ventajas de este clasificador se encuentra la falta de conocimiento previo de la distribución estadística de los datos de entrada [131]. Sin embargo, entre sus inconvenientes se encuentra la necesidad de ajustar varios hiperparámetros como el número de capas, neuronas ocultas e iteraciones [132].⁶

MLP aprende una función $f(\cdot) : R^m \rightarrow R^o$ entrenando al clasificador en un conjunto de datos donde m es la dimensionalidad de la entrada y o es el número de dimensiones de la salida. El conjunto de características (píxeles de la imagen) está representado por $X = x_1, x_2, x_3, \dots, x_m$ y la etiqueta de clase viene dada por y . La capa de entrada tiene un número de neuronas igual a m que representa las características de entrada. Cada neurona (excepto las de la capa de entrada) utiliza una función de aprendizaje no lineal $g(\cdot) : R \rightarrow R$ que conecta cada nodo con la capa siguiente, transformando su valor a través de pesos mediante un sumatorio lineal $w_1x_1 + w_2x_2 + w_3x_3 + \dots + w_mx_m$. Finalmente, los valores de salida (etiquetas de clase) se obtienen transformando los valores procedentes de la última capa oculta a la capa de salida. En la etapa de entrenamiento, MLP utiliza la retropropagación para calcular el descenso del gradiente. Comienza con pesos aleatorios y minimiza la función de pérdida actualizando repetidamente estos pesos. Comparando el resultado de la clase esperada con la salida, se obtiene un error que se utiliza para cambiar los pesos de conexión para cada entrada que se ha procesado.

⁶Adaptado del artículo [1]

6.3 | Algoritmos de Aprendizaje profundo

En esta sección se introducen los fundamentos clave de aprendizaje profundo en el contexto de los trabajos que se presentan. Se comienza con una breve introducción de las CNN. A continuación, se describen los nuevos modelos CNN desarrollados y aplicados en las publicaciones de esta Tesis. Para este fin, se han implementado modelos CNN en código de programación Python, utilizando los entornos de trabajo TensorFlow y Keras [133].

6.3.1 | Redes neuronales convolucionales

Las CNN son un tipo de modelos no lineales categorizados dentro de las redes profundas supervisadas. Como las ANN, su estructura está inspirada en el comportamiento de las neuronas en neurociencia visual. Las CNN se componen de un conjunto de bloques con unidades (o neuronas) capaces de transformar el volumen de datos de entrada en un volumen de salida de unidades (o neuronas). El volumen de neuronas de salida de los bloques anteriores será el bloque de entrada al bloque siguiente [134].

En términos generales, como cualquier ANN *feedforward*, la arquitectura de la CNN consta de una capa de entrada, capas ocultas y capa de salida. Las capas ocultas pueden ser de varios tipos, por ejemplo: las capas convolucionales compuestas por un conjunto de filtros (componente principal de las CNN), en las que se le aplica una función de activación no lineal; capas de agrupación (*pooling*), en las primeras etapas para reducir dimensionalidad de las características extraídas, y capas totalmente conectadas (*fully connected layer*), en las últimas etapas [118]. Por lo tanto, las capas ocultas se dividen en dos partes: la primera es el extractor de características y la segunda suele ser un MLP (cuyo funcionamiento está descrito en la sección 6.2.5), que asigna las etiquetas de clase finales. En otras palabras, este diseño consta de capas lineales y no lineales en las que las capas externas de una CNN extraen características básicas, mientras que el aprendizaje más complejo se produce jerárquicamente en las capas internas. Con respecto al MLP, las neuronas de una capa en una CNN no tienen por qué estar totalmente conectadas a todas las neuronas de la anterior pudiendo conectarse a una pequeña región del volumen de entrada anterior. Esta particularidad permite que los bloques de neuronas de una CNN funcionen como núcleos, operando sobre una pequeña región de la capa anterior. La retirada de las capas totalmente conectadas puede ser beneficiosa en términos de reducción de la complejidad y mejora de la explotación de la información espacial de los datos.

Las CNN se han aplicado con éxito a la clasificación de imágenes obtenidas de forma

remota. Su estructura multicapa puede explotar las ventajas del reparto natural de los pesos de las señales, con la agrupación de capas y las conexiones locales. La forma en que los datos de entrada se presentan a la red (en forma de múltiples matrices) la hace adecuada para procesar tanto imágenes multiespectrales como hiperespectrales [135].⁷

6.3.2 | Modelos de CNN propuestos

Para aplicar algoritmos de clasificación a las imágenes obtenidas de forma remota, se pueden implementar diferentes modelos de CNN. Estos modelos pueden considerar diferentes datos de entrada (por ejemplo información espectral, espacial y espectral-espacial [136]). En esta Tesis se han propuesto nuevos modelos CNN. En primer lugar, se ha propuesto un nuevo modelo CNN1D cuyos datos de entrada contienen la información espectral de cada pixel. También se ha propuesto un nuevo modelo CNN2D que explota la informa espacial-espectral, dado que tienen en cuenta la información del dominio espectral de cada pixel de la imagen, así como la de los píxeles vecinos.

6.3.2.1 | Arquitectura de CNN que explota la información espectral

La Arquitectura de la CNN con capa convolucional de una dimensión (CNN1D) propuesta en nuestro trabajo [2] y desarrollada en esta Tesis en [3; 4; 5; 6], está compuesta por las siguientes capas:

1. **Capa de entrada (o *input*):** acepta un tensor tridimensional formado por toda la información contenida en un sólo pixel.
2. **Capa convolucional 1D:** toma la información espectral de cada pixel y aplica 20 filtros (o *kernels*) de tamaño de kernel 12 (el número de bandas). Cada filtro se aplica multiplicando los valores de entrada correspondientes por los pesos del kernel. Después, la salida se obtiene tras sumar los productos ponderados. Cada filtro actúa como detector de características, buscando patrones en la información de entrada. Tras la operación de convolución, se aplica la función de activación ReLU (*Rectified Linear Unit*), que establece los valores negativos a cero y mantiene los valores positivos), mediante la que se introduce la no linealidad en la red.
3. **Capa (*flatten*):** reorganiza los datos que salen de la capa convolucional en un vector unidimensional.

⁷Adaptado del artículo [2]

4. **Capa completamente conectada (*dense*) con 128 neuronas:** funciona como una red neuronal tradicional en la que cada neurona está conectada con las neuronas de la capa anterior. Se encargan de combinar las características que han aprendido en las capas anteriores.
5. **Capa de normalización por lotes (*batch normalization*):** esta capa hace que los datos tengan una media cercana a cero y una desviación estándar cercana a uno. Estabiliza las activaciones dentro de cada lote, mejorando la estabilidad de entrenamiento y capacidad de generalización del modelo.
6. **Capa de activación ReLU:** introduce la no linealidad en la red neuronal, permitiendo que la red aprenda representaciones más complejas.
7. **Capa completamente conectada (*dense*):** está formada por igual número de neuronas que el número de clases que se van a detectar en la imagen. Se le aplica la función de activación *Softmax* para obtener las probabilidades de cada clase (probabilidad de ser una clase).
8. **Salida (*output*):** muestra los datos de predicción obtenidos con la CNN1D, los píxeles con mayor probabilidad de ser planta invasora.

La Fig. 6.1 muestra la arquitectura de CNN1D desarrollada para las contribuciones de esta Tesis Doctoral.

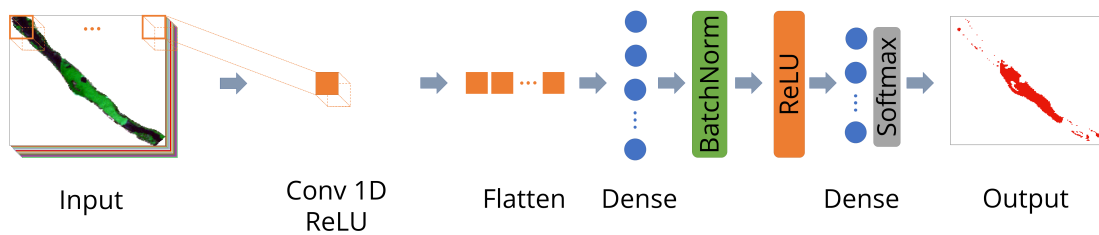


Figura 6.1: Arquitectura de la red neuronal convolucional de una dimensión (CNN1D) desarrollada. Los bloques tridimensionales dibujados sobre la imagen multiespectral representan los píxeles de la imagen. Los datos de entrada de este modelo se corresponden con la información espectral de cada pixel.

6.3.2.2 | Arquitecturas de la CNN que explotan la información espacio-espectral

En este caso, para la predicción de la clase a la que pertenece un pixel, la CNN tiene en cuenta su firma espectral y la de los píxeles vecinos. Para este fin, utilizando los entornos de trabajo TensorFlow y Keras se pueden implementar modelos CNN cuyas

arquitecturas incluyen capas convolucionales 2D (en los modelos CNN2D) o capas convolucionales 3D (en los modelos CNN3D). En el primer caso, en el modelo CNN2D, los datos de entrada a la capa convolucional pueden ser (ancho x alto x n° de bandas) de la imagen multiespectral y la capa crea un kernel de convolución espacial a lo largo de todas las bandas espectrales. Para el caso del modelo CNN3D, su capa convolucional 3D crea un kernel de convolución espacial sobre los datos de entrada que pueden tener las dimensiones (ancho x alto x n° imágenes x n° de bandas).

En nuestro trabajo [6] se tienen en cuenta estas dos tipos de CNN. En el preprocesado, a parte de las operaciones comunes al modelo anterior (extracción de ROI y gestión de los valores NoData), se realizan operaciones necesarias para preparar pequeñas regiones tridimensionales de información, que constituirán los datos de entrada del modelo CNN. Dichas operaciones se describen a continuación:

1. **Reflejo de la imagen a partir de los bordes (*reflect padding*):** *Padding* es el proceso de añadir información a la matriz (o cubo de datos) de la imagen de satélite multiespectral, antes de actuar las convoluciones. Refleja los propios datos de entrada alrededor del borde. La principal razón de este proceso es preservar las dimensiones espaciales del volumen de datos para que las dimensiones espaciales de salida sean las mismas que las de los datos de entrada. En otras palabras, en este caso se utiliza para que se tengan en cuenta en el proceso de clasificación de la imagen y también se haga la predicción de los píxeles de los bordes.
2. **Extracción de *patches*:** La imagen multiespectral se ha dividido en regiones tridimensionales cuadradas o *patches*. Por lo tanto, los *patches* de píxeles constituyen la capa de entrada (*input*) en el modelo CNN2D. De este modo, la información contenida en un píxel de la imagen y la información contenida en sus píxeles vecinos, se tiene en cuenta en el aprendizaje de características y en la predicción. Tras realizar varios experimentos probando diferentes tamaño de ventana (desde ventanas de 3 x 3 píxeles hasta tamaños de ventana de 9 x 9 píxeles), finalmente, se ha seleccionado un tamaño de ventana de 4 x 4 píxeles, para considerar la arquitectura CNN con el mejor rendimiento. Así, los parches constituyen regiones con 4 x 4 x 12 (dimensión espacial x número de bandas espectrales).

En la Fig. 6.2 se muestra la arquitectura del modelo CNN2D que ha obtenido mejores resultados en nuestros experimentos para la detección de plantas acuáticas invasoras. A continuación se describen dichas capas:⁸

⁸Adaptado del artículo [6]

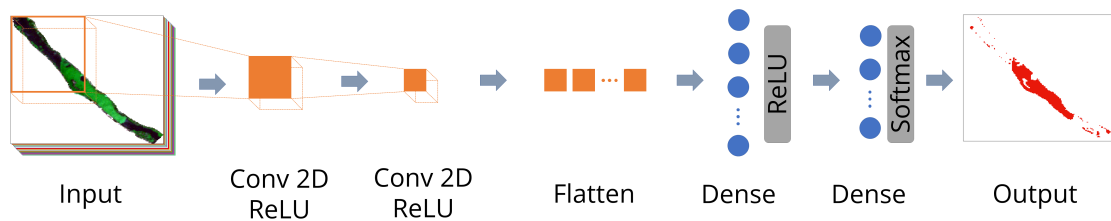


Figura 6.2: Arquitectura de la red neuronal convolucional de dos dimensiones (CNN2D) desarrollada. Los datos de entrada del modelo corresponden con la información espacial y espectral de cada bloque de píxeles (o *patch*).

1. **Capa de entrada (*input*):** consisten en los *patches* descritos anteriormente de dimensiones $4 \times 4 \times 12$ (ancho \times alto \times canales espectrales) que permiten explotar la información espectral y la espacial en la extracción de características del modelo CNN2D.
2. **Capa convolucional 2D:** aplica 32 filtros de convolución (de tamaño de ventana 3×3) sobre los *inputs*. Estos filtros se deslizan a lo largo de la imagen y realizan las operaciones de convolución. En esta operación se multiplican los elementos del filtro con los elementos correspondientes de la región local de la imagen de entrada y se suman los productos resultantes. Esta operación se repite para cada posición del filtro mientras se desliza por toda la imagen. Se van generando mapas de características según se aplican los filtros, captando patrones o características específicas de la imagen. Esta capa incluye la función de activación ReLU
3. **Capa de convolución 2D:** aplica 64 filtros de tamaño de ventana 2×2 e incluye la función de activación ReLU.
4. **Capa (*flatten*):** reorganiza los vectores tridimensionales que salen de las capas convolucionales 2D a un vector unidimensional.
5. **Capa completamente conectada (*dense*):** con 64 neuronas y función de activación ReLU.
6. **Capa completamente conectada (*dense*):** con 4 neuronas (número de clases con las que se ha clasificado la imagen multiespectral) y función *Softmax* (para obtener las probabilidades de pertenecer a una clase).
7. **Salida (*output*):** en la imagen mostramos los datos de predicción obtenidos con la CNN2D, seleccionando los píxeles con mayor probabilidad de ser planta invasora.

6.3.2.3 | Conjunto de entrenamiento para los modelos de CNN

Los modelos CNN, cuyas arquitecturas se han descrito, han sido entrenados con muestras de entrenamiento que han sido cuidadosamente seleccionadas por fotointerpretación de otras imágenes de alta resolución (PNOA) y extraídas de las imágenes de satélite multiespectrales (Sentinel-2), mediante técnicas SIG.

En el caso de los modelos que tienen en cuenta la información espacial-espectral de cada pixel, a partir de las muestras de entrenamiento seleccionadas, se ha creado un conjunto de datos más grande mediante una estrategia llamada *aumentación de datos* (*data augmentation*). Esta técnica, implementada utilizando la biblioteca Keras, ha permitido transformar las muestras de entrenamiento, girándolas o volteándolas aleatoriamente a lo largo del eje horizontal o vertical. De este modo, se consigue que el modelo sea más robusto a variaciones en los datos de entrada, ayudando a prevenir el sobreajuste (u *overfitting*), mejorando el rendimiento del modelo. Además, de cada muestra de entrenamiento, se extrae un *patch* con el tamaño de ventana con la que se ha configurado el modelo CNN.

6.4 | Métricas de evaluación de algoritmos

Para evaluar la eficacia de las distintas técnicas aplicadas a la detección de plantas acuáticas invasoras, suponemos que la diferencia entre los resultados y los datos reales se debe a errores de clasificación. Para ello, en las publicaciones se han mostrado matrices de confusión. En esta matriz, se muestran los verdaderos positivos (*True Positive (TP)*), los verdaderos negativos (*True Negative (TN)*), los falsos positivos (*False Positive (FP)*) y los falsos negativos (*False Negative (FN)*). Los valores reales están en filas que representan los valores en la imagen sintética de la verdad sobre el terreno. Las columnas de esta matriz contienen los valores predichos de cada clasificador. Como este estudio se centra en la detección de plantas acuáticas invasoras, la matriz de confusión es binaria (es decir, indica si se detectan o no las plantas invasoras).

Las métricas implementadas para evaluar la calidad de las predicciones de los algoritmos considerados son la precisión global o *overall accuracy* [Ec. (6.3)], la exactitud del usuario o *user's accuracy* [Ec. (6.4)], la exactitud del productor o *producer's accuracy* [Ec. (6.5)] (también conocidas como *recall*, sensibilidad o tasa de verdaderos positivos) y la puntuación F_1 o F_1 score [Ec. (6.6)]. Sus ecuaciones se describen a continuación:⁹

⁹Adaptado del artículo [2]

$$\text{Overall accuracy} = \frac{TP + TN}{TP + TN + FP + FN} \quad (6.3)$$

$$\text{User's accuracy} = \frac{TP}{TP + FP} \quad (6.4)$$

$$\text{Producer's accuracy} = \frac{TP}{TP + FN} \quad (6.5)$$

$$F_1 \text{ score} = \frac{2 * TP}{2 * TP + FP + FN} \quad (6.6)$$

Contribuciones de esta Tesis Doctoral

En este capítulo, en primer lugar, se realiza un resumen global y discusión de resultados. Además, se resumen los artículos que forman parte del compendio de publicaciones. También se muestran los principales resultados así como las contribuciones aportadas en los trabajos resultantes de esta Tesis.

7.1 | Resumen global de resultados y discusión

A continuación, se resumen y discuten globalmente las contribuciones de esta Tesis Doctoral orientadas, principalmente, al desarrollo de nuevos métodos y algoritmos que permiten la detección de plantas acuáticas invasoras en imágenes que se han obtenido de forma remota. Los resultados de esta Tesis demuestran que las técnicas de teledetección, SIG y algoritmos de inteligencia artificial facilitan las estrategias de gestión de este problema presente en varias partes de la geografía mundial y en concreto en el río Guadiana, a su paso por Extremadura.

La metodología propuesta en [1] hace viable el procesamiento de imágenes multiespectrales de alta resolución que requieren gran cantidad de memoria RAM para aplicar algoritmos de clasificación (en nuestro caso para clasificar distintos tipos de cubierta terrestre). Consiste en una estrategia de particionamiento espacial de imágenes teledetectadas en un paso previo a la predicción del conjunto de datos, por parte de un algoritmo de inteligencia artificial que va a clasificar cada pixel de la imagen. En concreto, se describe la división espacial del cubo de datos de una imagen multiespectral, adquirida por un dron que ha volado sobre una superficie dedicada al cultivo de olivar, recogiendo información de la radiación solar reflejada en los canales espectrales RGB, con una resolución de 3 cm por pixel. En este trabajo se evalúan los resultados de clasificación de los tipos de cobertura de suelo mediante diferentes algoritmos de clasificación su-

pervisada como RF, SVM, MLP y KNN, en varios experimentos. En ellos, se muestran los resultados de mapear un área de gran extensión (60 ha cuya imagen capturada por el dron contiene más de 140 millones de píxeles). Con la estrategia de procesamiento en ventana propuesta se obtienen buenos resultados de clasificación, superando el 90% en términos de *average precision*, *accuracy score* y *balanced accuracy score* en el mejor de los experimentos. Los resultados también muestran como el conjunto de muestras de entrenamiento, que se han recogido mediante técnicas SIG, influye en la predicción del tipo de cobertura terrestre. El tiempo de procesamiento de la imagen llevó unas 2.5 horas. Este proceso no hubiera sido posible realizarlo con un ordenador personal convencional.

Se han comprobado los buenos resultados de clasificación de cobertura terrestre mediante algoritmos de aprendizaje automático, en imágenes de alta resolución espacial, mediante la estrategia de procesamiento en ventana propuesta. Por ello, en [2] se propone una metodología para la generación de imágenes verdad-terreno sintéticas. En concreto, en nuestro trabajo demostramos que utilizando imágenes multiespectrales de alta resolución espacial (como las adquiridas por los vuelos del PNOA) se pueden generar imágenes mediante técnicas SIG que nos sirven para validar los resultados de los experimentos llevados a cabo en esta Tesis, en la que se utilizan algoritmos de clasificación de inteligencia artificial para procesar imágenes de satélite.

En ese sentido, en las siguientes publicaciones y resultados que se han llevado a cabo en esta Tesis Doctoral se han empleado imágenes multiespectrales de satélite Sentinel-2 (de resolución media y tiempo de revisita de 5 días). Los resultados demuestran cómo se pueden detectar, de forma automática, plantas acuáticas invasoras en imágenes de satélite mediante las metodologías descritas en los trabajos, con altas precisiones.

En la publicación [2], además se muestran los resultados de clasificación de cubierta terrestre en imágenes Sentinel-2 utilizando la estrategia de procesamiento completa (que incluye también la estrategia de preprocesamiento teniendo en cuenta los valores NoData) mediante algoritmos de inteligencia artificial. Los resultados muestran el éxito de aplicar algoritmos de clasificación tanto cuantitativamente como de forma visual. De esta forma los resultados reflejan que se obtienen mejores resultados de clasificación utilizando un algoritmo de aprendizaje profundo (CNN1D) seguido de un algoritmo de aprendizaje automático (RF) y por último un algoritmo de clasificación no supervisado como K-Means. Centrándonos en la detección de las plantas acuáticas invasoras, con el algoritmo K-Means se necesita una interpretación visual previa para seleccionar el número de *clusters* o agrupaciones con el que el algoritmo va a detectarlas mejor. Además, hay ciertas zonas en las orillas del río donde no diferencia las plantas invasoras de otra vegetación autóctona. Si atendemos a los resultados obtenidos con el algoritmo RF, las

plantas invasoras se detectan con precisión en gran parte de las zonas analizadas. Sin embargo, algunos contornos de la superficie del río ocupada por plantas invasoras no se detectan correctamente. Este fallo de predicción en la clasificación del tipo de píxel es mejorado mediante el algoritmo CNN1D. Esta interpretación visual también queda reflejada en los resultados estadísticos mostrados en la publicación. De esta forma, los resultados demuestran que con un número reducido de muestras de entrenamiento para entrenar los algoritmos de clasificación supervisada (RF y CNN1D) se pueden detectar plantas acuáticas invasoras con altas precisiones. Por el contrario, a pesar de que el algoritmo K-Means es menos complejo que los anteriores, requiere de un proceso de interpretación visual para llegar a unos resultados aceptables.

En los siguientes trabajos de esta Tesis, se han tenido en cuenta los resultados previos que demuestran el éxito en la detección de plantas invasoras para determinar su distribución espacial en una imagen concreta. En los estudios posteriores, se han utilizado algoritmos de aprendizaje profundo CNN1D, dado las mejores precisiones obtenidas para detectar plantas acuáticas invasoras en imágenes de satélite Sentinel-2. En la publicación [3] se ha descrito una metodología para monitorear la distribución de estas plantas a lo largo del tiempo. Para ello, el modelo CNN1D propuesto en la publicación anterior se ha entrenado con escasas muestras de entrenamiento para monitorear la distribución espacio temporal de plantas invasoras en una serie temporal de dos años. En concreto, los resultados muestran como con escasas muestras de entrenamiento se puede realizar una predicción acertada. Por lo tanto, tras analizar los resultados de la dinámica de la presencia de plantas invasoras en el río, el experimento que ofrece mejores resultados recoge muestras en únicamente 4 de las 62 imágenes analizadas de la serie temporal, identificando las plantas invasoras independientemente del estado fenológico en el que se encuentran. Se observa, por ejemplo, que hay más plantas invasoras cuando la planta se encuentra en estado de crecimiento vegetativo y por el contrario hay menos píxeles que contienen plantas invasoras cuando se encuentra en parada vegetativa. Además, los resultados muestran que al recoger muestras de entrenamiento hay que considerar la toma de muestras en las imágenes donde las plantas invasoras se presentan en color natural diferente, por ejemplo, cuando aparecen en color marrón (en diciembre, febrero y marzo) o en color verde (desde julio a diciembre).

En la publicación [4] se explora la disminución del conjunto de datos procedentes de las imágenes recogidas por el satélite Sentinel-2 necesarios para detectar las plantas invasoras. De esta forma, se compara la explotación de información contenida en cada píxel por parte de los algoritmos de inteligencia artificial. En las publicaciones anteriores se han explotado las 12 bandas espectrales proporcionadas por el satélite. En este trabajo se muestran los resultados de reducir el número de bandas gracias a la utilización de

composición de bandas o índices espectrales. Con la arquitectura CNN1D desarrollada en [2] se entrena el modelo de nuevo para predecir los píxeles que contienen plantas acuáticas invasoras en imágenes multiespectrales. Los resultados mostrados en la publicación muestran que se ofrecen mejores precisiones cuando se entrena el modelo con un número reducido de bandas espectrales. También se han generado los mismos resultados de mejora cuando se ha utilizado el algoritmo RF. Otro beneficio importante de usar índices espectrales en el entrenamiento (en lugar de todas las bandas) es que es más eficiente computacionalmente porque interviene menos información en el procesamiento de las imágenes.

Los avances obtenidos en los trabajos descritos anteriormente se ponen en práctica en la publicación [5], en la que se elabora una metodología en la que, mediante técnicas SIG, se trabaja con los mapas obtenidos por los modelos CNN1D que se han entrenado para detectar plantas acuáticas invasoras en una serie temporal. Dicha estrategia tiene su aplicación para mapear las áreas de acumulación de plantas acuáticas invasoras en un periodo de tiempo analizado. De tal forma, se muestran en los resultados los mapas de acumulación donde, gracias a la distinta tonalidad con la que se visualizan los píxeles, nos permite revelar las zonas donde suelen estar con mayor frecuencia. Por el contrario, también pueden darnos información de las localizaciones donde es menos frecuente que se acumulen estas plantas. Los mapas obtenidos también nos muestran el correcto funcionamiento de una barrera de contención instalada así como una necesidad de retirada de las plantas acumuladas para evitar que las plantas invadan las zonas del río aguas abajo de la barrera de contención.

En los resultados obtenidos en el trabajo [6] que aún no ha sido aceptado para publicación se propone una nueva arquitectura CNN2D. Esta arquitectura, a diferencia de la CNN1D en la que sólo tiene en cuenta la componente espectral para realizar la predicción de los píxeles de la imagen multiespectral, también considera la información de los píxeles vecinos. Mediante interpretación visual, se observa que los resultados obtenidos por el modelo CNN2D son altamente precisos. Esto puede comprobarse también en los altos % obtenidos en las distintas métricas de precisión empleadas. Los resultados muestran que el modelo CNN2D tiene un alto número de TN y TP y un bajo número de FN y FP. Se demuestra que la adición de la información espacial en el modelo de predicción de inteligencia artificial, es beneficioso para detectar plantas acuáticas invasoras en imágenes multiespectrales recogidas por el satélite Sentinel-2.

7.2 | Mapeado eficiente de grandes áreas en imágenes de alta resolución mediante estrategia de procesamiento en ventana

© 2021 IEEE. Reprinted, with permission, from Elena C. Rodríguez-Garlito and Abel Paz-Gallardo, *Efficiently Mapping Large Areas of Olive Trees Using Drones in Extremadura, Spain*, *IEEE Journal on Miniaturization for Air and Space Systems*, September 2021

El texto completo está incluido en el apéndice Publicaciones – Efficiently Mapping Large Areas of Olive Trees Using Drones in Extremadura, Spain.

7.2.1 | Resumen

Esta publicación utiliza datos RGB de alta resolución, recogidos por un vehículo aéreo no tripulado (UAV/dron), equipado con un sensor multiespectral y volado sobre un olivar en Extremadura (España), con fines de clasificación de la cobertura del suelo. Los vuelos de dron sobre grandes áreas agrícolas, recogiendo imágenes de alta resolución espacial como las del escenario estudiado, pueden ser tediosas de procesar, requiriendo una gran cantidad de memoria RAM. Para resolver este problema, se propone un nuevo enfoque para mapear la superficie dedicada a olivar aplicando una metodología de partición espacial que consiste en dividir la imagen automáticamente, antes de procesarla. Cada parte (conocida como ventana raster) se clasifica utilizando métodos de aprendizaje automático. Finalmente, se obtiene un mapa de clasificación tras procesar todas las ventanas. Entre los diferentes métodos clasificación espectral supervisada, se consideran los siguientes clasificadores: Random Forest (RF), Support Vector Machine (SVM), MultiLayer Perceptron (MLP), k-Nearest Neighbor (KNN), con el objetivo final de detectar olivos y distinguirlos de otros tipos de cobertura del suelo disponibles en la escena como suelo, sombras y maleza. Además, nuestros resultados experimentales demuestran que estos clasificadores pueden usarse para evitar tareas de campo que consumen mucho tiempo, facilitando el análisis de superficies agrícolas con vuelos UAV “a la carta”, lo que resulta en una alta precisión de clasificación. La Fig. 7.1 muestra el flujo de trabajo de esta publicación.

7.2.2 | Contribuciones de este artículo

A continuación, se enumeran las principales contribuciones de esta publicación:



Figura 7.1: Flujo de de trabajo para la detección de olivar.

1. Metodología para mapear imágenes de alta resolución espacial mediante un sistema de particionamiento en ventana.
2. Mapeado de una superficie agrícola (olivar) en imagen de dron mediante algoritmos de clasificación supervisada: RF, SVM, MLP y KNN.

7.2.3 | Esquema metodológico de estrategia de procesamiento en ventana

El problema de la viabilidad del procesamiento en imágenes de alta resolución se presenta debido a que la cantidad de memoria necesaria para utilizar los algoritmos de clasificación de la cubierta terrestre es muy exigente. Además, este asunto se agrava si la superficie a analizar es extensa. Para paliar este problema, se emplea una partición espacial automática (también conocida como partición de ventanas) antes de la predicción del conjunto de datos.

El particionamiento de ventanas divide el cubo de datos multispectral en ventanas o bloques de procesamiento situados contiguamente en el dominio espacial en el proceso de lectura de la imagen, de modo que cada ventana contiene información relativa a un subconjunto de píxeles de dicha imagen multispectral. El número de píxeles de cada ventana puede ajustarse en función de la imagen a procesar. En este estudio, dado que cada clasificador realiza la predicción píxel a píxel, se ha optado por dividir el cubo de datos en ventanas que contienen filas de píxeles de la imagen. Cada ventana contiene la información espectral asociada a una fila de píxeles. En primer lugar, los algoritmos se entrenan con muestras de entrenamiento seleccionadas. Este entrenamiento sólo se

realiza una vez y es válido para todas las ventanas de procesamiento. Después, los algoritmos de clasificación predicen la cobertura del suelo para la primera ventana leída. A continuación, se realiza un proceso de escritura parcial con esa ventana clasificada. Este proceso se repite ventana por ventana. Por último, se realiza el proceso de escritura de la última ventana clasificada. A continuación, se clasifica la imagen completa. En consecuencia, los algoritmos de aprendizaje automático son capaces de clasificar una imagen multispectral que sea incluso mayor que la memoria RAM disponible en el ordenador. La partición espacial también permite la paralelización entre distintos procesadores o máquinas. La Fig. 7.2 muestra el esquema de la metodología propuesta para el particionamiento en ventana de las imágenes previas a ser clasificadas mediante un algoritmo de aprendizaje automático.

7.2.4 | Mapeo de olivar

En este artículo, se llevaron a cabo tres experimentos para evaluar y validar los diferentes métodos de clasificación. En el *experimento n°1* se recogieron las muestras de entrenamiento (de olivos, suelo, malas hierbas y sombras) mediante operaciones SIG, seleccionándolas por interpretación visual. La Fig. 7.3 muestra el mapa resultado de la clasificación con uno de los algoritmos aplicados (RF). Este proceso llevó 2.5 h y no hubiera sido posible en un ordenador de especificaciones corrientes (Intel(R) Core(TM) i7-8700 procesador, 32GB memoria RAM y 1TB SSD) sin la estrategia de procesamiento en ventana propuesta. La Fig. 7.4 muestra mapas de clasificación para cada uno de los algoritmos de aprendizaje automático aplicado. Por otro lado, la Fig. 7.5(a) muestra las gráficas de precisión (*average precision*, *accuracy score* y *balanced accuracy score*) donde se ilustra clasificaciones con más de un 90 % de precisión, obtenidas (en orden creciente) por los clasificadores: RF, SVM, MLP y KNN.

Con el *experimento n°2*, del conjunto de entrenamiento del experimento anterior, se extrajeron de manera aleatoria diferentes conjuntos de entrenamiento (50, 100, 200, 400, 500, 600 y 700 muestras por clase). Como se muestra en la Fig. 7.5(b), todos los algoritmos se comportan de manera similar. Se puede ver cómo las precisiones aumentan a medida que aumenta el número de muestras de entrenamiento. Crecen de forma más pronunciada hasta que el número de muestras alcanza aproximadamente 200, y después siguen creciendo moderadamente. Además, se observa que cuando se han tomado 600 muestras de entrenamiento, se produce una disminución mínima que se corrige cuando el rendimiento se evalúa con la *balanced accuracy score*. También puede apreciar que los algoritmos de clasificación RF y SVM obtienen mejores resultados que MLP y KNN, que también se comportan de forma muy similar.

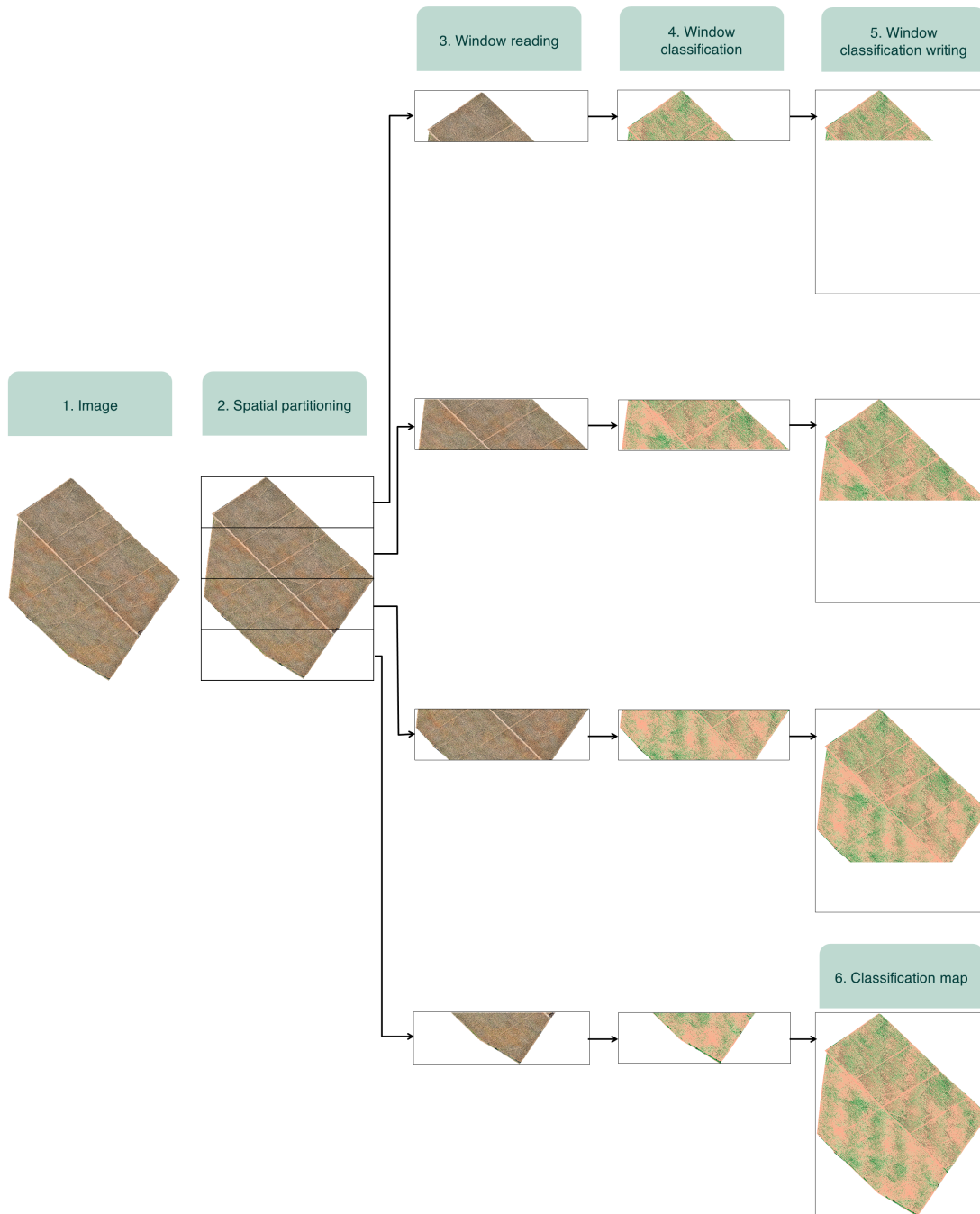


Figura 7.2: Estrategia de partición de ventanas en un ejemplo con cuatro ventanas.

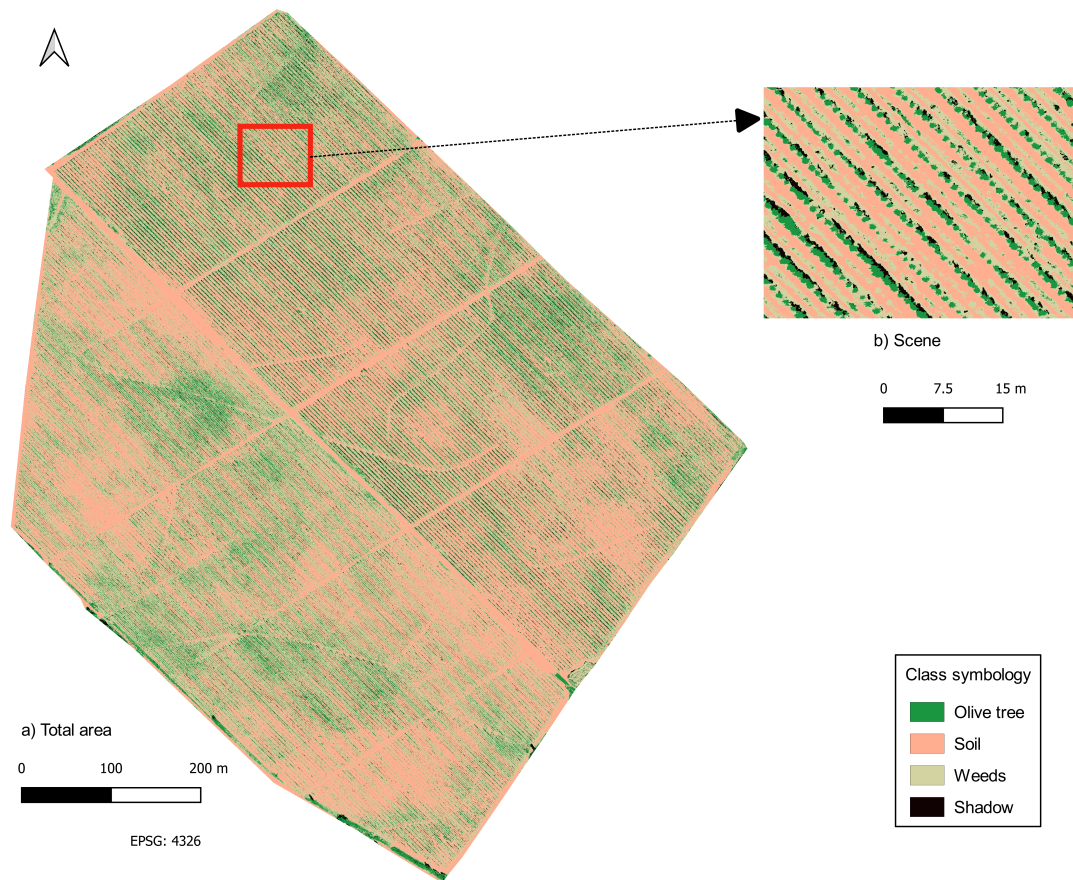


Figura 7.3: Mapa de clasificación del área total obtenido mediante partición de ventanas y RF (a) y mapa de clasificación de una escena ampliada (b).

Por último, con el *experimento n°3* se ha realizado una prueba de escalabilidad por clase en las que se han extraído aleatoriamente las muestras del *experimento n°1*, utilizando un factor de escala lineal ponderado según el número de píxeles asociados a cada clase en la imagen ground truth. Como se aprecia en la Fig. 7.5(c), los cuatro clasificadores analizados se comportan de forma similar, mejorando sus actuaciones cuando el número de muestras de entrenamiento crece. Crecen más significativamente al principio y luego tienden a estabilizarse. RF obtiene los mejores resultados. Comparando con el experimento anterior, los clasificadores obtienen mejores precisiones cuando se eligen muestras de entrenamiento variables por clase, de forma proporcional al número de muestras de cada clase en toda la escena.

Tras analizar estos tres experimentos, la principal conclusión es que las técnicas consideradas (especialmente, RF y SVM) pueden distinguir las diferentes clases de cobertura del suelo en la escena. Esto se debe principalmente a la alta resolución espacial de

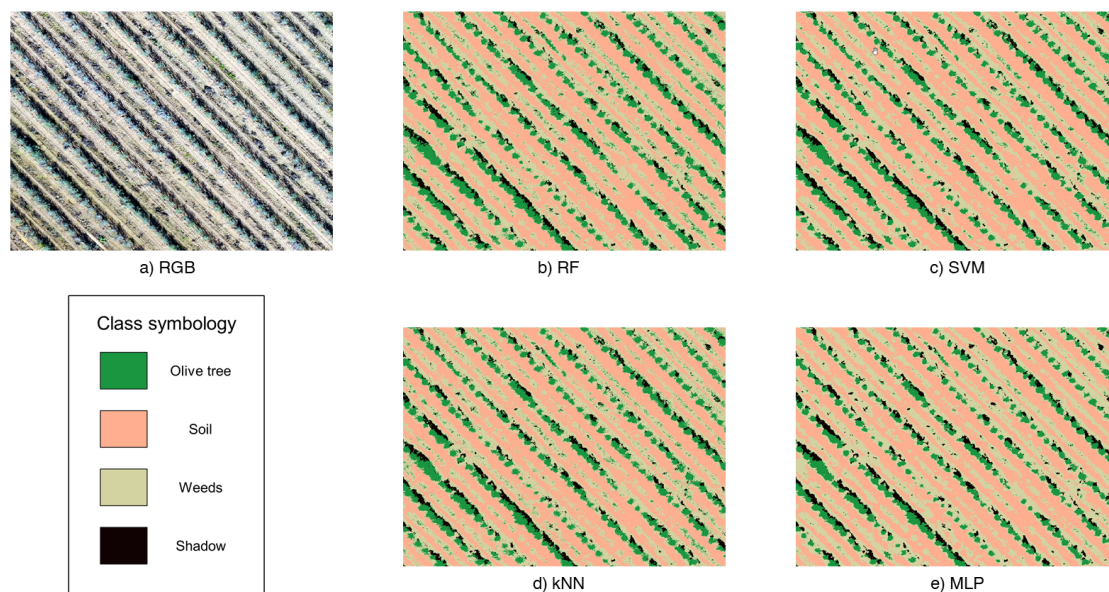


Figura 7.4: (a) Imagen RGB del conjunto de datos. Mapas de clasificación obtenidos por diferentes clasificadores: (b) RF, (c) SVM, (d) KNN y (e) MLP.

la escena (que no requiere una resolución espectral muy alta para proporcionar buenos resultados de clasificación). Además, se ha demostrado que, dada la homogeneidad del cultivo, se puede realizar una clasificación semiautomática de una gran explotación dedicada a los olivos, entrenando los algoritmos de clasificación con pocas muestras de entrenamiento. Si no se hubiera utilizado el aprendizaje automático, habría que realizar tareas manuales subjetivas recortando la imagen con un editor píxel a píxel, lo que sería inviable. Nuestros resultados demuestran que el aprendizaje automático aplicado a la agricultura ahorra mucho tiempo de trabajo de campo en la zona agrícola considerada y puede facilitar enormemente la gestión de las estrategias agrícolas.

7.3 | Detección automática de plantas acuáticas invasoras mediante algoritmos de aprendizaje automático y aprendizaje profundo

Adaptated and Translated from "Automatic Detection of Aquatic Weeds: A Case Study in the Guadiana River, Spain" under the Creative Commons License (CC BY 4.0).

El texto completo está incluido en el apéndice Publicaciones – Automatic Detection of Aquatic Weeds: A Case Study in the Guadiana River, Spain.

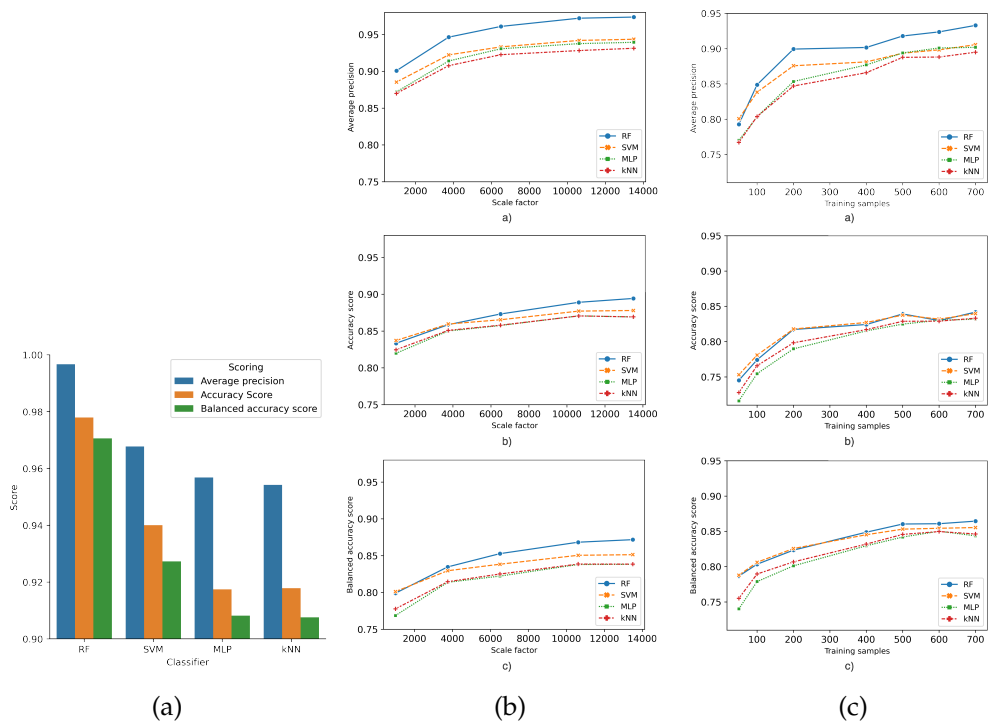


Figura 7.5: Métricas de precisión para evaluar los resultados de la clasificación (*average precision, accuracy score* y *balanced accuracy score*) para cada clasificador en: (a) Experimento 1, (b) Experimento 2 y (c) Experimento 3

7.3.1 | Resumen

El objetivo principal de este trabajo es desarrollar una metodología capaz de detectar automáticamente la geolocalización de plantas acuáticas invasoras utilizando técnicas de teledetección y aprendizaje automático o aprendizaje profundo. Para ello, se han aplicado varios algoritmos de clasificación a imágenes de satélite multispectrales de libre acceso, recogidas por el satélite Sentinel-2 de la ESA. Se realiza una evaluación cuantitativa y comparativa utilizando diferentes algoritmos de aprendizaje automático y profundo, desde métodos clásicos como K-means hasta métodos supervisados como random forest (RF) y redes neuronales convolucionales (CNN). Este estudio también propone una metodología para validar los resultados de clasificación obtenidos, generando imágenes verdad-terreno sintéticas, basadas en imágenes de alta resolución espacial disponibles. Los resultados obtenidos demuestran la idoneidad de algunos de los algoritmos considerados para la detección automática de maleza acuática, (como el jacinto de agua y el nenúfar mexicano) en imágenes de satélite con resolución espacial media.

7.3.2 | Contribuciones de este artículo

Las principales contribuciones de este artículo se resumen a continuación:

1. Establecimiento de una cadena de procesado completa de imágenes Sentinel-2 para detectar automáticamente plantas acuáticas invasoras en el río Guadiana utilizando herramientas de teledetección, SIG e inteligencia artificial. Esta metodología incluye preprocesado (con tratamiento de valores NoData), procesado y evaluación de resultados.
2. Propuesta de una nueva estrategia para validar los resultados de clasificación de los algoritmos de machine/deep learning mediante la generación de imágenes verdad-terreno, a partir de una imagen multispectral de alta resolución.
3. Comparación detallada entre algoritmos de aprendizaje automático (k-means, RF) y aprendizaje profundo (CNN) en el contexto de la detección de maleza acuática, en dos áreas en el río Guadiana, España. Se utilizan imágenes de satélite Sentinel-2 (de resolución media, que pueden ser recogidas con un tiempo de revisita frecuente (5 días) y están disponibles gratuitamente).

7.3.3 | Estrategia en el preprocesado de imágenes multispectrales para el tratamiento de los píxeles con valores nulos

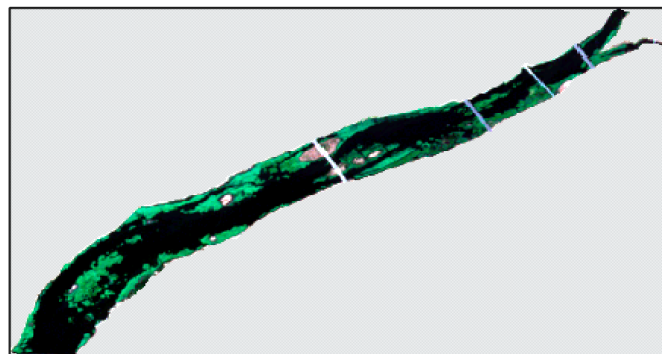
Trabajar con imágenes que no son cuadradas o rectangulares implica la presencia de valores nulos (o *NoData*), lo que supone una dificultad añadida tanto en el preprocesamiento como en el tratamiento de los datos. Estos valores *NoData* son valores en los que no hay información sobre la escena, debido principalmente a su geometría y no a errores de captura de datos del sensor, que puedan dar lugar a valores omitidos. Por lo tanto, trabajar con valores *NoData* puede ser un proceso tedioso, ya que hay que tenerlos en cuenta a nivel de SIG, cuando se muestran los datos y también a nivel de codificación, cuando se leen, procesan y escriben (guardan) las imágenes.

En esta investigación, los conjuntos de datos PNOA y Sentinel-2 se han obtenido en formato de 8 bits y, por tanto, los valores de los píxeles van de 0 a 255 en cada banda espectral. En primer lugar, se ha realizado una normalización de estos valores (dividiendo estos valores por 255) para que se muestren en un rango de 0 a 1. Con el fin de aplicar las técnicas de clasificación sólo sobre las zonas en las que queremos detectar las malas hierbas acuáticas, se ha aplicado una máscara previamente elaborada para mostrar sólo los datos dentro de cada ROI (como se ve en la Fig 7.6). En consecuencia, los conjuntos de datos tienen información y valores *NoData*. Para tratar los valores *NoData* y excluirlos

del entrenamiento, la predicción y la clasificación, se han asignado otros valores distintos de los valores dentro de las ROI. Se ha calculado el histograma de cada conjunto de datos y, dado que los píxeles que sí contienen información ROI saturan el rango (valores 0 ó 1), se ha cambiado el formato del conjunto de datos a coma flotante de 32 bits. A continuación, los valores *NoData* se asignan a 10 000, lo que evita dificultades para manejar los datos. Además, a nivel de codificación, se ha aplicado la máscara ROI de forma que sólo tenemos en cuenta los píxeles que están fuera de la máscara para aplicar las técnicas de clasificación.



(a)



 NoData Values

(b)

Figura 7.6: a) Imagen completa de Sentinel-2 para ROI-BA, b) ROI-ME recortado y valores *NoData* presentes en la imagen debido a su geometría.

7.3.4 | Estrategia para generación de imágenes verdad-terreno propuesta

Se ha implementado una estrategia novedosa para validar el rendimiento de los algoritmos de machine/deep learning en la aplicación considerada. En concreto, se propone una estrategia de generación de datos verdad-terreno sintéticos a partir de una imagen multiespectral de alta resolución. Para ello, se utilizan datos adquiridos por el Plan Nacional de Ortofotografía Aérea (PNOA), que proporciona conjuntos de datos de libre acceso. Estos datos se clasifican previamente utilizando una estrategia de procesamiento basada en ventanas explicada en nuestro trabajo anterior [1]. La Fig. 7.7 muestra un esquema para la generación de una imagen verdad-terreno sintética. Primero, se considera una imagen Sentinel-2 con un conjunto de píxeles representado por $X_S = \{x_{S_1}, x_{S_2}, x_{S_3}, \dots, x_{S_m}\}$. Entonces, se genera una malla en formato vectorial donde cada celda x_{G_i} es un cuadrado de 10×10 m simulando los contornos de los píxeles x_{S_i} . Como resultado, la malla $H \times W$ (donde H es la altura y W es el ancho de la imagen) tiene las mismas dimensiones que la imagen Sentinel-2, con la misma geolocalización. Por otro lado, el conjunto de datos del PNOA se ha clasificado y está compuesto por los píxeles $X_P = \{x_{P_1}, x_{P_2}, x_{P_3}, \dots, x_{P_m}\}$. Cada pixel es etiquetado como y_{p_i} , de acuerdo a la clase a la que pertenecen. Los píxeles x_{P_i} tienen una resolución espacial más alta que la de los píxeles x_{S_i} . En el siguiente paso, los centroides c_{P_i} de cada pixel x_{P_i} son identificados, adoptando sus etiquetas y_{p_i} y generando un archivo vectorial. A continuación, una imagen verdad-terreno sintética es generada situando la malla vectorial sobre el archivo vectorial. De tal forma que a cada celda x_{G_i} de la malla se le asigna una tabla de atributos equipada con tantas características como etiquetas y_{p_i} presenta el archivo vectorial. Finalmente, a cada celda se le asigna la etiqueta y_{p_i} por mayoría de votos. En consecuencia, una imagen sintética *Ground Truth (GT)* se desarrolla resultando una imagen de $H \times W$ con el mismo número de píxeles y resolución espacial que el conjunto de datos de Sentinel-2 dataset. La Fig. 7.8 muestra escenas del resultado de la generación de imágenes verdad-terreno para las dos regiones de interés.

7.3.5 | Mapeo de plantas acuáticas invasoras

La Fig. 7.9 y la Fig. 7.10 muestran los mapas de clasificación para ciertas escenas y para la zona completa de estudio para la ROI-BA y para ROI-ME en las Fig. 7.11 y Fig. 7.12.

La Tabla. 7.1 muestra las precisiones de clasificación. En ella se aprecia que los clasificadores supervisados se comportaron mejor que los no supervisados, no sólo porque RF y CNN pueden proporcionar buenos resultados con un número limitado de muestras

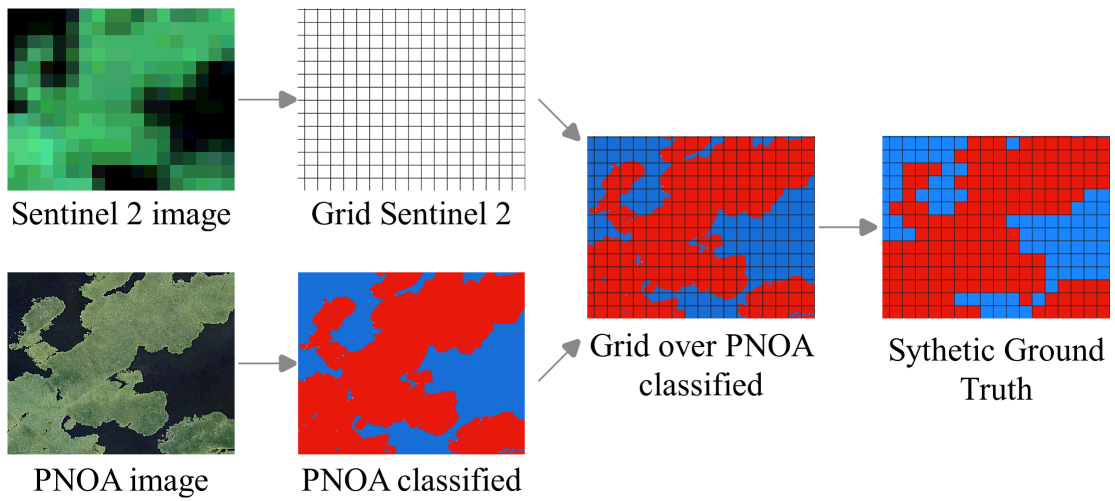


Figura 7.7: Principales pasos en la generación de la imagen verdad-terreno sintética (GT).

de entrenamiento, sino también porque el algoritmo no supervisado (*K-means*) necesita en última instancia un proceso de interpretación supervisado (basado en el análisis de imágenes de alta resolución para combinar algunos de los clusters obtenidos). El uso de un algoritmo u otro depende de los requisitos de cada caso de estudio, pero en nuestro contexto, el clasificador CNN se consideró la mejor opción.

Tabla 7.1: Métricas de precisión para el caso de Badajoz y el caso de Mérida

		Overall accuracy	User's accuracy	Producer's accuracy	F_1 score
Badajoz case	K-means	0.707	0.746	0.820	0.781
	RF	0.766	0.832	0.794	0.813
	CNN	0.779	0.784	0.901	0.839
Mérida Case	K-means	0.883	0.881	0.898	0.852
	RF	0.892	0.800	0.952	0.869
	CNN	0.903	0.843	0.911	0.876

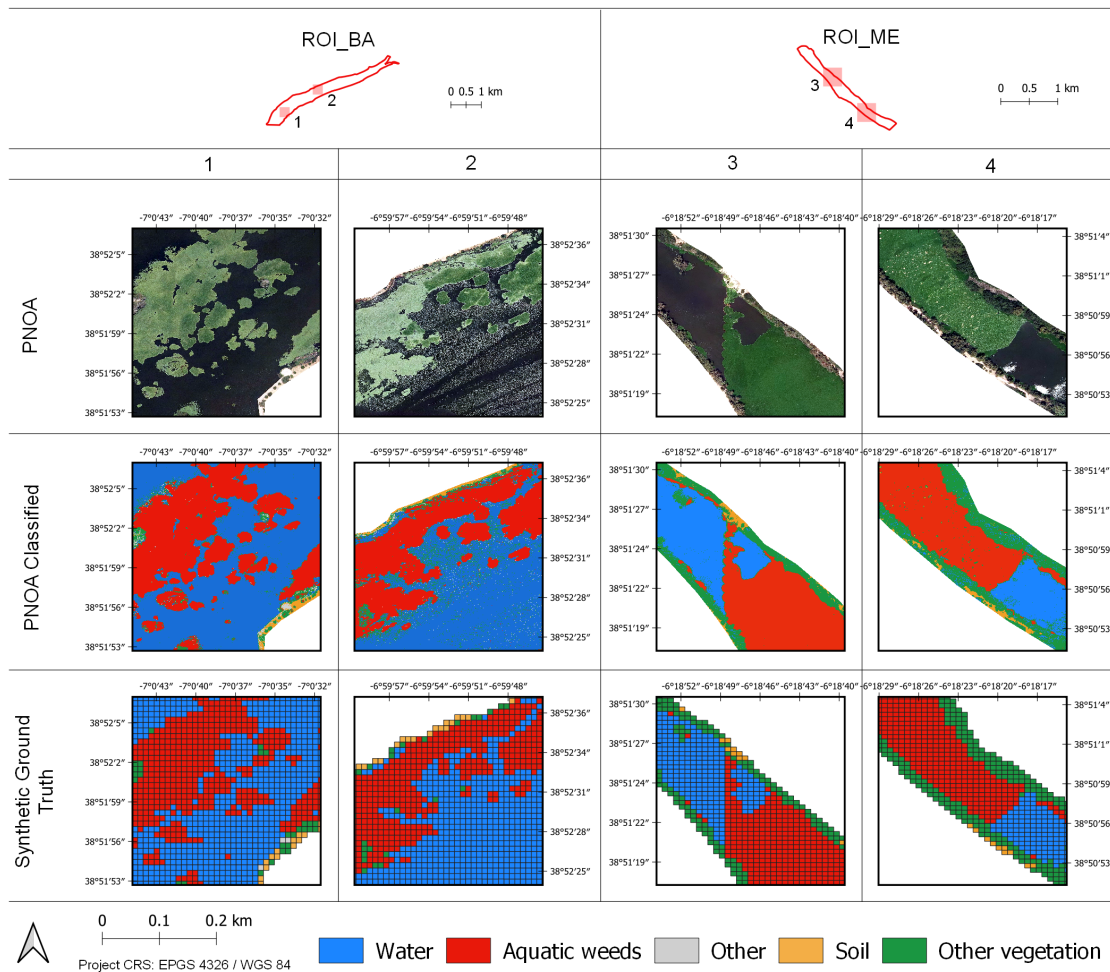


Figura 7.8: Algunas imágenes GT sintéticas generadas para cada región de interés considerada.

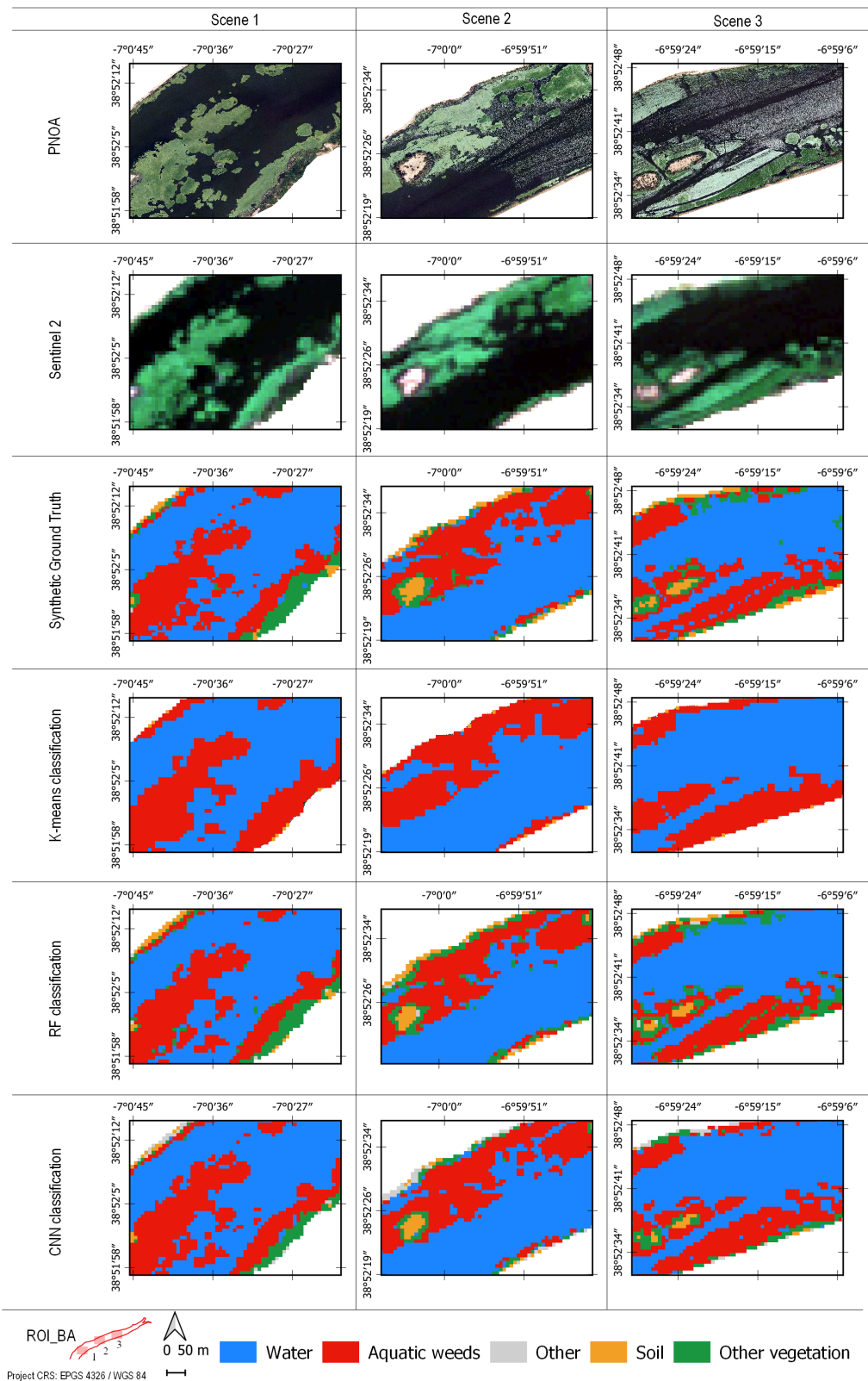


Figura 7.9: Mapas de clasificación de tres escenas representativas en ROI-BA (Badajoz).

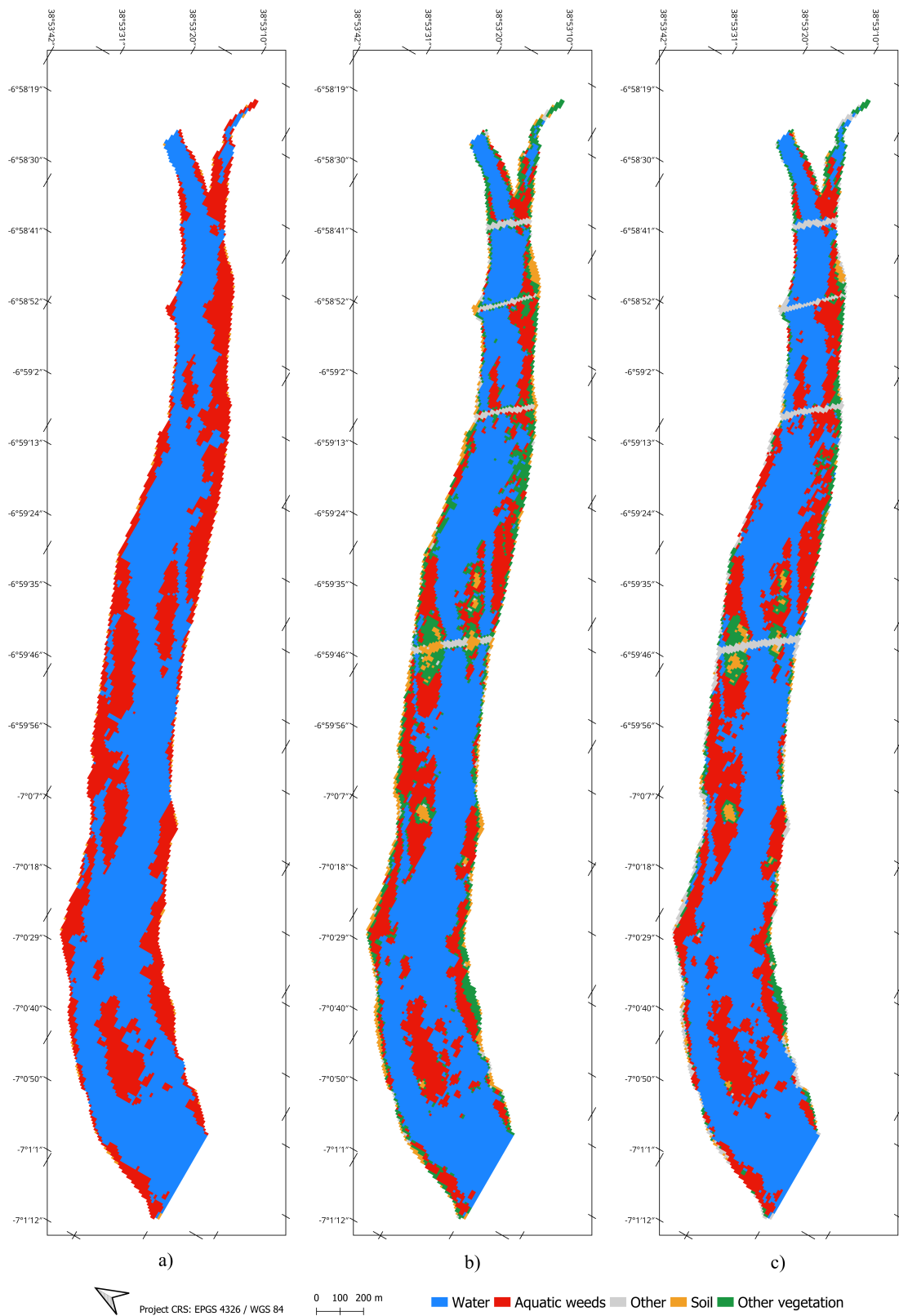


Figura 7.10: Mapas de clasificación en ROI-BA con diferentes clasificadores: a) K-means, b) RF y c) CNN.

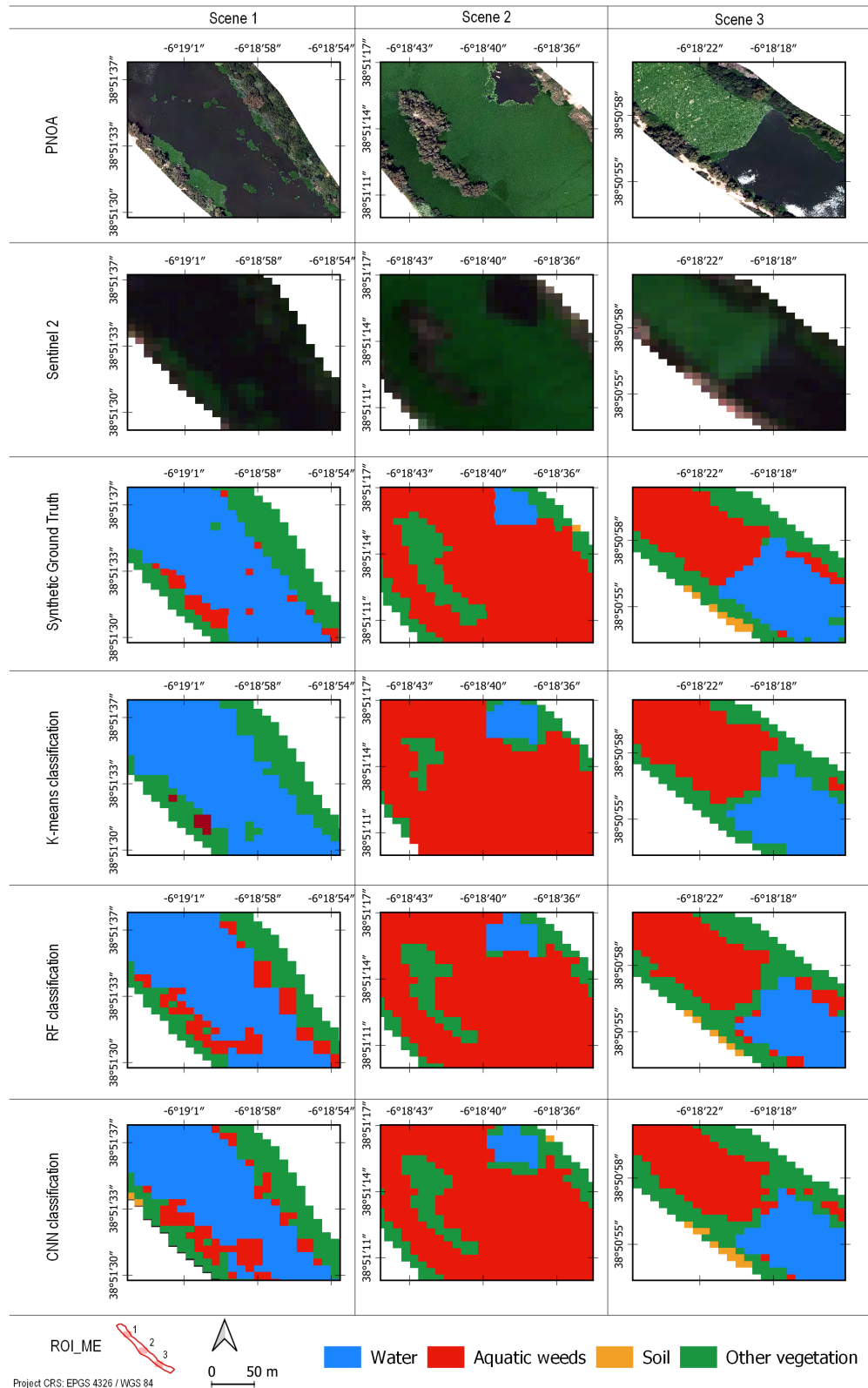


Figura 7.11: Mapas de clasificación de tres escenas representativas de ROI-ME (Mérida).

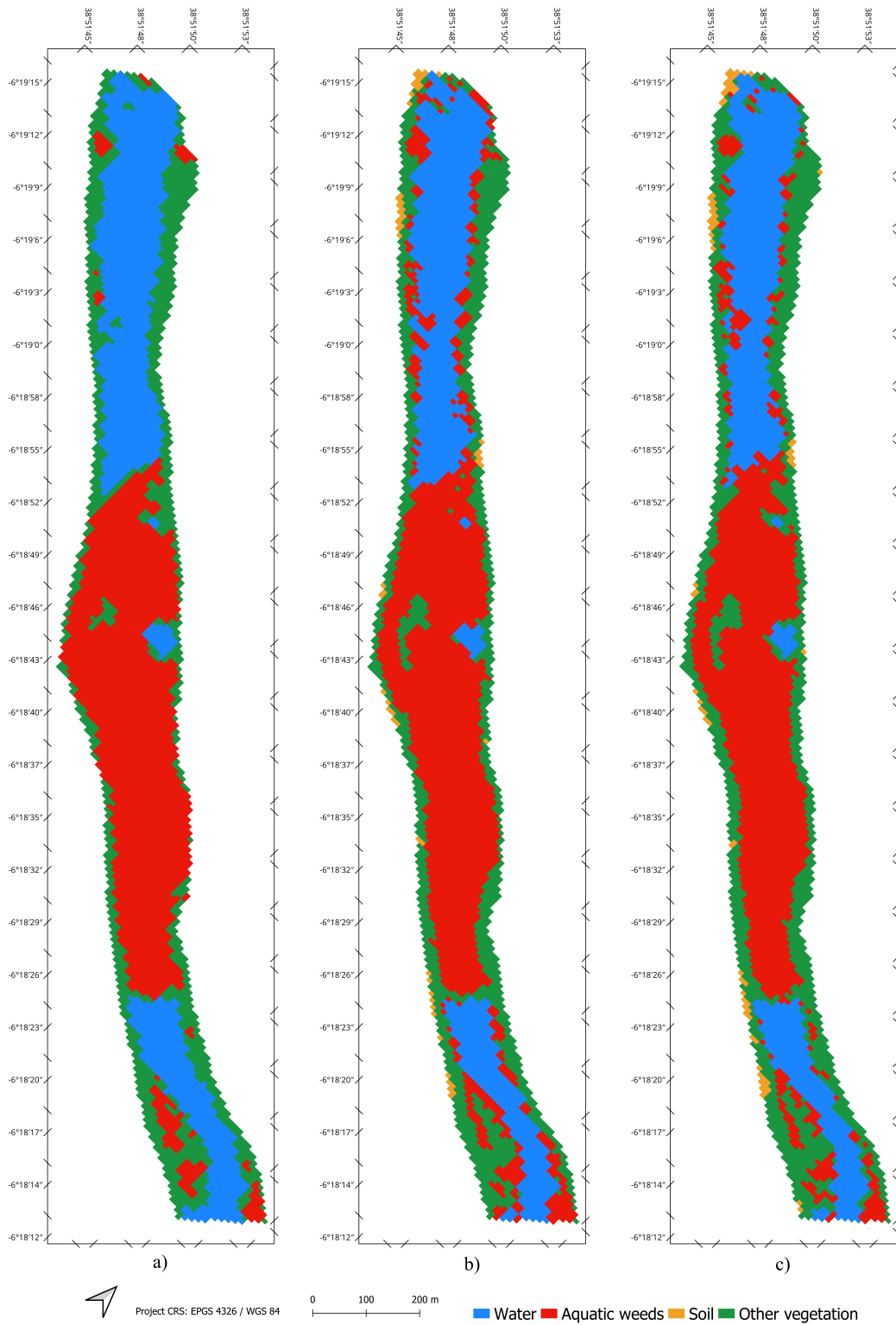


Figura 7.12: Mapas de clasificación en ROI-ME con diferentes clasificadores: a) K-means, b) RF y c) CNN.

7.4 | Monitoreo de la distribución espacio- temporal de plantas acuáticas invasoras en una serie temporal mediante un modelo de aprendizaje profundo entrenado con escasas muestras de entrenamiento

Adaptated and Translated from “Monitoring the Spatiotemporal Distribution of Invasive Aquatic Plants in the Guadiana River, Spain” under the Creative Commons License (CC BY 4.0).

El texto completo está incluido en el apéndice Publicaciones – Monitoring the Spatiotemporal Distribution of Invasive Aquatic Plants in the Guadiana River, Spain.

7.4.1 | Resumen

El seguimiento espaciotemporal de la distribución de plantas acuáticas invasoras es un reto en muchas regiones del mundo. En este trabajo, proponemos un sistema automático, basado en técnicas de teledetección y aprendizaje profundo, para monitorizar el jacinto de agua en el río Guadiana. En concreto, se realizó un análisis multitemporal durante dos años utilizando imágenes recogidas por el satélite Sentinel-2 de la ESA, analizadas con una red neuronal convolucional (CNN). Demostramos que, con nuestra estrategia, se puede monitorizar el río cada pocos días, siendo capaces de detectar automáticamente el jacinto de agua. Se han realizado tres experimentos para predecir la presencia de jacinto de agua a partir de unas pocas muestras de entrenamiento dispersas, que representan plantas invasoras en diferentes etapas fenológicas y con diferentes respuestas espectrales.

7.4.2 | Contribuciones de este artículo

Se enumeran las principales contribuciones de esta publicación:

1. Estrategia para evaluar la evolución multitemporal de plantas acuáticas invasoras en una serie temporal. Seleccionando como punto de partida el modelo CNN desarrollado en [2], se pueden discriminar de otros tipos de cobertura presentes (como agua, suelo y otra vegetación).
2. Entrenamiento de un modelo de aprendizaje profundo, minimizando el número de muestras recogidas. De este modo, las muestras de entrenamiento se han extraído de únicamente 4 de 62 imágenes multiespectrales del satélite Sentinel-2

analizadas. Dicho entrenamiento permite predecir la presencia de jacinto de agua (en un periodo de dos años) independientemente de los distintos estados fenológicos de la planta.

3. Monitorización de la distribución espacio-temporal de las plantas acuáticas invasoras cada pocos días. Esto se consigue utilizando datos adquiridos por el satélite Sentinel-2 (que permiten obtener una imagen sobre cualquier lugar del mundo cada cinco días) sin necesidad de volver a entrenar el modelo (es decir, reutilizando el mismo entrenamiento) y sin coste adicional en términos de adquisición de imágenes.

7.4.3 | Metodología propuesta para evaluar la evolución temporal

La Fig. 7.13 muestra la metodología propuesta y desarrollada en [3] para la monitorización del jacinto de agua presente en la superficie de los ríos. Este flujo de trabajo incluye el preprocesado de las imágenes obtenidas de forma remota, la detección automática de las plantas invasoras a través de un modelo CNN entrenado y la representación gráfica del seguimiento de la presencia de plantas invasoras en una serie temporal. Como se indica, se han llevado a cabo tres experimentos: El *experimento 1* recoge muestras de una sola imagen y utiliza ese conjunto de entrenamiento para predecir la geolocalización de las plantas invasoras en todas las imágenes de la serie temporal analizada. El diseño del *experimento 2* y del *experimento 3* está basado en los resultados del *experimento 1*. En esos últimos, se recogen muestras de entrenamiento de 4 imágenes de toda la serie temporal. En el *experimento 2* se utiliza el mismo conjunto de entrenamiento para todo el periodo temporal. Por el contrario, para el *experimento 3*, se utilizan 4 conjuntos para diferentes periodos anuales dependiendo del estado fenológico de la planta.

7.4.4 | Selección de un conjunto de entrenamiento adecuado para predecir la geolocalización del jacinto de agua en toda la serie temporal

En primer lugar, para el *experimento 1* se han extraído muestras de entrenamiento de una imagen de Sentinel-2 en la que el jacinto de agua se encuentra en una etapa de crecimiento vegetativo. Mediante interpretación visual (teniendo como referencia la imagen de alta resolución PNOA), se han podido seleccionar muestras de entrenamiento pertenecientes al jacinto de agua y las que pertenecen a diferentes tipos de cobertura del suelo (como el agua, el suelo y otros tipos de vegetación). Se han analizado una a una

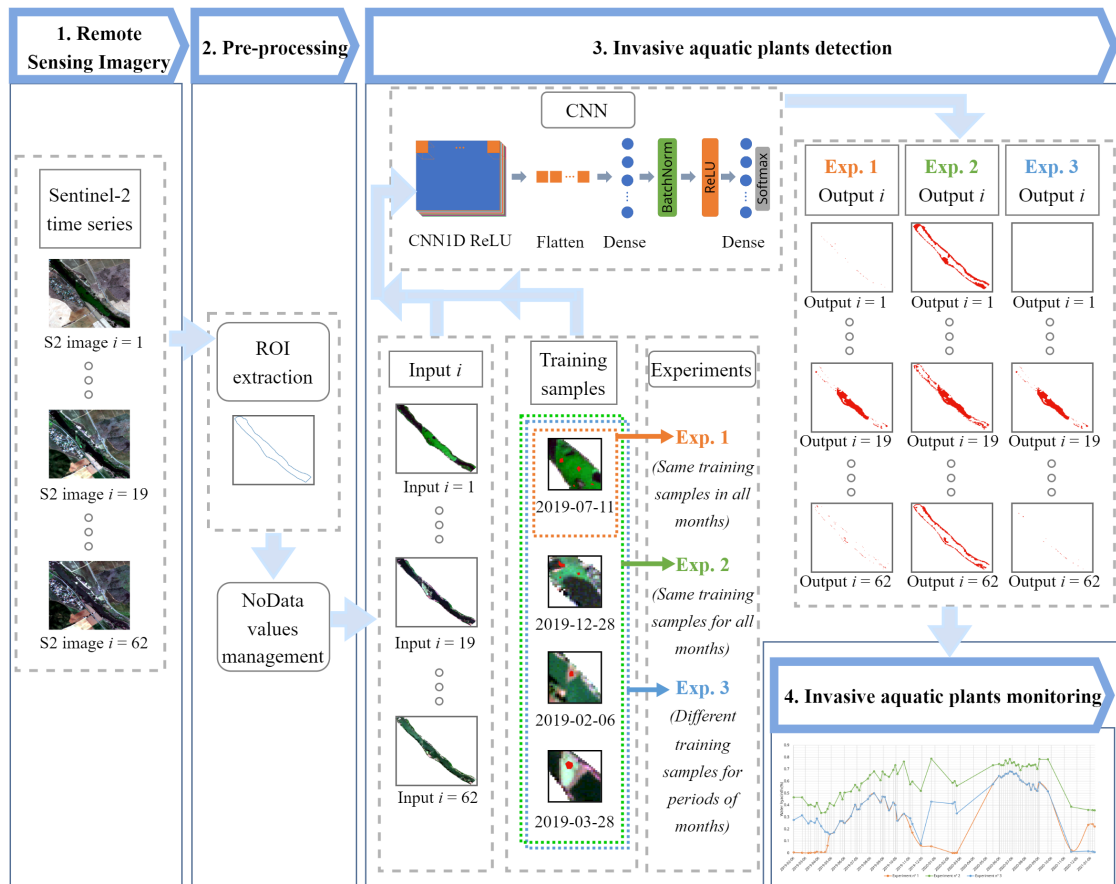


Figura 7.13: Flujo de trabajo del procedimiento de monitorización de la distribución espacio-temporal del jacinto de agua en el río Guadiana mediante tres experimentos diferentes. También se muestra la arquitectura de la CNN utilizada para el mapeo.

todas las imágenes clasificadas de la serie temporal para comprobar la idoneidad de este primer conjunto de entrenamiento para que el modelo CNN predijera correctamente el jacinto de agua en todas las imágenes. Se comprueba que las muestras de entrenamiento utilizadas en el *experimento 1* no son suficientes para una correcta detección de la planta invasora en el resto de meses del año, en los que se encuentra en distintos estados fenológicos

Para el *experimento 2* y *experimento 3*, se han extraído muestras de entrenamiento, además, de otras tres imágenes de Sentinel-2 adquiridas en fechas diferentes (una cuando el jacinto de agua está en parada vegetativa, otra cuando está en fase de floración y otra en parada vegetativa pero con diferente color verdadero —en marrón—). Como se ve en la Fig. 7.14, las firmas espectrales de las muestras de entrenamiento del jacinto de agua, presentan diferencias notables que justifican la recogida de muestras de jacinto de

agua en fechas diferentes. Como también se muestra en la composición de color RGB de las muestras Sentinel-2 en la Fig. 7.15 los diferentes colores del jacinto de agua dependen del ciclo vegetativo en el que se encuentren. Existen importantes variaciones en términos de reflectancia en las bandas RGB, especialmente en B03 (559,8 nm), lo que justifica los cambios de color de verde (fase de crecimiento vegetativo), al marrón (latencia).

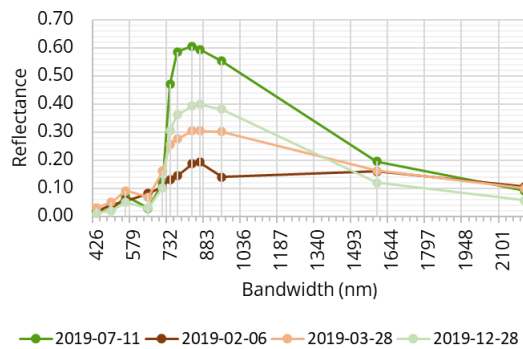


Figura 7.14: Firmas espectrales de las muestras de entrenamiento de jacinto de agua extraídas de imágenes Sentinel-2 (adquiridas en 4 fechas diferentes).

En la tabla 7.2 se describen los distintos conjuntos de entrenamiento considerados en estos experimentos. Teniendo en cuenta que cada una de las imágenes de Sentinel-2 que se procesan tienen 4471 píxeles etiquetados y que hay un total de 62 imágenes que se han procesado, el número de muestras de entrenamiento necesarias para cada experimento es bastante reducido.

Tabla 7.2: Número de muestras de entrenamiento (píxeles) usados en nuestros experimentos

	Experimento 1	Experimento 2	Experimento 3			
			Periodo 1	Periodo 2	Periodo 3	Periodo 4
Jacinto de agua	162	427	30	57	162	178
Otros tipos	288	288	288	288	288	288

7.4.5 | Resultados de monitorización del jacinto de agua en el río Guadiana en un periodo de dos años

En la Fig. 7.16 se ilustra la gráfica resultado de monitorear la presencia de jacinto de agua a lo largo del tiempo, para los tres experimentos realizados. Vemos que la dinámica se ajusta al comportamiento vegetativo de la planta. Por ejemplo, en los meses de crecimiento vegetativo el % de píxeles que contienen plantas invasoras aumenta. Por el

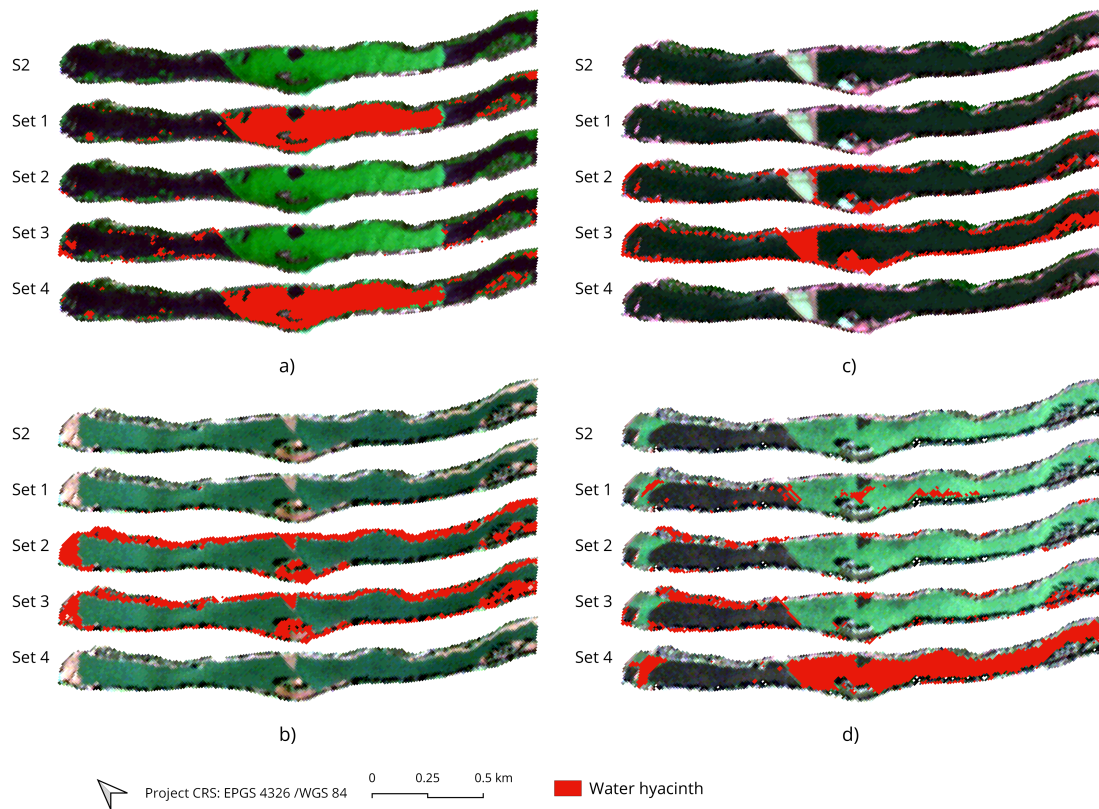


Figura 7.15: Justificación visual de la necesidad de recoger diferentes muestras de entrenamiento de imágenes de Sentinel-2 en 4 fechas diferentes. Se muestran los resultados obtenidos tras procesar con el modelo CNN las imágenes de Sentinel-2 adquiridas en las fechas: (a) 2019-07-11, (b) 2019-02-06, (c) 2019-03-28 y (d) 2019-12-28. Los píxeles que contienen jacinto de agua en la superficie del río están marcados en rojo. Para cada imagen, mostramos los resultados de detección obtenidos utilizando diferentes conjuntos de entrenamiento: muestras recogidas el 2019-07-11 (Conjunto 1), 2019-02-06 (Conjunto 2), 2019-03-28 (Conjunto 3) y 2019-12-28 (Conjunto 4). Las imágenes se visualizan en color verdadero (RGB).

contrario, cuando la planta se encuentra en la fase de parada vegetativa, ese % disminuye. La Fig. 7.17 muestra mapas elaborados a partir de las imágenes de salida del modelo CNN donde se ha detectado jacinto de agua en la serie temporal, por cada experimento considerado.

Evaluando uno a uno el resultado de aplicar el modelo de CNN sobre las imágenes de Sentinel-2 de toda la serie temporal, se ha demostrado que el seguimiento de la distribución espacio-temporal del jacinto no requiere observaciones de campo. De hecho, se puede monitorizar el estado de la planta cada cinco días utilizando imágenes de resolución espacial media, como las recogidas por el satélite Sentinel-2 de la ESA. También demostramos que sólo es necesario entrenar el modelo predictivo considerado (CNN) una vez, utilizando una imagen de alta resolución (en nuestro caso, la imagen PNOA) para extraer las muestras más representativas de la zona de estudio. Esto nos permite separar las plantas invasoras de otras superficies de la cubierta terrestre (como el agua, el suelo y otros tipos de vegetación) durante un periodo de al menos dos años. Para detectar el jacinto de agua en las distintas fases de su ciclo fenológico (teniendo en cuenta que presentan diferentes firmas espectrales), se recopiló un amplio conjunto de muestras de entrenamiento mediante la interpretación visual de las imágenes Sentinel-2. Como resultado, se necesitan muy pocas muestras de entrenamiento para hacer predicciones en el año siguiente.

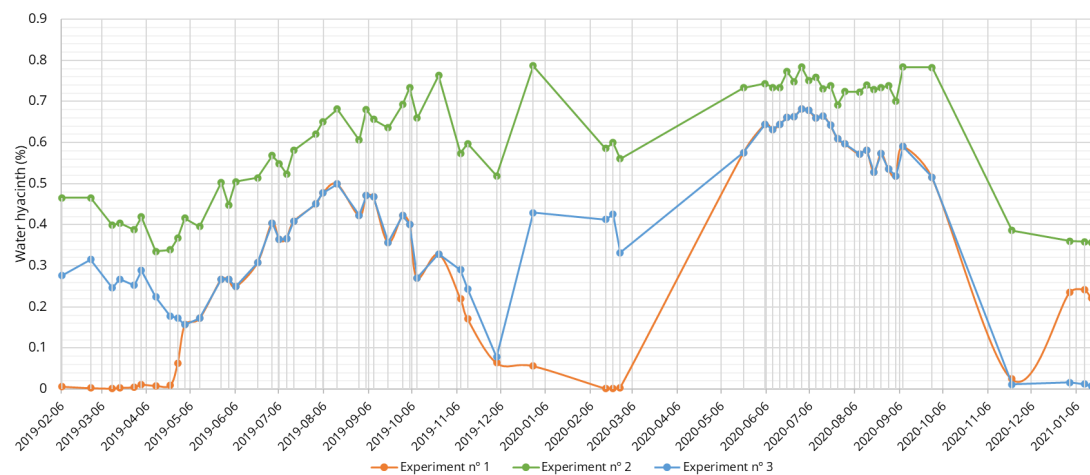


Figura 7.16: Porcentaje de píxeles de jacinto de agua en la ROI (excluidos los valores sin datos) obtenidos para la serie temporal completa (2019-2021) en cada experimento considerado.

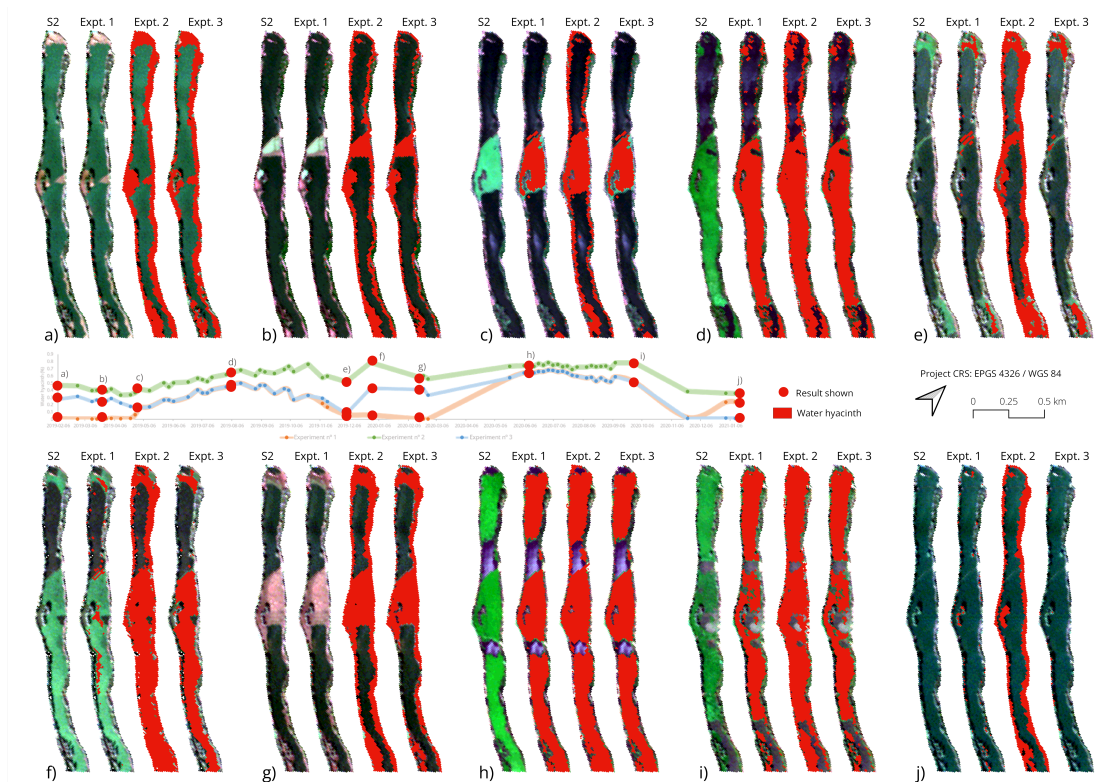


Figura 7.17: Resultados de la detección del jacinto de agua en algunas fechas de adquisición incluidas en la serie temporal estudiada: (a) 2019-02-06, (b) 2019-03-28, (c) 2019-05-02, (d) 2019-08-05, (e) 2019-12-03, (f) 2019-12-28, (g) 2020-02-16, (h) 2020-06-10, (i) 2020-09-28, y (j) 2020-01-16).

7.5 | Reducción del número de bandas espectrales del satélite Sentinel-2 necesarias para el mapeo de plantas acuáticas invasoras mediante modelos de aprendizaje profundo, entrenados con índices espectrales

Adaptated and Translated from "Mapping Invasive Aquatic Plants in Sentinel-2 Images Using Convolutional Neural Networks Trained with Spectral Indices" under the Creative Commons License (CC BY 4.0).

El texto completo está incluido en el apéndice Publicaciones – Mapping Invasive Aquatic Plants in Sentinel-2 Images Using Convolutional Neural Networks Trained With Spectral Indices.

7.5.1 | Resumen

En este trabajo, utilizamos diferentes índices espectrales para detectar plantas acuáticas invasoras en el río Guadiana, España. Nuestra metodología utiliza una red neuronal convolucional (CNN) como clasificador de base y es entrenada utilizando índices espectrales calculados utilizando diferentes combinaciones de bandas de Sentinel-2. En concreto, consideramos los siguientes índices espectrales: con dos bandas, calculamos el índice de vegetación de diferencia normalizada (NDVI), el índice de agua de diferencia normalizada (NDWI) y el índice infrarrojo de diferencia normalizada (NDII). Con tres bandas, calculamos la composición rojo-verde-azul (RGB) y el índice de algas flotantes (FAI). Por último, también utilizamos cuatro bandas para calcular el índice de suelo desnudo (BSI). En nuestros resultados, observamos que las CNN pueden cartografiar mejor las plantas acuáticas invasoras en el caso de estudio considerado cuando se entrenan utilizando índices espectrales en comparación con el uso de todas las bandas espectrales proporcionadas por el instrumento Sentinel-2.

7.5.2 | Contribuciones de este artículo

A continuación, se enumeran las principales contribuciones de esta publicación:

1. Metodología propuesta para la detección de plantas acuáticas invasoras en imágenes adquiridas por el satélite Sentinel-2, que simplifica la complejidad espectral que entra en el modelo CNN. En concreto, usamos índices espectrales para mejorar el proceso de entrenamiento de las CNN y determinar si los resultados obtenidos (calculados con un conjunto reducido de bandas de Sentinel-2 cuidadosamente seleccionadas) pueden mejorar los resultados que se obtienen cuando se utilizan todas las bandas disponibles.
2. Mapeado automático, con la nueva estrategia propuesta, en dos zonas del río Guadiana (España), muy afectadas por la presencia de plantas acuáticas invasoras (la primera zona afectada por el nenúfar mexicano y la segunda por el jacinto de agua) mediante el modelo CNN. Además se evalúan de forma cuantitativa y cualitativa los resultados.
3. Comparación cuantitativa y cualitativa de los resultados obtenidos con el modelo de la CNN y con otro clasificador clásico de aprendizaje, el RF, que se utilizó como estándar en otros estudios.

7.5.3 | Metodología para detectar plantas invasoras acuáticas entrenando un modelo CNN con un número reducido de bandas espectrales

La Fig. 7.18 muestra el flujo de trabajo necesario para detectar plantas invasoras acuáticas en imágenes de satélite Sentinel-2 con un modelo CNN entrenado con índices espectrales. En él, se indican las bandas espectrales que se utilizan para hacer las diferentes combinaciones de bandas descritas en 4.3 (RGB, NDVI, FAI, NDWI, BSI y NDII), las diferentes imágenes de entrada en el modelo CNN desarrollado, los diferentes conjuntos de entrenamiento y las imágenes de salida evaluadas de este estudio. También se ilustran las imágenes necesarias para una evaluación cuantitativa de los resultados.

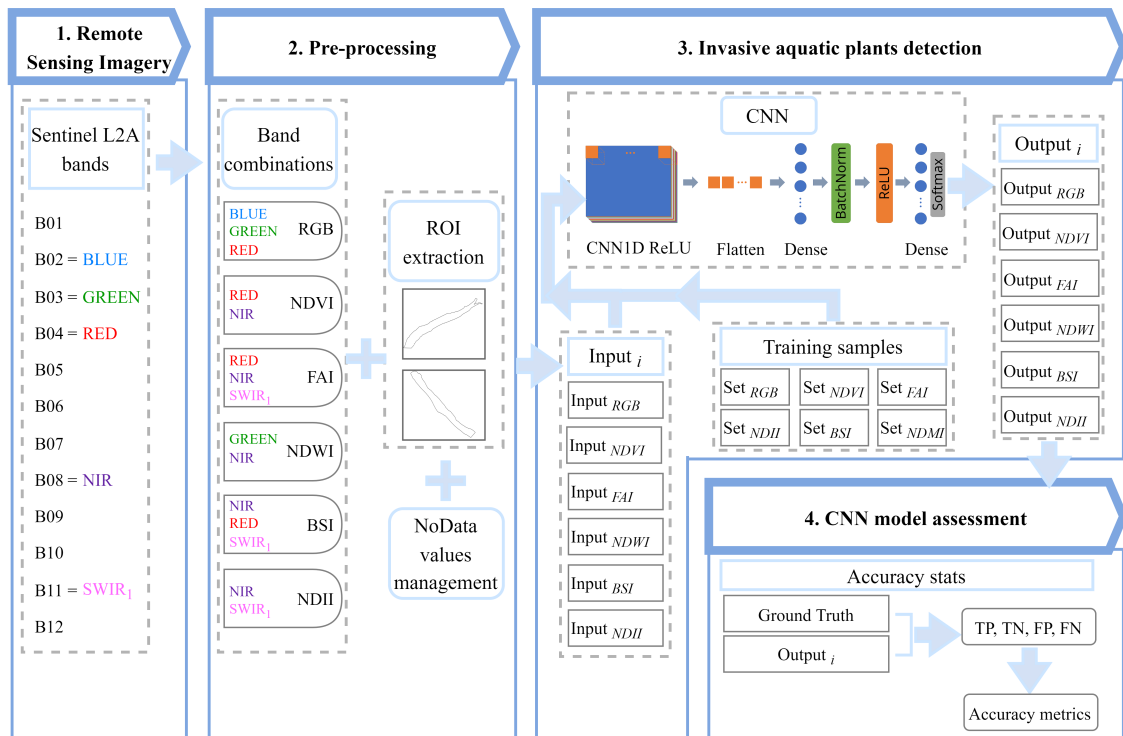


Figura 7.18: Flujo de trabajo del procedimiento de mapeado de plantas acuáticas invasoras en el río Guadiana utilizando un número reducido de las bandas espectrales ofrecidas por el satélite Sentinel-2. También se muestra la arquitectura de la CNN utilizada.

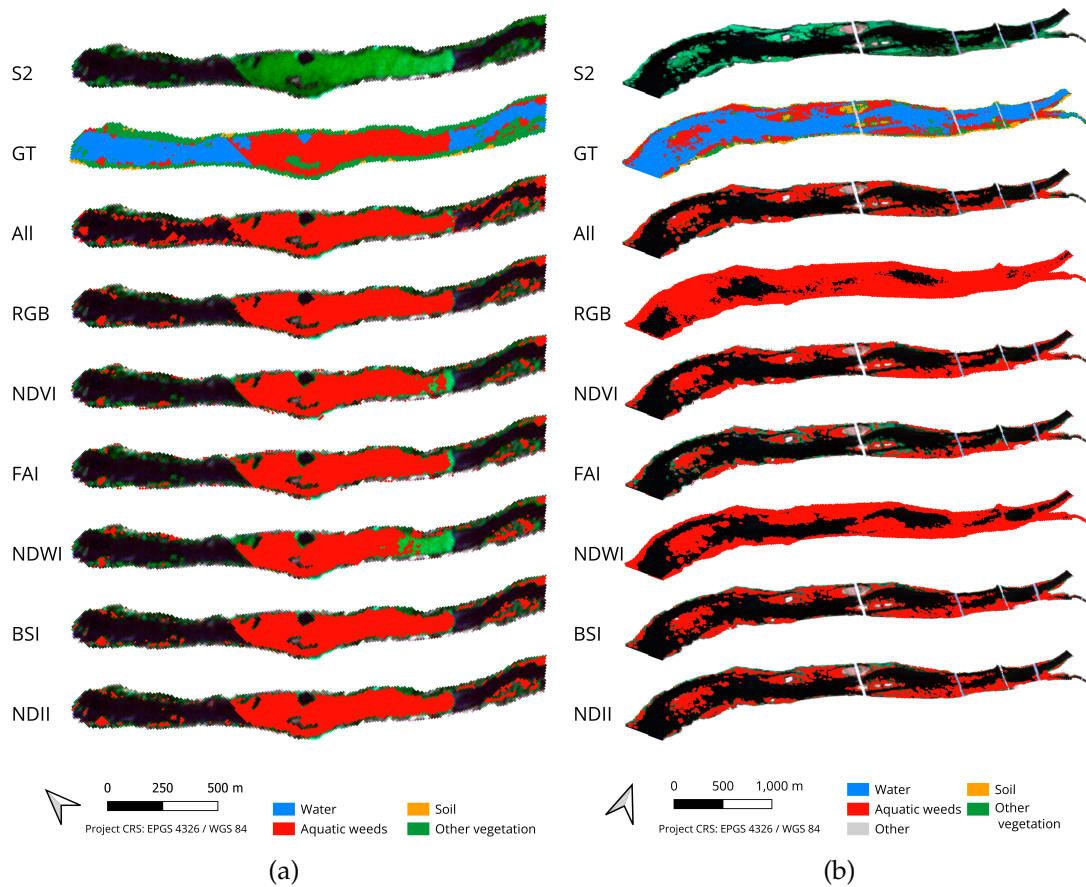


Figura 7.19: Resultados de la detección de plantas acuáticas invasoras utilizando diferentes índices para el modelo CNN: (a) Caso Badajoz. (b) Caso Mérida

7.5.4 | Mapeado de plantas invasoras acuáticas en el río Guadiana con el modelo CNN

La Fig. 7.19 muestra la detección del modelo CNN entrenado con índices espectrales y en la tabla 7.5 se muestran los resultados de las métricas de precisión de dicho modelo.

Los resultados representan una ventaja significativa respecto a trabajos anteriores, en los que la CNN se entrenaba con todas las bandas espectrales disponibles (lo que generalmente daba lugar a resultados de menor calidad a pesar de utilizar un mayor número de bandas espectrales). El índice con mejor precisión de detección depende de la métrica de evaluación que se considere, pero en general se puede concluir que la información proporcionada por los índices espectrales es más útil para el entrenamiento que los datos multispectrales brutos proporcionados por el satélite Sentinel-2.

Tabla 7.3: Evaluación del rendimiento para el caso de Mérida y el caso de Badajoz (los mejores resultados en negrita) utilizando el algoritmo CNN.

		Overall accuracy	User's accuracy	Producer's accuracy	F ₁ score
Caso Mérida	Todas las bandas	0.903	0.843	0.911	0.876
	RGB	0.933	0.892	0.935	0.913
	NDVI	0.920	0.924	0.857	0.889
	FAI	0.929	0.924	0.883	0.903
	NDWI	0.856	0.846	0.754	0.798
	BSI	0.925	0.887	0.917	0.902
	NDII	0.920	0.879	0.914	0.896
Caso Badajoz	Todas las bandas	0.779	0.784	0.901	0.839
	RGB	0.643	0.641	1.000	0.781
	NDVI	0.763	0.762	0.914	0.831
	FAI	0.691	0.813	0.669	0.734
	NDWI	0.658	0.652	0.997	0.788
	BSI	0.763	0.789	0.860	0.823
	NDII	0.746	0.795	0.811	0.803

7.5.5 | Mapeado de plantas invasoras acuáticas en el río Guadiana con el algoritmo RF

La Fig. 7.20 muestra los mapas resultantes de la utilización de RF como clasificador. En la tabla 7.4 se muestran las precisiones. A pesar de que las precisiones son también altas, son inferiores a las obtenidas con el modelo CNN. Mediante la utilización de RF como clasificador, la detección es más óptima cuando se utilizan todas las bandas proporcionadas cuando atendemos a casi todas las métricas de precisión en el caso de Badajoz (excepto con el valor de producer's accuracy para el NDWI) y muy similares en el caso de Mérida pero más altas cuando se reducen el número de bandas necesarias (como en el caso de RGB y NDVI).

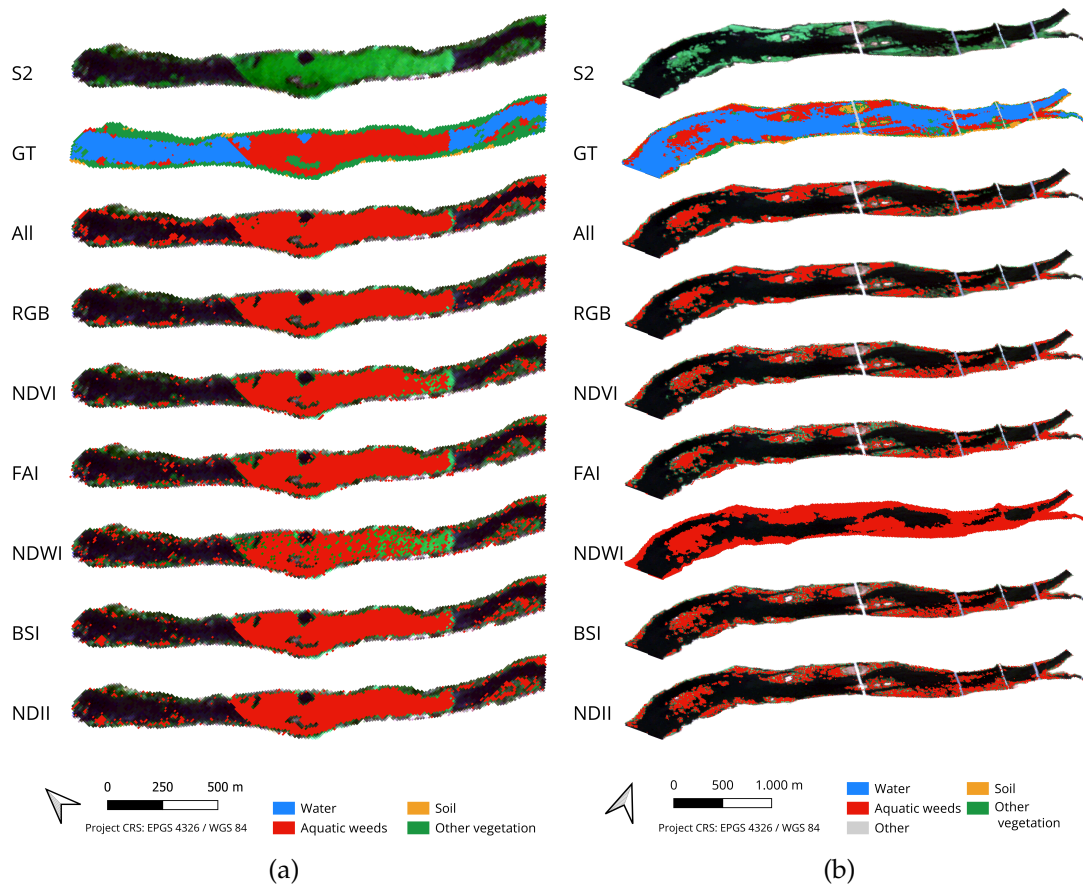


Figura 7.20: Resultados de la detección de plantas acuáticas invasoras utilizando diferentes índices con el algoritmo RF: (a) Caso Mérida. (b) Caso Badajoz.

Tabla 7.4: Evaluación del rendimiento para los casos de Mérida y Badajoz (los mejores resultados en negrita) utilizando el algoritmo RF.

		Overall accuracy	User's accuracy	Producer's accuracy	F_1 score
Caso Mérida	Todas las bandas	0.892	0.800	0.952	0.869
	RGB	0.924	0.876	0.930	0.902
	NDVI	0.900	0.877	0.855	0.866
	FAI	0.897	0.852	0.880	0.866
	NDWI	0.783	0.727	0.676	0.701
	BSI	0.909	0.857	0.910	0.883
	NDII	0.906	0.847	0.916	0.880
	Caso Badajoz	Todas las bands	0.766	0.832	0.794
RGB		0.642	0.736	0.643	0.686
NDVI		0.694	0.803	0.690	0.743
FAI		0.662	0.805	0.621	0.701
NDWI		0.658	0.652	0.997	0.788
BSI		0.703	0.802	0.710	0.753
NDII		0.702	0.791	0.724	0.756

7.6 | Mapeo de las áreas de acumulación de plantas acuáticas invasoras en una serie temporal de imágenes multiespectrales mediante modelo de aprendizaje profundo y SIG

© 2023 IEEE. Reprinted, with permission, from Elena C. Rodríguez-Garlito, Abel Paz-Gallardo and Antonio Plaza, *Mapping the Accumulation of Invasive Aquatic Plants in the Guadiana River, Spain, using Multitemporal Remote Sensing*, IEEE Geoscience and Remote Sensing Letters, - 2023

El texto completo está incluido en el apéndice Publicaciones – Mapping the Accumulation of Invasive Aquatic Plants in the Guadiana River, Spain, Using Multitemporal Remote Sensing.

7.6.1 | Resumen

Las imágenes multiespectrales son muy eficaces para la detección de diferentes tipos de cubierta terrestre. Se han obtenido resultados satisfactorios en el seguimiento de distintos tipos de tipos de cubierta vegetal mediante imágenes de satélite, incluidas las zonas conquistadas por plantas acuáticas invasoras, como el jacinto de agua. Varios países de todo el mundo están sufriendo los efectos negativos causados por la rápida propagación de estas plantas. Por ejemplo, se han llevado a cabo varias estrategias para su control en el río Guadiana (España). En este trabajo, desarrollamos una nueva metodología capaz de localizar automáticamente las zonas más frecuentes de acumulación de invasoras en el río Guadiana. Nuestra estrategia explota series temporales multiespectrales adquiridas por el satélite Sentinel-2 de la ESA. Una vez detectadas las plantas invasoras mediante deep learning (una red neuronal convolucional), se lleva a cabo un análisis posterior mediante SIG para cartografiar las zonas en las que se encuentran con mayor frecuencia las masas superficiales de jacinto de agua. De este modo, demostramos que la gestión de las plantas acuáticas invasoras en el río Guadiana puede llevarse a cabo con éxito.

7.6.2 | Contribuciones de este artículo

A continuación, se enumeran las principales contribuciones de este artículo:

1. Metodología propuesta para detectar las áreas de acumulación de plantas invasoras acuáticas en una serie temporal de imágenes de satélite Sentinel-2. A partir de un modelo CNN entrenado, se detectan las plantas en cada una de las imágenes de la serie. Por último, se explica una estrategia de análisis SIG para determinar las zonas de acumulación.
2. Mapeo de áreas de acumulación para tres series temporales así como su posterior análisis.

7.6.3 | Metodología para detectar las áreas de acumulación de plantas invasoras acuáticas en una serie temporal de imágenes de satélite

En la Fig. 7.21 se muestra el esquema de trabajo. Los pasos iniciales de esta metodología contemplan el preprocesado de datos multiespectrales. También describe la detección automática de las planta invasoras en la serie temporal analizada mediante el modelo de *deep learning*. El modelo CNN está basado en el explorado en [2] y desarrollado en [3]) para monitorear la distribución espacio-temporal en una serie temporal independientemente del estado fenológico de la planta. Además, se desarrolla un nuevo método en el que, mediante técnicas SIG, se opera con los mapas de detección (las salidas del modelo de CNN). Finalmente, mediante operaciones vectoriales y rasters se obtiene una imagen raster que muestre, en una rampa de color, las veces que se ha acumulado jacinto de agua en el periodo estudiado y para cada geolocalización. En estos mapas, cada pixel muestra el número de veces que el jacinto de agua se ha detectado en el periodo de tiempo analizado, pudiendo comprobar las áreas donde se tienden a acumular estas plantas. Con esta información, se pueden obtener estadísticas útiles para las tareas de control y gestión.

7.6.4 | Análisis de los mapas de acumulación para diferentes periodos temporales

La Fig. 7.25(a) muestra el mapa de acumulación final generado a partir de las imágenes de salida del algoritmo CNN para la serie temporal completa de 62 imágenes. Este mapa revela la geolocalización de las zonas donde las plantas acuáticas invasoras se acumulan con mayor frecuencia. Podemos ver que hay muchas zonas en las que el jacinto de agua se ha detectado repetidamente en casi todas las imágenes Sentinel-2 de la serie temporal analizada (unas 55 imágenes). Estas zonas (mostradas en color rojo oscuro) se concen-

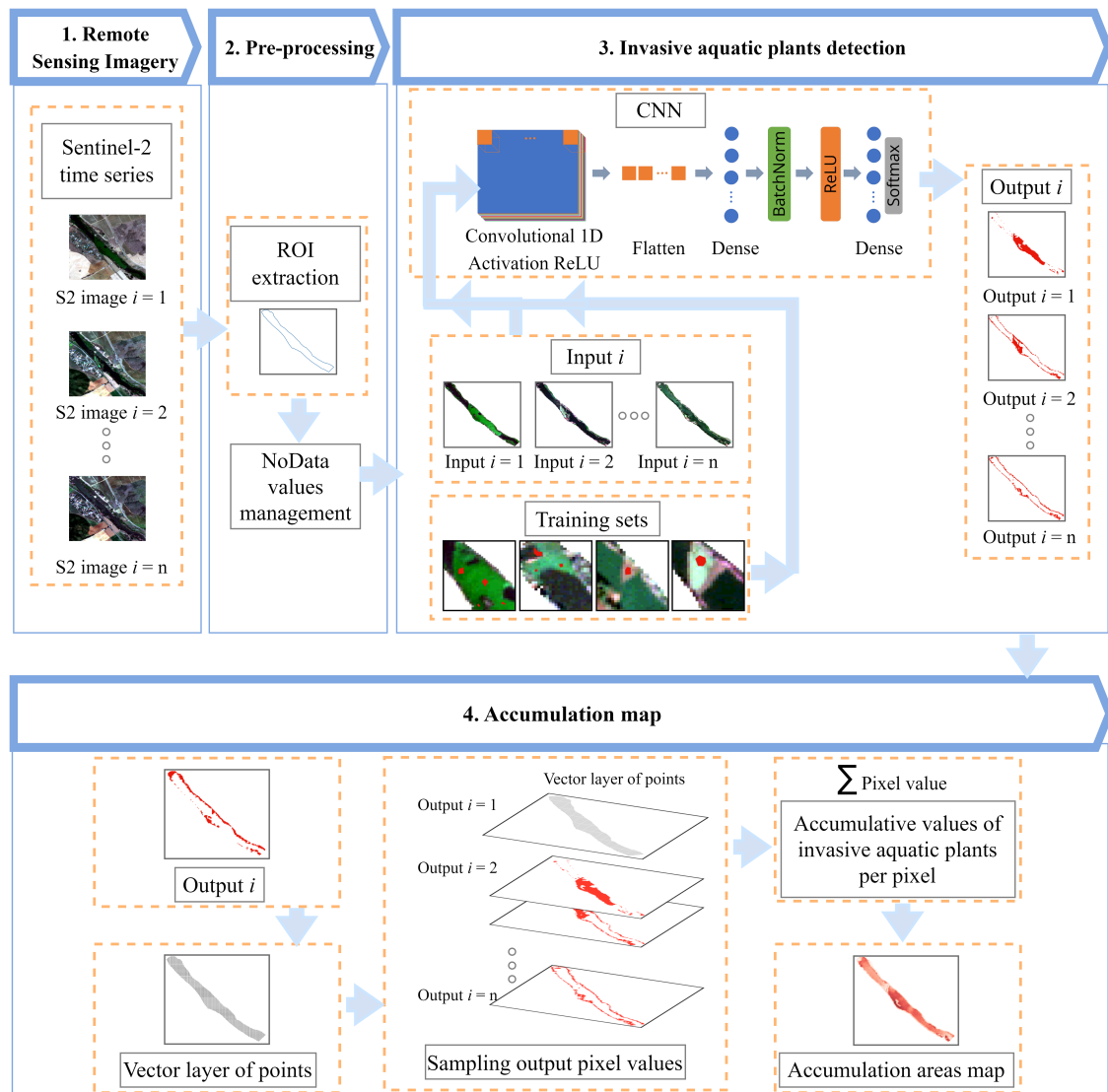


Figura 7.21: Flujo de trabajo del procedimiento de generación de mapas de acumulación de jacinto de agua en el río Guadiana.

tran sobre todo en las orillas de los ríos, en pequeñas islas y en las zonas cercanas a una barrera de contención de jacintos de agua (instalada durante el periodo estudiado). Por el contrario, las zonas en las que se ha detectado jacinto de agua en pocas imágenes de la serie temporal completa, se muestran en un color rojo más claro.

La Fig. 7.23 muestra el histograma de los resultados de acumulación de píxeles. Cada barra del histograma (también conocida como *bin* o *bucket*) representa rangos de número de imágenes (eje X). A continuación, el número de píxeles que contienen especies invasoras se muestra para cada bin en el eje Y. El gráfico de línea sobre las barras representa la estimación de la densidad del núcleo (*Kernel Density estimation (KDE)*), un método conocido de suavizado del núcleo para mostrar la forma de la distribución estadística. Este gráfico revela que, en el periodo de dos años considerado, hay un gran número de píxeles con plantas acuáticas invasoras en más de la mitad de las imágenes analizadas, alcanzando un máximo de unos 400 píxeles (10% del total) en unas 30-40 imágenes, y un mínimo de unos 50 píxeles en 55 imágenes. El histograma también muestra un valor medio de unos 200 píxeles con plantas invasoras en el periodo estudiado.

Esta metodología se repitió para el seguimiento de periodos de tiempo específicos. Por ejemplo, analizando las imágenes Sentinel-2 adquiridas entre abril y mayo de 2019 (6 imágenes), el mapa de la Fig. 7.25(b) muestra que la mayor acumulación de jacinto de agua se ha producido en las inmediaciones de la barrera de contención (como era de esperar). Por otro lado, la Fig. 7.25(c) muestra el mapa generado para el periodo de junio a agosto (verano) de 2020 (17 imágenes). Aquí, la acumulación de jacinto de agua se distribuye de manera más uniforme en toda la ROI. Esto se debe al hecho de que las plantas acuáticas invasoras están en crecimiento vegetativo, y la gran cantidad de biomasa presente en la superficie del río ha atravesado la barrera. Este último mapa revela la necesidad de eliminar las plantas acumuladas para evitar que invadan el cauce del río aguas abajo.

El enfoque propuesto proporciona conocimientos valiosos para el seguimiento y control de las plantas acuáticas invasoras. En nuestro caso concreto de estudio, la geolocalización de las zonas más frecuentes de acumulación de jacinto de agua es relevante para la posterior eliminación de la planta de la superficie del río. También puede utilizarse para predecir la ubicación de nuevas barreras de retención del jacinto de agua.

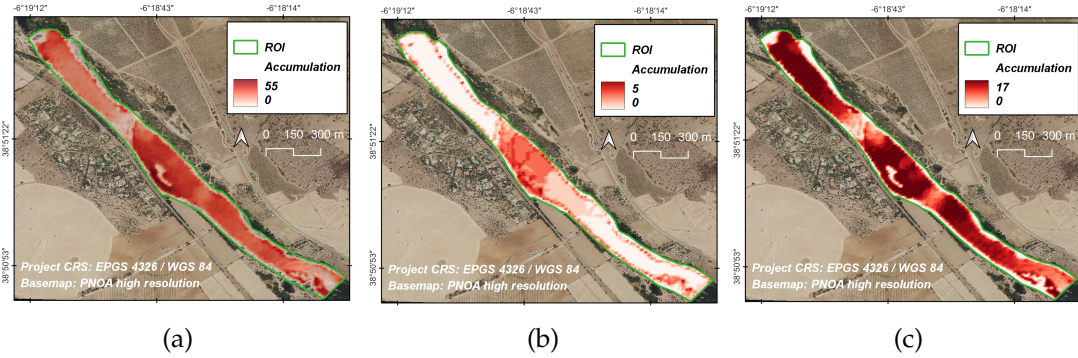


Figura 7.22: Mapas de acumulación de jacinto de agua para distintos periodos: (a) Serie temporal completa. (b) Desde 2019-04-12 hasta 2019-05-27. (c) Desde 2020-06-05 hasta 2020-08-29.

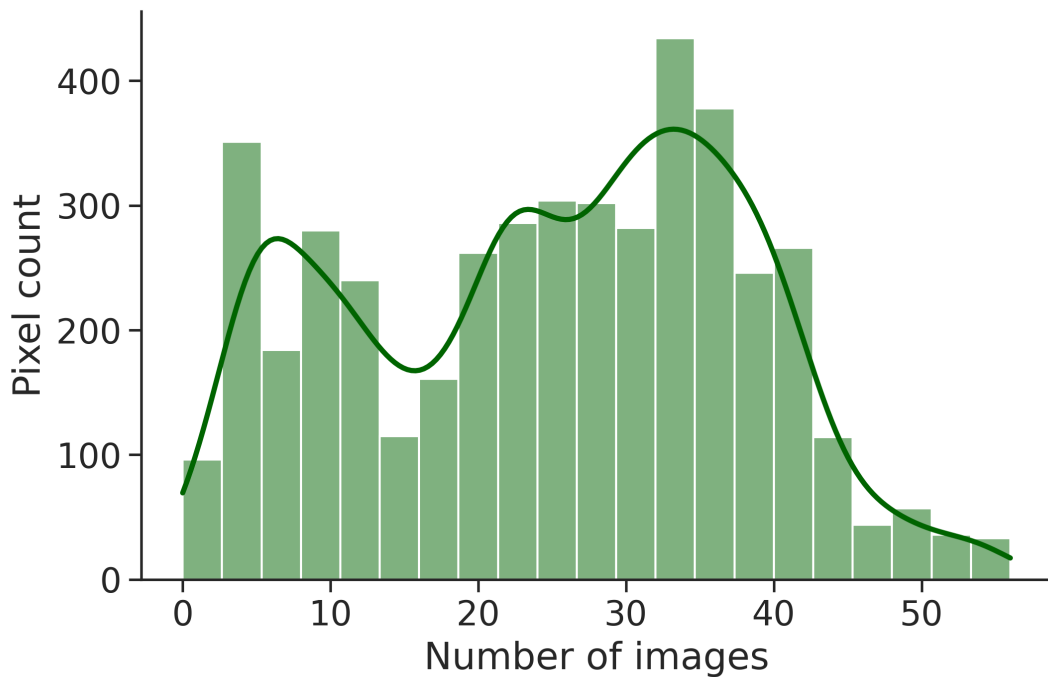


Figura 7.23: Histograma que muestra el número de píxeles detectados como jacinto de agua para la serie temporal completa.

7.7 | Comprobación del impacto de añadir la componente espacial en el modelo CNN

Adaptado del artículo pendiente de aceptación "Spectral-Spatial Mapping of Invasive Aquatic Plants in the Guadiana River, Spain, Using Convolutional Neural Networks".

7.7.1 | Resumen

Las imágenes de teledetección son cruciales para encontrar patrones espaciales y temporales en la vegetación. El río Guadiana (situado en el suroeste de España) ha sido invadido desde principios de la década de los 2000 por plantas acuáticas flotantes con una rápida capacidad de reproducción, causando efectos negativos en el ecosistema. Conocer con precisión la distribución espacio-temporal de las plantas acuáticas invasoras es importante para prevenir su propagación. Hemos explorado el uso de redes neuronales convolucionales (CNN) para cartografiar, monitorizar y analizar la distribución de plantas acuáticas invasoras, contribuyendo a las tareas de gestión. Aquí examinamos el rendimiento en la detección de plantas acuáticas invasoras de un nuevo modelo de CNN que realiza análisis de características espectrales-espaciales. Los resultados experimentales se comparan con otros modelos en los que sólo se considera como dato de entrada la información espectral de cada pixel. Nuestros resultados demuestran una mejora en la tarea de detección de plantas acuáticas invasoras cuando se añade información espacial a los datos de entrada.

7.7.2 | Contribuciones de este artículo

Las principales contribuciones de este artículo son:

1. Propuesta metodológica para detectar plantas acuáticas invasoras en imágenes de satélite adquiridas por Sentinel-2 que incluye: preprocesado (con extracción de ROI, con tratamiento de valores *NoData*, con relleno (o *padding*) del tipo reflejo, extracción de *patches*), procesado de la imagen utilizando una nueva arquitectura CNN2D así como la evaluación del modelo.
2. Mapeado automático de dos ROI afectados por plantas invasoras acuáticas mediante el modelo CNN2D propuesto, así como evaluación cualitativa y cuantitativa de los resultados.
3. Comparación de los resultados de detección de plantas acuáticas invasoras para los modelos CNN2D propuesto y CNN1D propuesto en los trabajos previos.

7.7.3 | Estrategia metodológica propuesta

Propuesta metodológica para detectar plantas acuáticas invasoras en imágenes de satélite adquiridas por Sentinel-2 que incluye: preprocesado (con extracción de ROI, con tratamiento de valores *NoData*, con relleno (o *padding*) del tipo reflejo, extracción de *patches*), procesado de la imagen utilizando una nueva arquitectura CNN2D así como la evaluación del modelo

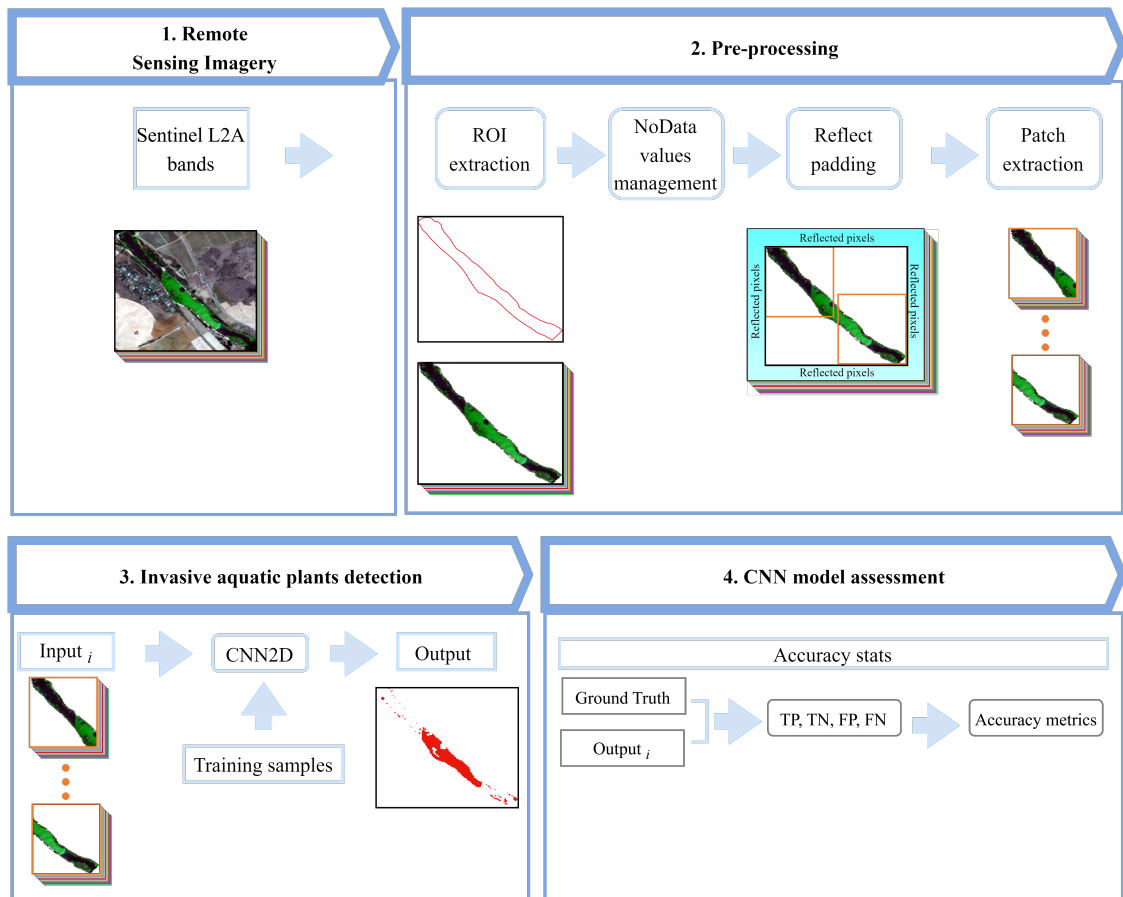


Figura 7.24: Flujo de trabajo del procedimiento de mapeo de plantas acuáticas invasoras en el río Guadiana utilizando el modelo CNN2D.

7.7.4 | Mapeo de plantas acuáticas invasoras con CNN2D en dos ROI

Las Fig. 7.25(a) y 7.25(b) ilustran los resultados de detección de plantas invasoras para el caso de Mérida y para el caso de Badajoz, respectivamente. En concreto, se muestran

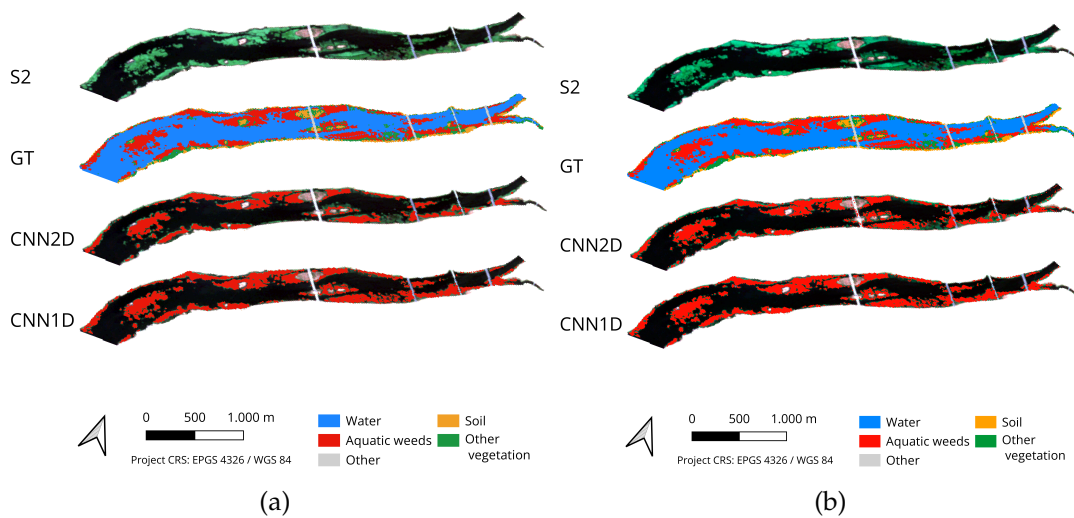


Figura 7.25: Resultados de detección de plantas acuáticas invasoras usando los modelos CNN2D y CNN1D para: (a) Caso Mérida. (b) Caso Badajoz.

los resultados del desarrollo de la nueva CNN2D propuesta donde los píxeles que contienen plantas invasoras de la imagen de salida de cada modelo aparecen en color rojo, sobre la capa base Sentinel-2. También se muestran los resultados visuales del rendimiento del modelo CNN1D, cuya arquitectura fue propuesta y desarrollada en nuestro trabajo anterior. Además, para cada ROI, se ilustran la imagen en color real de Sentinel-2 (S2), la imagen en color real (GT) y los resultados de los modelos.

Centrándonos en los resultados del nuevo modelo CNN2D propuesto en este trabajo, observamos que la detección del jacinto de agua en el caso de Mérida y del nenúfar en el caso de Badajoz es visualmente muy precisa cuando se compara con la imagen GT. Este modelo ha procesado eficazmente los datos espectrales y espectrales proporcionados dentro de cada ventana de píxeles (o *patch*, capturando las complejas relaciones entre píxeles vecinos y sus valores espectrales. En el caso de Mérida, el buen uso de la información espacial-espectral combinada se refleja en la correcta identificación de la gran masa flotante de jacinto de agua que ocupa aproximadamente el centro de la imagen, por ejemplo. También se han identificado los píxeles de jacinto de agua presentes en las orillas del río y los que están rodeados de otro tipo de vegetación. Los resultados de detección en el caso de Badajoz son una prueba más del robusto rendimiento del modelo CNN2D y de su capacidad para distinguir la clase de planta invasora de otras clases presentes en la escena. Esto se refleja en la correcta detección de masas con contornos irregulares rodeadas de agua, así como masas de plantas invasoras que limitan con otras clases como otro tipo de vegetación.

7.7.5 | Comparación de las actuaciones del modelo CNN2D con el modelo CNN1D para mapear plantas acuáticas invasoras

Basándose en las métricas reflejadas en la tabla 7.5, CNN2D obtiene en general mejores resultados que el modelo CNN1D en las imágenes multiespectrales evaluadas. CNN2D muestra una mayor precisión global, precisión del usuario y puntuación F1 en ambas imágenes, lo que indica un mejor rendimiento a la hora de clasificar con precisión las plantas acuáticas invasoras. Aunque el resultado del modelo CNN1D muestra resultados más altos en términos de precisión del productor que el modelo CNN2D, ambos valores son muy similares. Por lo tanto, la adición del componente espacial a los datos espectrales de los datos de entrada es favorable para detectar plantas acuáticas invasoras.

Tabla 7.5: Evaluación del rendimiento para el caso de Mérida y el caso de Badajoz utilizando la CNN1D y la CNN2D

		Overall accuracy	User's accuracy	Producer's accuracy	F_1 score
Mérida Case	CNN2D	0.9592	0.9381	0.9548	0.9464
	CNN1D	0.903	0.843	0.911	0.876
Badajoz Case	CNN2D	0.9198	0.8651	0.8228	0.8434
	CNN1D	0.9013	0.7839	0.8592	0.8198

Conclusiones finales

Los resultados de esta Tesis Doctoral han contribuido en la detección, monitorización y análisis de la presencia de especies exóticas invasoras como el jacinto de agua y el nenúfar mexicano, presentes en el río Guadiana (suroeste de España). Con las investigaciones desarrolladas, que aplican técnicas de teledetección, técnicas de aprendizaje automático y aprendizaje profundo, y técnicas SIG, se obtienen las conclusiones que se detallan a continuación:

1. La estrategia propuesta y desarrollada de procesamiento automático de ventanas para cartografiar grandes áreas en imágenes de alta resolución, como las imágenes agro obtenidas mediante el vuelo de un dron sobre olivos en la región de Extremadura (España), hace factible la utilización de algoritmos de clasificación de aprendizaje automático y profundo para el procesamiento de imágenes multispectrales computacionalmente pesadas.
2. La metodología propuesta y desarrollada que comprende etapas de preprocesamiento, procesamiento (mediante un modelo de CNN1D) y evaluación, demuestran la factibilidad de geolocalizar automáticamente, con precisión alta, las especies invasoras (camalote y nenúfar mexicano) presentes en el río Guadiana.
3. La monitorización espacio-temporal de especies exóticas invasoras como el jacinto de agua se puede llevar a cabo cada pocos días mediante imágenes gratuitas (5 días en el caso de las recogidas por el satélite Sentinel-2 de la ESA). Mediante el entrenamiento adecuado de un modelo predictivo de aprendizaje profundo (CNN1D) se puede conseguir, con escasas muestras de entrenamiento pertenecientes a un número reducido de imágenes, la detección de las plantas acuáticas invasoras en cualquier estado de su ciclo fenológico.

4. El entrenamiento del modelo predictivo CNN1D, basado en combinaciones de bandas o índices, representa ventajas significativas en términos de eficiencia y eficacia computacional frente a la utilización de las 12 bandas, ofrecidas por el producto S2L2A de Sentinel-2.
5. La metodología ofrecida y aplicada para mapear la acumulación de plantas invasoras, detectadas mediante modelos de CNN en una serie temporal de imágenes multiespectrales, proporciona información útil de análisis que simplifican las tareas de control de la propagación de estas plantas.
6. La metodología propuesta y desarrollada, que comprende etapas de preprocesamiento, procesamiento (mediante modelos de CNN que tienen en cuenta la información espacial y espectral de los píxeles que se predicen) y evaluación, demuestran el impacto positivo en la mejora de las precisiones frente a modelos CNN que únicamente tienen en cuenta la información espectral de cada pixel.

Con las contribuciones de esta Tesis Doctoral se ha comenzado una línea de trabajo para gestionar la problemática de las plantas acuáticas invasoras en cuerpos de agua dulce, como en el río Guadiana, mediante la aplicación de inteligencia artificial para la detección automática sobre imágenes obtenidas de forma remota, gratuitas, obtenidas por el satélite Sentinel-2 de la ESA. En futuros estudios, pueden considerarse otras imágenes teledetectadas, de alta resolución espacial, comerciales. También, pueden considerarse otros modelos de aprendizaje profundo. Además, se contempla seguir explotando la información de series temporales de imágenes multiespectrales mediante la utilización de modelos CNN3D para la monitorización de estas plantas en imágenes de satélite. Del mismo modo, se considera la explotación de secuencia de imágenes de satélite mediante modelos de redes neuronales recurrentes (*Recurrent Neural Network (RNN)*) para aprender patrones del pasado en series temporales y realizar predicciones futuras.

Bibliografía

- [1] E. C. Rodríguez-Garlito and A. Paz-Gallardo, "Efficiently mapping large areas of olive trees using drones in Extremadura, Spain," *IEEE Journal on Miniaturization for Air and Space Systems*, vol. 2, pp. 148–156, 3 2021.
- [2] E. C. Rodríguez-Garlito, A. Paz-Gallardo, and A. Plaza, "Automatic detection of aquatic weeds: A case study in the Guadiana River, Spain," *IEEE Journal of Selected Topics in Applied Earth Observations and Remote Sensing*, vol. 15, pp. 8567–8585, 2022.
- [3] —, "Monitoring the spatiotemporal distribution of invasive aquatic plants in the Guadiana river, Spain," *IEEE Journal of Selected Topics in Applied Earth Observations and Remote Sensing*, vol. 16, pp. 228–241, 2022.
- [4] —, "Mapping invasive aquatic plants in sentinel-2 images using convolutional neural networks trained with spectral indices," *IEEE Journal of Selected Topics in Applied Earth Observations and Remote Sensing*, vol. 16, pp. 2889–2899, 2023.
- [5] —, "Mapping the accumulation of invasive aquatic plants in the Guadiana river, Spain, using multitemporal remote sensing," *IEEE Geoscience and Remote Sensing Letters*, vol. 20, pp. 1–5, 2023.
- [6] —, "Spectral-spatial mapping of invasive aquatic plants in the Guadiana river, Spain, using convolutional neural networks," vol. En revisión, pp.–, 2023.
- [7] V. H. Smith and D. W. Schindler, "Eutrophication science: where do we go from here?" *Trends in Ecology & Evolution*, vol. 24, pp. 201–207, 4 2009.
- [8] R. G. Hartzler and D. D. Buhler, *Ecological management of agricultural weeds*, 2001.
- [9] S. Patel, *Threats, management and envisaged utilizations of aquatic weed Eichhornia crassipes: an overview*. Springer, 7 2012, vol. 11.
- [10] A. M. Villamagna and B. R. Murphy, "Ecological and socio-economic impacts of invasive water hyacinth (*Eichhornia crassipes*): A review," *Freshwater Biology*, vol. 55, pp. 282–298, 2010.

- [11] K. H. Thamaga and T. Dube, "Remote sensing of invasive water hyacinth (*Eichhornia crassipes*): A review on applications and challenges," *Remote Sensing Applications: Society and Environment*, vol. 10, pp. 36–46, 2018.
- [12] B. Gopal, *Water hyacinth. (Aquatic Plant Studies 1)*. Cambridge University Press, 1987.
- [13] Y. Ghoussein, H. Nicolas, J. Haury, A. Fadel, P. Pichelin, H. A. Hamdan, and G. Faour, "Multitemporal remote sensing based on an FVC reference period using Sentinel-2 for monitoring *Eichhornia crassipes* on a Mediterranean River," *Remote Sensing*, vol. 11, p. 1856, 2019.
- [14] A. Malik, "Environmental challenge vis a vis opportunity: The case of water hyacinth," *Environment International*, vol. 33, pp. 122–138, 2007.
- [15] N. Jafari, "Ecological and socio-economic utilization of water hyacinth (*Eichhornia crassipes* Mart Solms)," *Journal of Applied Sciences and Environmental Management*, vol. 14, 8 2010.
- [16] Q. Mahmood, P. Zheng, E. Islam, Y. Hayat, M. J. Hassan, G. Jilani, and R. C. Jin, "Lab scale studies on water hyacinth (*Eichhornia crassipes* Mart Solms) for biotreatment of textile wastewater," *Caspian Journal of Environmental Sciences Caspian J. Env. Sci*, vol. 3, 2005.
- [17] A. Mary Lissy P N and G. Madhu, "Removal of heavy metals from waste water using water hyacinth," *ACEEE Int. J. on Transportation and Urban Development*, vol. 01, 2011.
- [18] J. Lu, Z. Fu, and Z. Yin, "Performance of a water hyacinth (*Eichhornia crassipes*) system in the treatment of wastewater from a duck farm and the effects of using water hyacinth as duck feed," *Journal of Environmental Sciences*, vol. 20, pp. 513–519, 2008.
- [19] P. Saha, O. Shinde, and S. Sarkar, "Phytoremediation of industrial mines wastewater using water hyacinth," *International Journal of Phytoremediation*, vol. 19, pp. 87–96, 1 2017.
- [20] W. H. Ting, I. A. Tan, S. F. Salleh, and N. A. Wahab, "Application of water hyacinth (*Eichhornia crassipes*) for phytoremediation of ammoniacal nitrogen: A review," *Journal of Water Process Engineering*, vol. 22, pp. 239–249, 4 2018.
- [21] G. K. Gaurav, T. Mehmood, L. Cheng, J. J. Klemeš, and D. K. Shrivastava, "Water hyacinth as a biomass: A review," *Journal of Cleaner Production*, vol. 277, 12 2020.
- [22] F. Li, X. He, A. Srishti, S. Song, H. T. W. Tan, D. J. Sweeney, S. Ghosh, and C. H. Wang, "Water hyacinth for energy and environmental applications: A review," *Bioresource Technology*, vol. 327, 5 2021.
- [23] A. Salas-Ruiz and M. del Mar Barbero-Barrera, "Performance assessment of water hyacinth–cement composite," *Construction and Building Materials*, vol. 211, pp. 395–407, 6 2019.
- [24] N. Merry M. Mitan, "Water hyacinth: Potential and threat," vol. 19. Elsevier Ltd, 2019, pp. 1408–1412.
- [25] A. A. Adelodun, U. O. Hassan, and V. O. Nwachuckwu, "Environmental, mechanical, and biochemical benefits of water hyacinth (*Eichhornia crassipes*)," *Environmental Science and Pollution Research* 2020 27:24, vol. 27, pp. 30 210–30 221, 5 2020.

- [26] "Global Invasive Species Database." [Online]. Available: http://www.iucngisd.org/gisd/100_worst.php
- [27] "Dynamism and abundance of water hyacinth in the Winam Gulf of Lake Victoria: Evidence from remote sensing and seasonal-climate data," *International Journal of Environmental Studies*, vol. 62, pp. 449–465, 8 2005.
- [28] C. Perna and D. Burrows, "Improved dissolved oxygen status following removal of exotic weed mats in important fish habitat lagoons of the tropical Burdekin River floodplain, Australia," vol. 51, 2005, pp. 138–148.
- [29] V. D. Tobias, J. L. Conrad, B. Mahardja, and S. Khanna, "Impacts of water hyacinth treatment on water quality in a tidal estuarine environment," *Biological Invasions*, vol. 21, pp. 3479–3490, 12 2019.
- [30] A. M. Villamagna and B. R. Murphy, "Ecological and socio-economic impacts of invasive water hyacinth (*Eichhornia crassipes*): A review," *Freshwater Biology*, vol. 55, pp. 282–298, 2010.
- [31] Z. H. Zhang and J. Y. Guo, "Biology of water hyacinth," 2017.
- [32] "Centre for Agricultural Bioscience International - eichhornia crassipes (water hyacinth)." [Online]. Available: <https://www.cabi.org/isc/datasheet/20544#tosummaryOffInvasiveness>
- [33] T. R. Téllez, E. M. de Rodrigo López, G. L. Granado, E. A. Pérez, R. M. López, and J. M. S. Guzmán, "The water hyacinth, *Eichhornia crassipes*: An invasive plant in the Guadiana River Basin (Spain)," *Aquatic Invasions*, vol. 3, pp. 42–53, 2008.
- [34] E. P. Albano and D. T. R. Téllez, "Reproducción sexual del jacinto de agua (*Eichhornia crassipes*): germinación, anatomía y banco de semillas."
- [35] E. A. Pérez, T. R. Téllez, S. R. Maqueda, P. J. Linares, F. M. Pardo, P. L. Medina, J. L. Moreno, F. L. Gallego, J. G. Cortés, and J. M. Guzmán, "Seed germination and risks of using the invasive plant *Eichhornia crassipes* (Mart.) Solms-Laub. (water hyacinth) for composting, ovine feeding and biogas production," *Acta Botanica Gallica*, vol. 162, pp. 203–214, 7 2015.
- [36] "www.chguadiana.es," Último acceso: 26 de febrero de 2023. [Online]. Available: <https://www.chguadiana.es/>
- [37] J. A. Coetsee, M. P. Hill, T. Ruiz-Téllez, U. Starfinger, and S. Brunel, "Monographs on invasive plants in europe n° 2: *Eichhornia crassipes* (Mart.) Solms," *Botany Letters*, vol. 164, pp. 303–326, 2017.
- [38] A. Rodríguez-Merino, P. García-Murillo, S. Cirujano, and R. Fernández-Zamudio, "Predicting the risk of aquatic plant invasions in europe: How climatic factors and anthropogenic activity influence potential species distributions," *Journal for Nature Conservation*, vol. 45, pp. 58–71, 2018.
- [39] F. MT Aguiar and Ferreira, "Plant invasions in the rivers of the Iberian Peninsula, south-western Europe: A review," *Plant Biosystems-An International Journal Dealing with all Aspects of Plant Biology*, vol. 147, pp. 1107–1119, 2013.
- [40] V. Mozaffarian and B. Yaghoubi, "New record of *Eichhornia crassipes* (waterhyacinth) from north of Iran," *Rostaniha*, vol. 16, pp. 208–209, 2015.

- [41] J. Caudill, J. D. Madsen, W. Pratt, and C. Llp, "Operational aquatic weed management in the California Sacramento-San Joaquin River Delta," *Journal of Aquatic Plant Management*, vol. 59, pp. 2–15, 2021.
- [42] E. V. Wyk and B. W. V. Wilgen, "The cost of water hyacinth control in South Africa: a case study of three options," *African Journal of Aquatic Science*, vol. 27, pp. 141–149, 1 2002.
- [43] B. Greenfield, M. Blankinship, and T. McNabb, "Control costs, operation, and permitting issues for non-chemical plant control: case studies in the San Francisco Bay-Delta Region, California," *Journal of Aquatic Plant Management*, vol. 44, pp. 40–49, 2006.
- [44] B. K. Greenfield, G. S. Siemering, J. C. Andrews, M. Rajan, S. P. Andrews, and D. F. Spencer, "Mechanical shredding of water hyacinth (*Eichhornia crassipes*): Effects on water quality in the Sacramento-San Joaquin River Delta, California," *Estuaries and Coasts*, vol. 30, pp. 627–640, 2007.
- [45] "index @ www.invasep.eu," Último acceso: 26 de febrero de 2023. [Online]. Available: <http://www.invasep.eu/>
- [46] "index @ camaloteaceca.eu," Último acceso: 26 de febrero de 2023. [Online]. Available: https://camaloteaceca.eu/?page_id=620&lang=en
- [47] M. P. Hill and J. A. Coetzee, "Integrated control of water hyacinth in Africa 1," *EPPO bulletin*, vol. 38, pp. 452–457, 2008.
- [48] J. jun Chu, Y. Ding, and Q. jia Zhuang, "Invasion and control of water hyacinth (*Eichhornia crassipes*) in China," *Journal of Zhejiang University. Science. B.*, vol. 7, pp. 623–626, 2006.
- [49] N. J. Waltham and S. Fixler, "Aerial herbicide spray to control invasive water hyacinth (*Eichhornia crassipes*): Water quality concerns fronting fish occupying a tropical floodplain wetland," *Tropical Conservation Science*, vol. 10, 12 2017.
- [50] M. H. Julien, "Biological control of water hyacinth with arthropods: a review to 2000," 2000.
- [51] J. A. Coetzee and M. P. Hill, "The role of eutrophication in the biological control of water hyacinth, *Eichhornia crassipes*, in South Africa," pp. 247–261, 4 2012.
- [52] L. A. Wainger, N. E. Harms, C. Magen, D. Liang, G. M. Nesslage, A. M. McMurray, and A. F. Cofrancesco, "Evidence-based economic analysis demonstrates that ecosystem service benefits of water hyacinth management greatly exceed research and control costs," *PeerJ*, vol. 6, 2018.
- [53] R. Gerardo and I. P. D. Lima, "Assessing the potential of Sentinel-2 data for tracking invasive water hyacinth in a river branch," *Journal of Applied Remote Sensing*, vol. 16, 2022.
- [54] Y. Ghoussein, H. Nicolas, J. Haury, A. Fadel, P. Pichelin, H. A. Hamdan, and G. Faour, "Multitemporal remote sensing based on an FVC reference period using Sentinel-2 for monitoring *Eichhornia crassipes* on a Mediterranean river," *Remote Sensing*, vol. 11, 2019.
- [55] B. Song and K. Park, "Detection of aquatic plants using multispectral UAV imagery and vegetation index," *Remote Sensing*, vol. 12, 2020.

- [56] D. Bubenheim, V. Genovese, J. D. Madsen, and E. Hard, "Remote sensing and mapping of floating aquatic vegetation in the Sacramento – San Joaquin River Delta," *J. Aquat. Plant Manage*, pp. 46–54, 2021.
- [57] D. Xu, Y. Pu, M. Zhu, Z. Luan, and K. Shi, "Automatic detection of algal blooms using Sentinel-2 MSI and Landsat OLI images," *IEEE Journal of Selected Topics in Applied Earth Observations and Remote Sensing*, vol. 14, pp. 8497–8511, 2021.
- [58] G. Singh, C. Reynolds, M. Byrne, and B. Rosman, "A remote sensing method to monitor water, aquatic vegetation, and invasive water hyacinth at national extents," *Remote Sensing*, vol. 12, pp. 1–24, 12 2020.
- [59] C. Ade, S. Khanna, M. Lay, S. L. Ustin, and E. L. Hestir, "Genus-level mapping of invasive floating aquatic vegetation using Sentinel-2 satellite remote sensing," *Remote Sensing*, vol. 14, p. 3013, 6 2022.
- [60] Z. Qiu, D. Mao, K. Feng, M. Wang, H. Xiang, and Z. Wang, "High-resolution mapping changes in the invasion of *Spartina Alterniflora* in the Yellow River Delta," *IEEE Journal of Selected Topics in Applied Earth Observations and Remote Sensing*, vol. 15, pp. 6445–6455, 2022.
- [61] E. K. Cheruiyot, C. Mito, M. Menenti, B. Gorte, R. Koenders, and N. Akdim, "Evaluating MERIS-based aquatic vegetation mapping in Lake Victoria," *Remote Sensing*, vol. 6, pp. 7762–7782, 2014.
- [62] M. Schmidt, "Monitoring aquatic weeds in a river system using SPOT 5 satellite imagery," *Journal of Applied Remote Sensing*, vol. 4, p. 043528, 2010.
- [63] E. L. Hestir, S. Khanna, M. E. Andrew, M. J. Santos, J. H. Viers, J. A. Greenberg, S. S. Rajapakse, and S. L. Ustin, "Identification of invasive vegetation using hyperspectral remote sensing in the California Delta ecosystem," *Remote Sensing of Environment*, vol. 112, pp. 4034–4047, 2008.
- [64] K. J. Sheffield, D. Clements, D. J. Clune, A. Constantine, and T. M. Dugdale, "Detection of aquatic alligator weed (*Alternanthera philoxeroides*) from aerial imagery using random forest classification," *Remote Sensing*, vol. 14, 2022.
- [65] V. Akbari, M. Simpson, S. Maharaj, A. Marino, D. Bhowmik, G. N. Prabhu, S. Rupavatharam, A. Datta, A. Kleczkowski, and J. R. Sujeetha, "Monitoring aquatic weeds in indian wetlands using multi-temporal remote sensing data with machine learning techniques," *International Geoscience and Remote Sensing Symposium (IGARSS)*, vol. 2021-July, pp. 6847–6850, 2021.
- [66] C. Nyamekye, S. A. Ofori, R. Arthur, G. Osei, L. B. Appiah, S. Kwofie, B. Ghansah, and D. Bryniok, "Evaluating the spatial and temporal variations of aquatic weeds (biomass) on Lower Volta River using multi-sensor Landsat images and machine learning," *Heliyon*, vol. 7, 2021.
- [67] M. E. Paoletti, J. M. Haut, J. Plaza, and A. Plaza, "A new deep convolutional neural network for fast hyperspectral image classification," *ISPRS Journal of Photogrammetry and Remote Sensing*, vol. 145, pp. 120–147, 2018.
- [68] T. Kattenborn, J. Leitloff, F. Schiefer, and S. Hinz, "Review on convolutional neural networks (CNN) in vegetation remote sensing," *ISPRS Journal of Photogrammetry and Remote Sensing*, vol. 173, pp. 24–49, 3 2021.

- [69] H. Li, J. Lu, G. Tian, H. Yang, J. Zhao, and N. Li, "Crop classification based on GDSSM-CNN using multi-temporal RADARSAT-2 SAR with limited labeled data," *Remote Sensing*, vol. 14, 8 2022.
- [70] G. Fontanelli, A. Lapini, L. Santurri, S. Pettinato, E. Santi, G. Ramat, S. Pilia, F. Baroni, D. Tapete, F. Cigna, and S. Paloscia, "Early-season crop mapping on an agricultural area in Italy using x-band dual-polarization SAR satellite data and convolutional neural networks," *IEEE Journal of Selected Topics in Applied Earth Observations and Remote Sensing*, vol. 15, pp. 6789–6803, 2022.
- [71] H. Zhao, Z. Chen, H. Jiang, W. Jing, L. Sun, and M. Feng, "Evaluation of three deep learning models for early crop classification using Sentinel-1A imagery time series—a case study in Zhanjiang, China," *Remote Sensing*, vol. 11, 11 2019.
- [72] C. Liao, J. Wang, Q. Xie, A. A. Baz, X. Huang, J. Shang, and Y. He, "Synergistic use of multi-temporal RADARSAT-2 and VEN μ S data for crop classification based on 1d convolutional neural network," *Remote Sensing*, vol. 12, 3 2020.
- [73] H. Zhao, S. Duan, J. Liu, L. Sun, and L. Reymondin, "Evaluation of five deep learning models for crop type mapping using Sentinel-2 time series images with missing information," *Remote Sensing*, vol. 13, 7 2021.
- [74] X. Wang, J. Zhang, L. Xun, J. Wang, Z. Wu, M. Henchiri, S. Zhang, S. Zhang, Y. Bai, S. Yang, S. Li, and X. Yu, "Evaluating the effectiveness of machine learning and deep learning models combined time-series satellite data for multiple crop types classification over a large-scale region," *Remote Sensing*, vol. 14, 5 2022.
- [75] D. Spiller, L. Ansalone, F. Carotenuto, and P. P. Mathieu, "Crop type mapping using PRISMA hyperspectral images and one-dimensional convolutional neural network," in *International Geoscience and Remote Sensing Symposium (IGARSS)*. Institute of Electrical and Electronics Engineers Inc., 2021, pp. 8166–8169.
- [76] D. Guidici and M. L. Clark, "One-dimensional convolutional neural network land-cover classification of multi-seasonal hyperspectral imagery in the San Francisco Bay area, California," *Remote Sensing*, vol. 9, 6 2017.
- [77] W. Yang, T. Nigon, Z. Hao, G. D. Paiao, F. G. Fernández, D. Mulla, and C. Yang, "Estimation of corn yield based on hyperspectral imagery and convolutional neural network," *Computers and Electronics in Agriculture*, vol. 184, 5 2021.
- [78] K. Nogueira, J. A. D. Santos, N. Menini, T. S. F. Silva, P. C. Morellato, R. Da, and S. Torres, "Spatio-temporal vegetation pixel classification by using convolutional networks," *IEEE Geoscience and Remote Sensing Letters*, vol. 16, pp. 1665–1669, 2019.
- [79] F. H. Wagner, A. Sanchez, Y. Tarabalka, R. G. Lotte, M. P. Ferreira, M. P. Aïdar, E. Gloor, O. L. Phillips, and L. E. Aragão, "Using the u-net convolutional network to map forest types and disturbance in the Atlantic rainforest with very high resolution images," *Remote Sensing in Ecology and Conservation*, vol. 5, pp. 360–375, 12 2019.
- [80] T. Kattenborn, J. Eichel, S. Wisser, L. Burrows, F. E. Fassnacht, and S. Schmidtlein, "Convolutional neural networks accurately predict cover fractions of plant species and communities in unmanned aerial vehicle imagery," *Remote Sensing in Ecology and Conservation*, vol. 6, pp. 472–486, 12 2020.

- [81] B. G. Weinstein, S. Marconi, S. Bohlman, A. Zare, and E. White, "Individual tree-crown detection in rgb imagery using semi-supervised deep learning neural networks," *Remote Sensing*, vol. 11, 6 2019.
- [82] W. Pi, J. Du, Y. Bi, X. Gao, and X. Zhu, "3D-CNN based UAV hyperspectral imagery for grassland degradation indicator ground object classification research," *Ecological Informatics*, vol. 62, 5 2021.
- [83] M. A. Ghazal, A. Mahmoud, A. Aslantas, A. Soliman, A. Shalaby, J. A. Benediktsson, and A. El-Baz, "Vegetation cover estimation using convolutional neural networks," *IEEE Access*, vol. 7, pp. 132 563–132 576, 2019.
- [84] D. Ibanez, R. Fernandez-Beltran, F. Pla, and N. Yokoya, "DAT-CNN: Dual attention temporal CNN for time-resolving Sentinel-3 vegetation indices," *IEEE Journal of Selected Topics in Applied Earth Observations and Remote Sensing*, vol. 15, pp. 2632–2643, 2022.
- [85] S. Ji, C. Zhang, A. Xu, Y. Shi, and Y. Duan, "3D convolutional neural networks for crop classification with multi-temporal remote sensing images," *Remote Sensing*, vol. 10, 1 2018.
- [86] B. Zhang, L. Zhao, and X. Zhang, "Three-dimensional convolutional neural network model for tree species classification using airborne hyperspectral images," *Remote Sensing of Environment*, vol. 247, 9 2020.
- [87] A. Plaza, J. Plaza, A. Paz, and S. Sanchez, "Parallel hyperspectral image and signal processing [applications corner]," *IEEE Signal Processing Magazine*, vol. 28, pp. 119–126, 2011.
- [88] E. Kroupi, M. Kesa, V. D. Navarro-Sánchez, S. Saeed, C. Pelloquin, B. Alhaddad, L. Moreno, A. Soria-Frisch, and G. Ruffini, "Deep convolutional neural networks for land-cover classification with Sentinel-2 images," <https://doi.org/10.1117/1.JRS.13.024525>, vol. 13, p. 024525, 6 2019.
- [89] D. Phiri, M. Simwanda, S. Salekin, V. R. Ryirenda, Y. Murayama, M. Ranagalage, N. Oktaviani, H. A. Kusuma, T. Zhang, J. Su, C. Liu, W. H. Chen, H. Liu, G. Liu, M. Cavur, H. S. Duzgun, S. Kemeç, D. C. Demirkan, R. Chairat, Y. B. Salem, M. Aoun, Z. Kiala, O. Mutanga, J. Odindi, and K. Peerbhay, "Sentinel-2 data for land cover / use mapping : A review," *Remote Sensing*, vol. 42, p. 14, 2019.
- [90] "<https://sentinel.esa.int/web/sentinel/missions/sentinel-2>," Último acceso: 26 de febrero de 2023. [Online]. Available: <https://sentinel.esa.int/web/sentinel/missions/sentinel-2>
- [91] L. Alonso, J. Picos, G. Bastos, and J. Armesto, "Detection of very small tree plantations and tree-level characterization using open-access remote-sensing databases," *Remote Sensing*, vol. 12, 2020.
- [92] M. Padial-Iglesias, P. Serra, M. Ninyerola, and X. Pons, "A framework of filtering rules over ground truth samples to achieve higher accuracy in land cover maps," *Remote Sensing*, vol. 13, pp. 1–36, 2021.
- [93] F. Alonso-Sarria, C. Valdivieso-Ros, and F. Gomariz-Castillo, "Isolation forests to evaluate class separability and the representativeness of training and validation areas in land cover classification," *Remote Sensing*, vol. 11, 2019.
- [94] "Index @ inspire.ec.europa.eu," Último acceso: 26 de febrero de 2023. [Online]. Available: <https://inspire.ec.europa.eu/>

- [95] "index @ pnoa.ign.es," Último acceso: 26 de febrero de 2023. [Online]. Available: <https://pnoa.ign.es/>
- [96] "eBee Plus - senseFly," Último acceso: 26 de febrero de 2023. [Online]. Available: <https://www.sensefly.com/drone/ebee-plus-survey-drone/>
- [97] "senseFly S.O.D.A. - senseFly," Último acceso: 26 de febrero de 2023. [Online]. Available: <https://www.sensefly.com/camera/sensefly-soda-photogrammetry-camera/>
- [98] J. J. W. Rouse, R. H. Haas, J. A. Schell, and D. W. Deering, "Monitoring vegetation systems in the great plains with ERTS," in *NASA. Goddard Space Flight Center 3d ERTS-1 Symp., Vol. 1, Sect. A*, vol. 351, 1974, p. 309.
- [99] C. Hu, "A novel ocean color index to detect floating algae in the global oceans," *Remote Sensing of Environment*, vol. 113, pp. 2118–2129, 10 2009.
- [100] B.-C. Gao, "NDWI—a normalized difference water index for remote sensing of vegetation liquid water from space," *Remote Sensing of Environment*, vol. 58, pp. 257–266, 1996.
- [101] S. Miyatake and A. Rikimaru, "Development of forest canopy density mapping and monitoring model using indices of vegetation, bare soil and shadow," in *Proceedings of the 18th Asian Conference on Remote Sensing*, 1997.
- [102] M. A. Hardisky, V. Klemas, and R. M. Smart, "The influence of soil salinity, growth form, and leaf moisture on-the spectral radiance of *Spartina Alterniflora* Canopies," *Photogrammetric Engineering and Remote Sensing*, vol. 49, pp. 77–83, 1 1983.
- [103] E. R. Hunt and B. N. Rock, "Detection of changes in leaf water content using near-and middle-infrared reflectances," *Remote Sensing of Environment*, vol. 30, pp. 43–54, 1989.
- [104] O. Strashok, M. Ziemiańska, and V. Strashok, "Evaluation and correlation of Sentinel-2 NDVI and NDMI in Kyiv (2017-2021)," *Journal of Ecological Engineering*, vol. 23, pp. 212–218, 2022.
- [105] M. Sánchez, A. Cuartero, M. Barrena, and A. Plaza, "A new method for positional accuracy analysis in georeferenced satellite images without independent ground control points," *Remote Sensing*, vol. 12, p. 4132, 2020.
- [106] E. C. Enoguanbhor, F. Gollnow, J. O. Nielsen, T. Lakes, and B. B. Walker, "Land cover change in the abuja city-region, nigeria: Integrating GIS and remotely sensed data to support land use planning," *Sustainability*, 2019.
- [107] J. Cavender-Bares, J. A. Gamon, and P. A. Townsend, *Remote sensing of plant biodiversity*, 2020.
- [108] K. Kaku, "Satellite remote sensing for disaster management support: A holistic and staged approach based on case studies in Sentinel Asia," *International Journal of Disaster Risk Reduction*, vol. 33, pp. 417–432, 2019.
- [109] M. Tadese, L. Kumar, R. Koech, and B. K. Kogo, "Mapping of land-use/land-cover changes and its dynamics in Awash river basin using remote sensing and GIS," *Remote Sensing Applications: Society and Environment*, vol. 19, p. 100352, 2020.

- [110] D. Apostolopoulos and K. Nikolakopoulos, "A review and meta-analysis of remote sensing data, gis methods, materials and indices used for monitoring the coastline evolution over the last twenty years," *European Journal of Remote Sensing*, vol. 54, pp. 240–265, 2021.
- [111] E. C. Rodríguez-Garlito and A. Nieto, "Publicación de datos de los bienes de interés cultural de la provincia de Cáceres en un geoportal," pp. 39–54, 2018.
- [112] Q. D. Team, "Qgis geographic information system," 2020.
- [113] G. Contributors, "Gdal: Geospatial data abstraction library," <https://gdal.org>, 2023.
- [114] Mapbox, "rasterio: Geospatial raster data i/o for python programmers," <https://rasterio.readthedocs.io/en/latest>, 2023.
- [115] J. E. Ball, D. T. Anderson, and C. S. Chan, "A comprehensive survey of deep learning in remote sensing: Theories, tools and challenges for the community," *Journal of Applied Remote Sensing*, vol. 11, 2017.
- [116] B. Y. Courville Aaron Goodfellow Ian, *Deep Learning*, 2016.
- [117] Y. Bengio, *Learning deep architectures for AI*, 2009, vol. 2.
- [118] M. E. Paoletti, J. M. Haut, J. Plaza, and A. Plaza, "Deep learning classifiers for hyperspectral imaging: A review," *ISPRS Journal of Photogrammetry and Remote Sensing*, vol. 158, pp. 279–317, 2019.
- [119] F. Pedregosa, G. Varoquaux, A. Gramfort, V. Michel, B. Thirion, O. Grisel, M. Blondel, P. Prettenhofer, R. Weiss, V. Dubourg, J. Vanderplas, A. Passos, D. Cournapeau, M. Brucher, M. Perrot, and E. Duchesnay, "Scikit-learn: Machine learning in Python," *Journal of Machine Learning Research*, vol. 12, pp. 2825–2830, 2011.
- [120] L. Breiman, "Random forests," *Machine Learning*, vol. 45, pp. 5–32, 2001.
- [121] R. E. Blahut, *Fast Algorithms for Signal Processing*.
- [122] T. Hastie, J. Friedman, and R. Tibshirani, *The Elements of Statistical Learning*. Springer New York, 2009.
- [123] V. N. Vapnik, *Statistical Learning Theory*, ny: wiley ed., New York, 1998.
- [124] A. J. Izenman, "Support Vector Machines," in *Learning with Kernels: Support Vector Machines, Regularization, Optimization, and Beyond*. MITP, 2013, pp. 369–406.
- [125] F. Melgani and L. Bruzzone, "Classification of hyperspectral remote sensing images with support vector machines," *IEEE Transactions on Geoscience and Remote Sensing*, vol. 42, no. 8, pp. 1778–1790, 2004.
- [126] P. Ghamisi, M. S. Couceiro, and J. A. Benediktsson, "A Novel Feature Selection Approach Based on FODPSO and SVM," *IEEE Transactions on Geoscience and Remote Sensing*, vol. 53, no. 5, pp. 2935–2947, 2015.

- [127] T. Cover and P. Hart, "Nearest neighbor pattern classification," *IEEE Transactions on Information Theory*, vol. 13, no. 1, pp. 21–27, 1967.
- [128] F. Maselli, G. Chirici, L. Bottai, P. Corona, and M. Marchetti, "Estimation of Mediterranean forest attributes by the application of k-NN procedures to multitemporal Landsat ETM+ images," *International Journal of Remote Sensing*, vol. 26, no. 17, pp. 3781–3796, 2005.
- [129] A. E. Maxwell, T. A. Warner, and F. Fang, "Implementation of machine-learning classification in remote sensing: an applied review," *International Journal of Remote Sensing*, vol. 39, no. 9, pp. 2784–2817, 2018.
- [130] D. E. Rumelhart, G. E. Hinton, and R. J. Williams, "Learning representations by back-propagating errors," *Nature*, vol. 323, no. 6088, pp. 533–536, 1986.
- [131] J. A. Benediktsson, "Statistical methods and neural network approaches for classification of data from multiple sources," Ph.D. dissertation, School of Elect. Eng., Purdue Univ., West Lafayette, IN, 1990.
- [132] J. A. Richards, "Analysis of remotely sensed data: The formative decades and the future," in *IEEE Transactions on Geoscience and Remote Sensing*, vol. 43, no. 3, mar 2005, pp. 422–432.
- [133] F. Chollet *et al.*, "Keras," <https://keras.io>, 2015.
- [134] M. E. Paoletti, J. M. Haut, J. Plaza, and A. Plaza, "A new deep convolutional neural network for fast hyperspectral image classification," *ISPRS Journal of Photogrammetry and Remote Sensing*, vol. 145, pp. 120–147, 2018.
- [135] Y. Lecun, Y. Bengio, and G. Hinton, "Deep learning," *Nature*, vol. 521, pp. 436–444, 2015.
- [136] L. Zhang, L. Zhang, and B. Du, "Deep learning for remote sensing data: A technical tutorial on the state of the art," *IEEE Geoscience and Remote Sensing Magazine*, vol. 4, pp. 22–40, 6 2016.

Resultados de esta Tesis Doctoral

Publicaciones en el compendio

1. Publicación [1]: **E. C. Rodríguez-Garlito** and A. Paz-Gallardo, "Efficiently Mapping Large Areas of Olive Trees Using Drones in Extremadura, Spain", in IEEE Journal on Miniaturization for Air and Space Systems, vol. 2, no. 3, pp. 148-156, Sept. 2021. DOI: 10.1109/JMASS.2021.3067102
2. Publicación [2]: **E. C. Rodríguez-Garlito**, A. Paz-Gallardo and A. Plaza, "Automatic Detection of Aquatic Weeds: A Case Study in the Guadiana River, Spain", in IEEE Journal of Selected Topics in Applied Earth Observations and Remote Sensing, vol. 15, pp. 8567-8585, 2022. DOI: 10.1109/JSTARS.2022.3210373. [IF(2022)=5.5].
3. Publicación [3]: **E. C. Rodríguez-Garlito**, A. Paz-Gallardo and A. Plaza, "Monitoring the Spatiotemporal Distribution of Invasive Aquatic Plants in the Guadiana River, Spain", in IEEE Journal of Selected Topics in Applied Earth Observations and Remote Sensing, vol. 16, pp. 228-241, 2023. DOI: 10.1109/JSTARS.2022.3225201. [IF(2022)=5.5].
4. Publicación [4]: **E. C. Rodríguez-Garlito**, A. Paz-Gallardo and A. Plaza, "Mapping Invasive Aquatic Plants in Sentinel-2 Images Using Convolutional Neural Networks Trained With Spectral Indices", in IEEE Journal of Selected Topics in Applied Earth Observations and Remote Sensing, vol. 16, pp.2889-2899, 2023. DOI: 10.1109/JSTARS.2023.3257142. [IF(2022)=5.5].
5. Publicación [5]: **E. C. Rodríguez-Garlito**, A. Paz-Gallardo and A. Plaza, "Mapping the Accumulation of Invasive Aquatic Plants in the Guadiana River, Spain, Using

Multitemporal Remote Sensing”, in IEEE Geoscience and Remote Sensing Letters, vol. 20, pp. 1-5, 2023. DOI: 10.1109/LGRS.2023.3277366. [IF(2022)=4.8].

Otros resultados pendientes de publicar

1. Publicación [6]: **E. C. Rodríguez-Garlito**, A. Paz-Gallardo and A. Plaza, “Spectral-Spatial Mapping of Invasive Aquatic Plants in the Guadiana River, Spain, Using Convolutional Neural Networks”

Capítulo de libro

1. Publicación [111]: **E. C. Rodríguez-Garlito**, A. Nieto Masot . "Publicación de datos de los Bienes de Interés Cultural de la provincia de Cáceres en un Geoport". En A. Nieto Masot y G. Cárdenas Alonso (Eds.), Sistema de Información geográfica y teledetección: aplicaciones en el análisis territorial pp. 39-54, 2018. ISBN 9788409037490 Universidad de Extremadura.

Comunicaciones

1. **E. C. Rodríguez-Garlito**, A. Paz-Gallardo and A. Plaza, “Detección de plantas invasoras en agua usando imágenes de satélite mediante algoritmos de inteligencia artificial”. III Jornadas Doctorales. Universidad de Extremadura. Badajoz 29 noviembre 2019.
2. **E. C. Rodríguez-Garlito**, A. Paz-Gallardo and A. Plaza, “Inteligencia artificial para detección de olivos en imagen de dron”. IV Jornadas Doctorales. Universidad de Extremadura. 27 noviembre 2020.
3. **E. C. Rodríguez-Garlito**, A. Paz-Gallardo and A. Plaza, “Teledetección e inteligencia artificial para la monitorización de plantas acuáticas invasoras”. V Jornadas Doctorales de la Universidad de Extremadura. 05 noviembre 2021.
4. **E. C. Rodríguez-Garlito**, A. Paz-Gallardo and A. Plaza, “Teledetección e inteligencia artificial para la monitorización de plantas acuáticas invasoras”. IV Jornadas de Divulgación Científica G-9. Bilbao 18-20 de mayo 2022.

Premios

1. **E. C. Rodríguez-Garlito**, A. Paz-Gallardo and A. Plaza, "Inteligencia artificial para detección de olivos en imagen de dron". Póster seleccionado por la Uex en la Rama de Ingeniería y Arquitectura. IV Jornadas Doctorales. Universidad de Extremadura. 27 noviembre 2020.
2. **E. C. Rodríguez-Garlito**, A. Paz-Gallardo and A. Plaza, "Teledetección e inteligencia artificial para la monitorización de plantas acuáticas invasoras". Póster seleccionado por la Uex en la Rama de Ingeniería y Arquitectura. V Jornadas Doctorales. Universidad de Extremadura. 05 noviembre 2021.
3. **E. C. Rodríguez-Garlito**, A. Paz-Gallardo and A. Plaza, "Teledetección e inteligencia artificial para la monitorización de plantas acuáticas invasoras". Póster seleccionado por el Grupo de Universidades (G-9) en la Rama de Ingeniería y Arquitectura, en las IX Jornadas Doctorales G-9. Bilbao 18-19 mayo 2022.
4. **E. C. Rodríguez-Garlito**. Ganadora II Edición del Concurso de Divulgación #HiloTesis, por la Universidad de Extremadura. Badajoz 3 junio 2022.
5. **E. C. Rodríguez-Garlito**. Ganadora a nivel nacional de la II Edición del Concurso de Divulgación #HiloTesis, por CRUE Universidades Españolas. 29 junio 2022.

Otra divulgación

1. "Ella aplica la inteligencia artificial al nenúfar". Difusión en prensa escrita. Periódico HOY. 6 junio 2022
2. "Badajoz - #HiloTesis sobre el Nenúfar" Difusión radio. rtve play radio reportajes emisoras. 21 junio 2022.

Participación en proyectos de I+D+I regionales

1. Procesamiento de imágenes hiperespectrales. Referencia GR18060. IP: Antonio Plaza Miguel. Duración (29/05/2018 – 04/11/2021). Financiación 167402,84€.
2. Ayuda del programa propio de la UEx para el grupo de investigación "Computación Hiperespectral". Referencia 2021/00421/001. IP: Antonio Plaza Miguel. Duración (31/12/2021 – 31/12/2022). Financiación 65000€.

Publicaciones

© 2021 IEEE. Reprinted, with permission, from Elena C. Rodríguez-Garlito and Abel Paz-Gallardo, *Efficiently Mapping Large Areas of Olive Trees Using Drones in Extremadura, Spain*, *IEEE Journal on Miniaturization for Air and Space Systems*.

Reprinted from “Automatic Detection of Aquatic Weeds: A Case Study in the Guadiana River, Spain” under the Creative Commons License (CC BY 4.0).

Reprinted from “Monitoring the Spatiotemporal Distribution of Invasive Aquatic Plants in the Guadiana River, Spain” under the Creative Commons License (CC BY 4.0).

Reprinted from “Mapping Invasive Aquatic Plants in Sentinel-2 Images Using Convolutional Neural Networks Trained with Spectral Indices” under the Creative Commons License (CC BY 4.0).

© 2023 IEEE. Reprinted, with permission, from Elena C. Rodríguez-Garlito, Abel Paz-Gallardo and Antonio Plaza, *Mapping the Accumulation of Invasive Aquatic Plants in the Guadiana River, Spain, using Multitemporal Remote Sensing*, *IEEE Geoscience and Remote Sensing Letters*.

Efficiently Mapping Large Areas of Olive Trees Using Drones in Extremadura, Spain

Escuela Politécnica
Av. de la Universidad, S/N, 10003
Teléfono: 0034927257000. Ext. 51662
correo electrónico: apazgal, aplaza @unex.es
Cáceres, España

Dr. Abel Francisco Paz Gallardo y Dr. Antonio Plaza Miguel, como directores de la Tesis Doctoral titulada “Desarrollo de nuevos métodos y algoritmos de análisis y clasificación de imágenes multiespectrales orientadas a la gestión y monitorización de plantas acuáticas invasoras”, certificamos el factor de impacto y la categorización de la siguiente publicación incluida en la Tesis Doctoral. Del mismo modo, se especifica la aportación de la doctoranda. Para cualquier otra información o aclaración, por favor, no duden en contactar con nosotros.

Titulo de la publicación: Efficiently Mapping Large Areas of Olive Trees Using Drones in Extremadura, Spain

Autores: **Elena C. Rodríguez-Garlito**, Abel Paz-Gallardo

Revista: IEEE Journal on Miniaturization for Air and Space Systems

Otros datos: vol 2, págs 148-156, año 2021

DOI: 10.1109/JMASS.2021.3067102

Factor de impacto 2022: -

Abstract: Remotely sensed multispectral (MS) images have been widely used in different areas of research in recent years, allowing their exploitation in many domains like precision agriculture. This study uses high-resolution RGB data, collected by an unmanned aerial vehicle (UAV/drone), equipped with a camera sensor and flown over an olive tree field in Extremadura (Spain), for land-cover classification purposes. Drone flights over large agricultural areas, collecting high spatial resolution images such as the scenario studied, can be tedious to process, requiring a large amount of random-access memory (RAM). To solve this issue, a new olive tree cover mapping approach is proposed by applying a spatial partitioning methodology that consists of splitting the image automatically, before processing. Each part (known as the raster window) is classified by using machine learning methods. Finally, a classification map is obtained after processing all windows. Among different supervised spectral classification methods, the following classifiers are considered: random forest (RF), support vector machine (SVM), multilayer perceptron (MLP), and k-nearest neighbor (kNN), with the ultimate goal of detecting olive trees and distinguishing them from other land-cover types available in the scene, such as soil, shadows, and weeds. In addition, our experimental results demonstrate that these classifiers can be used to avoid time-consuming fieldwork tasks, facilitating the analysis of agricultural fields with “a la carte” UAV flights resulting in high classification accuracy.

Contribución de la doctoranda: Planteamiento de la hipótesis, conceptualización, búsqueda bibliográfica, metodología, análisis y discusión de resultados, elaboración de tablas y figuras, escritura del manuscrito borrador y redacción de la revisión.

Efficiently Mapping Large Areas of Olive Trees Using Drones in Extremadura, Spain

Elena C. Rodríguez-Garlito¹ and Abel Paz-Gallardo²

Abstract—Remotely sensed multispectral (MS) images have been widely used in different areas of research in recent years, allowing their exploitation in many domains like precision agriculture. This study uses high-resolution RGB data, collected by an unmanned aerial vehicle (UAV/drone), equipped with a camera sensor and flown over an olive tree field in Extremadura (Spain), for land-cover classification purposes. Drone flights over large agricultural areas, collecting high spatial resolution images such as the scenario studied, can be tedious to process, requiring a large amount of random-access memory (RAM). To solve this issue, a new olive tree cover mapping approach is proposed by applying a spatial partitioning methodology that consists of splitting the image automatically, before processing. Each part (known as the raster window) is classified by using machine learning methods. Finally, a classification map is obtained after processing all windows. Among different supervised spectral classification methods, the following classifiers are considered: random forest (RF), support vector machine (SVM), multilayer perceptron (MLP), and k -nearest neighbor (kNN), with the ultimate goal of detecting olive trees and distinguishing them from other land-cover types available in the scene, such as soil, shadows, and weeds. In addition, our experimental results demonstrate that these classifiers can be used to avoid time-consuming fieldwork tasks, facilitating the analysis of agricultural fields with “a la carte” UAV flights resulting in high classification accuracy.

Index Terms—Drones, land-cover classification, machine learning.

I. INTRODUCTION

MULTISPECTRAL (MS) and hyperspectral (HS) imaging are important techniques in remote sensing (RS). These images comprise three dimensions [1]: two of them represent the spatial location of each pixel in the image and the

Manuscript received December 12, 2020; revised February 21, 2021; accepted March 16, 2021. Date of publication March 18, 2021; date of current version August 23, 2021. This work was supported by the European Social Fund (Resolución de 10 de mayo de 2017, de la Secretaría General de Ciencia, Tecnología e Innovación, por la que se resuelve la convocatoria de ayudas para la financiación de contratos predoctorales para formación de Doctores en los centros públicos de I+D pertenecientes al Sistema Extremeño de Ciencia, Tecnología e Innovación en el ejercicio 2017 (expediente PD16001)). (Corresponding author: Elena C. Rodríguez-Garlito.)

The authors are with the Hyperspectral Computing Laboratory, Department of Technology of Computers and Communications, Escuela Politécnica, University of Extremadura, 10003 Cáceres, Spain (e-mail: elenacristinarg@unex.es; apazgal@unex.es).

Digital Object Identifier 10.1109/JMASS.2021.3067102

third dimension describes the spectral singularity of each pixel at different wavelength channels. Therefore, these images can be described as a data cube [2]. MS and HS sensors are typically installed on airborne or spaceborne platforms. Sentinel-2, from the European Space Agency (ESA) [3], is an example of the MS sensor and the airborne visible/infrared imaging spectrometer (AVIRIS) [4] from the National Aeronautics and Space Administration (NASA), an example of the HS sensor.

In recent years, advances in the development of MS and HS sensors and the existence of a great variety of sensors with different technical specifications (spatial and spectral resolution, spectral range, and image acquisition costs, among others) have allowed their use in different research areas, such as environmental studies, military and intelligence applications, monitoring wild land and forests fires, chemical/biological contamination, urban planning, and agricultural management [5]. MS sensors are only capable of obtaining information in tens of spectral bands whereas through HS measuring instruments of very high spatial and spectral resolution, the information in hundred of bands is collected. In this study, an MS image (with low spectral resolution) is used, specifically a three-band MS image corresponding to the three bands of the visible spectrum (RGB: Red, Green, and Blue). Although each pixel in the image records information in only three wavelengths channels, it has a very high spatial resolution.

Over the last few years, the use of unmanned aerial vehicles (UAVs/drones) has increased due to recent technological advances such as the installation of high-resolution sensors or the integration of a thermal camera that allow practical applications, such as environmental monitoring [6], crop management [7], and precision agriculture [8], among others. They have gained considerable interest in both scientific research and applications in the private sector. Specifically, in the field of agriculture, the advantages of using UAVs are remarkable due to their small size, the ability to collect flights over a large area of land in a short time, and the important advantage of being able to collect data from the same area as often as desired.

In the literature, different techniques have been applied to analyze and interpret MS images, such as atmospheric and geometric correction, data recovery, dimensional reduction, detection of targets and anomalies, change detection, spectral unmixing, and land-cover classification [9]. In this article, we focus on classification techniques, where a label is assigned to

each pixel of an MS image, corresponding to the association of a pixel with a certain class. Among many applications of classification [10], this technique has been widely used in precision agriculture.

RS using drones through an MS sensor allows to fly over large areas to monitor crops, identify diseases, and locate weeds quickly. In other words, the introduction of new technologies in the agricultural sector allows for the improvement of agricultural tasks and the increase of crop productivity.

The region of Extremadura (Spain) has large portions of land dedicated to agriculture. Specifically, the olive grove holds an area of 287 000 ha approximately [11]. Land-cover classification of this particular crop contributes significantly to improving agronomic knowledge of the region.

Numerous machine learning methods have been developed for HS/MS image analysis. In land-cover classification, diverse studies have evaluated the performances of machine learning methods [12]–[15]. In this study, the performance of four nonparametric classifiers (classifiers that do not require any assumptions on the distribution of the input data) is examined and compared for land-cover classification purposes by using drone-collected image data over the region of Extremadura. These classifiers are random forest (RF), support vector machine (SVM), k -nearest neighbor (kNN), and multilayer perceptron (MLP). These classifiers are all supervised in nature, where a set of representative training samples (samples whose labels are known) are used to train the classifier.

The main goal of this article is to develop an efficient window partitioning processing strategy for olive tree cover mapping feasibility of agricultural drone MS images. In the agricultural domain, drone flights over olive trees are made to obtain high-resolution images for agronomic analysis: counting applications, fault inspection, crop diseases, etc. A small area can be inspected on foot. However, a lot of time is required to inspect larger areas, which is the usual scenario in agriculture. The scenario studied has 60 hectares (ha) approximately, where long-duration drone flights are needed to cover the entire farm. This study represents those “a la carte” UAV long flights for whole farms to make an agronomic analysis on the entire olive surface. In other words, this methodology is applicable to MS images of large areas of land (not only inspection flights of a specific area) which are very heavy because they collect a lot of high-resolution data. Additionally, high memory amounts are required to use machine learning algorithms for land-cover classification. With the strategy developed, it is possible to make a classification of large farms efficiently without the need of a machine with the high amount of memory or a supercomputer.

This article is organized as follows. In Section II, the classification algorithms used in this research are reviewed and the spatial partitioning strategy is explained. Section III defines the experimental environment and discusses the performance and classification results obtained by each selected method on an MS drone image. Section IV concludes this article and provides hints at plausible future research lines.

II. METHODS

The adopted classifiers can be categorized according to the availability of training samples. In supervised classifiers, a set of representative samples for each class are labeled in advance. On the contrary, unsupervised classifiers do not need the training sample labels of the input data. As an intermediate method, semisupervised classifiers are based on both labeled training samples and unlabeled samples [16].

In this article, we focus on supervised approaches as they are often the most reliable ones in precision agriculture applications. To differentiate between several land-cover classes, the machine learning algorithms used interpret an MS image denoted by $X \in \mathbb{R}^{H \times W \times R}$, where H is the height of the data cube, W is the width, and R is the number of spectral bands. Then, a mapping function $\mathcal{M}_\theta : X \rightarrow Y$ assigns each x_i to a corresponding land-cover label y_i . In other words, the supervised classifiers used in this study need to be fitted with two arrays: 1) a sparse or dense array X of size $[n_samples, n_features]$, holding the training samples and 2) an array Y of size $[n_samples]$, holding the target values (class labels) for the training samples. In unsupervised methods like clustering (where each pixel is associated with one of the clusters selected previously), the algorithms implement a fitting method to find the clusters on training samples and a function returns an array of integer labels corresponding to the different classes or clusters. Finally, a final classification map $Y \in \mathbb{R}^{H \times W}$ is obtained.

A. Random Forest

The RF algorithm was first introduced in [17] as an effective tool in prediction for classification and regression. RF belongs to the family of ensemble methods, where an ensemble of classifiers is trained by combining the predictions of several estimators in order to improve generalization. Particularly, this method builds several randomized decision trees independently, and then averages their predictions.

The operation of RF can be explained in several steps. In the first step, this algorithm uses the so-called “bagging” since a “bootstrapped” sample from the training set is created. In other words, samples are randomly selected from the original training dataset, allowing the same sample to be taken more than once whereas others may not be chosen at all. In a second step, a decision tree is created by using the bootstrapped data set, but only random variables are used in each step. The first step is now repeated, resulting in a wide variety of decision trees. The implementation used in this study calculates the final classification by averaging the probabilistic prediction of each decision tree.

Although this algorithm combines techniques designed for trees, it offers several advantages [18] since the bootstrapping procedure reduces the variance of the model without increasing the bias. It is also not sensitive to overtraining or noise compared with other methods based on boosting, in addition to flexible, easy, and fast to evaluate [16].

These important points have allowed successful studies based on the RF in the field of land-cover classification. RF classifiers were successfully explored for RS applications

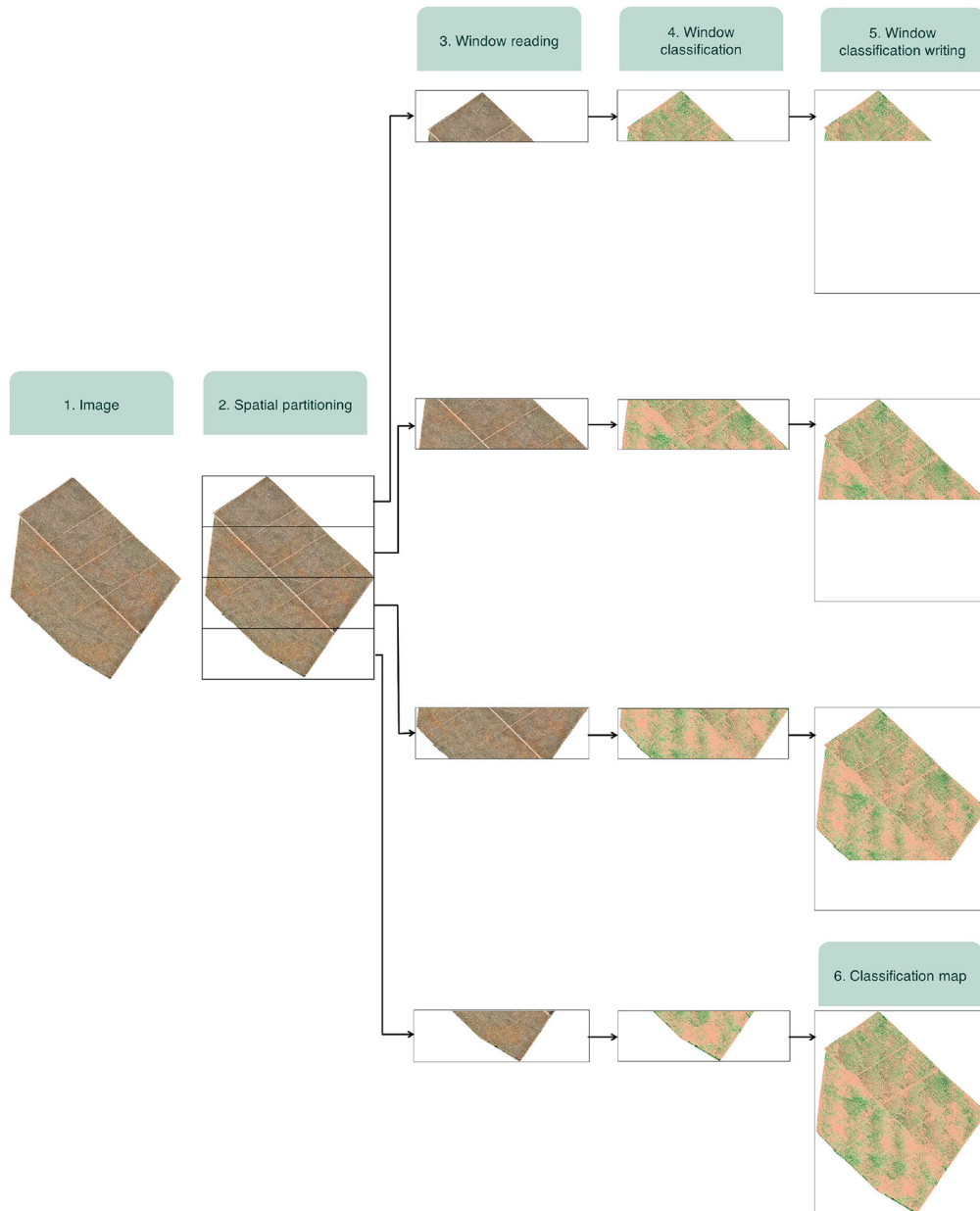


Fig. 1. Window partitioning strategy using an example with four windows.

in [19], where it was concluded that their performance is comparable to other ensemble methods in terms of accuracy. However, RFs are much faster in terms of training when compared to other ensemble methods. In addition, the RF was suggested in [20] as an advantageous classification method in terms of accuracy instead of other widely used statistical classification methods. Numerous applications of the RF have been recently developed in the area of RS [21].

B. Support Vector Machine

The SVM method was developed in [22] and has been widely used for HS/MS image classification and regression problems. A kernel is used for solving linear and nonlinear problems by projecting the pixel vectors into a higher dimensional space [23]. Specifically, the SVM finds the optimal hyperplane that separates two classes, maximizing the distance

between the separating hyperplane and the closest training sample. Support vectors are the closest training samples to the hyperplane. This hyperplane has different mathematical formulations depending on how the data are separated. Therefore, there are different kernel functions used [linear, polynomial, radial basis function (RBF), and sigmoid, among others] [24].

The SVM method is capable of performing binary and multiclass classification. Moreover, the SVM can handle the classification of high-dimensional data with a limited number of training samples due to the fact that only the samples that are closest to the class boundaries are actually needed to locate the optimal separating hyperplane [25].

C. *k*-Nearest Neighbors

The kNN algorithm was proposed in [26] to assign each unclassified sample the label of the nearest of a set of

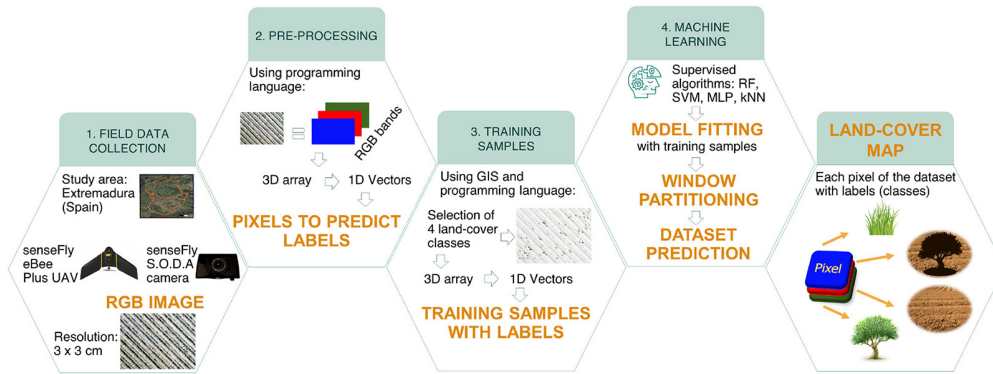


Fig. 2. General overview of land-cover classification workflow.

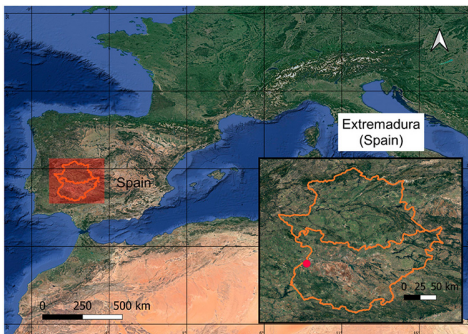


Fig. 3. Region of Extremadura, Spain.

previously classified samples. Despite being considered a relatively simple method, it has been applied in numerous classification and regression problems. Moreover, it is a nonparametric method that can get successful results in problems where the decision boundaries are irregular.

The classification of each query sample is computed by a simple majority vote of the closest neighbors. In other words, an unknown sample is assigned the label which has the most representatives within the nearest neighbors of the sample. Each unknown sample is compared against the original training data and it is not trained to produce a model, as opposed to other classifiers [27].

kNN classifiers predict the label of a sample through a constant k (integer value) that is defined by the user and represents the number of training samples that are closest to it. It must be taken into account that the choice of k is data dependent [28], due to the fact that a complex decision boundary may be produced for very low values of k , while very large values of k reduce noise but introduce larger generalization.

D. Multilayer Perceptron

The MLP is a supervised nonparametric artificial neural network (ANN) algorithm that has been widely used in classification and regression problems. The performance of ANNs resembles that of the biological brain, as they move the information from the nodes (or neurons) of the input layer to the output neurons of the output layer, using one or more hidden layers that form an interconnected network. The

MLP classifier is a class of ANN that uses a backpropagation algorithm introduced in [29].

The MLP learns a function $f(\cdot) : R^m \rightarrow R^o$ by training the classifier on a dataset, where m is the dimensionality of the input and o is the number of dimensions of the output. The set of features (pixels of the image) is represented by $X = x_1, x_2, x_3, \dots, x_m$ and the class label is given by y . The input layer has a number of neurons equal to m that represents the input features. Each neuron (except for those in the input layer) uses a nonlinear learning function $g(\cdot) : R \rightarrow R$ that connects every node to the following layer, transforming its value through weights by means of a linear summation $w_1x_1 + w_2x_2 + w_3x_3 + \dots + w_mx_m$. Finally, the output values (class labels) are obtained by transforming the values coming from the last hidden layer to the output layer. In the training stage, the MLP uses backpropagation to calculate the gradient descent. It starts with random weights and minimizes the loss function by repeatedly updating these weights. By comparing the expected class result to the output, an error is obtained that is used to change the connection weights for each input that has been processed.

Among the main advantages of this classifier is the lack of prior knowledge of the statistical distribution of the input data [30]. However, its drawbacks include the requirement to tune several hyperparameters, such as the number of layers, hidden neurons, and iterations [31].

E. Spatial Partitioning

As described in Section I, the problem of processing feasibility is presented due to the fact that the amount of memory required to use land-cover classification algorithms described before is very demanding. Moreover, this matter gets worst because of drone flights over large agricultural areas collecting high-resolution images for agronomic studies results in very heavy images. To alleviate this issue, an automatic spatial partitioning (also known as window partitioning) is employed before dataset prediction.

Window partitioning splits the cube of MS data in processing windows or blocks located contiguously in the spatial domain in the process of reading of the image, so that each window contains information relative to a subset of pixels in the MS image. The number of pixels in each window can

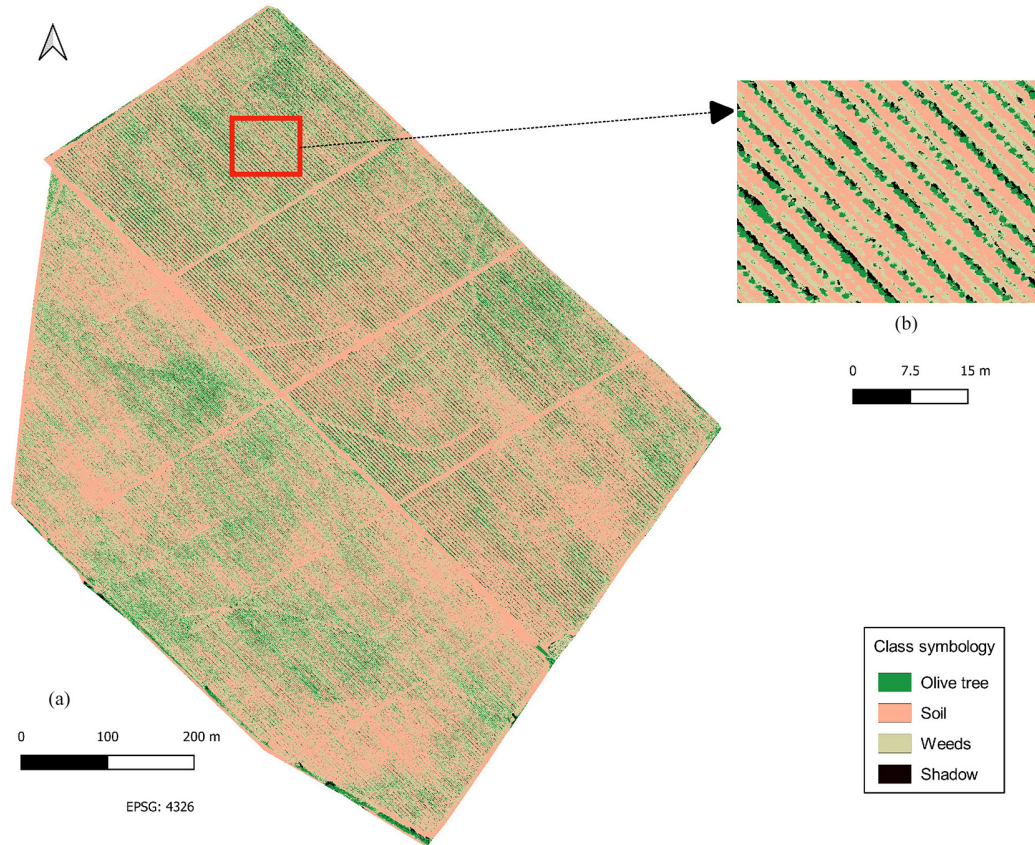


Fig. 4. (a) Classification map of the total area obtained by window partitioning and RF. (b) Classification map of a zoomed scene.

be adjusted according to the image to be processed. In this study, since each classifier makes the prediction pixel by pixel, it has been chosen to split the data cube in windows that contain rows of pixels of the MS image. Each window contains the spectral information associated with a row of pixels. First, algorithms are trained with selected training samples. This training is only performed once and is valid for all processing windows. Next, classification algorithms predict land cover for the first window read. Afterward, a partial write process is performed with that classified window. This process is repeated window by window. Finally, the writing process of the last classified window takes place. Then, the complete image is classified. Consequently, machine learning algorithms are capable to classify an MS image that is even larger than computer available RAM. Spatial partitioning also supports parallelization between different processors or machines. A general overview of this approach is given in Fig. 1 with an example splitted in four windows.

III. RESULTS

A general overview of our experimental validation is given in Fig. 2. First, we perform data collection using different kinds of drones, obtaining the high-resolution image data. Then, we perform preprocessing and collection of training samples. Next, we perform window partitioning and classification based on machine learning, obtaining a land-cover map that can be validated to ground truth (GT). In the following, we explain the dataset evaluated, the MS sensor and the

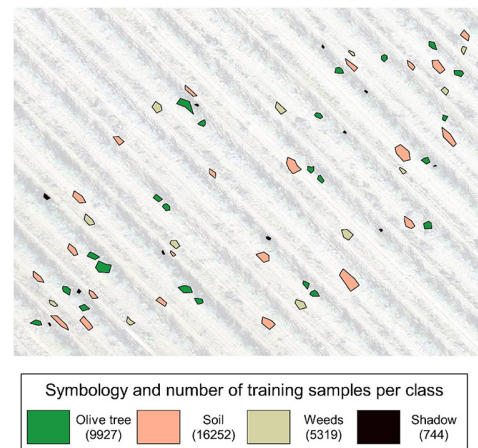


Fig. 5. Training samples extracted by the handcrafted feature-based method. The number of pixels selected per class is in brackets.

platform where it is carried out (UAV/drone), the experimental environment, the setup for the different classifiers, and the experimental results.

A. Multispectral Datasets

The considered classifiers have been evaluated on MS data captured by a drone in Extremadura, Spain, as shown in Fig. 3. The data were collected in December 2019. The drone was operated over an agricultural area with olive trees of 60 ha in a flight time of 45 min. The spatial resolution is 3 cm per pixel.

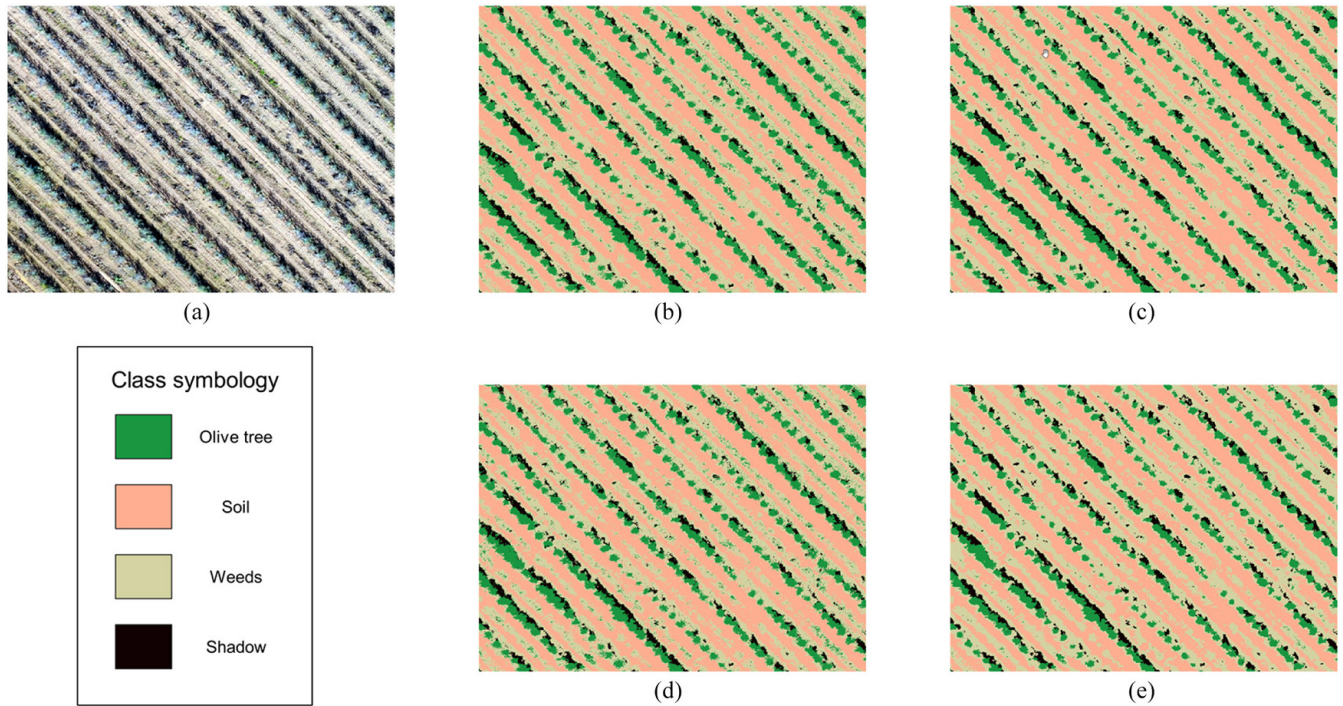


Fig. 6. (a) RGB image of the dataset. Classification maps obtained by different classifiers: (b) RF, (c) SVM, (d) kNN, and (e) MLP.

The MS image, with dimensions of $34\,167 \times 41\,184$ pixels, covers an extension of olive grove land and consists of different classes, including soil, olive trees, olive trees shadows, and weeds. The drone has three data channels (RGB) with spectral coverage of 475 nm (blue channel), 560 nm (green channel), and 668 nm (red channel).

B. Sensor and UAV/Drone Platform Specifications

The described dataset was acquired using a senseFly eBee Plus UAV carrying the senseFly S.O.D.A camera. The technical features of the senseFly eBee Plus UAV [32] include a wingspan of 110 cm (43.3 in), weight (including camera and battery) 1.1 kg (2.4 lb), radio link range of 3 km nominal (up to 8 km)/1.86 mi (up to 4.97 mi), automatic 3-D flight planning, cruise speed of 40–110 km/h (11–30 m/s or 25–68 mph), wind resistance of up to 45 km/h (12 m/s or 28 mph), maximum flight time of 59 min, and maximum flight range of 45 km (28 mi). The technical features of the senseFly S.O.D.A camera [33] include an RGB lens of F/2.8-11, 10.6 mm (35 mm equivalent: 29 mm), RGB resolution of 5472×3648 pixels (3:2), exposure compensation of ± 2.0 (1/3 increments), RGB shutter is global shutter 1/30 – 1/2000 s, different white balance modes, ISO range of 25–6400, RTK/PPK support, and image formats in JPEG and DNG+JPEG.

C. Hardware/Software Environment

The hardware environment used for this study was a computer with an Intel Core i7-8700 processor, 32-GB RAM memory, and 1-TB SSD. The window partitioning strategy and machine learning algorithms have been implemented by

developing the algorithms in Python 3.8 programming language, due to it eases integration with other components, is convenient to use given its wide variety of libraries and is open source.

D. Window Partitioning Processing

To evaluate the window partitioning processing strategy implemented in this study, land-cover classification is performed by using the RF classifier over the entire olive tree MS image. The MS data cube, which collects information from a surface area of 60 ha in RGB bands, contains more than 140 million pixels. The results show that thanks to this spatial partitioning processing strategy, it is feasible to classify large agricultural areas. This processing took 2.5 h and it would not have been possible to do it with a computer with normal specifications without manually partitioning the image in several parts, process part by part and merging the results.

In Fig. 4, we show the olive tree cover map. The area used in the following experiments is also shown. Given the homogeneity of the complete image, we focus on a small scene which corresponds to a fragment of 0.146 ha of the total area, with dimensions of 1095×1475 pixels.

E. Experiments

To evaluate and validate the different methods (RF, SVM, MLP, and kNN) in the considered application domain, several experiments have been carried out, categorized into three groups according to how many training samples have been extracted from the MS dataset in the preprocessing stage. In every scenario, for the SVM classifier, it has been proven that better results are obtained with the RBF kernel.

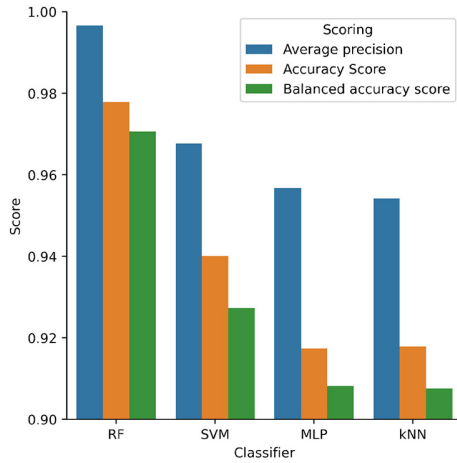


Fig. 7. Classification performance of different classifiers in experiment 1, using different metrics: (a) average precision, (b) accuracy score, and (c) balanced accuracy score.

1) *Experiment 1 (Handcrafted Feature-Based Method)*: First, a classical handcrafted feature-based method has been applied by using the QGIS software [34] to extract features that represent the dataset. Four land-cover classes can be observed in the data: 1) olive trees; 2) soil; 3) weeds; and 4) olive tree shadow over the soil. Training samples for each of these classes have been extracted from the RGB image through GIS tools, as shown in Fig. 5, where the polygons belonging to each of the classes are highlighted in different colors. The dataset is then transformed from a data cube of three dimensions to three vectors (corresponding to the reflectance values of the pixels of each of the training samples in one vector with three bands). Each of the three vectors has three other associated vectors corresponding to the known labels. Finally, classifiers are applied to build a model constructed with training samples to make predictions for the dataset, labeling every pixel of the image. The obtained classification maps are shown in Fig. 6. As can be seen by comparing the classification results with the RGB image, such classification maps provide a relatively good characterization of the features that appear in the scene.

The performance of different approaches is compared in Fig. 7 using the following classification metrics: average precision, accuracy score, and balanced accuracy score. All these metrics range between zero and one, the higher the better. The experiments have been repeated five times, taking as the score value to be compared the mean of five executions. In each of the three metrics, the predicted labels (pixel classes) of the RGB image are compared with the GT image (validated in the agricultural area by technicians). Fig. 7 shows that the accuracy of all classifiers is close to optimal, with the RF classifier providing the best scores.

2) *Experiment 2*: In this experiment, the image is classified with the different number of training samples randomly extracted from the training samples of experiment 1, specifically: 50, 100, 200, 400, 500, 600, and 700 training samples per class. The metrics used to measure classification performance are the same as those used in experiment 1 (average precision, accuracy score, and balanced accuracy score). Fig. 8 reports the mean of the scores after repeating

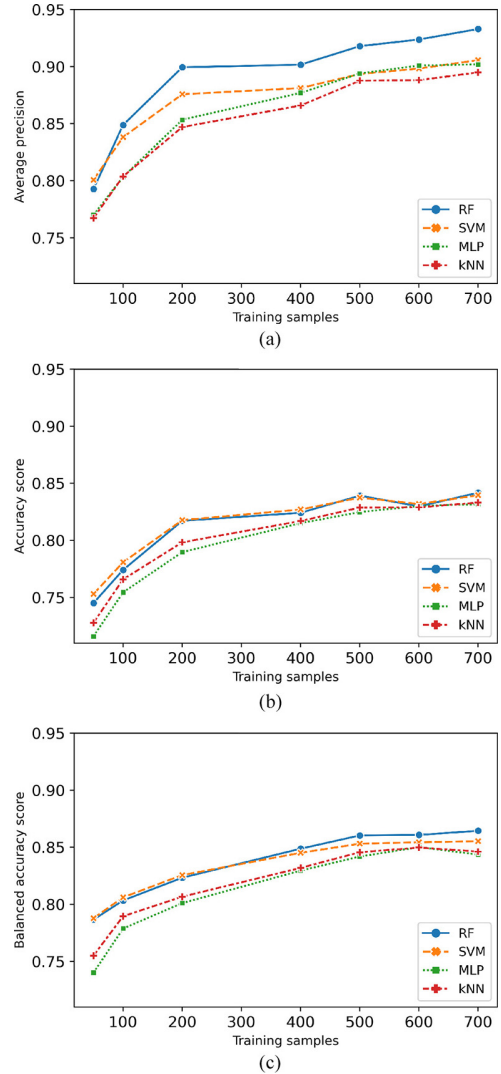


Fig. 8. Classification performance of different classifiers in experiment 2, using different metrics: (a) average precision, (b) accuracy score, and (c) balanced accuracy score.

each experiment five times. As it is shown, all the classification algorithms behave in a similar way. It can be seen how the accuracies increase as the number of training samples increases. They grow in a more pronounced way until the number of samples reaches approximately 200, and then continue growing moderately. In addition, it can be observed that when 600 training samples have been taken, there is a minimum decrease that is corrected when the performance is evaluated with the balanced accuracy score. Furthermore, it can be appreciated that the RF and SVM classification algorithms obtain better results over MLP and kNN, which also behave in a very similar way.

3) *Experiment 3*: For this experiment, a scalability test has been performed where a variable number of training samples per class have been randomly extracted from the training samples of experiment 1, using a linear scale factor, weighted according to the number of pixels associated with each class in the GT image. Table I shows the number of training samples per class in each step chosen for this experiment. Moreover, as

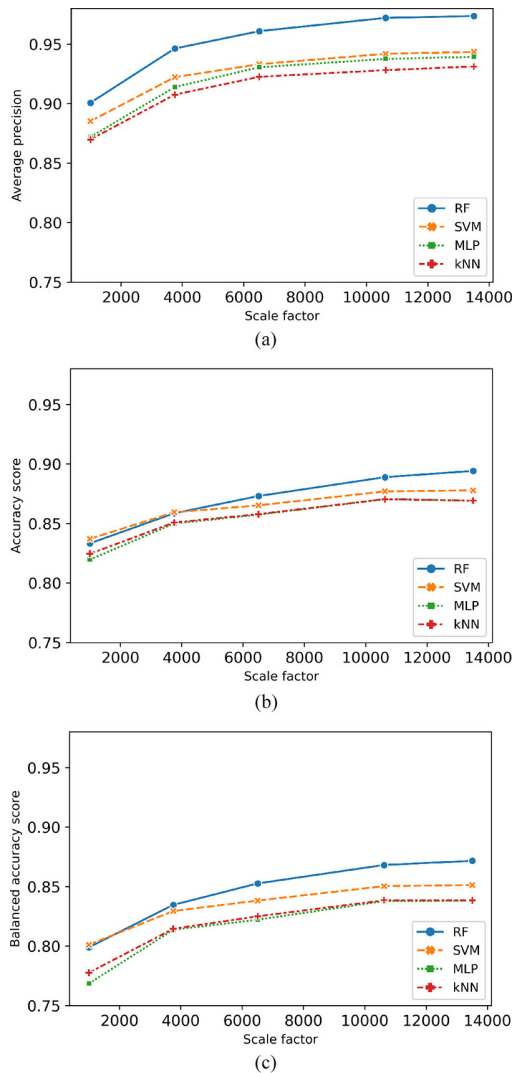


Fig. 9. Classification performance of different classifiers in experiment 3, using different metrics: (a) average precision, (b) accuracy score, and (c) balanced accuracy score.

TABLE I

NUMBER OF TRAINING SAMPLES PER CLASS ACCORDING TO THE WEIGHTED SCALE FACTOR USED

Classes	Weights	Scale factor				
		1000	3750	6500	10620	13500
Olive	16 %	160	600	1040	1699	2160
Soil	42 %	420	1575	2730	4460	5670
Weeds	38 %	380	1425	2470	4036	5130
Shadow	4 %	40	150	260	425	540

in the other two experiments, each test has been repeated five times, to measure the average precision, accuracy score, and balanced accuracy score, showing the mean of such accuracies in Fig. 9. As it is shown, the four classifiers analyzed behave in a very similar way, improving their performance as the number of training samples increases. They grow more significantly first and then tend to stabilize. The RF classifier stands out over the other three classifiers due to its better results. Compared to the previous experiment, the performance of the classifiers is more accurate when variable training samples are

chosen per class, in a way that is proportional to the number of samples of each class in the entire scene.

IV. CONCLUSION

In this article, a new strategy is developed to map large agricultural areas through high-resolution MS images, obtained by a drone flown over olive trees in the region of Extremadura (Spain), by implementing an automatic window processing method. Consequently, heavy MS image processing (from viewpoint of computational memory) becomes feasible to apply machine learning classifiers. Besides, the land-cover map obtained, through an automatic spatial partitioning, significantly reduces the time that would have been spent cropping areas of the MS image manually, using clip tools in GIS, for example. Additionally, different machine learning classification methods (RF, SVM, kNN, and MLP) have been applied to make a semi-automatic classification of MS data. Three experiments have been carried out to measure the performance of classification algorithms, obtaining accurate classification maps. The main conclusion is the techniques considered (especially, RF and SVM) can distinguish the different land-cover classes in the scene. This is mainly due to the high spatial resolution of the scene (which does not require very high spectral resolution to provide good classification results).

Furthermore, it has been shown that given the homogeneity of the crop, a semi-automatic classification of a large farm dedicated to olive trees can be executed, training the classification algorithms with few training samples. If machine learning had not been used, it would have to be done with subjective manual tasks by cropping the image with a pixel-by-pixel editor, which would be unfeasible. Our results demonstrate that machine learning applied in agriculture save a lot of time in terms of field work in the considered agricultural area and can greatly facilitate management of agricultural strategies.

Several agronomic applications can be achieved with the results of this study, such as detection of weeds (a main challenge in agronomic scenarios), future work on counting olive trees to estimate productions, as well as detecting diseases and growth problems of olive trees (avoid growth inequalities). In the future, more advanced classifiers like convolutional neural networks (CNNs) will be compared to the simpler (and faster) classifiers considered in this article.

ACKNOWLEDGMENT

The authors gratefully acknowledge Greenfield Technologies S.L. for providing the drone dataset used in the experiments. Some icons shown in the figures were collected from the free database of Flaticon and Freepik.

REFERENCES

- [1] C.-I. Chang, *Hyperspectral Imaging: Techniques for Spectral Detection and Classification—Chen-I Chang*. New York, NY, USA: Kluwer Acad., 2003.
- [2] A. Plaza, J. Plaza, A. Paz, and S. Sanchez, "Parallel hyperspectral image and signal processing [applications corner]," *IEEE Signal Process. Mag.*, vol. 28, no. 3, pp. 119–126, May 2011.
- [3] *Sentinel-2*. Accessed: Dec. 12, 2020. [Online]. Available: <https://www.esa.int>

- [4] AVIRIS—Airborne Visible/Infrared Imaging Spectrometer—General Overview. Accessed: Dec. 12, 2020. [Online]. Available: <https://aviris.jpl.nasa.gov/aviris/index.html>
- [5] C. A. Lee, S. D. Gasster, A. Plaza, C. I. Chang, C. I. Chang, and B. Huang, “Recent developments in high performance computing for remote sensing: A review,” *IEEE J. Sel. Topics Appl. Earth Observ. Remote Sens.*, vol. 4, no. 3, pp. 508–527, Sep. 2011.
- [6] S. Manfreda *et al.*, “On the use of unmanned aerial systems for environmental monitoring,” *Remote Sens.*, vol. 10, no. 4, p. 641, 2018.
- [7] F. Vanegas, D. Bratanov, K. Powell, J. Weiss, and F. Gonzalez, “A novel methodology for improving plant pest surveillance in vineyards and crops using UAV-based hyperspectral and spatial data,” *Sensors*, vol. 18, no. 1, p. 260, Jan. 2018.
- [8] M. D. Yang, H. H. Tseng, Y. C. Hsu, and H. P. Tsai, “Semantic segmentation using deep learning with vegetation indices for rice lodging identification in multi-date UAV visible images,” *Remote Sens.*, vol. 12, no. 4, p. 633, Feb. 2020.
- [9] G. Shaw and D. Manolakis, “Signal processing for hyperspectral image exploitation,” *IEEE Signal Process. Mag.*, vol. 19, no. 1, pp. 12–16, Jan. 2002.
- [10] B. Ayhan *et al.*, “Vegetation detection using deep learning and conventional methods,” *Remote Sens.*, vol. 12, no. 15, p. 2502, Aug. 2020.
- [11] INE Instituto Nacional de Estadística. Accessed: Dec. 12, 2020. [Online]. Available: <https://www.ine.es/>
- [12] M. E. Paoletti, J. M. Haut, J. Plaza, and A. Plaza, “Neighboring region dropout for hyperspectral image classification,” *IEEE Geosci. Remote Sens. Lett.*, vol. 17, no. 6, pp. 1032–1036, Jun. 2020.
- [13] M. E. Paoletti, J. M. Haut, X. Tao, J. P. Miguel, and A. Plaza, “A new GPU implementation of support vector machines for fast hyperspectral image classification,” *Remote Sens.*, vol. 12, no. 8, p. 1257, 2020.
- [14] J. M. Haut, M. E. Paoletti, J. Plaza, A. Plaza, and J. Li, “Visual attention-driven hyperspectral image classification,” *IEEE Trans. Geosci. Remote Sens.*, vol. 57, no. 10, pp. 8065–8080, Oct. 2019.
- [15] N. He, L. Fang, S. Li, A. Plaza, and J. Plaza, “Remote sensing scene classification using multilayer stacked covariance pooling,” *IEEE Trans. Geosci. Remote Sens.*, vol. 56, no. 12, pp. 6899–6910, Dec. 2018.
- [16] P. Ghamisi, J. Plaza, Y. Chen, J. Li, and A. J. Plaza, “Advanced spectral classifiers for hyperspectral images: A review,” *IEEE Geosci. Remote Sens. Mag.*, vol. 5, no. 1, pp. 8–32, Mar. 2017.
- [17] L. Breiman, “Random forests,” *Mach. Learn.*, vol. 45, no. 1, pp. 5–32, 2001.
- [18] V. F. Rodriguez-Galiano, B. Ghimire, J. Rogan, M. Chica-Olmo, and J. P. Rigol-Sanchez, “An assessment of the effectiveness of a random forest classifier for land-cover classification,” *ISPRS J. Photogrammetry Remote Sens.*, vol. 67, pp. 93–104, Jan. 2012.
- [19] P. O. Gislason, J. A. Benediktsson, and J. R. Sveinsson, “Random forests for land cover classification,” *Pattern Recognit. Lett.*, vol. 27, no. 4, pp. 294–300, 2006.
- [20] B. Waske, J. A. Benediktsson, K. Arnason, and J. R. Sveinsson, “Mapping of hyperspectral AVIRIS data using machine-learning algorithms,” *Can. J. Remote Sens.*, vol. 35, no. S1, pp. S106–S116, 2009.
- [21] M. Belgiu and L. Drăgu, “Random forest in remote sensing: A review of applications and future directions,” *ISPRS J. Photogrammetry Remote Sens.*, vol. 114, pp. 24–31, Apr. 2016.
- [22] V. N. Vapnik, *Statistical Learning Theory*. New York, NY, USA: Wiley, 1998.
- [23] A. J. Izenman, “Support vector machines,” in *Learning With Kernels: Support Vector Machines, Regularization, Optimization, and Beyond*. Cambridge, MA, USA: MIT Press, 2013, pp. 369–406.
- [24] F. Melgani and L. Bruzzone, “Classification of hyperspectral remote sensing images with support vector machines,” *IEEE Trans. Geosci. Remote Sens.*, vol. 42, no. 8, pp. 1778–1790, Aug. 2004.
- [25] P. Ghamisi, M. S. Couceiro, and J. A. Benediktsson, “A novel feature selection approach based on FODPSO and SVM,” *IEEE Trans. Geosci. Remote Sens.*, vol. 53, no. 5, pp. 2935–2947, May 2015.
- [26] T. Cover and P. Hart, “Nearest neighbor pattern classification,” *IEEE Trans. Inf. Theory*, vol. IT-13, no. 1, pp. 21–27, Jan. 1967.
- [27] F. Maselli, G. Chirici, L. Bottai, P. Corona, and M. Marchetti, “Estimation of mediterranean forest attributes by the application of k -NN procedures to multitemporal landsat ETM+ images,” *Int. J. Remote Sens.*, vol. 26, no. 17, pp. 3781–3796, 2005.
- [28] A. E. Maxwell, T. A. Warner, and F. Fang, “Implementation of machine-learning classification in remote sensing: An applied review,” *Int. J. Remote Sens.*, vol. 39, no. 9, pp. 2784–2817, 2018.
- [29] D. E. Rumelhart, G. E. Hinton, and R. J. Williams, “Learning representations by back-propagating errors,” *Nature*, vol. 323, no. 60881, pp. 533–536, 1986.
- [30] J. A. Benediktsson, “Statistical methods and neural network approaches for classification of data from multiple sources,” Ph.D. dissertation, School Elect. Eng., Purdue Univ., West Lafayette, IN, USA, 1990.
- [31] J. A. Richards, “Analysis of remotely sensed data: The formative decades and the future,” *IEEE Trans. Geosci. Remote Sens.*, vol. 43, no. 3, pp. 422–432, Mar. 2005.
- [32] eBee Plus—SenseFly. Accessed: Mar. 26, 2021. [Online]. Available: <https://www.sensefly.com/solution/survey-360-survey-drone-solution/>
- [33] SenseFly S.O.D.A.—SenseFly. Accessed: Dec. 12, 2020. [Online]. Available: <https://www.sensefly.com/camera/sensefly-soda-photogrammetry-camera/>
- [34] QGIS Geographic Information System, QGIS Develop. Team, 2020. [Online]. Available: <https://www.qgis.org/>



Elena C. Rodríguez-Garlito received the B.Sc. degree in civil engineering and the M.Sc. degree in geographical information systems (GIS) and remote sensing from the University of Extremadura, Cáceres, Spain, in 2013 and 2014, respectively, where she is currently pursuing the Ph.D. degree with predoctoral contracts for the training of Doctors in public RD centers belonging to the Extremadura System of Science, Technology, and Innovation.

She is currently a member of the Hyperspectral Computing Laboratory, Department of Technology of Computers and Communications, University of Extremadura. Her research interests include GIS, remote sensing, and machine learning.



Abel Paz-Gallardo received the B.S. degree in computer engineering and the M.Sc. and Ph.D. degrees in computer science from the University of Extremadura, Cáceres, Spain, in 2007, 2009, and 2011, respectively.

His Ph.D. and main research interests comprise remotely sensed hyperspectral image analysis, signal processing, and efficient implementations of large-scale scientific problems on high-performance computing architectures, such as clusters and graphical processing units (GPUs). From 2006 to 2007, he was a Research Assistant with the Computer Architecture Department, University of Extremadura, where he became an Associate Professor in 2008. At the same time, he started working with the Minimally Invasive Surgery Center Jesús Usón, Cáceres. In 2010, he started working for Bull Spain S.A. to deploy at CETA-Ciemat, Trujillo, Spain, the biggest GPGPU Cluster in Spain and one of the biggest ones in Europe. Since November 2010, he has been an Associate Professor with the Computer Architecture Department, University of Extremadura. From October 2011 to July 2018, he was the IT Manager (CIO) of CETA-Ciemat, where he achieved the GPU Research Centre mention from NVIDIA as a Principal Investigator. Since 2018, he has been the Chief Information Officer of Greenfield Technologies, a precision agriculture company that provides recommendations to farmers, through the use of different innovative technologies (such as drones, satellites, sensors, and artificial intelligence) and applied research. He has participated in more than 30 international projects and has authored more than 40 publications, including 14 journal citation report (JCR) papers (most of them published by IEEE journals) and over 30 peer-reviewed international conference papers.

Dr. Paz-Gallardo was also awarded with the *IEEE Signal Processing Magazine* Best Column Award Paper from the IEEE Signal Processing Society in November 2015.

Automatic Detection of Aquatic Weeds: A Case Study in the Guadiana River, Spain

Escuela Politécnica
Av. de la Universidad, S/N, 10003
Teléfono: 0034927257000. Ext. 51662
correo electrónico: apazgal, aplaza @unex.es
Cáceres, España

Dr. Abel Francisco Paz Gallardo y Dr. Antonio Plaza Miguel, como directores de la Tesis Doctoral titulada “Desarrollo de nuevos métodos y algoritmos de análisis y clasificación de imágenes multiespectrales orientadas a la gestión y monitorización de plantas acuáticas invasoras”, certificamos el factor de impacto y la categorización de la siguiente publicación incluida en la Tesis Doctoral. Del mismo modo, se especifica la aportación de la doctoranda. Para cualquier otra información o aclaración, por favor, no duden en contactar con nosotros.

Título de la publicación: Automatic Detection of Aquatic Weeds: A Case Study in the Guadiana River, Spain

Autores: **Elena C. Rodríguez-Garlito**, Abel Paz-Gallardo y Antonio Plaza

Revista: IEEE Journal of Selected Topics in Applied Earth Observations and Remote Sensing

Otros datos: vol 15, págs 8567-8585, año 2022

DOI: 10.1109/JSTARS.2022.3210373

Factor de impacto 2022: 5.5

Abstract: The spread of aquatic invasive plants is a major concern in several zones of the world's geography. These plants, which are not part of the natural ecosystem, cause a negative impact to the environment, as well as to economy and society. In Spain, large areas of Guadiana (the second-longest river in Spain) have been invaded by such plants. Among the strategies to address this problem, monitoring and detection play an important role to control the spatiotemporal distribution of the invasive plants. The main objective of this work is to develop a methodology able to automatically detect the geolocation of aquatic invasive plants using remote sensing and machine learning techniques. To this end, several classification algorithms have been applied to freely available multispectral satellite imagery, collected by ESA's Sentinel-2 satellite. A quantitative and comparative assessment is conducted using different machine and deep learning algorithms from classical methods, such as unsupervised K-means to supervised random forests and convolutional neural networks. This study also proposes a methodology for validating the obtained classification results, generating synthetic ground truth images based on available high spatial resolution imagery. The obtained results demonstrate the suitability of some of the considered algorithms for automatic detection of aquatic weeds in satellite images with medium spatial resolution.

Contribución de la doctoranda: Planteamiento de la hipótesis, conceptualización, búsqueda bibliográfica, metodología, análisis y discusión de resultados, elaboración de tablas y figuras, escritura del manuscrito borrador y redacción de la revisión.

Automatic Detection of Aquatic Weeds: A Case Study in the Guadiana River, Spain

Elena C. Rodríguez-Garlito , *Student Member, IEEE*, Abel Paz-Gallardo , and Antonio Plaza , *Fellow, IEEE*

Abstract—The spread of aquatic invasive plants is a major concern in several zones of the world’s geography. These plants, which are not part of the natural ecosystem, cause a negative impact to the environment, as well as to economy and society. In Spain, large areas of Guadiana (the second-longest river in Spain) have been invaded by such plants. Among the strategies to address this problem, monitoring and detection play an important role to control the spatiotemporal distribution of the invasive plants. The main objective of this work is to develop a methodology able to automatically detect the geolocation of aquatic invasive plants using remote sensing and machine learning techniques. To this end, several classification algorithms have been applied to freely available multispectral satellite imagery, collected by ESA’s Sentinel-2 satellite. A quantitative and comparative assessment is conducted using different machine and deep learning algorithms from classical methods, such as unsupervised K-means to supervised random forests and convolutional neural networks. This study also proposes a methodology for validating the obtained classification results, generating synthetic ground truth images based on available high spatial resolution imagery. The obtained results demonstrate the suitability of some of the considered algorithms for automatic detection of aquatic weeds in satellite images with medium spatial resolution.

Index Terms—Aquatic weeds, deep learning (DL), detection, invasive plants, machine learning (ML), remote sensing (RS), Sentinel-2.

I. INTRODUCTION

REMOTE sensing (RS) and geographical information systems (GISs) are two disciplines on the rise in recent decades. Together, they provide an ideal analysis framework in many disciplines [1]. Based on RS technology, multispectral

(MS) or hyperspectral (HS) sensors installed on airborne (airplanes/drones) or spaceborne (satellites) platforms measure the energy that an object in the Earth’s surface reflects and absorbs. In this way, MS or HS images record measurements in discrete and discontinuous portions of the spectral range, with tens (MS) or hundreds (HS) of nearly contiguous spectral bands. As a result, RS data contain a vast amount of information in the spatial and spectral domains and can be represented as data cubes, as they comprise data in three dimensions [2]. In other words, each pixel is composed of tens or hundreds of measurements in different wavelengths.

On the other hand, GIS technology facilitates the understanding of the information in the pixels that make up the data cube by taking advantage of the information available in the spatial domain. In this way, maps can be created displaying the spectral observations in a georeferenced way. This also allows for the arrangement of different layers of georeferenced information for better assessment of the data using GIS techniques in computer applications.

The exploitation of RS together with GIS exhibits the potential to improve the understanding of the land surface, thanks to the detailed information that RS images provide, consequently allowing for a precise analysis and GIS-based interpretation that is applicable to several fields, such as urban planning [3], biodiversity [4], disaster management [5], precision agriculture [5], land cover mapping [6], monitoring of oil spills and other events [7], among many others. In particular, classification allows distinguishing water bodies from other impervious surfaces (e.g., urban environments), including soil and vegetation. This allows us to address problems related to (for instance) the excessive growth of vegetation in water (the most important resource on the planet).

The inefficient management of domestic, agricultural, or industrial waste contributes to the excess of nutrients in aquatic ecosystems (e.g., phosphorus and nitrogen), which pollute the water through a process called eutrophication [8]. Important ecological impacts, such as the loss of water quality, stem from the enrichment of nutrients in the water. This enrichment also causes an excessive growth of certain plant species known as aquatic weeds [9]. An excessive presence of such weeds could lead to the fact that a large amount of oxygen dissolved in the water is consumed during their growth and putrefaction, introducing a large amount of organic matter in the water [10]. Most notably, floating aquatic weeds tend to create a mantle on the surface of the water that absorbs light, reducing the amount of illumination in benthic habitats and, therefore, reducing biodiversity [11].

Manuscript received 18 July 2022; revised 5 September 2022; accepted 26 September 2022. Date of publication 28 September 2022; date of current version 12 October 2022. This work was supported in part by European Social Fund (Resolución de 10 de mayo de 2017, de la Secretaría General de Ciencia, Tecnología e Innovación, por la que se resuelve la convocatoria de ayudas para la financiación de contratos predoctorales para formación de Doctores en los centros públicos de I+D pertenecientes al Sistema Extremeño de Ciencia, Tecnología e Innovación en el ejercicio 2017 expediente PD16001), in part by the Consejería de Economía, Ciencia y Agenda Digital of the Junta de Extremadura and the European Regional Development Fund (ERDF) of the European Union under Grant GR21040, in part by Spanish Ministerio de Ciencia e Innovación under Grant PID2019-110315RB-I00 (APRISA), and in part by European Union’s Horizon 2020 Research and Innovation Program under Grant 734541 (EOXPOSURE). (*Corresponding author: Antonio Plaza.*)

The authors are with the Hyperspectral Computing Laboratory, Department of Technology of Computers and Communications, Escuela Politécnica, University of Extremadura, 10003 Cáceres, Spain (e-mail: elenacristinarg@unex.es; apazgal@unex.es; aplaza@unex.es).

Digital Object Identifier 10.1109/JSTARS.2022.3210373

Occasionally, in specific geographical areas on the water's surface, there is vegetation that is not part of that particular ecosystem. Such kind of vegetation is also referred to as alien species. These are invasive species introduced intentionally or accidentally, e.g., due to globalization (trade, transport of goods, etc.). Due to their invasive nature, these species also pose a significant threat to the species of the native ecosystem [12]. Therefore, the removal of these so-called invasive plants is much needed to reduce the impact introduced in the environment and water quality, and also to reduce the negative economic impact [13]. As a specific case study, the Guadiana river basin in Extremadura (a region in the southwest of Spain) contains invasive species, such as water hyacinth (*Eichhornia crassipes*), since the beginning of the 2000s. It is possible to perform mechanical elimination of these species by chemical or biological means [14], [15], as well as to adopt other methods to control their spread [16].

In order to monitor and control invasive aquatic plants, mapping their distribution is a critical step. RS plays an important role in this task, since satellite images provide rich spatial and temporal information. In recent decades, we have seen a tremendous growth of RS studies in which image analysis and different sensor specifications have been exploited to map and detect aquatic invasive plants [17], [18], [19], [20], [21]. However, in the literature, there are few studies aimed at monitoring and controlling of aquatic invasive plants using machine learning (ML) techniques [22], [23], [24].

Artificial intelligence (AI) approaches provide a wide variety of regression and classification algorithms for the interpretation of RS images. Besides, depending on the availability of labeled samples to train the models, they can be categorized into unsupervised, supervised, or semisupervised methods (a hybrid of the first-two). Popular examples of unsupervised methods are clustering algorithms. These algorithms find natural groups with similar spectral behavior, such as the well-known K-means. Due to its simplicity, this method has been widely used to group samples of data in clusters [25]. On the other hand, supervised algorithms, such as random forests (RFs) [26], support vector machines [27], K-nearest neighbor [28], or multilayer perceptron (MLP), require training samples. MLP is in fact an artificial neural network (ANN), which mimics the behavior of neurons in the human brain. ANN-based algorithms have significantly developed in recent years, thanks to the advent of computer hardware, such as graphics processing units, and have evolved into a subfield of ML called deep learning (DL). Numerous studies have considered DL algorithms [29]. Among them, convolutional neural networks (CNNs) have become extremely popular due to their outstanding performance in many classification tasks (e.g., to recognize objects [30], scenes [31], pixel classification of a scene [32], or subpixel detection [33]).

The main goal of this work is to develop an ML/DL methodology to automatically detect the spatial-temporal distribution of aquatic invasive plants in the Guadiana river. To the best of our knowledge, there are no previous studies about the detection of aquatic weeds in this river combining GIS, RS, and AI techniques [34]. Specifically, we could not find any works using

DL to address this problem. The main innovative contributions of our work can be summarized as follows.

- 1) We establish a full processing chain, including preprocessing, processing, and evaluation, of Sentinel-2 images, using RS and GIS tools (with treatment of NoData values), to automatically detect invasive aquatic weeds in the Guadiana river.
- 2) We have implemented a novel strategy to validate the performance of ML/DL algorithms in the considered application. To be specific, we generate synthetic ground truth (GT) data from a high-resolution MS image. For this purpose, we use data acquired by the (Spanish) National Plan of Aerial Orthophotography (PNOA) that provides open-access datasets that have been preclassified using a window-based processing strategy [35].
- 3) We carry out a detailed comparison between ML and DL algorithms in the context of aquatic weeds detection. In order to show that invasive aquatic plants can be monitored using ML/DL techniques, two areas in the Guadiana river, Spain, have been carefully selected and studied. K-means clustering and the RF algorithm have been applied to them, and a CNN architecture has also been configured for this study. We use Sentinel-2 medium-resolution MS images to conduct the study, as they can be collected with a frequent revisit time (five days) and are freely available to the scientific community. We also report results on the full Sentinel-2 flightlines for reference.

The rest of this article is organized as follows. Section II describes some challenges related to the detection of aquatic weeds in the Guadiana river. Section III outlines some available open-access RS datasets to detect aquatic weeds in the Guadiana river. Section IV describes the adopted ML/DL techniques. Section V explains the materials and methods used in our work. Section VI discusses the obtained experimental results. Finally, Section VII concludes this article.

II. AQUATIC WEEDS IN THE GUADIANA RIVER: BACKGROUND AND CHALLENGES

The challenge of preventing and controlling the existence and spread of invasive aquatic weeds extends over a large part of the world geography. As an illustration, the water hyacinth (*Eichhornia crassipes*) is one of the most invasive species on the Earth. Its geographical distribution reaches almost every continent [36]. In Africa, it is present in many places, such as the Lake Victoria or Niger river. In Asia, it can be found at the Al Kabir river. In Australia, it covers the Burdeki River and. And, in North and South America, it is present in the Rio Grande and several lagoons outside the Amazon, among others. In Europe, these aquatic weeds are also living in France, Italy, Portugal, Germany, and Spain, where the second-largest river (Guadiana) is largely affected.

The Guadiana river's basin is located at the Iberian Peninsula and covers an area of about 67 129.38 km². The river flows in a course of about 829 km from east to west, extending for the most part in the southwest of Spain. The Spanish basin crosses the regions of Andalucía, Castilla La Mancha, and Extremadura,



Fig. 1. *Nymphaea mexicana* in the Guadiana river, photographed by Tomás Rodríguez.

distributed in an area of 55 508.28 km² [37]. In this work, we focus on two areas located in Extremadura, where the basin of the Guadiana river occupies an area of 23 443.73 km². Moreover, Extremadura has about 1500 km of inland coastline, the largest in Western Europe.

In addition to *Eichhornia crassipes*, other invasive aquatic plant species have spread in the Guadiana river, such as *Nymphaea mexicana* (see Fig. 1) and *Azolla filiculoides*. They all have American origin. Moreover, as shown in Fig. 1, their tapestry-like distribution on the surface of the water prevents the passage of light and affects native vegetation as well as aquatic invertebrates [38], [39], [40]. The negative ecological and socioeconomic impacts caused by these invasive plants have motivated different control mechanisms, as well as eradication attempts by public institutions. In this sense, several extraction and surveillance actions have been carried out, requiring large economic investments. Some of these actions have been framed within international projects [41], [42], including LIFE + INVASEP “Combat invasive species in the Tajo and Guadiana drainage basins in the Iberian Peninsula,” Interreg Spain–Portugal LIFE10/NAT/ES 000582, and ACECA Project—cofinanced by the European Regional Development Fund (i.e., FEDER)—with budgets of 2 895 267 and 5 560 221.66 euros in 2012–2016 and 2014–2020 periods, respectively.

The current strategies carried out for the eradication of invasive aquatic plants have not achieved their total elimination. In this regard, new financial investments for control strategies are planned for the 2021–2027 period for *Eichhornia crassipes* and *Nymphaea mexicana* [43], respectively. For this reason, monitoring and mapping aquatic weeds are necessary. RS and GIS techniques for image acquisition and processing are powerful tools for this purpose.

III. OPEN-ACCESS RS DATASETS

There is a wide variety of currently operational RS instruments able to capture spectral radiance or reflectance of the Earth’s surface, with different numbers of spectral channels covering a diversity of spectral ranges. On the one hand, HS sensors collect data in hundreds of nearly contiguous spectral bands. On the other hand, MS images usually have a lower discrete number of bands. RS sensors are flown on airborne or spaceborne instruments, taking part in different space missions or national plans, which provide coverage throughout international and national territories, in several formats and resolution in the spatial, spectral, and temporal domains. RS imagery are often available for free or under request. In our research, medium-resolution images (acquired with frequent revisit times) have been targeted to monitor the spread of aquatic invasive plants. Whenever available, open-access databases have been chosen. In that sense, the MS dataset provided by PNOA and datasets collected by Sentinel-2 have been selected.

Several research efforts have considered digital aerial orthophotographs collected by PNOA for photointerpretation tasks, due to their high spatial resolution [44], [45], [46]. Some projects managed by the Ministry of Development (Spain) follow the INSPIRE Directive [47], which establishes a spatial data infrastructure for geographic data in Europe to provide geometric and temporal coherence of cartographic and geographic databases. In this way, aerial photography constitutes a basis for the realization of information on urban planning, land occupation, hydrography, forest management, and cartography for territories belonging to the European Community. Within the PNOA framework, it is possible to perform photogrammetric flights using planes equipped with a high-resolution digital camera, four MS sensors, and a panchromatic sensor, collecting high spatial resolution images (25 or 50 cm) of the entire Spanish

TABLE I
SENTINEL-2 BANDS

Band name	B01	B02	B03	B04	B05	B06	B07	B08	B8A	B09	B10	B11	B12
Resolution (m)	60	10	10	10	20	20	20	10	20	60	60	20	20
Bandwidth (nm)	442.7	492.4	559.8	664.6	704.1	740.5	782.8	832.8	864.7	945.1	1373.5	1613.7	2202.4
Application	Coastal aerosol	Blue	Green	Red	Vegetation red edge	Vegetation red edge	Vegetation red edge	NIR	Narrow NIR	Water vapour	Cirrus	SWIR	SWIR

territory within a period of 2 or 3 years (depending on the area) [48]. Among the products offered, PNOA provides free MS images with high spatial resolution and three RGB spectral bands in the European Terrestrial Reference System (ETRS89) geodetic system. Furthermore, upon request, digital frames of PNOA flights can be purchased. These images comprise four bands, three for the visible (RGB) part of the spectrum and one for near-infrared (NIR), all georeferenced in the ETRS89 geodetic Cartesian reference framework, with high spatial resolution images (0.22 or 0.45 m).

Last but not least, the European Space Agency (ESA) developed (as part of the Copernicus programme) a family of Earth observations missions called Sentinels. In this work, given their success for land cover classification [49], [50], an MS medium-resolution optical imagery provided by Sentinel-2 mission (focused on land monitoring [51]) is considered. Sentinel-2 provides coverage over all land areas, except Antarctica, via two identical satellites, which are composed by an MS instrument (whose technical characteristics allow a revisit time of five days). Sentinel-2 offers two types of products: 1) Level-1 C (S2L1C); and 2) Level-2 A (S2L2A). Both of them are available for free, and they are composed of $100 \times 100 \text{ km}^2$ tiles, which are orthoimages in UTM/WGS84 projection. S2L1C is a top-of-atmosphere reflectance product and S2L2A a bottom-of-atmosphere reflectance product. S2L2A is the result of applying atmospheric correction techniques to S2L1C images (thanks to a processing algorithm called Sen2Cor, developed by ESA). As a result, the reflection and scattering of light by the atmosphere before reaching the ground is corrected. Each S2L1C image is composed of 13 spectral bands, containing reflectance values from the visible and NIR to the shortwave infrared, with spatial resolutions of 10-, 20-, and 60-m per pixel (depending on the wavelength). In this way, the four visible spectral bands have spatial resolution of 10-m per pixel, the six NIR bands have 20-m spatial resolution, and the three shortwave infrared bands have 60-m spatial resolution. In case of S2L2A, the B10 band (used for cirrus cloud detection) is excluded, because it does not contain any information at the bottom of the atmosphere (see Table I [52]).

IV. MACHINE/DEEP LEARNING TECHNIQUES

To the best of our knowledge, AI methods have not been fully explored as of yet to automatically map the spatiotemporal distribution of aquatic invasive plants. In this section, we describe some ML/DL techniques that we have used to perform automatic invasive plants detection.

Let an MS image be defined by $X \in \mathbb{R}^{H \times W \times B}$, where H and W denote the height and width of the data cube, respectively, and B is the number of spectral bands. The goal is to find a mapping function $\mathcal{M}_\theta : X \rightarrow Y$ that assigns each pixel x_i to a corresponding label y_i (including aquatic weed), producing a classification map $Y \in \mathbb{R}^{H \times W}$. In this sense, ML/DL algorithms build a model based on learning to make predictions. In supervised approaches, training samples are collected and labels for some pixels are available (e.g., by means of a human-based annotation process). On the contrary, unsupervised approaches group similar pixels together by discovering patterns of similarity. Last but not least, semisupervised methods combine labeled and unlabeled data during the training process.

Recent advances in ML/DL algorithms, high-performance computing, and Big Data accessibility have led to the adoption of ANNs for classification tasks [53]. DL, which can be considered as a subfield of ML [54], exploits many ANN layers that are stacks of functions able to extract features at different levels [55]. Their structure exhibits great advantages over traditional ML algorithms. Specifically, DL models can be adapted to supervised and unsupervised classification tasks; their learning procedure allows to extract linear and nonlinear features, and they exhibit great flexibility in their architectures, thanks to their diversity in terms of both the types of layer that can be arranged and their number (depth) [56].

In the following, general aspects of the ML/DL algorithms adopted in our work are given. Specifically, we use an unsupervised method widely known for its simplicity (i.e., K-means clustering), a supervised (i.e., RF) based on decision trees, and a supervised DL method (i.e., CNN).

1) *K-means*: K-means is a popular unsupervised method among clustering techniques where data are grouped in clusters such that samples in the same group (or cluster) are more similar to each other than those in other groups. The goal of this algorithm is to choose centroids within a cluster sum-of-squares criterion given by

$$\sum_{i=0}^n (\|x_i - \mu_j\|^2) \quad (1)$$

where n is the number of groups of equal variance in which samples are separated and x_i are the samples (divided into k disjoint clusters C described by the mean μ_j). The operation of this algorithm can be described in several steps.

- a) In the first step, parameter k (corresponding to the number of clusters to be identified in the data) is set. Then, the centroids of the clusters are chosen and each sample is assigned to its nearest centroid.

b) In the second step, new centroids are created by taking the mean value of all the samples assigned to each previous centroid. The difference between the new centroids and the old ones is computed, and this process is repeated until there are no more changes in the location of the centroids.

2) *Random Forest*: RF is an ensemble learning approach first introduced in [57]. In particular, this method classifies pixels by creating a multitude of randomized decision trees (supervised and nonparametric classifiers) where the final prediction is an average of the probabilistic ones of each decision tree. In other words, it performs a bagging strategy by building the trees from top to bottom based on the “divide and conquer” concept [58], achieving error compensations. First, in order to carry out the (supervised) classification, a training set is defined. RF operates by means of a bagging procedure in which training samples are randomly selected from the original training set. As a result, some samples may not be used and others may be chosen more than once. Next, each decision tree is built with different training sets by using a bootstrapped dataset. This technique improves the generalization of the learning process by avoiding the tendency to overfitting of decision trees. It is advantageous for reducing model variance without increasing bias. Other methods based on “boosting” are more sensitive to overtraining and noise [59].

3) *Convolutional Neural Networks*: CNNs are a kind of nonlinear models categorized within a supervised deep network (discriminative deep networks). Their structure is inspired by the behavior of neurons in visual neuroscience. CNNs comprise a set of blocks with units (or neurons) capable to transform the input data volume to an output volume of units (or neurons). The output volume of neurons of the previous blocks will be the input block to the following block [32]. In general terms, as any feedforward neural network, the architecture of the CNN consists of an input layer, hidden layers, and output layer. The hidden layers are divided in two parts: a) the first one is the feature extractor; and b) the second part is often an MLP, which assigns the final class labels. In other words, this design consists of multiple layers where the outer layers of a CNN extract basic features, whereas more complex learning is hierarchically produced in the inner layers. With regards to the MLP, the neurons of a layer are not fully connected to all neurons of the previous one, because they are connected to a small region of previous input volume. This particularity allows the blocks of neurons in a CNN to work as kernels, operating over a small region of the previous layer. The withdrawal of fully connected layers can be beneficial in terms of reducing complexity and enhancing the exploitation of spatial information in the data. CNNs have been successfully applied to perform RS image classification. Their multilayer structure can exploit the advantages of natural signal sharing weights, with pooling layers and local connections. The way input data are presented to the network (in the form of multiple arrays), makes it suitable to process both MS and HS images [60]. The main types of hierarchical structures are convolutional layers with nonlinear operation and pooling layers in the first stages and fully connected layers in the last stages [56]. The CNN applies weights and biases to the input data in each hidden layer. CNNs use an activation function and perform convolutions. Among the different types of CNN

models for RS data classification (spectral CNN, spatial CNN, and spectral–spatial CNN) [61], we focus on spectral CNNs [62] where the procedure repeated in the convolutional layers l can be described as

$$l : X_k^l = \sigma(K_1^{l-1} * X^{l-1} + b_k^{l-1}) \quad (2)$$

where the feature map created at each layer l is X_k , K is a set of kernels $K = \{K_1, K_2, K_3, \dots, W_k\}$, the b applied biases are $\gamma = \{b_1, b_2, b_3, \dots, b_k\}$, the input RS dataset is convolved using the $*$ operation, and the nonlinear transform function is denoted by $\sigma(\cdot)$ [29]

V. MATERIALS AND METHODS

A. Study Area

Our study has been conducted at the Guadiana river in Extremadura, Spain. Two portions of a section affected by aquatic weeds in the river have been analyzed. The first region of interest (ROI) corresponds to a section affected by *Nymphaea mexicana* that crosses the city of Badajoz (denoted hereinafter as BA_zone) with an area of 192 ha approximately, which extends between $7^\circ 01' - 6^\circ 58'$ W latitude and $38^\circ 51' - 38^\circ 53'$ N longitude. The second study area (about 45 ha) is affected by *Eichhornia crassipes* in the city of Mérida (denoted hereinafter as ME_zone) in which an invasive plant control barrier has been installed in the river for mechanical removal. This area extends between $6^\circ 19' - 6^\circ 18'$ W latitude and $38^\circ 50' - 38^\circ 51'$ N longitude, respectively (see Fig. 2).

B. MS Datasets

In our experiments, several datasets collected by different MS sensors (PNOA and Sentinel-2) have been considered. First, to facilitate the training and validation for aquatic weeds detection, the PNOA dataset has been obtained over BA_zone and ME_zone. The orthophotographs have been obtained for free from National Geographic Institute’s Download Center (IGN) [63]. By analyzing the metadata of each image, we can see that the date in which they were collected was July 10, 2019. These PNOA datasets include three RGB bands and their dimensions are $18\,630 \times 9747$ and 7443×6321 pixels (width \times height) for the BA_zone and ME_zone, respectively. As will be explained later, both images acquired by the PNOA are rectangular and include both ROIs for Badajoz and Mérida (i.e., ROI_BA and ROI_ME), corresponding to the river areas being analyzed, as well as some NoData values (pixels where there is no information). There are 27 448 554 and 6 432 601 pixels with information in ROI_BA and ROI_ME, respectively, with a spatial resolution of 0.25-m per pixel. These datasets were downloaded in Unit 8 (unsigned integer 8 bits) format, where each pixel values range from 0 to 255.

Our study aims to detect aquatic weeds by using free high spatial resolution satellite images with a frequent revisit time over the ROI, allowing for the monitoring and control of the weeds. For this purpose, datasets S2L2A (acquired by an MS sensor onboard Sentinel-2) have been downloaded from a satellite imagery provider called SentinelHub [64]. These datasets are

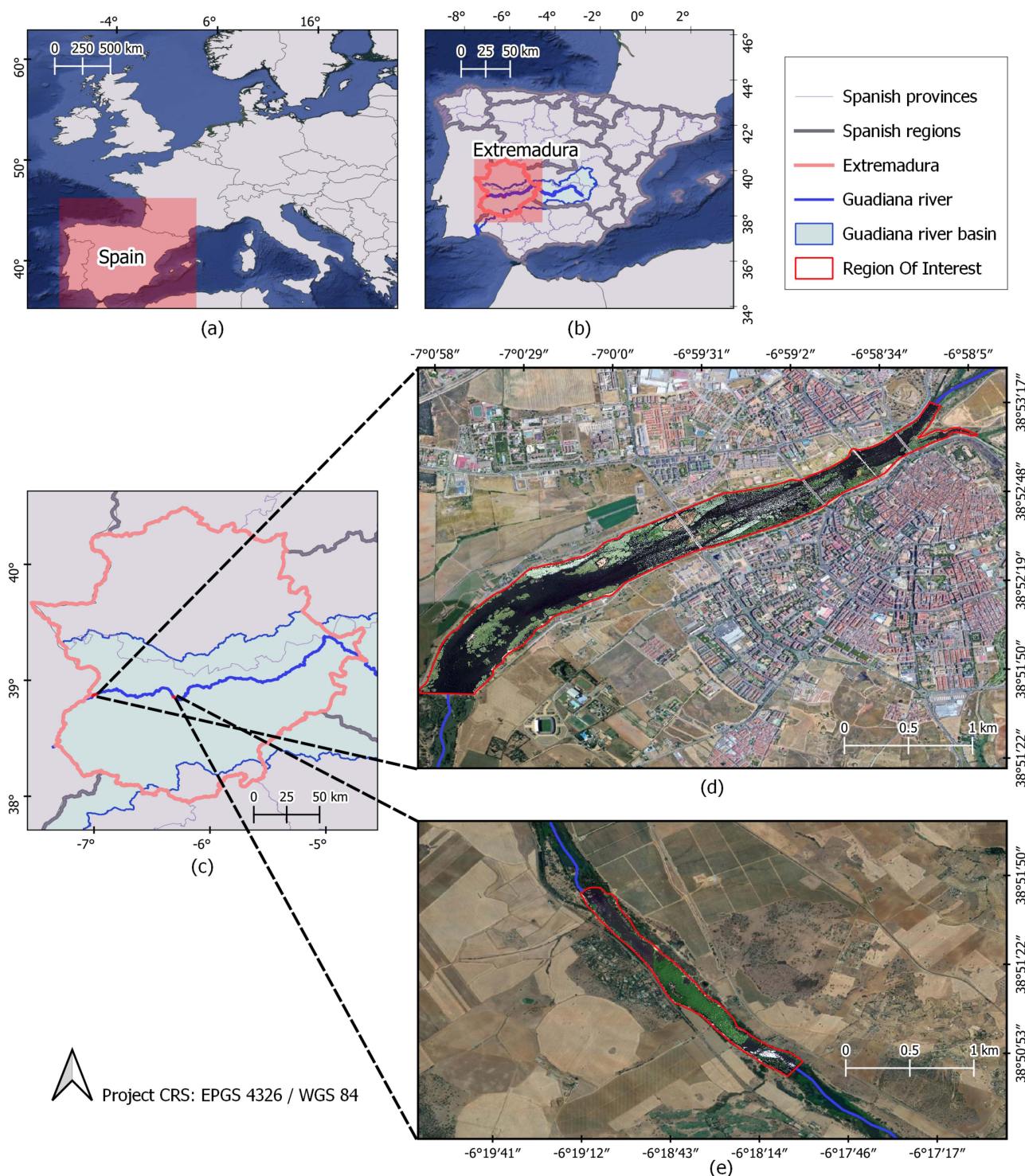


Fig. 2. (a) Geographical location of Spain. (b) Geographical location of the region of Extremadura, the Guadiana river, and the Guadiana river basin. (c) Zoom of the Extremadura region, depicting the Guadiana river and its basin. (d) Zoom of an area affected by aquatic weeds in Badajoz city (BA_zone). (e) Zoom of an area affected by aquatic weeds in Mérida city (ME_zone).

atmospherically corrected so they are not foggy in appearance (as it is the case of S2L1C datasets). Since Sentinel-2 has a revisit time of five days, the closest date to the PNOA datasets has been chosen. For BA_zone and ME_zone, images from July 11, 2019, have been downloaded. These MS datasets contain 12 bands ranging from 442.7 to 2202.4 nm, with spatial resolution of 10-

20-, or 60-m per pixel, depending on the wavelength. Table III gives the corresponding bands. After applying a clipping mask with ROI_BA, the S2L2A dataset for BA_zone has dimensions of 451×236 pixels, being 16 240 pixels with information (the rest are NoData values). In the case of ME_zone, the S2L2A dataset has dimensions of 189×173 , with 4471 pixels with

information. Both MS images have been downloaded in 8 bit format (unsigned integer 8 bits), where the pixel values range from 0 to 255.

C. Hardware/Software Environment

The hardware environment used in the experiments is composed by an Intel(R) Core(TM) i7-8700 processor, 32 GB random access memory (RAM) memory, and 1 TB SSD. The window partitioning strategy and the ML/DL frameworks have been implemented in Python 3.8 programming language, selected because of its open-source nature, its versatility, and flexible integration with other components, in addition to the existence of numerous libraries. In addition, a very popular DL framework has been used, i.e., TensorFlow, which is an end-to-end open-source platform which is very easy to use through the high-level library Keras (a DL application programming interface). Regarding image preprocessing operations, most of them have been carried out using QGIS software [65], as well as tools developed in QGIS. In general terms, GIS techniques have been used for the following.

- 1) Visualization of images (PNOA, Sentinel-2, and classified images).
- 2) Treatment of NoData values, i.e., to query pixel values, and to analyze histograms, spectral signatures, etc.
- 3) *Training sample collection process*: This has been accomplished by means of vectors (polygons) drawing over the Sentinel-2 image, having as a reference layer, the PNOA high-resolution image. The samples were extracted from the Sentinel-2 image.
- 4) *Data preprocessing and postprocessing*: All previous tools were used directly on QGIS, but also implemented in Python to automate processes.
- 5) Maps layout design (for better understanding when displaying results).
- 6) The synthetic GT generation (described in Section V-G2) was performed using a Python script to automate all GIS processes needed (crop geolocation, centroids generation, vectorial data calculations, etc.).

D. Classification Methods

In order to verify that aquatic weeds can be automatically detected by ML/DL algorithms, the following methods have been adopted.

- 1) *K-Means*: The number of classification groups (the same number of centroids generated) has been set empirically using different values (between 3 and 6) in order to classify the two scenarios according to their most representative classes (four and five classes for ROI_ME and ROI_BA, respectively).
- 2) *Random Forest*: The number of estimators has been set to 100 after checking that the obtained results did not improve much by increasing the number of decision trees. They have been tested with an increasing value of tree depth, since the algorithm takes longer after a certain depth, but the accuracy remains the same.
- 3) *Convolutional Neural Network*: The CNN is applied in such a way that the spectral signature of each pixel is considered

TABLE II
NUMBER OF TRAINING SAMPLES (PIXELS) USED FOR TRAINING THE RF AND CNN CLASSIFIERS IN THE BADAJOZ AND MÉRIDA CASES

Number of training samples (pixels)	Badajoz case	Mérida case
Water	176	101
Aquatic weeds	195	162
Soil	8	10
Other vegetation	22	177
Other	18	-
Total number and percentage of training samples used	419 (2.58%)	450 (10.06%)
Total number of labeled pixels inside each ROI	16 240	4471

The numbers in the parentheses are the percentage of the total number of labeled samples used for training in each case (rest of the labeled samples were used for testing)

as the input vector. Therefore, the CNN receives as many input vectors as the number of pixels in the MS image. It is assumed each pixel is labeled as one class. The structure of our CNN classifier consists of several layers, i.e., convolutional, reshaping, fully connected, normalization, and activation, as shown in Fig. 3. In this study, the CNN does not use spatial information (only spectral information), due to the fact that we are using a 1-D convolutional network (CNN1D). This makes a fair comparison with the other ML algorithms used (i.e., K-means and RF).

E. Training and Validation

In order to apply supervised classification algorithms, we choose a set of training samples from Sentinel-2 images for each of the scenarios analyzed in this article. Since the PNOA images have higher spatial resolution and have been taken at the same date as the Sentinel-2 images, two training datasets have been defined by photointerpretation over PNOA images. The first training dataset has been selected according to the predominant classes in the ROI_BA scenario, so that representative samples have been collected from each of them. Specifically, five classes (i.e., water, aquatic weeds, soil, other vegetation, and other as bridges) were defined in ROI_BA. Similarly, samples from four representative classes (i.e., water, aquatic weeds, soil, and other vegetation) have been selected in ROI_ME. First, samples were taken with pixels containing only a single class. As we were mainly interested in locating invasive plants in this study, for greater accuracy of results, we proceeded to take training samples of mixed pixels containing invasive plants among other classes. The segmentation process of these training samples was carried out using GIS tools in QGIS software. Table II gives the total number of pixels used for training the RF and CNN classifiers in both scenarios. The numbers in the parentheses are the percentage of available labeled samples used for training, while the rest of the labeled samples were used for testing. As it can be seen in Table II, the RF and CNN classifiers are trained with a very limited number of the available labeled pixels (2.58% of the labeled samples for the Badajoz case and 10.06% of the labeled samples for the Mérida case).

The training sets (one for BA_zone and one for ME_zone) include samples of invasive plants and other classes that are not invasive plants (with other kinds of vegetation among

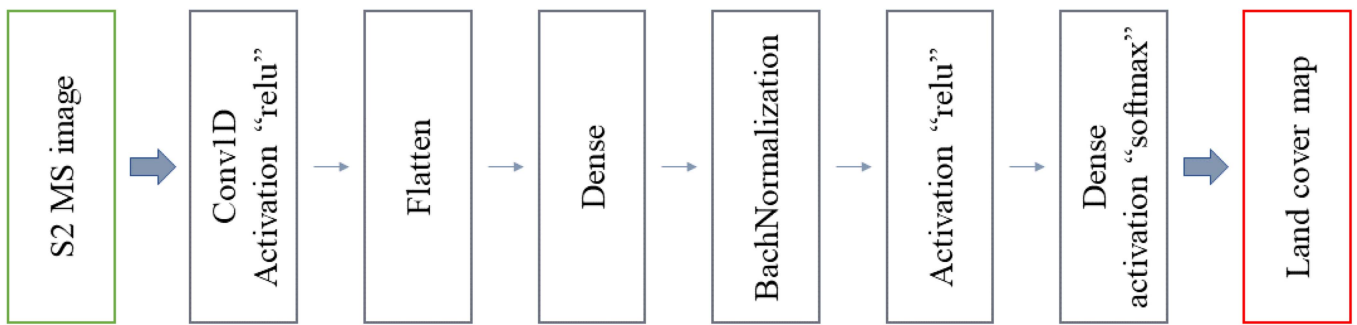


Fig. 3. Architecture of the considered CNN.

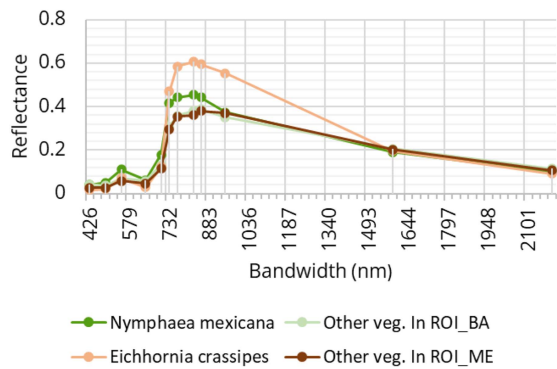


Fig. 4. Spectral signatures of the vegetation differentiated in the training sets, i.e., *Eichhornia crassipes*, other vegetation in ROI_ME, *Nymphaea mexicana*, and other vegetation in ROI_BA.

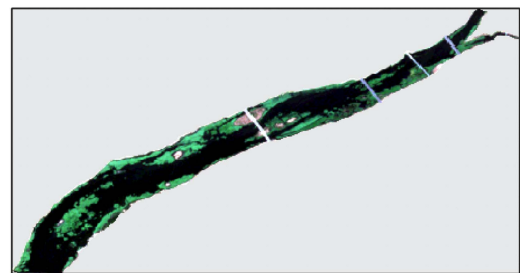
them). In Fig. 4, the spectral signatures of *Eichhornia crassipes*, *Nymphaea mexicana*, and other vegetation species in ROI_ME and ROI_BA are shown. As it can be seen, the signatures exhibit a similar spectral pattern, but there are some spectral differences between them. These nuances are usually enough for classification algorithms to distinguish them. The fact that invasive plant species can be distinguished from other vegetation species has also been taken into account in other studies [66]. Fig. 4 suggests that the spectral signatures of invasive plant species can be separated from those of other kinds of vegetation species.

F. Image Preprocessing: Dealing With NoData Values

In many research works in which RS techniques have been applied for classification purposes, the analyzed images have a square or rectangular shape. That is because such techniques are often applied to identify every class and all of them are of equal importance in the study. In addition, working with images that are not square or rectangular implies the presence of NoData values, resulting in added difficulty in both preprocessing and data processing. NoData values are values where there is no information about the scene, due mainly to its geometry and not to sensor data capture errors that may result in missing values. Therefore, working with NoData values can be a tedious process, since they have to be considered at GIS level, when data are displayed, and also at coding level, when reading, processing, and writing (saving) the images.



a)



□ NoData Values

b)

Fig. 5. (a) Full Sentinel-2 image for ROI_BA. (b) Clipped ROI_BA and NoData values present in the image due to its geometry.

In this research, PNOA and Sentinel-2 datasets have been obtained from the mentioned platforms in 8-bit format, and hence pixel values range from 0 to 255 in each spectral band. First, a normalization of these values has been carried out (dividing these values by 255) so that they are displayed in a range from 0 to 1. In order to apply classification techniques only over the areas in which we want to detect aquatic weeds, a previously elaborated mask has been applied to show only the data within each ROI (as shown in Fig. 5). Consequently, datasets have information and NoData values. To deal with NoData values and exclude them from training, prediction, and classification, other values different than the values inside the ROIs have been assigned. The histogram of each dataset has been calculated, and given that the pixels that do contain ROI information saturate the range (0 or 1 values), the dataset format has been changed to 32-bit floating point. Then, NoData values are assigned to

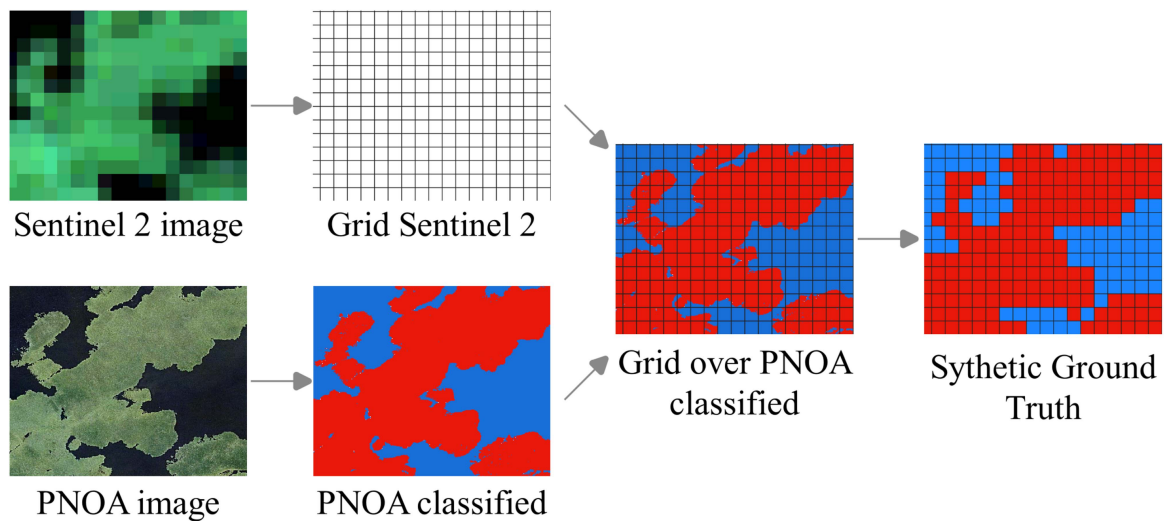


Fig. 6. Main steps in synthetic GT generation.

10 000, avoiding difficulties to handle the data. In addition, at coding level, the ROI mask has been applied so that we only take into account the pixels that are outside the mask to apply the classification techniques.

G. Evaluation of Classification Techniques

In this work, a strategy has been developed to evaluate invasive plants classification. It involves GIS techniques and their implementation in programming languages. Since PNOA MS images have very high spatial resolution, training and validation samples could be chosen by photointerpretation. Furthermore, they can also be used to validate the classification made in the Sentinel-2 dataset. For this purpose, we need to compare the classified pixels in the Sentinel-2 image with the classified pixels in the PNOA dataset. The classification of the latter has been possible by resorting to spatial partitioning. Both datasets have different spatial resolutions; so in order to conduct this operation, we elaborated a synthetic image of the classified PNOA dataset. Thus, the resulting PNOA classified image pixels have 10 m of spatial resolution (the same as Sentinel-2 datasets). In this way, a synthetic GT can be generated and used to compute different evaluation metrics.

1) *Window Partitioning for the PNOA Dataset:* Since PNOA datasets are very high-resolution images and due to the big dimensions of the ROIs studied, a lot of information is collected. Consequently, the MS data cube requires a large amount of RAM to be able to process the pixels. To solve this problem, we apply the window partitioning methodology presented in [35]. Resulting from this, the PNOA data cube is split in contiguous processing blocks. These neighboring blocks in the spatial domain contain subsets of pixels of the complete dataset with their associated spectral information and can be processed in block by block fashion.

2) *Synthetic GT Generation:* The main steps in the synthetic GT generation are shown in Fig. 6. First, we consider the Sentinel-2 image with a set of pixels represented by

$X_S = x_{S1}, x_{S2}, x_{S3}, \dots, x_{Sm}$. Then, a vector grid is generated where each cell x_{Gi} is a square of 10×10 m, simulating the contours of the pixel x_{Si} . As a result, the $H \times W$ grid (where H is the height and W is the width of the image) has the same dimensions as the Sentinel-2 image, with the same geolocation. On the other hand, the PNOA dataset has been classified by using the RF algorithm, and it is composed of pixels $X_P = \{x_{P1}, x_{P2}, x_{P3}, \dots, x_{Pm}\}$. Each pixel is labeled as y_{pi} , according to the class where it belongs. The pixels x_{Pi} have a higher spatial resolution than that of x_{Si} . Then, the centroids c_{Pi} of each pixel x_{Pi} are identified, adopting their labels y_{pi} and generating a vector file. Afterwards, a synthetic GT is generated by placing the vector grid on a vector file. Next, each cell x_{ci} of the grid is assigned an attribute table equipped with as many features as labels y_{pi} are present on the vector file. Finally, each cell is assigned with a label y_{pi} by majority voting. Consequently, a synthetic GT is developed resulting in an $H \times W$ image with the same number of pixels and spatial resolution as the Sentinel-2 dataset. We emphasize that after having the synthetic GT generated, it was validated and refined by visual comparisons with field observations to guarantee the accuracy of the labels. For illustrative purposes, some synthetic GT scenes generated for the considered ROIs are shown in Fig. 7.

VI. EXPERIMENTAL RESULTS

The results of the application of the considered ML/DL algorithms to the Sentinel-2 datasets are explained in this section. The classification maps and statistics obtained after applying the precision metrics described in the following section are discussed for the Badajoz and Mérida cases. This section concludes with a brief discussion on the obtained results.

A. Metrics for Accuracy Assessment

In order to evaluate the efficiency of different techniques, we assume that the difference between the results and the GT data are due to classification errors. For this purpose, a confusion

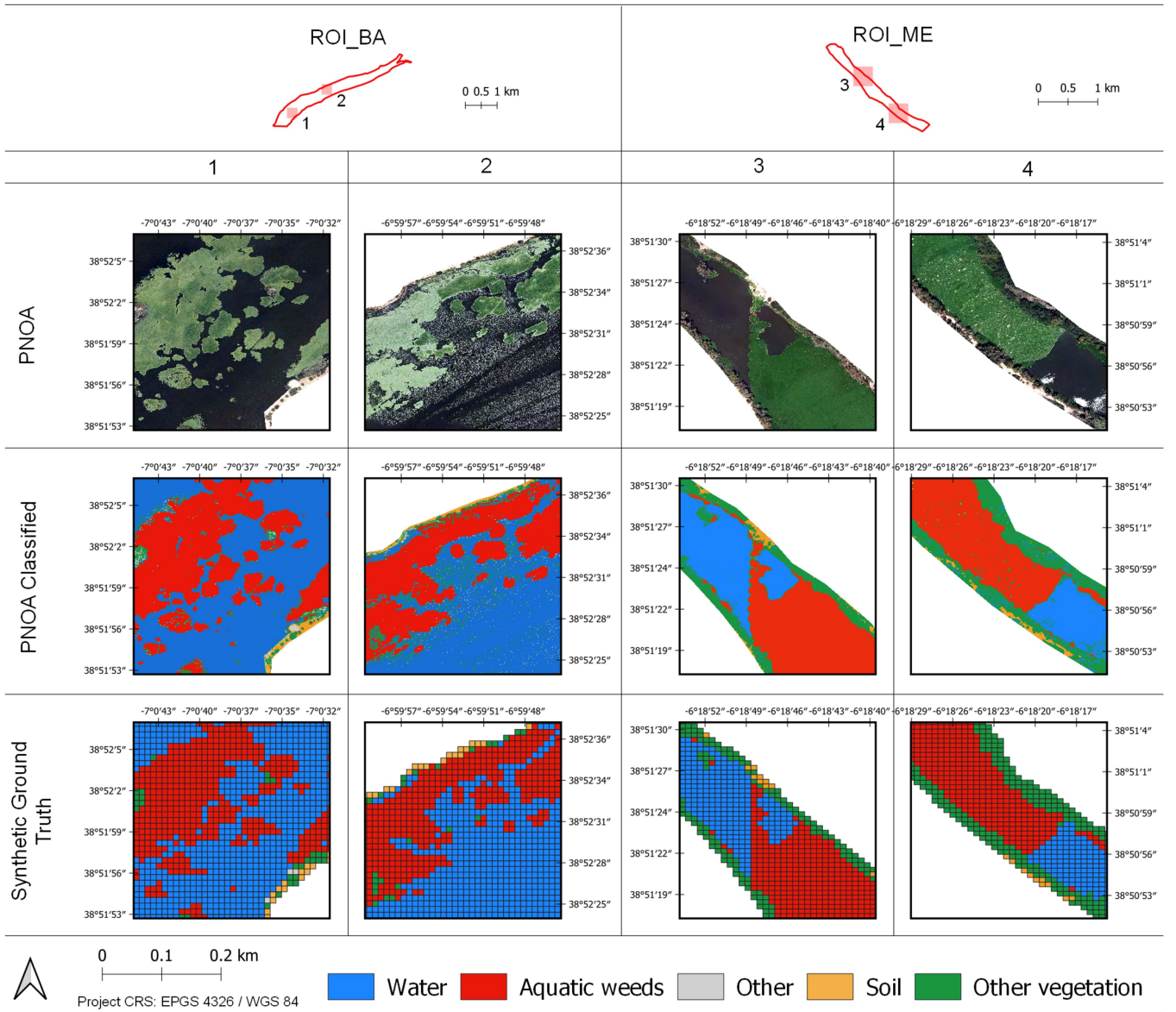


Fig. 7. Some synthetic GT images generated for each considered ROI.

matrix is computed for each of them. In this matrix, true positives (TPs), true negatives (TNs), false positives (FPs), and false negatives (FNs) are shown. The real values are in rows, representing the values in the synthetic GT image. The columns in this matrix contain the predicted values of each classifier. As this study is focused on the detection of aquatic weeds, the confusion matrix is binary (i.e., it indicates whether the invasive plants are detected or not).

The metrics implemented to evaluate the quality of the considered algorithm predictions are overall accuracy [see (3)], user's accuracy [see (4)], producer's accuracy [see (5)] (also known as recall, sensitivity, or TP rate), and F_1 score [see (6)]. Their equations are described as follows:

$$\text{Overall accuracy} = \frac{TP + TN}{TP + TN + FP + FN} \quad (3)$$

$$\text{User's accuracy} = \frac{TP}{TP + FP} \quad (4)$$

$$\text{Producer's accuracy} = \frac{TP}{TP + FN} \quad (5)$$

$$F_1 \text{ score} = \frac{2 * TP}{2 * TP + FP + FN} \quad (6)$$

B. Visual Interpretation of Results: Badajoz Case

Fig. 8 shows the performance of the classification algorithms employed in this study for the detection of aquatic weeds in the Guadiana river (three scenes, one per column, all in Badajoz). In this figure, the first row depicts the PNOA data. The second row depicts the Sentinel-2 data. The third row shows the synthetic GT. The fourth row provides the K-means classification results. The fifth row reports the RF classification results. Finally, the

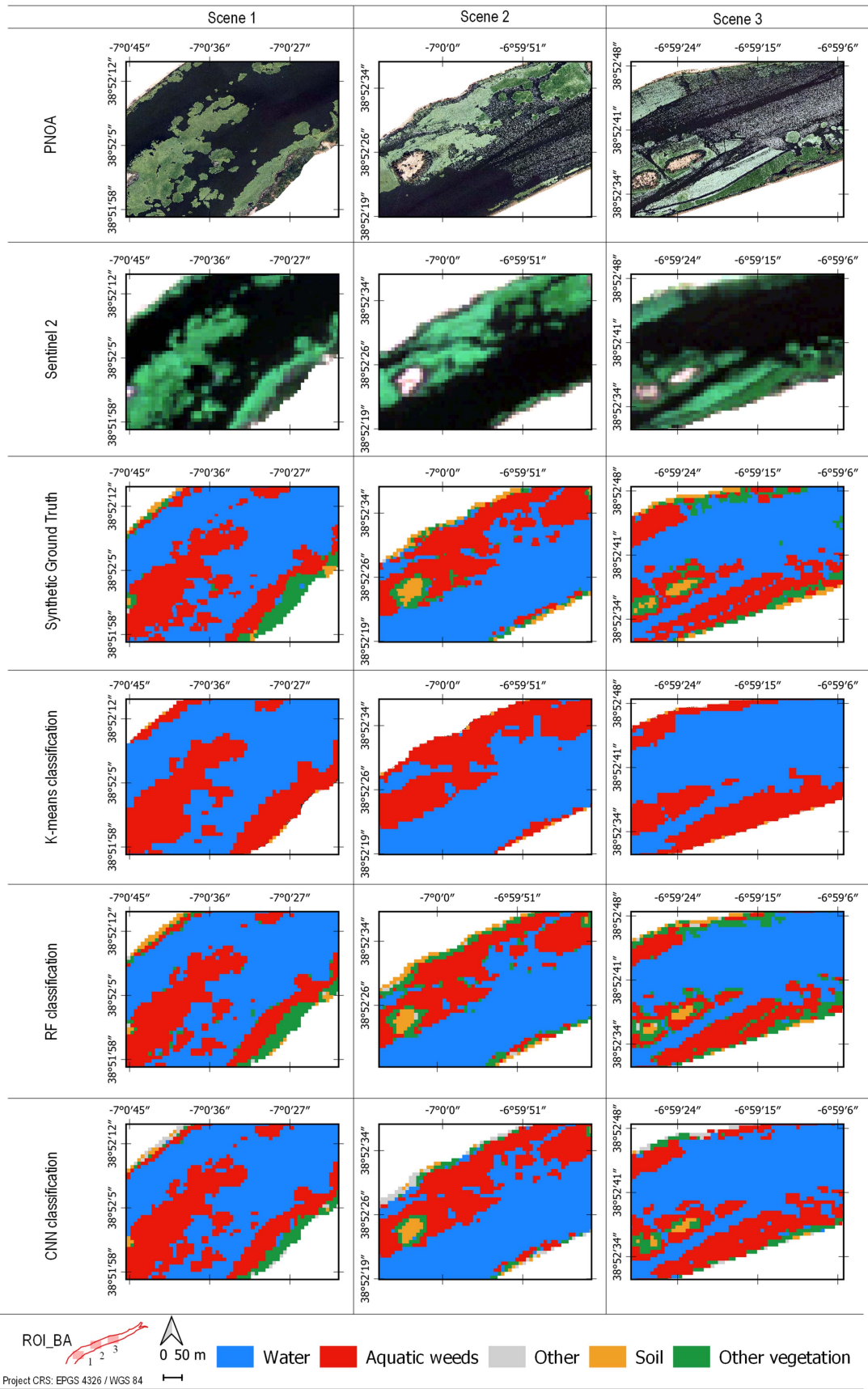


Fig. 8. Classification maps for three representative scenes in ROI_BA (Badajoz).

sixth row contains the CNN classification results. We report results for three representative scenes in ROI_BA. As it is shown, by comparing the RGB image (the PNOA dataset) and the synthetic GT with the results of applying the different classification algorithms on the MS dataset (Sentinel-2 image), we can conclude that they can all detect the presence of aquatic weeds. In the following, we describe the specific results obtained by each algorithm and shown in Fig. 8.

1) *Results of K-Means*: K-means is an unsupervised algorithm. It has been tested with different numbers of clusters. Five clusters were finally chosen, which are in agreement with the number of classes with which the two supervised algorithms (i.e., RF and CNN) have been trained. In this case, a single cluster is not associated with the aquatic weeds class. Specifically, two clusters represent almost all the aquatic weeds present in the water. However, these clusters do not distinguish the weeds from other types of vegetation. Water can be distinguished well, and part of the soil is also well-differentiated. Another cluster represents different classes, water, and contours of aquatic weeds (mixed pixels). In most cases, this cluster represents areas close to the contours of the masses of aquatic weeds, which are often water areas, although (rarely) they can also contain some pixels associated to aquatic weeds.

2) *Results of RF*: The RF classification maps have been obtained after a training process with five classes. In the resulting images, aquatic weeds can be distinguished from other classes present in the scenes. Soil, water, and other vegetation areas can be also distinguished. However, some parts of the contour of the masses of aquatic weeds are classified as other vegetation.

3) *Results of CNN*: The maps obtained by the CNN are in close agreement with the GT. It can be visually seen that this classifier improves the aquatic weeds detection results obtained by the other algorithms.

To conclude this section, Fig. 9 shows the full classification maps obtained by the three considered classifiers for the entire Badajoz scene. It can be seen that supervised classifiers (i.e., RF and CNN) provide more consistent results than the K-means with a better delineation of the river area and the bridges over the river (belonging to the soil class).

C. Visual Interpretation of Results: Mérida case

Fig. 10 shows the obtained classification results in Mérida (three scenes, one per column, all in Mérida). In the following, we describe the results obtained by each classifier in this case.

1) *Results of K-Means*: After different iterations with different numbers of centroids, we finally considered that the K-means performance with five clusters is the best. With this number of clusters, the classifications of two clusters needed to be grouped to reflect the distribution of invasive plants. Moreover, there are two clusters showing water, which have been grouped with the same color for visualization purposes. Regarding the classification with four clusters, invasive plants were detected, but we could not differentiate them from the vegetation on the river banks.

2) *Results of RF*: The performance results of the RF classifier improved with regards to the K-means algorithm, as it was already seen in the ROI_BA case study.

3) *Results of CNN*: The performance results of the CNN classifier improved with regards to the K-means and RF algorithms, as it was already seen in the ROI_BA case study. Specifically, the CNN produced a very good delineation of water bodies and accurate detection results of aquatic invasive plants.

To conclude this section, Fig. 11 shows the full classification maps obtained by the three considered classifiers for the entire Mérida scene. Once again, supervised classifiers (i.e., RF and CNN) provide more consistent results than the K-means with a better identification of soil areas.

D. Statistical Analysis of the Classification Results

The obtained confusion matrices are shown in Fig. 12. It can be seen in these matrices that the accuracy of aquatic weeds detection increases according to the complexity of the algorithm applied. The lowest accuracy is obtained by the K-means algorithm. RF and CNN algorithms outperform K-means and result in similar accuracies, with acceptable FN and FP rates. It is worth noting that the three considered classifiers achieve better performance in ROI_ME than in ROI_BA. As it can be seen in Fig. 9, ROI_BA contains more separate and irregularly shaped masses of aquatic weeds. This leads to the existence of mixed pixels (aquatic weeds with water and aquatic weeds with other vegetation), decreasing the overall classification accuracies. Nevertheless, as it can be seen in Table III (which reports the quantitative metrics calculated, such as the F_1 score, overall accuracy, producer's accuracy, and user's accuracy), the obtained results are close to 1, indicating that good accuracies could be obtained in the ROI_BA case when RF and CNN classifiers are adopted. Table III also gives that the scores for ROI_ME are even superior, with both RF and CNN providing close to optimal results in this case study.

We also compared how accuracies change depending on the number of samples used for the training process. Table IV gives the accuracies for different numbers of training samples. We selected the samples randomly and ran the algorithm ten times, and then we calculated the mean accuracy between executions. Fig. 13 shows that there is not a significant impact in the overall accuracy when reducing the number of samples. This is because a lot of time was spent in this study to carefully select the most representative samples through validation supported by the high-resolution image.

E. Discussion

The two scenarios considered in experiments cover large irregular areas of the Guadiana river (from one margin of the river to the other). Our methodology has been shown to be able to provide accurate classification of invasive plants in large areas of the river, enabling for a detailed monitoring of all river sections affected. Specifically, a preprocessing strategy has been adopted to treat the NoData values present in the pixels outside the analyzed river contour of the whole rectangular image, as the datasets do not have a perfectly rectangular shape.

In addition, different ML/DL classification techniques have been evaluated from clustering algorithms, such as K-means, to more complex supervised classification algorithms, such as RF and CNN. The spatiotemporal distribution of aquatic invasive

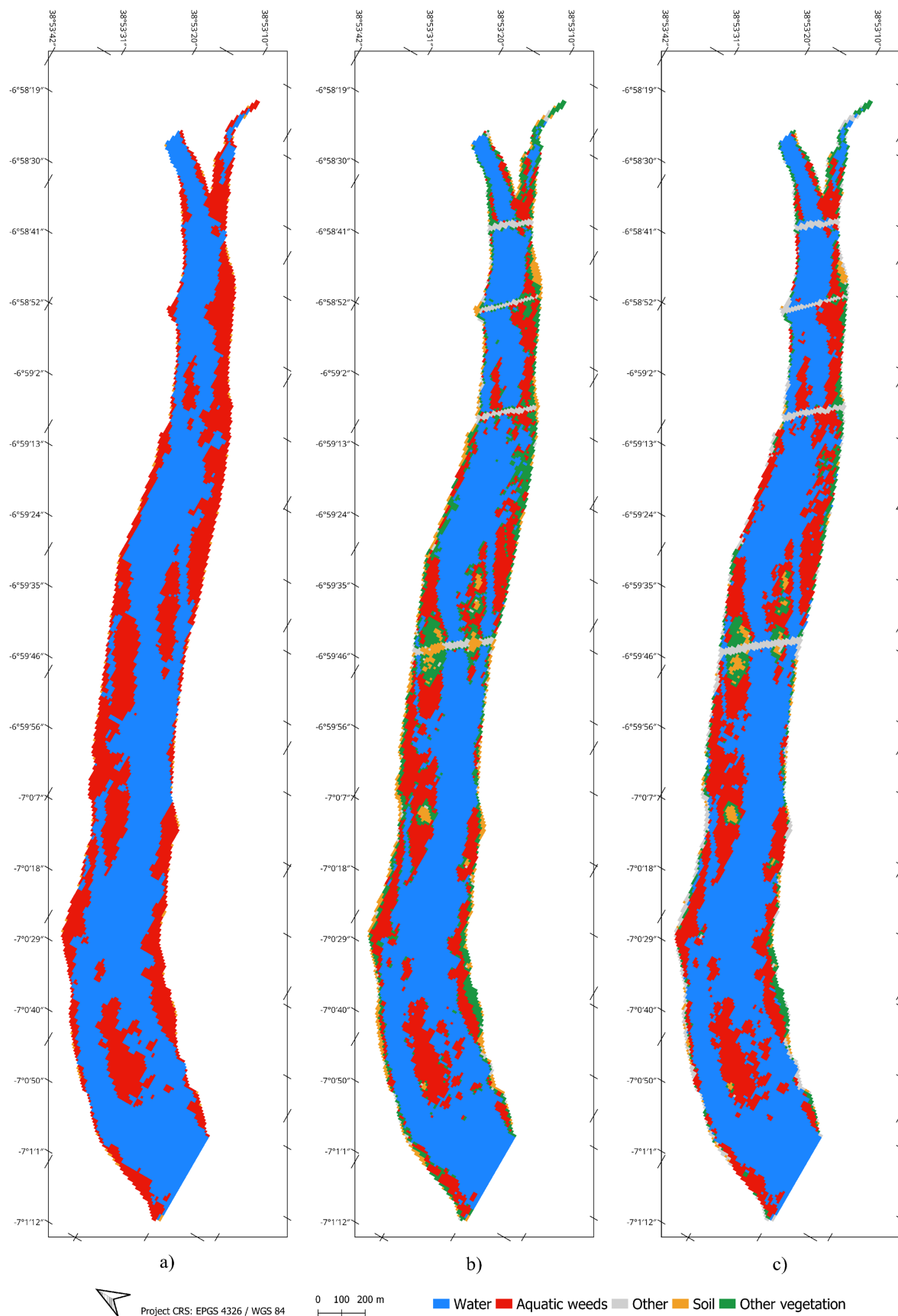


Fig. 9. Classification maps in ROI_BA with different classifiers. (a) K-means. (b) RF. (c) CNN.

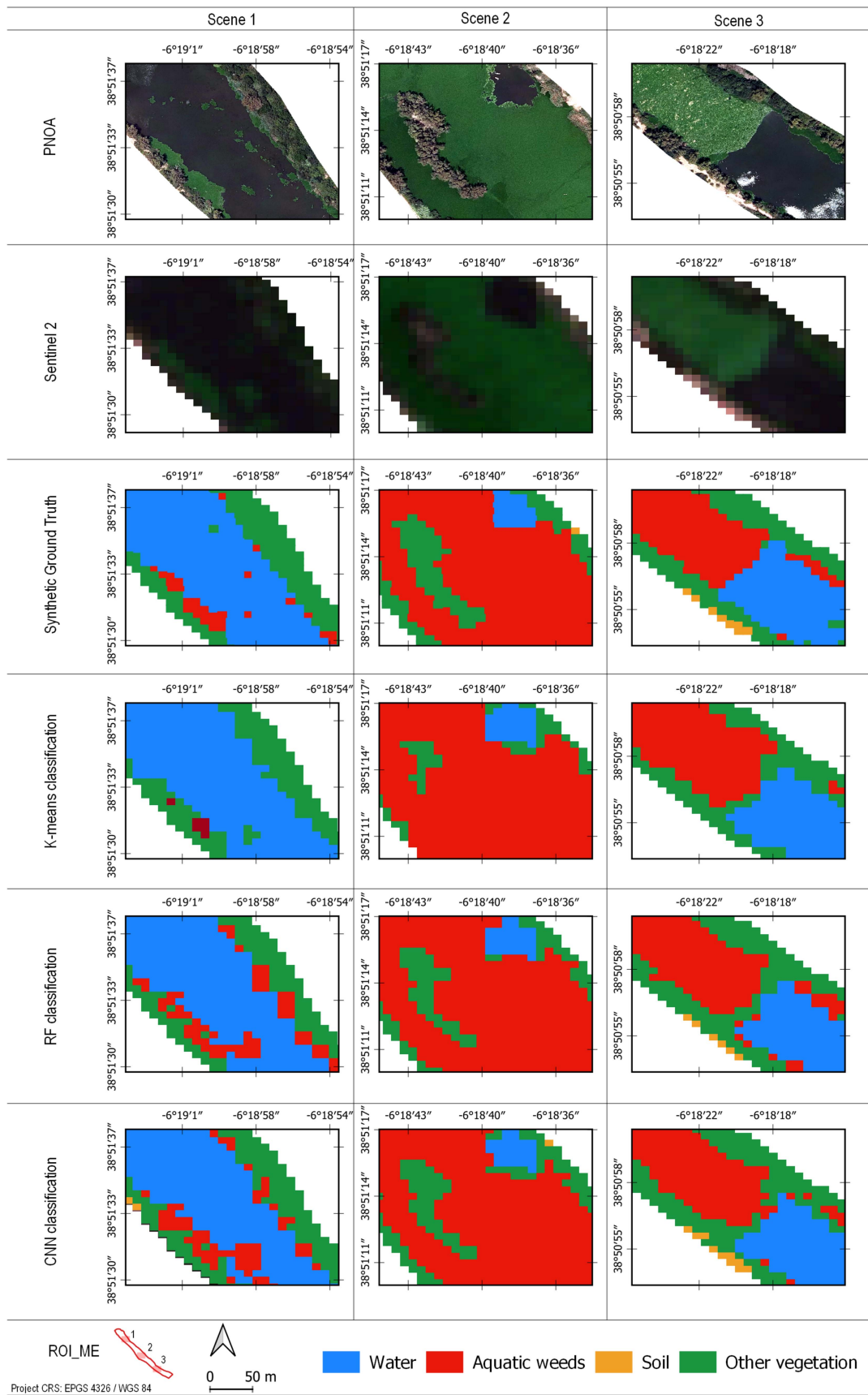


Fig. 10. Classification maps for three representative scenes in ROI_ME (Mérida).

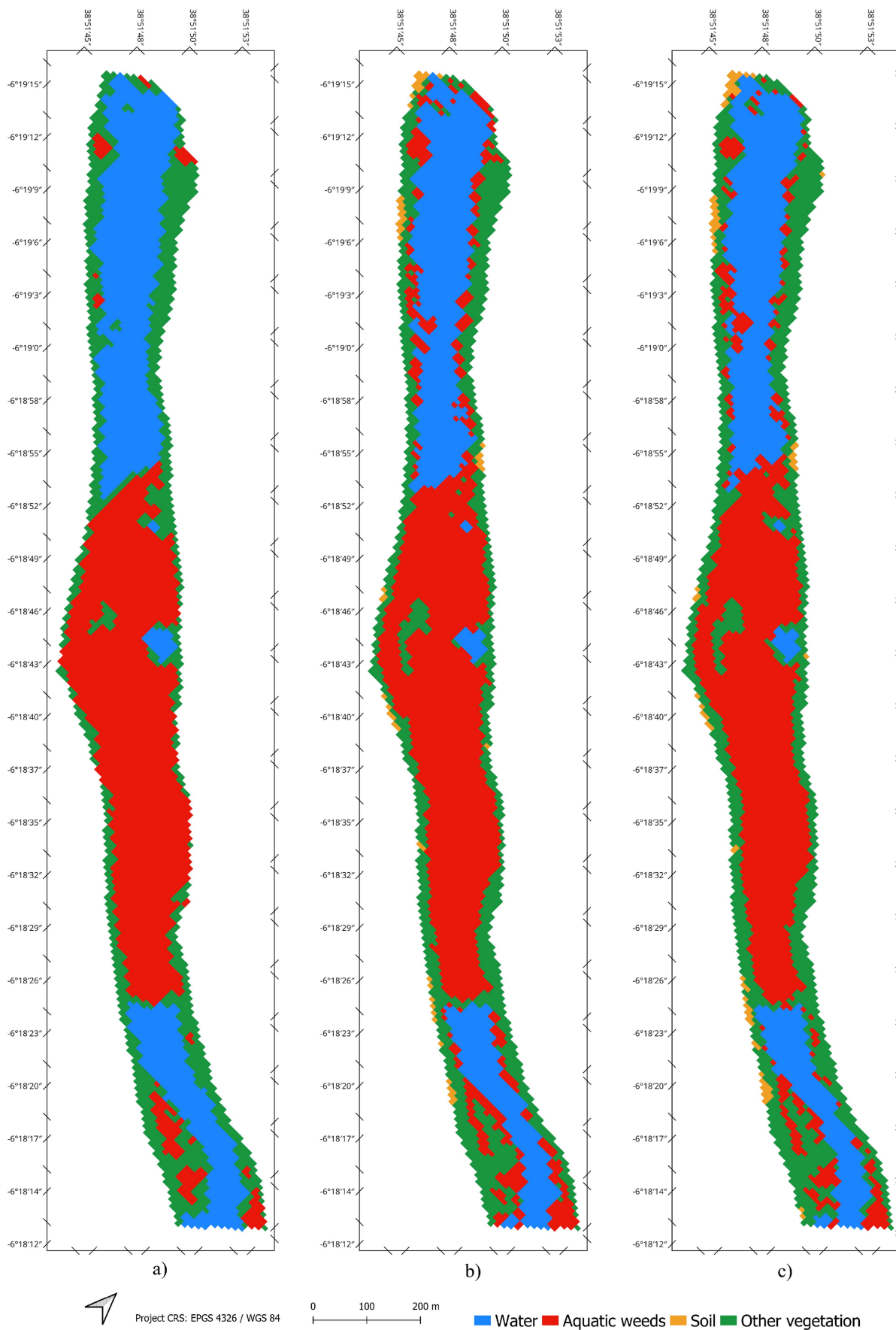


Fig. 11. Classification maps in ROI_ME with different classifiers. (a) K-means. (b) RF. (c) CNN.

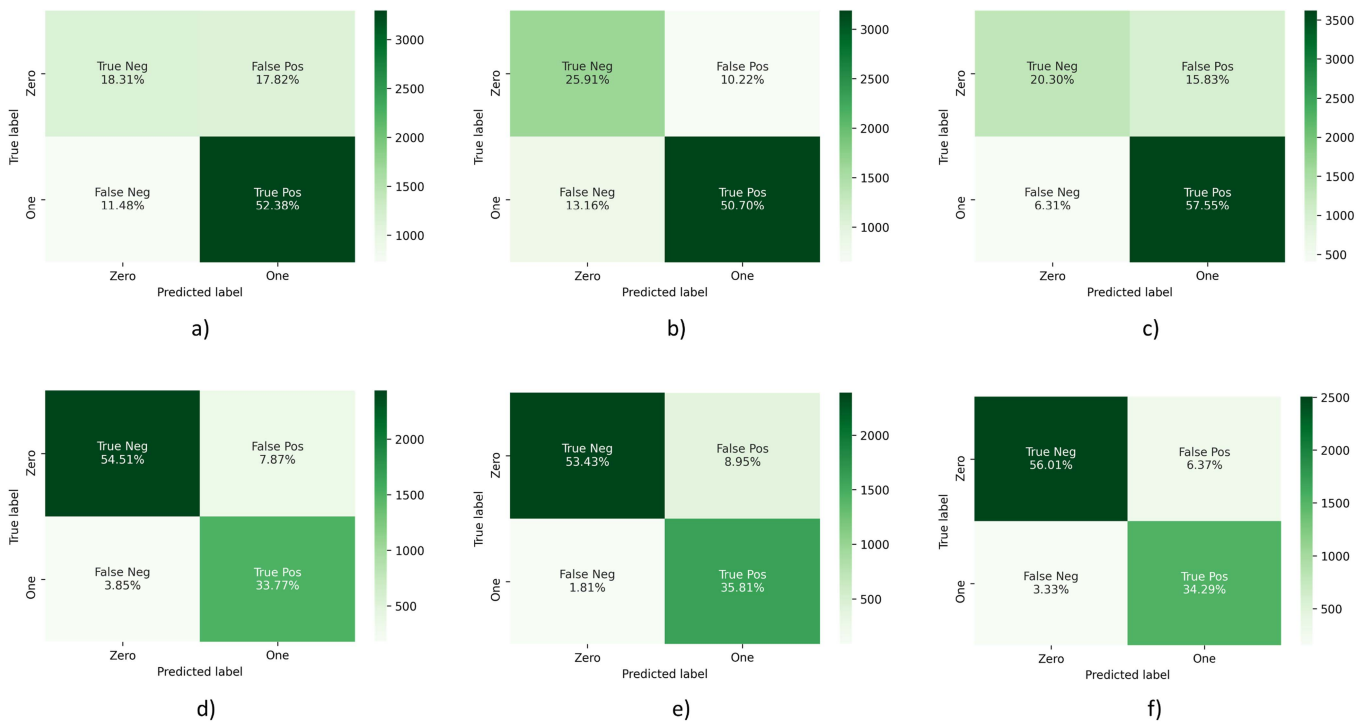


Fig. 12. Confusion matrices. (a) K-means applied to ROI_BA. (b) RF applied to ROI_BA. (c) CNN applied to ROI_BA. (d) K-means applied to ROI_ME. (e) RF applied to ROI_ME. (f) CNN applied to ROI_ME.

TABLE III
PERFORMANCE METRICS FOR THE BADAJOZ AND MÉRIDA CASES

		Overall accuracy	User's accuracy	Producer's accuracy	F_1 score
Badajoz case	K-means	0.707	0.746	0.820	0.781
	RF	0.766	0.832	0.794	0.813
	CNN	0.779	0.784	0.901	0.839
Mérida case	K-means	0.883	0.881	0.898	0.852
	RF	0.892	0.800	0.952	0.869
	CNN	0.903	0.843	0.911	0.876

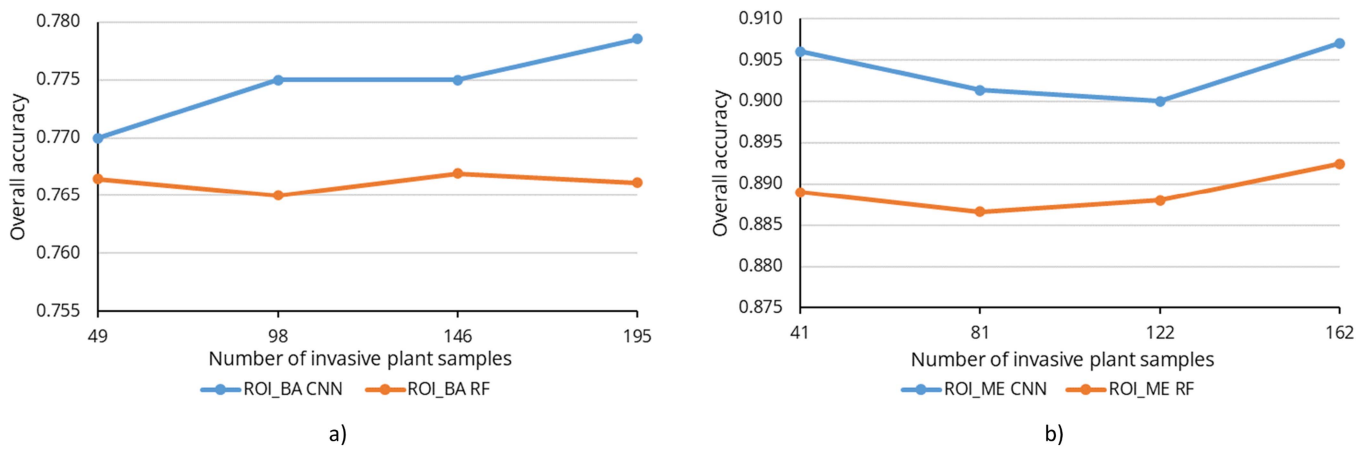


Fig. 13. Graphical representation of the overall classification accuracy obtained using different numbers of training samples. (a) ROI_BA. (b) ROI_ME.

TABLE IV
OVERALL CLASSIFICATION ACCURACY OBTAINED USING DIFFERENT
NUMBERS OF TRAINING SAMPLES FOR THE BADAJOZ AND MÉRIDA CASES

Badajoz case	Number of samples	41	81	122	162
	RF	0.766	0.765	0.767	0.766
	CNN	0.770	0.775	0.775	0.779
Mérida case	Number of samples	49	98	146	195
	RF	0.889	0.887	0.888	0.892
	CNN	0.900	0.902	0.900	0.903

The bold entities indicate the best result of the comparison methods.

plants has been accurately mapped by RF and CNN classifiers using a limited number of training samples. Our results demonstrate the success of these approaches in terms of quantitative accuracy and visual appearance of the obtained results.

Specifically, we have observed that CNNs provide better classification results and can therefore detect aquatic invasive plants very accurately. They are followed in decreasing order of accuracy by RF and K-means. The advantage of using K-means is the fact that the algorithm is unsupervised, and hence does not require collecting training samples. On the other hand, K-means needs to identify the classes detected by the clusters, which may be difficult in practice.

Another important observation is that better results are obtained when the masses are distributed in the water surface, forming fewer blankets than in the case in which they are distributed in separated masses and with irregular contours, which favors the existence of mixed pixels that decrease the overall accuracy. In this sense, training supervised classifiers, such as RF and CNN, can be useful to carry out predictions in other river datasets. In this study, these classifiers have achieved reasonable accuracies (between 77% and 90% in terms of overall accuracy) with a small percentage of training samples (only 2.58% of the available labeled samples in the Badajoz case and 10.08% of the available labeled samples in the Mérida case). Thus, considering the classifier that has obtained the highest accuracy (CNN), the area occupied by the invasive plants is about 18 ha in ROI_ME and about 46 ha in ROI_BA.

Moreover, the results obtained show that similar classification accuracies can be achieved with high-resolution images, such as PNOA data (which are expensive and costly to process), than with medium-resolution images, such as Sentinel-2 images (which are free and require less processing time). The strategy developed for validation of the results has been possible thanks to the synthetic GT generated from high-resolution classified images that required using a window processing strategy (due to the large amount of RAM memory needed).

To conclude this section, we note that ML/DL algorithms can also be applied to the PNOA dataset, but the classification accuracy cannot be calculated because the PNOA image is the one that we use as our baseline for creating the GT. Sentinel-2 data are easier to work with due to their size (PNOA images are about 800 times heavier due to their high spatial resolution). This is why our goal is to detect invasive plants in Sentinel-2 medium spatial resolution images instead of high resolution expensive

PNOA flights that are used in this work as a starting point for generating a high-quality GT.

VII. CONCLUSION

In this study, we have developed a full processing chain for automatic detection of aquatic invasive plants in satellite images. Specifically, our methodology comprises preprocessing, processing, and evaluation stages, able to accurately geolocate invasive vegetation weeds present in the Guadiana river, Spain, achieving high detection accuracies. In our work, supervised classifiers performed better than unsupervised ones, not only because RF and CNN can provide good results with a limited number of training samples, but also because the unsupervised algorithm (K-means) ultimately needs a supervised interpretation process (based on analyzing high-resolution images to combine some of the obtained clusters). The use of one algorithm or another depends on the requirements of each case study, but in our context, the CNN classifier was regarded as the best tool of choice.

Continuous monitoring and control of aquatic invasive plants require early detection of the growth of existing masses in the water. To achieve this goal, future work will be oriented toward the development of methods able to assess the spatio-temporal evolution of aquatic weeds, given that Sentinel-2 captures images with a five-day revisit time, which allows to conduct change detection studies in that time frame. In addition, other DL approaches can be considered in future studies. For instance, the spatial information of the input image may be considered besides the spectral signature of each pixel by using a spatial CNN (CNN2D) classifier. A spatial-spectral CNN (CNN3D) architecture may also be used for even more refined classification.

ACKNOWLEDGMENT

The authors would like to thank *Confederación Hidrográfica del Guadiana* for corroborating the geolocation of invasive plants species in the two scenarios analyzed and Associate Editor and the two Anonymous Reviewers for their outstanding comments and suggestions that greatly helped us to improve the technical content and presentation of our manuscript.

REFERENCES

- [1] M. Sánchez, A. Cuartero, M. Barrera, and A. Plaza, "A new method for positional accuracy analysis in georeferenced satellite images without independent ground control points," *Remote Sens.*, vol. 12, 2020, Art. no. 4132.
- [2] A. Plaza, J. Plaza, A. Paz, and S. Sánchez, "Parallel hyperspectral image and signal processing [applications corner]," *IEEE Signal Process. Mag.*, vol. 28, no. 3, pp. 119–126, May 2011.
- [3] E. C. Enoguanbhor, F. Gollnow, J. O. Nielsen, T. Lakes, and B. B. Walker, "Land cover change in the Abuja city-region, Nigeria: Integrating GIS and remotely sensed data to support land use planning," *Sustainability*, vol. 11, 2019, Art. no. 1313.
- [4] J. Cavender-Bares, J. A. Gamon, and P. A. Townsend, *Remote Sensing of Plant Biodiversity*. Berlin, Germany: Springer, 2020.
- [5] K. Kaku, "Satellite remote sensing for disaster management support: A holistic and staged approach based on case studies in Sentinel Asia," *Int. J. Disaster Risk Reduction*, vol. 33, pp. 417–432, 2019.

- [6] M. Tadese, L. Kumar, R. Koech, and B. K. Kogo, "Mapping of land-use/land-cover changes and its dynamics in Awash River Basin using remote sensing and GIS," *Remote Sens. Appl.: Soc. Environ.*, vol. 19, 2020, Art. no. 100352.
- [7] D. Apostolopoulos and K. Nikolakopoulos, "A review and meta-analysis of remote sensing data, GIS methods, materials and indices used for monitoring the coastline evolution over the last twenty years," *Eur. J. Remote Sens.*, vol. 54, pp. 240–265, 2021.
- [8] V. H. Smith and D. W. Schindler, "Eutrophication science: Where do we go from here?," *Trends Ecol. Evol.*, vol. 24, pp. 201–207, Apr. 2009.
- [9] R. G. Hartzler and D. D. Buhler, *Ecological Management of Agricultural Weeds*. Cambridge, U.K.: Cambridge Univ. Press, 2001.
- [10] S. Patel, *Threats, Management and Envisaged Utilizations of Aquatic Weed Eichhornia Crassipes: An Overview*, vol. 11. Berlin, Germany: Springer, Jul. 2012.
- [11] A. M. Villamagna and B. R. Murphy, "Ecological and socio-economic impacts of invasive water hyacinth (*Eichhornia crassipes*): A review," *Freshwater Biol.*, vol. 55, pp. 282–298, 2010.
- [12] A. Hussner, "Alien aquatic plant species in European countries," *Weed Res.*, vol. 52, pp. 297–306, 2012.
- [13] N. Hanley and M. Roberts, "The economic benefits of invasive species management," *People Nat.*, vol. 1, pp. 124–137, 2019.
- [14] K. J. Murphy, "Aquatic weed problems and their management: A review. II. Physical control measures," *Crop Protection*, vol. 7, pp. 283–302, 1988.
- [15] K. J. Murphy, "Aquatic weed problems and their management: A review I. The worldwide scale of the aquatic weed problem," *Crop Protection*, vol. 7, pp. 232–248, 1988.
- [16] E. O. O. Gangstad, *Weed Control Methods for River Basin Management*. Boca Raton, FL, USA: CRC Press, 2018.
- [17] D. Bubenheim, V. Genovese, J. D. Madsen, and E. Hard, "Remote sensing and mapping of floating aquatic vegetation in the Sacramento–San Joaquin River Delta," *J. Aquatic Plant Manage.*, vol. 59, pp. 46–54, 2021.
- [18] B. Song and K. Park, "Detection of aquatic plants using multispectral UAV imagery and vegetation index," *Remote Sens.*, vol. 12, 2020, Art. no. 387.
- [19] E. K. Cheruiyot, C. Mito, M. Menenti, B. Gorte, R. Koenders, and N. Akdim, "Evaluating MERIS-based aquatic vegetation mapping in Lake Victoria," *Remote Sens.*, vol. 6, pp. 7762–7782, 2014.
- [20] M. Schmidt, "Monitoring aquatic weeds in a river system using SPOT 5 satellite imagery," *J. Appl. Remote Sens.*, vol. 4, 2010, Art. no. 043528.
- [21] E. L. Hestir et al., "Identification of invasive vegetation using hyperspectral remote sensing in the California Delta ecosystem," *Remote Sens. Environ.*, vol. 112, pp. 4034–4047, 2008.
- [22] K. J. Sheffield, D. Clements, D. J. Clune, A. Constantine, and T. M. Dugdale, "Detection of aquatic alligator weed (*Alternanthera philoxeroides*) from aerial imagery using random forest classification," *Remote Sens.*, vol. 14, 2022, Art. no. 2674.
- [23] V. Akbari et al., "Monitoring aquatic weeds in Indian wetlands using multitemporal remote sensing data with machine learning techniques," in *Proc. IEEE Int. Geosci. Remote Sens. Symp.*, 2021, pp. 6847–6850.
- [24] C. Nyamekye et al., "Evaluating the spatial and temporal variations of aquatic weeds (Biomass) on Lower Volta River using multi-sensor Landsat Images and machine learning," *Heliyon*, vol. 7, 2021, Art. no. e07080.
- [25] C. M. Viana, I. Girão, and J. Rocha, "Long-term satellite image time-series for land use/land cover change detection using refined open source data in a rural region," *Remote Sens.*, vol. 11, 2019, Art. no. 1104.
- [26] A. D. Kulkarni and B. Lowe, "Random forest algorithm for land cover classification," *Int. J. Recent Innov. Trends Comput. Commun.*, vol. 4, pp. 58–63, 2016.
- [27] S. E. Jodzani, B. A. Johnson, and D. Chen, "Comparing deep neural networks, ensemble classifiers, and support vector machine algorithms," *Remote Sens.*, vol. 11, 2019, Art. no. 1713.
- [28] V. L. Diengdoh, S. Ondei, M. Hunt, and B. W. Brook, "A validated ensemble method for multinomial land-cover classification," *Ecological Inform.*, vol. 56, 2020, Art. no. 101065.
- [29] L. Ma, Y. Liu, X. Zhang, Y. Ye, G. Yin, and B. A. Johnson, "Deep learning in remote sensing applications: A meta-analysis and review," *ISPRS J. Photogrammetry Remote Sens.*, vol. 152, pp. 166–177, 2019.
- [30] Z.-Q. Zhao, P. Zheng, S.-T. Xu, and X. Wu, "Object detection with deep learning: A review," *IEEE Trans. Neural Netw. Learn. Syst.*, vol. 30, no. 11, pp. 3212–3232, Nov. 2019.
- [31] D. Zeng et al., "Deep learning for scene classification: A survey," vol. abs/2101.10531, 2021, *arXiv:2101.10531*. [Online]. Available: <https://arxiv.org/abs/2101.10531>
- [32] M. E. Paoletti, J. M. Haut, J. Plaza, and A. Plaza, "A new deep convolutional neural network for fast hyperspectral image classification," *ISPRS J. Photogrammetry Remote Sens.*, vol. 145, pp. 120–147, 2018.
- [33] D. He, Y. Zhong, X. Wang, and L. Zhang, "Deep convolutional neural network framework for subpixel mapping," *IEEE Trans. Geosci. Remote Sens.*, vol. 59, no. 11, pp. 9518–9539, Nov. 2021.
- [34] L. Pádua et al., "Water hyacinth (*Eichhornia crassipes*) detection using coarse and high resolution multispectral data," *Drones*, vol. 6, 2022, Art. no. 47.
- [35] E. C. Rodríguez-Garrito and A. Paz-Gallardo, "Efficiently mapping large areas of olive trees using drones in Extremadura, Spain," *IEEE J. Miniaturization Air Space Syst.*, vol. 2, no. 3, pp. 148–156, Sep. 2021.
- [36] K. H. Thamaga and T. Dube, "Remote sensing of invasive water hyacinth (*Eichhornia crassipes*): A review on applications and challenges," *Remote Sens. Appl.: Soc. Environ.*, vol. 10, pp. 36–46, 2018.
- [37] A. Rodríguez-Merino, P. García-Murillo, S. Cirujano, and R. Fernández-Zamudio, "Predicting the risk of aquatic plant invasions in Europe: How climatic factors and anthropogenic activity influence potential species distributions," *J. Nat. Conservation*, vol. 45, pp. 58–71, 2018.
- [40] F. C. F. Aguiar and M. T. Ferreira, "Plant invasions in the rivers of the Iberian Peninsula, South-Western Europe: A review," *Plant Biosyst.*, vol. 147, pp. 1107–1119, 2013.
- [41] Accessed: Jun. 2022. [Online]. Available: <http://www.invasp.eu/>
- [42] Accessed: Jun. 2022. [Online]. Available: https://camaloteaceca.eu/?page_id=620&lang=en
- [43] C. H. del Guadiana, "Gobernanza y estrategias para la lucha contra las especies exóticas invasoras en la cuenca del guadiana," 2021. Accessed: Jun. 2021. [Online]. Available: https://www.chguadiana.es/sites/default/files/2021-05/REVISI%C3%93N_ESTRATEGIA%20DE%20EEI%202021%20COMPLETA_firmada.pdf
- [44] L. Alonso, J. Picos, G. Bastos, and J. Armesto, "Detection of very small tree plantations and tree-level characterization using open-access remote-sensing databases," *Remote Sens.*, vol. 12, 2020, Art. no. 2276.
- [45] M. Padial-Iglesias, P. Serra, M. Ninyerola, and X. Pons, "A framework of filtering rules over ground truth samples to achieve higher accuracy in land cover maps," *Remote Sens.*, vol. 13, 2021, Art. no. 2662.
- [46] F. Alonso-Sarria, C. Valdivieso-Ros, and F. Gomariz-Castillo, "Isolation forests to evaluate class separability and the representativeness of training and validation areas in land cover classification," *Remote Sens.*, vol. 11, 2019, Art. no. 3000.
- [47] Accessed: Jun. 2022. [Online]. Available: <https://inspire.ec.europa.eu/>
- [48] Accessed: Jun. 2022. [Online]. Available: <https://pnoa.ign.es/>
- [49] E. Kroupi et al., "Deep convolutional neural networks for land-cover classification with Sentinel-2 images," *J. Appl. Remote Sens.*, vol. 13, Jun. 2019, Art. no. 024525, doi: [10.1117/1.JRS.13.024525](https://doi.org/10.1117/1.JRS.13.024525).
- [50] D. Phiri et al., "Sentinel-2 data for land cover/use mapping: A review," *Remote Sens.*, vol. 12, 2020, Art. no. 2291.
- [51] Accessed: Jun. 2022. [Online]. Available: <https://sentinel.esa.int/web/sentinel/missions/sentinel-2>
- [52] Copernicus-sentinel-2. Accessed: Jun. 2022. [Online]. Available: <https://eoportal.org/web/eoportal/satellite-missions/c-missions/copernicus-sentinel-2>
- [53] J. E. Ball, D. T. Anderson, and C. S. Chan, "A comprehensive survey of deep learning in remote sensing: Theories, tools and challenges for the community," *J. Appl. Remote Sens.*, vol. 11, 2017, Art. no. 042609.
- [54] L. Goodfellow and A. Courville, *Deep Learning*. Cambridge, MA, USA: MIT Press, 2016.
- [55] Y. Bengio, *Learning Deep Architectures for AI*, vol. 2. Boston, MA, USA: Now Publishers, 2009.
- [56] M. E. Paoletti, J. M. Haut, J. Plaza, and A. Plaza, "Deep learning classifiers for hyperspectral imaging: A review," *ISPRS J. Photogrammetry Remote Sens.*, vol. 158, pp. 279–317, 2019.
- [57] L. Breiman, "Random forests," *Mach. Learn.*, vol. 45, pp. 5–32, 2001.
- [58] R. E. Blahut, *Fast Algorithms for Signal Processing*. New York, NY, USA: Cambridge Univ. Press, 2010.
- [59] T. Hastie, J. Friedman, and R. Tibshirani, *The Elements of Statistical Learning*. New York, NY, USA: Springer, 2009.
- [60] Y. Lecun, Y. Bengio, and G. Hinton, "Deep learning," *Nature*, vol. 521, pp. 436–444, 2015.

- [61] L. Zhang, L. Zhang, and B. Du, "Deep learning for remote sensing data: A technical tutorial on the state of the art," *IEEE Geosci. Remote Sens. Mag.*, vol. 4, no. 2, pp. 22–40, Jun. 2016.
- [62] W. Hu, Y. Huang, L. Wei, F. Zhang, and H. Li, "Deep convolutional neural networks for hyperspectral image classification," *J. Sensors*, vol. 2015, 2015, Art. no. 258619.
- [63] Accessed: Jun. 2022. [Online]. Available: <https://centrodedescargas.cnig.es/CentroDescargas/>
- [64] Accessed: Jun. 2022. [Online]. Available: <https://www.sentinel-hub.com/explore/sentinelplayground/>
- [65] S. Madry, *Introduction to QGIS: Open Source Geographic Information System*. Locate Press, 2021. [Online]. Available: <https://books.google.es/books?id=biJozgEACAAJ>
- [66] K. H. Thamaga and T. Dube, "Understanding seasonal dynamics of invasive water hyacinth (*Eichhornia crassipes*) in the Greater Letaba river system using Sentinel-2 satellite data," *GIScience Remote Sens.*, vol. 56, pp. 1355–1377, 2019.



Elena C. Rodríguez-Garlito (Student Member, IEEE) received the B.Sc. degree in civil engineering and the M.Sc. degree in geographical information systems and remote sensing, in 2013 and 2014, respectively, from the University of Extremadura, Cáceres, Spain, where she is currently working toward the Ph.D. degree in the area of invasive aquatic plants detection using remote sensing techniques, with pre-doctoral contracts for the training of Doctors in public RD centers belonging to the Extremadura System of Science, Technology, and Innovation.

She is currently a Member of Hyperspectral Computing Laboratory, Department of Technology of Computers and Communications, University of Extremadura. Her research interests include GIS, remote sensing, and machine/deep learning.



Abel Paz-Gallardo received the B.S. degree in computer engineering and the M.Sc. and Ph.D. degrees in computer science from the University of Extremadura, Cáceres, Spain, in 2007, 2009, and 2011, respectively.

During 2006 and 2007, he was a Research Assistant with Computer Architecture Department, University of Extremadura, where he became an Associate Professor in 2008. At the same time, he started working with Minimally Invasive Surgery Center Jesús Usón, Cáceres. In 2010, he started working with Bull Spain

S.A. to deploy at CETA-Ciemat, Trujillo, Spain, the biggest GPGPU Cluster in Spain and one of the biggest ones in Europe. Since November 2010, he has been an Associate Professor with Computer Architecture Department. From October 2011 to July 2018, he was the IT Manager (CIO) with CETA-Ciemat, where he achieved the GPU Research Centre mention from NVIDIA as Principal Investigator. Since July 2018, he has been the Chief Information Officer with Greenfield Technologies, a precision agriculture company that provides recommendations to farmers through the use of different innovative technologies, such as drones, satellites, sensors, and artificial intelligence, and applied research. He has participated in more than 40 international projects and has authored or coauthored more than 40 publications, including 14 journal citation report papers (most of them published by IEEE journals) and more than 30 peer-reviewed international conference papers. His research interests include remotely sensed hyperspectral image analysis, signal processing, and efficient implementations of large-scale scientific problems on high-performance computing architectures, such as clusters and graphical processing units.

Dr. Paz-Gallardo was the recipient of the IEEE Signal Processing Magazine Best Column Award Paper from the IEEE Signal Processing Society in November 2015.



Antonio Plaza (Fellow, IEEE) received the M.Sc. and Ph.D. degrees in computer engineering from the University of Extremadura, Cáceres, Spain, in 1999 and 2002, respectively.

He is currently a Full Professor and the Head of Hyperspectral Computing Laboratory, Department of Technology of Computers and Communications, University of Extremadura. He has authored or coauthored more than 600 publications, including 364 JCR journal papers (265 in IEEE journals), 24 book chapters, and 330 peer-reviewed conference proceeding papers, in the field of his research interests, including hyperspectral data processing and parallel computing of remote sensing data.

Prof. Plaza has guest edited ten special issues on hyperspectral remote sensing for different journals. He is a Fellow of IEEE "for contributions to hyperspectral data processing and parallel computing of Earth observation data" and a Member of Academia Europaea, The Academy of Europe. He was the recipient of the Recognition of Best Reviewers of IEEE GEOSCIENCE AND REMOTE SENSING LETTERS (in 2009), the Recognition of Best Reviewers of IEEE TRANSACTIONS ON GEOSCIENCE AND REMOTE SENSING (in 2010) for which he was an Associate Editor in 2007–2012, the Best Column Award of the IEEE Signal Processing Magazine in 2015, the 2013 Best Paper Award of the IEEE JOURNAL OF SELECTED TOPICS IN APPLIED EARTH OBSERVATIONS AND REMOTE SENSING (JSTARS), the most highly cited paper (2005–2010) in the Journal of Parallel and Distributed Computing, and best paper awards at the IEEE Workshop on Hyperspectral Image and Signal Processing: Evolution in Remote Sensing, the IEEE International Conference on Space Technology, and the IEEE Symposium on Signal Processing and Information Technology. He is an Associate Editor for IEEE ACCESS (receiving the recognition of Outstanding Associate Editor for the journal in 2017) and was a Member of the Editorial Board of *IEEE Geoscience and Remote Sensing Newsletter* (2011–2012), *IEEE Geoscience and Remote Sensing Magazine* (2013), and of the steering committee of the JSTARS. He was the Director of Education Activities for the IEEE Geoscience and Remote Sensing Society (GRSS) in 2011 and 2012, and the President of the Spanish Chapter of IEEE GRSS in 2012 and 2016. He is a Chair of the Publications Awards Committee of IEEE GRSS and a Vice Chair of the Fellow Evaluations Committee of IEEE GRSS. He has reviewed more than 500 manuscripts for more than 50 different journals. He was the Editor-in-Chief of IEEE TRANSACTIONS ON GEOSCIENCE AND REMOTE SENSING journal for five years (2013–2017) and IEEE JOURNAL ON MINIATURIZATION FOR AIR AND SPACE SYSTEMS (2019–2020). He has been included in the 2018–2021 Highly Cited Researchers List (Clarivate Analytics).

Monitoring the Spatiotemporal Distribution of Invasive Aquatic Plants in the Guadiana River, Spain

Escuela Politécnica
Av. de la Universidad, S/N, 10003
Teléfono: 0034927257000. Ext. 51662
correo electrónico: apazgal, aplaza @unex.es
Cáceres, España

Dr. Abel Francisco Paz Gallardo y Dr. Antonio Plaza Miguel, como directores de la Tesis Doctoral titulada “Desarrollo de nuevos métodos y algoritmos de análisis y clasificación de imágenes multiespectrales orientadas a la gestión y monitorización de plantas acuáticas invasoras”, certificamos el factor de impacto y la categorización de la siguiente publicación incluida en la Tesis Doctoral. Del mismo modo, se especifica la aportación de la doctoranda. Para cualquier otra información o aclaración, por favor, no duden en contactar con nosotros.

Titulo de la publicación: Monitoring the Spatiotemporal Distribution of Invasive Aquatic Plants in the Guadiana River, Spain

Autores: **Elena C. Rodríguez-Garlito**, Abel Paz-Gallardo y Antonio Plaza

Revista: IEEE Journal of Selected Topics in Applied Earth Observations and Remote Sensing

Otros datos: vol 16, págs 228-241, año 2023

DOI: 10.1109/JSTARS.2022.3210373

Factor de impacto 2022: 5.5

Abstract: Monitoring the spatiotemporal distribution of invasive aquatic plants is a challenge in many regions worldwide. One of the most invasive species on Earth is the water hyacinth. These plants are harmful to biodiversity and create negative impacts on society and economy. The Guadiana river (one of the most important ones in Spain) has suffered from this problem since the early 2000s. Several efforts have been made to mitigate it. However, invasive plants, such as the water hyacinth, are still present in seed banks at the bottom of the river and can germinate even more than a decade after. In this article, we propose an automatic methodology, based on remote sensing and deep learning techniques, to monitor the water hyacinth in the Guadiana river. Specifically, a multitemporal analysis was carried out during two years using images collected by ESA’s Sentinel-2 satellite, analyzed with a convolutional neural network. We demonstrate that, with our strategy, the river can be monitored every few days, and we are able to automatically detect the water hyacinth. Three experiments have been carried out to predict the presence of water hyacinth from a few scattered training samples, which represent invasive plants in different phenological stages and with different spectral responses.

Contribución de la doctoranda: Planteamiento de la hipótesis, conceptualización, búsqueda bibliográfica, metodología, análisis y discusión de resultados, elaboración de tablas y figuras, escritura del manuscrito borrador y redacción de la revisión.

Monitoring the Spatiotemporal Distribution of Invasive Aquatic Plants in the Guadiana River, Spain

Elena C. Rodríguez-Garlito , *Student Member, IEEE*, Abel Paz-Gallardo , and Antonio Plaza , *Fellow, IEEE*

Abstract—Monitoring the spatiotemporal distribution of invasive aquatic plants is a challenge in many regions worldwide. One of the most invasive species on Earth is the water hyacinth. These plants are harmful to biodiversity and create negative impacts on society and economy. The Guadiana river (one of the most important ones in Spain) has suffered from this problem since the early 2000s. Several efforts have been made to mitigate it. However, invasive plants, such as the water hyacinth, are still present in seed banks at the bottom of the river and can germinate even more than a decade after. In this article, we propose an automatic methodology, based on remote sensing and deep learning techniques, to monitor the water hyacinth in the Guadiana river. Specifically, a multitemporal analysis was carried out during two years using images collected by ESA's Sentinel-2 satellite, analyzed with a convolutional neural network. We demonstrate that, with our strategy, the river can be monitored every few days, and we are able to automatically detect the water hyacinth. Three experiments have been carried out to predict the presence of water hyacinth from a few scattered training samples, which represent invasive plants in different phenological stages and with different spectral responses.

Index Terms—Deep learning (DL), invasive aquatic species, multitemporal remote sensing, water hyacinth.

I. INTRODUCTION

THE water hyacinth (*eichhornia crassipes*) is an aquatic perennial macrophyte native to Brazilian habitats [1]. This aquatic plant (that floats freely on the surface of freshwater) has spread to different parts of the world [2], being distributed in more than 50 countries across five continents. These species, considered as a valuable resource with several qualities [3], exhibit unique properties. Some authors have emphasized the ecological and socioeconomic application of the water hyacinth [4].

Manuscript received 30 September 2022; revised 5 November 2022; accepted 24 November 2022. Date of publication 28 November 2022; date of current version 7 December 2022. This work was supported in part by European Social Fund (Resolución de 10 de mayo de 2017, de la Secretaría General de Ciencia, Tecnología e Innovación, por la que se resuelve la convocatoria de ayudas para la financiación de contratos predoctorales para formación de Doctores en los centros públicos de I+D pertenecientes al Sistema Extremeño de Ciencia, Tecnología e Innovación en el ejercicio 2017, expediente PD16001), in part by Consejería de Economía, Ciencia y Agenda Digital of the Junta de Extremadura, in part by European Regional Development Fund (ERDF) of the European Union under Grant GR21040, in part by Spanish Ministerio de Ciencia e Innovación under Project PID2019-110315RB-I00 (APRISA), and in part by European Union's Horizon 2020 Research and Innovation Program under Grant 734541 (EOXPOSURE). (*Corresponding author: Elena Cristina Rodríguez-Garlito.*)

The authors are with the Hyperspectral Computing Laboratory, Department of Technology of Computers and Communications, Escuela Politécnica, University of Extremadura, 10003 Cáceres, Spain (e-mail: elenacristinarg@unex.es; apazgal@unex.es; aplaza@unex.es).

Digital Object Identifier 10.1109/JSTARS.2022.3225201

It absorbs heavy metals and organic contaminants, allowing its utilization in wastewater treatments [5], [6], [7] and for heavy metal removal [8], [9]. It also has potential use as water hyacinth biomass in biochar [10], bio-oil, and syngas [11]. Its use is also common in energy production, water treatment, agriculture (as a chemical and biological resource), and as an alternative to conventional construction materials [12]. However, its presence threatens the environment and produces a negative socioeconomic impact [13].

With high toleration in extreme environmental conditions [14], it outcompetes native vegetation, therefore affecting biodiversity. Moreover, climate change makes native plant species more vulnerable, also favoring invasive plant species that adapt better to changes. As a result, the water hyacinth is considered as one of the worst invasive alien species, and it is included in the Global Invasive Species Database [15]. The highly invasive nature of this plant is due, in part, to its rapid reproductive capacity (it can double its biomass in 6–12 days [16]). The plant is generally distributed in floating mats in the surface of rivers. These dense mats negatively affect important physiochemical water quality parameters. Dissolved oxygen concentration (the most important variable for aquatic fauna) is reduced with the growth of invasive plants [17], [18]. The patches that cover the water block the light needed for photosynthesis by other submersed vegetation. These patches also absorb nutrients from the water (impacting on ecological communities as well), decreasing phytoplankton distribution, and changing zooplankton abundance and diversity [19].

Water hyacinth invasion also creates a negative impact on different human activities, such as navigability, boating access, and recreation [20]. From an economic perspective, the invasion of hyacinth entails high costs in management [21], equipment, treatment, and qualified personnel for the tasks of control, removal, and elimination in the affected water bodies [22], [23], [24]. Given the difficulty of eradicating the invasive plants in affected watercourses, management efforts are aimed at reducing their biomass through various strategies. For this purpose, mechanical control or manual removal have been used [25], along with chemical [26], [27] or biological control [28], [29].

There is a legal framework in Europe that discourages a profitable economy around this kind of invasive species, prohibiting possession, and trade and trafficking of live specimens. Confederación Hidrográfica del Guadiana (CHG) is a public Spanish organization in charge of managing the Guadiana river basin. As shown in Fig. 1, the water hyacinth first appeared (following a tapestry-like distribution) in the Guadiana river



Fig. 1. Water hyacinth (*Eichhornia crassipes*) being removed by machinery in the Guadiana river, Spain.

basin in 2004, causing negative impacts as discussed above. This plant has also affected recreational activities in the Guadiana river, such as canoeing, as it completely invades sections of the river. Its accumulation on the piers affects navigation.

Several strategies have been adopted to mitigate the negative impact of invasive plants, with large economic investments. Some of these actions have been focused on manual and mechanized removals. Control infrastructures (such as containment and removal barriers) have been created. However, the Spanish legislation does not allow the use of herbicides in natural watercourses. In 2021, it was reported that a total of 150 783 092 tons of hyacinth were extracted since 2005 [30]. Surveillance activities have also been carried out to prevent its proliferation and expansion. The current focus is on control and early detection. Economic analyses have been conducted to demonstrate the benefits to the ecosystem of invasive species management [31]. In this way, an investment of 27 800 000 € has been foreseen for water hyacinth control and eradication measures for the 2021–2027 period.

The reproductive biology of water hyacinth allows for sexual and asexual reproductions [32], [33]. Asexual reproduction, through the formation of stolons, is the main cause of the rapid spread of water hyacinth [34]. On the other hand, sexual reproduction from a seed bank is also possible [35], [36]. According to reports from CHG, total elimination of the water hyacinth from the surface of the Guadiana river was accomplished on December 2020 [30]. However, the seeds still remain at the bottom of the river and they can germinate after a few years [35]. An important aspect to control their reproduction is early detection, allowing to taking removal measures. Invasive water species have a great capacity to reproduce and adapt to the environment in which they develop. Consequently, continuous monitoring and control of affected areas is necessary.

The seasonal growth of water hyacinth in Brazil was studied in [37], suggesting tactics for managing hyacinth with herbicide applications. The phenology and growth stages of the plant were described in a study conducted in a lake in Florida [38]. There, it was concluded that its growth phases exhibit adaptivity to the environment, ease of dispersal, reproduction, and repopulation after severe losses (particularly, in winter). Therefore, it is important to understand the phenological behavior of the plant and the

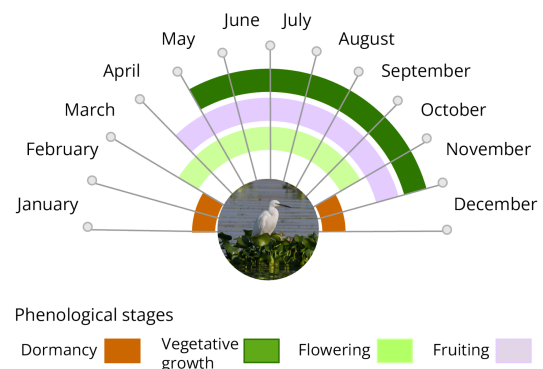


Fig. 2. Illustration of the phenological stages of water hyacinth in the Guadiana river, Spain.

dynamics of the changes it undergoes over time. Fig. 2 shows the phenology of water hyacinth in the Guadiana river basin (Spain). This figure has been elaborated from published reports by the CHG [30], [39], using field observations. It is important to note that the behavior shown in Fig. 2 can vary according to climatic aspects. In May, the vegetative growth period usually begins; the rapid development of the plant facilitates its asexual reproduction, which is capable of multiplying individuals in a very short time. Flowering usually begins in April and continues throughout the summer months. The flowers are blue and remain open from two to five days [40]. Flowering continues throughout the warm months and increases in June and August. After flowering, the fruit is produced. In November or December, the plants begin their dormancy period.

The main goal of this study is to develop a new technique to automatically detect and monitor the water hyacinth every five days [Sentinel-2 (S2) satellite revisit time] in a time series of remote sensing images spanning two years. Our aim is to determine seasonal changes in the spatial and temporal distributions of its biomass. We also analyze how many remote sensing images are required to collect suitable training samples for automatically detecting water hyacinth in the considered time series. Our goal is to minimize the number of images needed to obtain an accurate geolocation of the plant; thus, being able to model its phenological cycle. Specially, in this study we give particular

importance to accurately mapping the water hyacinth during the vegetative growth and propagation phases of the invasive plant. The main contributions of our work can be summarized as follows.

- 1) Following our previous work in [41], a deep learning (DL) model capable of identifying automatically water hyacinth has been selected as a baseline for evaluating the multitemporal evolution of the plant in a two-year time series. The selected model is able to discriminate invasive plants from the rest of the land cover, separating them from other types of vegetation.
- 2) A careful training of the DL model has been carried out by minimizing the number of samples collected. In this way, training samples have been extracted from only four multispectral S2 satellite images. Such training allows us to predict the presence of water hyacinth (in a two-year period) independently of the different phenological stages of the plant.
- 3) Using the trained model, we can monitor the spatiotemporal distribution of aquatic invasive plants every few days. This is accomplished by using S2 data (which allows obtaining an image over any location in the world every five days) without the need to retrain the model (i.e., by reusing the same training) with no additional cost in terms of image acquisition.

The rest of this article is organized as follows. Section II describes some related works. Section III explains the materials and methods used in our work. Section IV justifies the experimental design, shows the experimental results, interprets the water hyacinth dynamics, and assesses the adopted convolutional neural network (CNN) model. Section V discusses the obtained experimental results. Finally, Section VI concludes this article with some remarks and hints at plausible future research lines.

II. RELATED WORKS

In recent years, there has been an increase in the use of remote sensing techniques for mapping and monitoring water hyacinth. Different remote sensing instruments (such as Landsat Thematic Mapper, MODIS, RapidEye, WorldView-2, WorldView-3, SPOT 5, among others) with different specifications and acquisition costs have been reported in published studies [42]. Studies using remote sensing techniques take advantage of available images to identify and detect invasive plants [43]. Remote sensing images record measurements of the energy reflected and absorbed by the surface of the Earth. For instance, multispectral images, such as those collected by satellite instruments as ESA's S2, contain detailed spectral and spatial information [44] that can be used to create maps of the distribution of invasive plants [45]. Some studies applied remote sensing methods to satellite imagery by taking advantage of available indices. For example, the normalized difference vegetation index (NDVI) [46] was used to detect water hyacinth in Lake Tana, Ethiopia, by using monthly S2 images. There, satellite MODIS data were used to evaluate NDVI trends, concluding that the expansion of invasive plants is favored by fluctuations at the lake level. In [47], the NDVI

and the normalized difference water index were used to monitor the water hyacinth in Mondego river, Portugal, showing also the potential of multispectral S2 data to assist in the development of strategies for controlling the invasion of aquatic weeds. In [2], fractional vegetation cover was used to estimate the area invaded in Al Kabir river, Lebanon, using S2 time series.

The wide variety of existing machine learning algorithms allows for the detailed interpretation of remote sensing images [48]. Classification techniques exhibit the potential to automatically classify image pixels containing invasive species [49]. For example, in [50], a Naïve Bayes classifier was used to map water hyacinth in Saigon river, Vietnam. In [51], the random forest (RF) classifier was applied to S2 images allowing for the detection of water hyacinth (among other land covers). In [52], a linear discriminant analysis was used on S2 images acquired in the Greater Letaba river system, South Africa. An ensemble learning approach based on the RF algorithm was applied for the same purpose in [53]. DL algorithms, such as CNNs [54], offer flexibility in their architecture that are quite appealing for remote sensing data processing [55], but have not been widely applied to the detection of water hyacinth according to our knowledge.

In the context of the management of invasive plants in the Guadiana river, the competent institution has been monitoring the river by using aircraft flights, field data, and S2 images. In our previous work [41], we proposed a methodology for preprocessing, processing, and evaluation of satellite images using different machine learning/DL techniques to automatically detect aquatic invasive plants in the Guadiana river, Spain. Moreover, we carried out a comprehensive comparison between unsupervised and supervised classifiers, such as K-means, RF, and CNNs. In addition, we proposed a strategy to quantitatively assess classification performance in our context. This validation strategy consisted in generating a synthetic ground truth image from a high spatial resolution image, explained in detail in [56]. In this way, we demonstrated that aquatic invasive plants could be detected automatically. We also observed in the obtained classification maps and performance metrics that the CNN classifier achieved better detection accuracies than other classifiers. As a result, in this work, we adopt the CNN classifier as a baseline to perform multitemporal monitoring of water hyacinth in the Guadiana river.

III. MATERIALS AND METHODS

Fig. 3 graphically shows the workflow adopted to monitor water hyacinth in the analyzed time series. After the acquisition of S2 images in the two-year period analyzed, a preprocessing of these images is carried out. Then, automatic detection of invasive plants takes place by means of a trained CNN (in fact, three different trained models are considered in this work according to different experiments). The final classification outputs are used for the monitoring stage, which provides the percentage of water hyacinth detected over time.

A. Study Area

A section of the Guadiana river affected by water hyacinth has been selected for experiments. The region of interest (ROI)

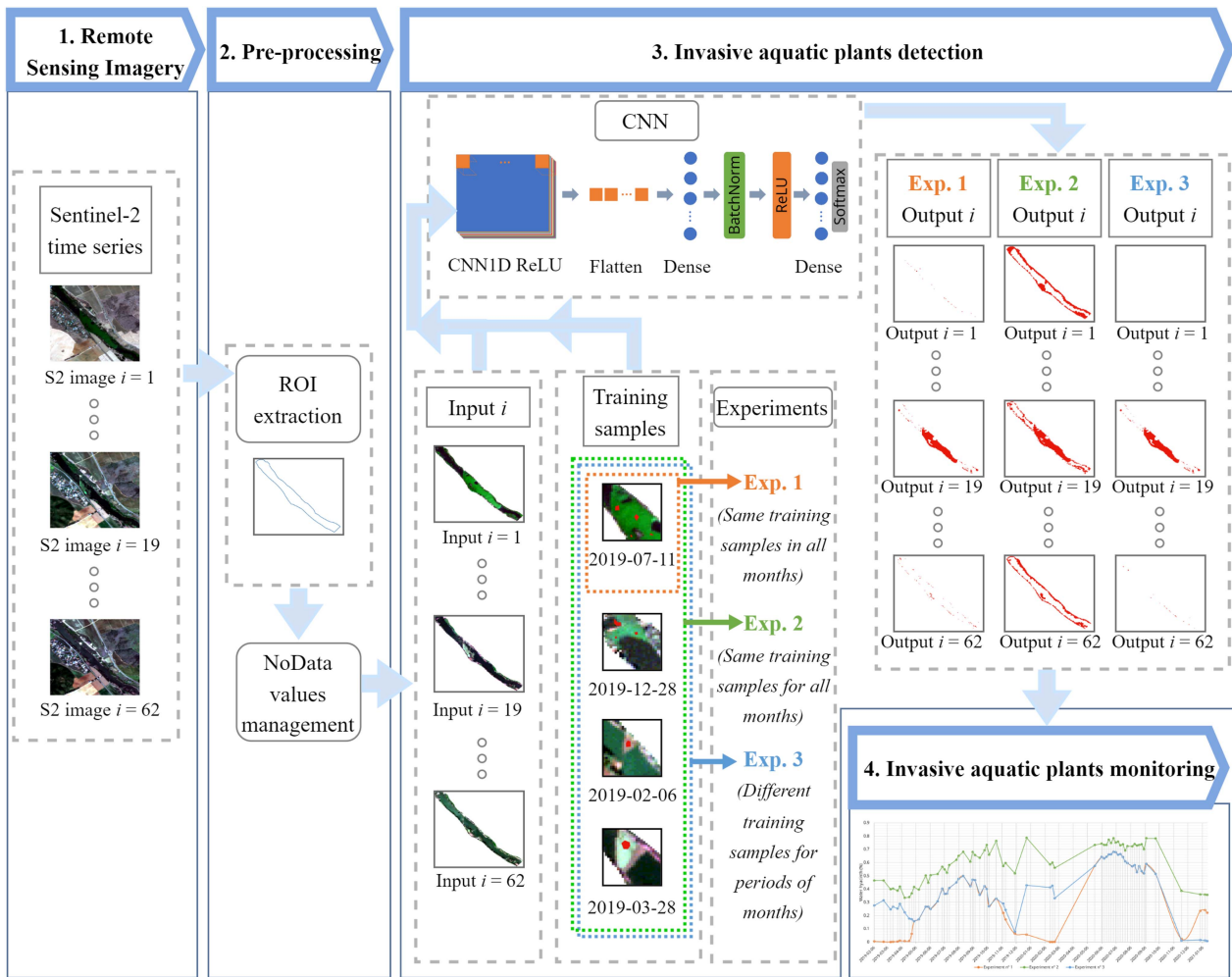


Fig. 3. Workflow of the procedure for monitoring the spatiotemporal distribution of water hyacinth in the Guadiana river using three different experiments. The architecture of the CNN used for mapping is also displayed.

TABLE I
DESCRIPTION OF S2 BANDS

Band name	B01	B02	B03	B04	B05	B06	B07	B08	B8A	B09	B10	B11	B12
Resolution (m)	60	10	10	10	20	20	20	10	20	60	60	20	20
Bandwidth (nm)	442.7	492.4	559.8	664.6	704.1	740.5	782.8	832.8	864.7	945.1	1373.5	1613.7	2202.4
Application	Coastal aerosol	Blue	Green	Red	Vegetation red edge	Vegetation red edge	Vegetation red edge	NIR	Narrow NIR	Water vapor	Cirrus	SWIR	SWIR

corresponds to an area affected by *Eichhornia crassipes*, close to the city of Mérida (ME_zone) in which an invasive plant control barrier has been installed in the river for mechanical removal. It covers an area of about 45 ha, between $38^{\circ}50' - 38^{\circ}51'N$ longitude and $6^{\circ}19' - 6^{\circ}18'W$ latitude (see Fig. 4), respectively.

B. Multitemporal Dataset

Among the advanced instruments capable of capturing the spectral response of the Earth's surface, satellites launched by ESA (as part as the Copernicus programme) have been incorporated in this study. The S2 mission provides open-access

multispectral datasets that offer the potential to monitor water hyacinth in rivers [47]. In particular, the level-2 A (S2L2A) products (with atmospheric correction) of the time series described in Table III have been acquired from SentinelHub [57]. The S2L2A imagery is composed of $100 \times 100 \text{ km}^2$ tiles in the Universal Transverse Mercator/World Geodetic System-84 projection, collected using a revisit time of five days. In Table I, we give the spatial and spectral resolutions of these images in each of the 12 available spectral bands. In our study, a period of two years has been monitored using a total of 62 S2 images (collected between January 2019 and January 2021), discarding those datasets in which the ROI was covered by clouds. Table II reports the final set of images used in our study.

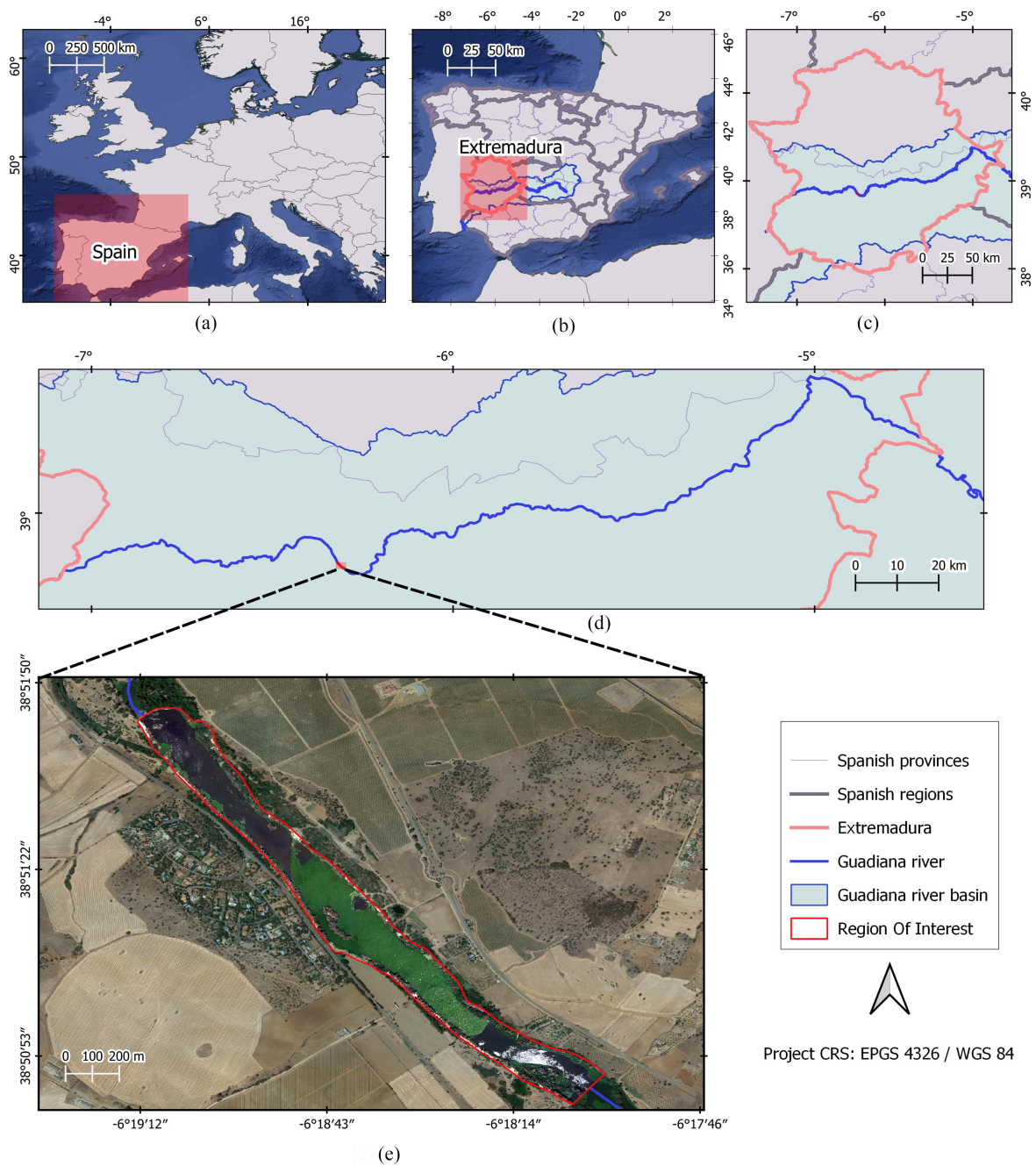


Fig. 4. (a) Geographical location of Spain. (b) Geographical location of the region of Extremadura, the Guadiana river, and the Guadiana river basin. (c) Zoom of Extremadura region, depicting the Guadiana river and its basin. (d) Zoom of the Guadiana river in the Extremadura region. (e) Zoom of a high-resolution image, including an area affected by water hyacinth, close to the city of Mérida.

TABLE II
S2 IMAGES PROCESSED PER MONTH AND YEAR

Year	Jan.	Feb.	Mar.	Apr.	May	Jun.	Jul.	Aug.	Sep.	Oct.	Nov.	Dec.	Total
2019	0	2	3	4	3	3	5	3	4	3	2	2	34
2020	0	3	0	0	1	6	6	5	3	0	1	0	25
2021	3	0	0	0	0	0	0	0	0	0	0	0	3
Total (images per month)	3	5	3	4	4	9	11	8	7	3	3	2	62

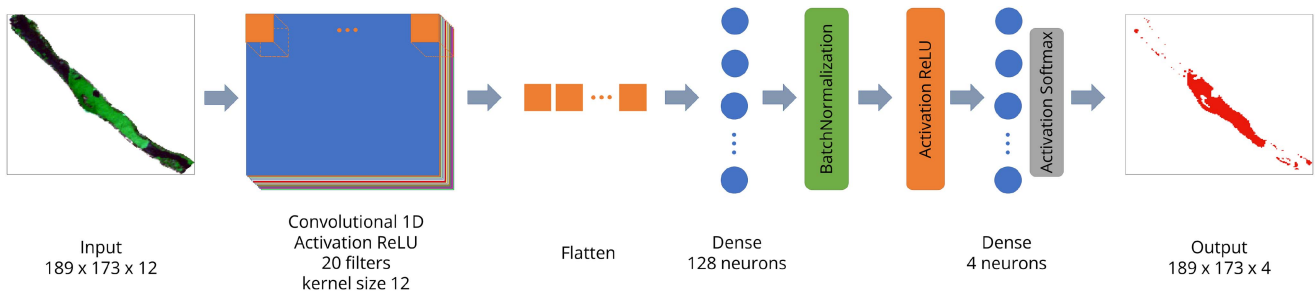


Fig. 5. Architecture of the considered CNN.

C. Hardware/Software Environment

The hardware environment in which our experiments were run comprises an Intel(R) Core(TM) i9-10900 k processor, 64-GB RAM memory, and 2-TB SSD. All the codes were implemented in Python 3.10 using TensorFlow and Keras frameworks. On the other hand, QGIS software was used for all preprocessing operations (such as raster clipping, image analysis, sample selection, etc.).

D. Image Preprocessing

After downloading the images, we manually extracted the ROIs in which we wanted to detect invasive plants. Resulting from the change of geometry to a dataset that does not have a square shape, pixels with no-data values appear. These no-data values are treated as explained in [41] to exclude them from training, prediction, and classification. For that purpose, a normalization of the pixel values of each band of the dataset has been carried out to scale them between 0 and 1. Furthermore, the format has been changed from 8 to 32 bits.

E. Image Analysis

We use a CNN algorithm to implement a model of water hyacinth detection, able to identify water hyacinth on S2 images and make predictions in other different images. CNNs have been widely used in spatial and spectral pattern analyses [55] to perform pixel classification studies, becoming a suitable algorithm for separating different vegetation types [58], [59], [60], [61]. Recent studies have demonstrated the effectiveness of CNNs in the task of mapping vegetation species in remote sensing images [62]. The CNN design consists of sets of blocks with neurons. The input data are transformed to an output volume of neurons connected through weights and biases. In this way, the output volume becomes the input of the next block [63]. The design of CNNs allows to process input data in the form of multiple arrays [64], including multispectral images. As the traditional multilayer perceptron, the CNN has hidden layers. There, patterns are exploited in at least one convolutional layer. Some studies apply CNNs to analyze the spatial patterns of the input image data. Others consider spectral information, and some works consider both the spatial and spectral information contained in the data [55]. In this study, the spectral pixels are considered as the input data. Our CNN architecture receives as many input vectors as pixels are present in the original S2 image.

The adopted classification scheme is shown in Fig. 5 where our CNN architecture comprises the following layers.

- 1) A convolutional 1-D layer with ReLU activation, including 20 filters and kernel size of 12.
- 2) A reshaping (flatten) layer.
- 3) A fully connected (dense) layer with 128 neurons.
- 4) A batch normalization layer with ReLU activation.
- 5) A fully connected (dense) layer with four neurons and *Softmax* activation.

This architecture has achieved an overall classification accuracy of 90% when identifying aquatic invasive plants in our study area [41], outperforming other state-of-the-art methods.

As shown in Fig. 3, the CNN model has been trained with different training samples. The different training sets used by the CNN model define the three experiments performed in this work. The design of experiments 2 and 3 depends on the results of experiment 1. All conducted experiments are described in the following section.

IV. EXPERIMENTAL RESULTS

A. Experimental Design

In order to detect water hyacinth in the Guadiana river, a multitemporal study has been carried out. A supervised CNN has been trained to process a two-year time series of S2 imagery. Before applying the CNN algorithm, we train the predictive model to be able to distinguish water hyacinth from other species and land covers. For this purpose, training samples of invasive plants have been collected, together with other training samples from different land cover types present in our case study. Three experiments are described as follows, where experiments 2 and 3 have been defined based on the results of water hyacinth detection in experiment 1.

1) *Experiment 1*: In this experiment, a single set of training samples are collected from an S2 image and used for prediction in the complete time series. First, to be able to identify the water hyacinth, the main land cover types present in the river have been identified by visual interpretation from a high-resolution image. For this purpose, we have chosen an orthophotograph acquired by the (Spanish) National Plan of Aerial Orthophotography (PNOA) using a photogrammetric flight. These flights are carried out over the whole Spanish territory. It has been obtained for free, from the National Geographic Institute [65]. The high spatial resolution PNOA dataset was collected in 2019. It is a multispectral image with three RGB bands of 7443 ×

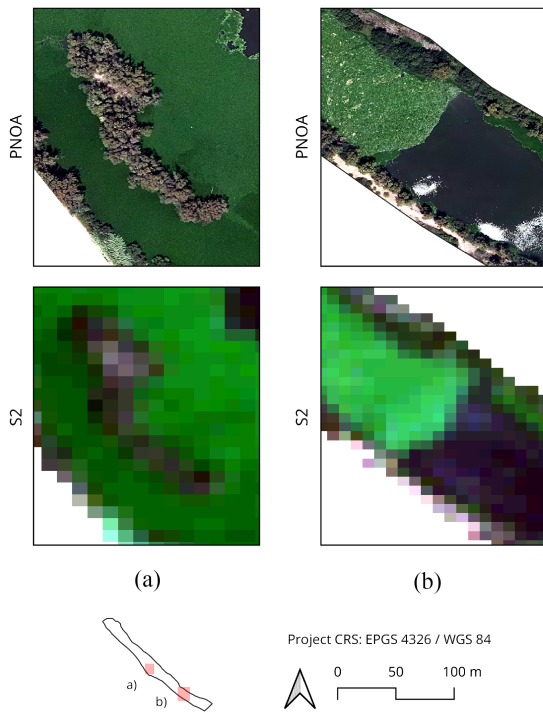


Fig. 6. (a) and (b) PNOA and S2 datasets. By visual interpretation, water hyacinth training samples are collected and differentiated from the rest of land cover types.

6321 pixels, in 8-bit format, with a spatial resolution of 0.25 m per pixel. Since the date of acquisition of the PNOA dataset belongs to the time series studied (July 2019), we have been able to accurately extract training samples on the July S2 image by using GIS tools. Specifically, we have collected training samples of water hyacinth and other land cover types from the ROI extracted from the image acquired by S2 on July 11, 2019. In this month, as shown in Fig. 2, water hyacinth is in a vegetative growth stage, and the plant can flower and produce fruits. As shown in Fig. 6, the high-resolution PNOA image acquired in July 2019 is suitable to separate the invasive plants from other species in the image. In this way, by visual interpretation, training samples can be collected by selecting those that belong to water hyacinth and those that belong to different land cover types (such as water, soil, and other kinds of vegetation).

The definition of the next experiments was established after analyzing the 62 images obtained after applying the CNN to each of the training sets. With the purpose of collecting a minimum number of samples from the S2 images, the results were considered acceptable when the detection of the invasive plants was adequate for all the months in the time series studied.

2) *Experiment 2*: In this experiment, we use a single set of training samples collected from several S2 images for predicting the presence of water hyacinth in the complete time series. Here, we consider a single training set (considering the different phenological stages of water hyacinth) for predicting its presence in every month in the multitemporal dataset. On the one hand, samples of different land cover types (except water hyacinth) were collected on July 11, 2019, from the S2

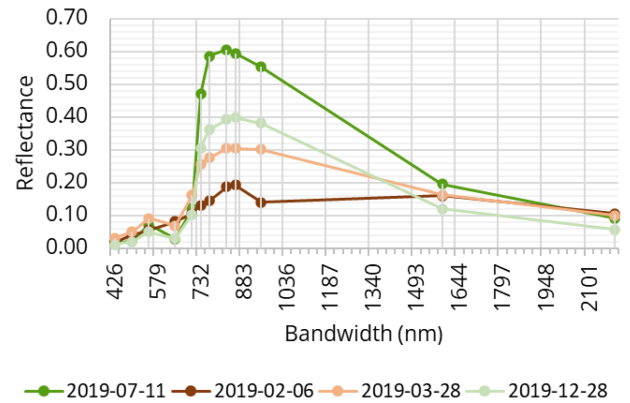


Fig. 7. Spectral signatures of the training samples of water hyacinth.

dataset by resorting to visual inspection of the high spatial resolution PNOA dataset and GIS techniques. We rely on field reports and technical consultations with CHG to conclude that the spatial resolution of S2 images is acceptable to collect water hyacinth samples by visual interpretation (from areas that are large enough and are fully occupied by the plant) on different phases of the vegetative cycle. In addition, to avoid collecting erroneous training samples, S2 images have been visualized with indices that highlight vegetation and water types (such as NDVI and moisture index). In this way, samples have been extracted at four different dates (since the training samples used in experiment 1 are not sufficient for a correct detection of the invasive plant in all the months of the year). These dates are as follows.

- 1) February 6, 2019, when the water hyacinth is in dormancy.
- 2) March 28, 2019, when it is in flowering stage.
- 3) July 11, 2019, when it is in vegetative growth.
- 4) December 28, 2019, when it is also in dormancy, but with different natural color.

The spectral signatures of water hyacinth in the dates reported above are shown in Fig. 7. They follow a similar trend as that of conventional spectral signatures of vegetation, with absorption features in the red and blue wavelengths and high reflectance in the green and near infrared (NIR) wavelengths [66]. Despite that, they exhibit notable differences that justify the collection of water hyacinth samples on different dates. As it is also shown on the RGB color composition of the S2 image in Fig. 10, the different water hyacinth colors depend on the vegetative cycle in which they are. There are significant variations in terms of reflectance in the RGB bands, especially in B03 (559.8 nm), justifying the color changes from green (vegetative growth stage) to brown (dormancy).

3) *Experiment 3*: In this experiment, we collected a set of training samples belonging to different phenological stages of the water hyacinth that notably affect its spectral signature. First, after analyzing all the images, we assumed that other land cover types are common in each training set, so they were extracted on July 11, 2019, by visual interpretation, as reported in previous experiments. Second, water hyacinth samples were acquired on the same dates, as in the previous experiment. On the contrary, every training set is considered just for a specific period of the

TABLE III
NUMBER OF TRAINING SAMPLES (PIXELS) USED IN OUR EXPERIMENTS

	Experiment 1	Experiment 2	Experiment 3			
			Period 1	Period 2	Period 3	Period 4
Water hyacinth	162	427	30	57	162	178
Other land cover types	288	288	288	288	288	288

year. Accordingly, the first training set (collected on February 6, 2019) is only considered for February. The second set (collected on March 28, 2019) is considered for March and April. The third one (collected on July 11, 2019) is used in the May–October period. Finally, the samples collected on December 28, 2019, are used in the November–January period.

Table III describes the different training sets considered in this experiment. Considering that an S2 image has 4471 labeled pixels and that there are a total of 62 images that have been processed, the number of training samples required for each experiment is quite small.

B. Experimental Results

This section describes the obtained detection results and justifies the consideration of different dates to collect training samples. Experiments 2 and 3 arise from the fact that new training samples need to be collected in order to reflect the phenological stage of the plant in different months of the year.

Fig. 9 shows the dynamics presented by the water hyacinth in the Guadiana river study areas. Specifically, it reports the detection results obtained after applying the CNN algorithm to four different cases, with four different training sets collected on different dates (i.e., July, December, February, and March). On the other hand, Fig. 10 displays some of the obtained invasive plant detection results with different training sets.

Regarding the results in Fig. 9, we note that the use of the training set collected on July 11, 2019, (referred to hereinafter as set 1, collected during the growing stage of the plant) reveals an increase in the percentage of pixels containing water hyacinth with regards to the ROI in May 2019. It can also be seen that the percentage of detected pixels reaches a maximum in the summer months. At this point, there is a slow decline (i.e., a decrease in the percentage of pixels labeled as water hyacinth in the ROI). Such decline is steeper in November, when the plant is in dormancy. In this case, the training samples were collected by visual interpretation using a high-resolution image (PNOA) from the same date. As a consequence, the detection results in Fig. 8 can be considered quite accurate. Particularly, the large mass of invasive plants accumulated behind the barrier is perfectly detected [see Fig. 10(a)]. On the contrary, when the training samples from February (set 2) and March (set 3) are used, the invasive plants are hardly detected. This can be seen in Fig. 9; with the July 2019 training set, almost no water hyacinth is detected in February and March. On the other hand, the use of training samples collected in December (set 4) also seems suitable for accurate detection of hyacinth in the S2 image acquired in July, as shown in Fig. 10(a). This is confirmed by

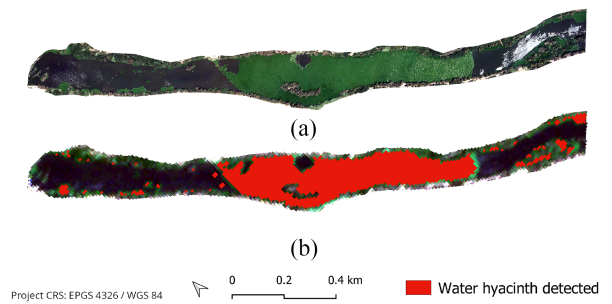


Fig. 8. (a) S2 image was collected at the same date as the PNOA reference image. (b) Water hyacinth detection results on the S2 image.

the correlation of the plots obtained after using the December and July training sets in Fig. 9. However, no correlation can be appreciated from August to December.

According to the results in Fig. 9, with the set of samples collected in July, no hyacinth could be detected in February. However, as shown in Fig. 10, invasive plants can be seen in the S2 images. It should be noted that, in February, the hyacinth is in a period of vegetative standstill and has brown color. With the samples collected in February (set 2), the detection results are accurate. With the samples collected in March (set 3), the hyacinth can be also detected, but not in all covered areas. The same happens with the samples collected in December (set 4), i.e., the invasive plants cannot be detected in the February image.

As shown in Fig. 2, in March, the plant starts flowering. As shown in Fig. 9, with the samples collected in July, the plants are not detected in March. On the contrary, as shown in Fig. 10(c), the plant appears in brown and green colors. Consequently, there is a need to collect training samples in March, since set 3 is the only training set that allows for a correct detection of the water hyacinth in this period. In other words, to avoid nondetections of water hyacinth in February and March, we need training samples collected in those months (although the corresponding sets do not describe well the status of the plant in the rest of the months of the year).

Finally, as we can see in Fig. 10(d), the water hyacinth appears with green color in December and can only be correctly detected with the training samples collected on the same month (set 4). These detection results can also be appreciated in Fig. 9. Similar results were obtained in the two analyzed years, revealing that the seasonal behavior of water hyacinth is quite stable.

C. Interpretation of Water Hyacinth Dynamics

In this section, we discuss the dynamics of the invasive plant over time, taking as reference Fig. 11 that reports the detection

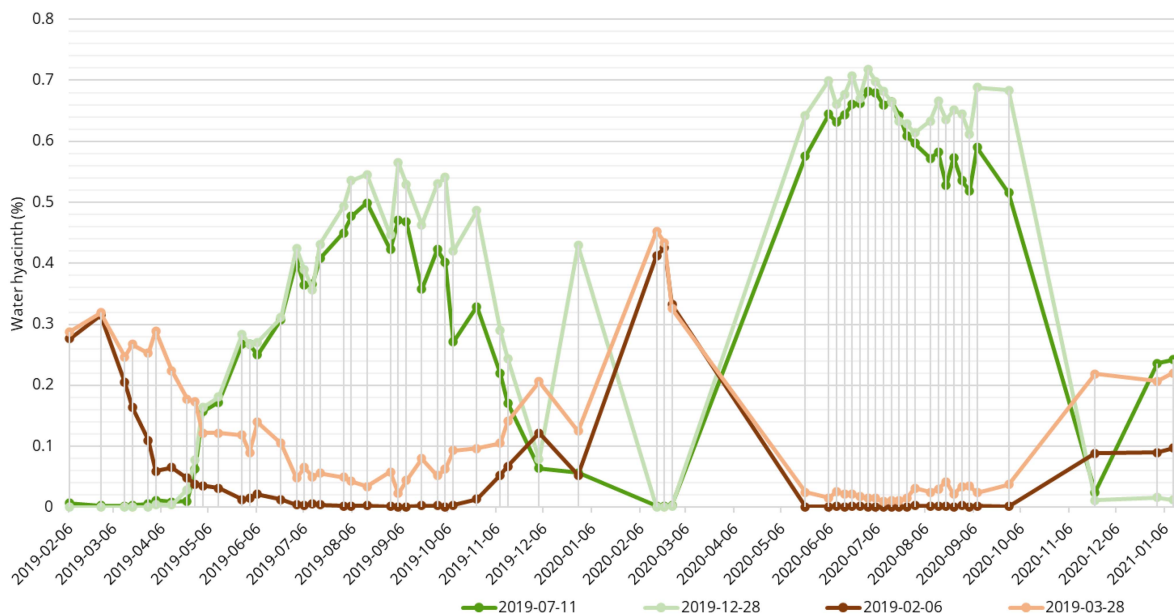


Fig. 9. Water hyacinth detection results (% of pixels detected in the ROI, excluding no-data values) for the time series (2019–2021) using the considered training sets: Set 1 (July 11, 2019), set 2 (February 6, 2019), set 3 (March 28, 2019), and set 4 (December 28, 2019).

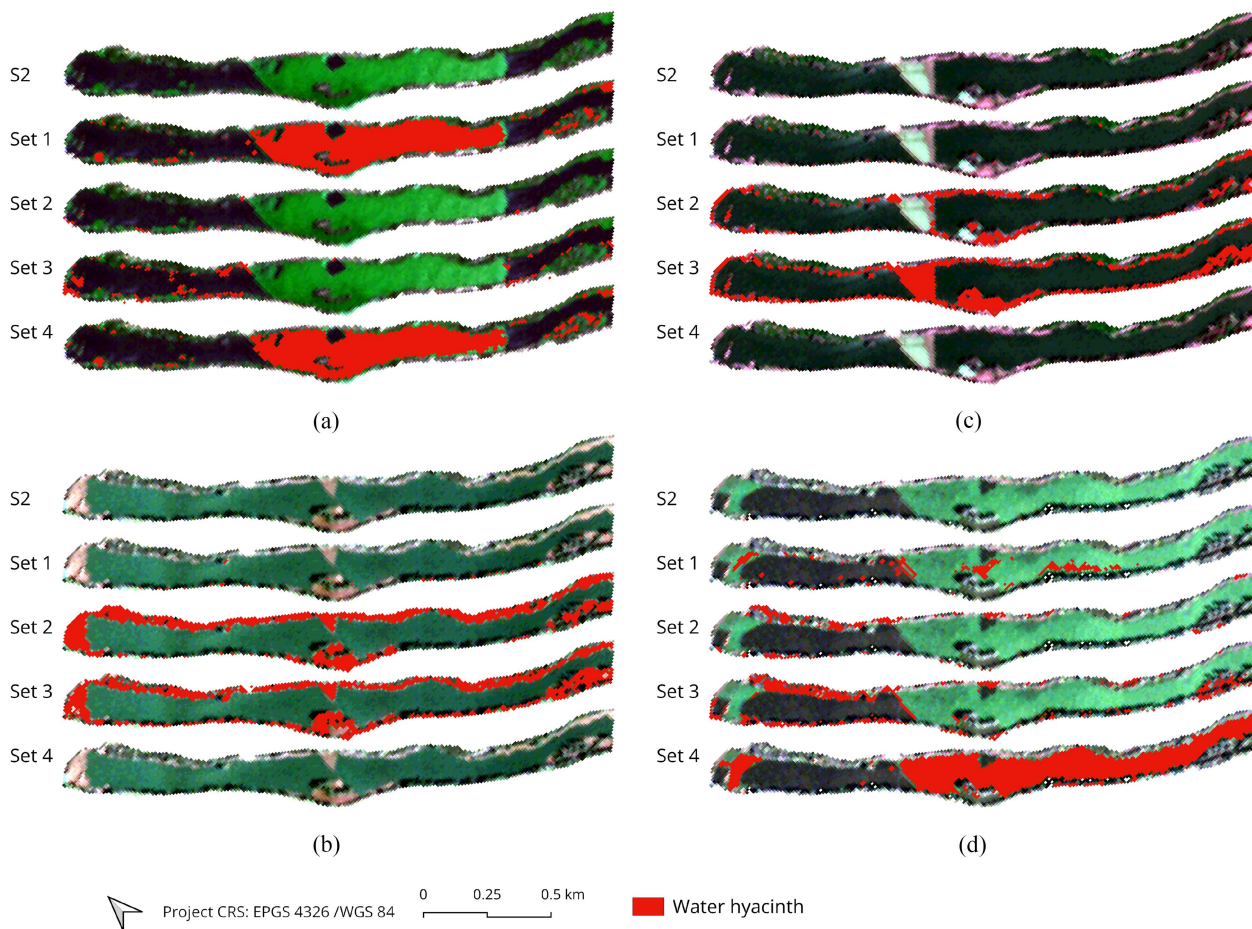


Fig. 10. Results obtained after applying the CNN to the S2 images acquired on the following dates. (a) July 11, 2019. (b) February 6, 2019. (c) March 28, 2019. (d) December 28, 2019. Pixels containing water hyacinth on the surface of the river are marked in red. For each image, we show the detection results obtained by using different training sets; samples collected on July 11, 2019 (set 1), February 6, 2019 (set 2), March 28, 2019 (set 3), and December 28, 2019 (set 4). The images are visualized in natural color (RGB).

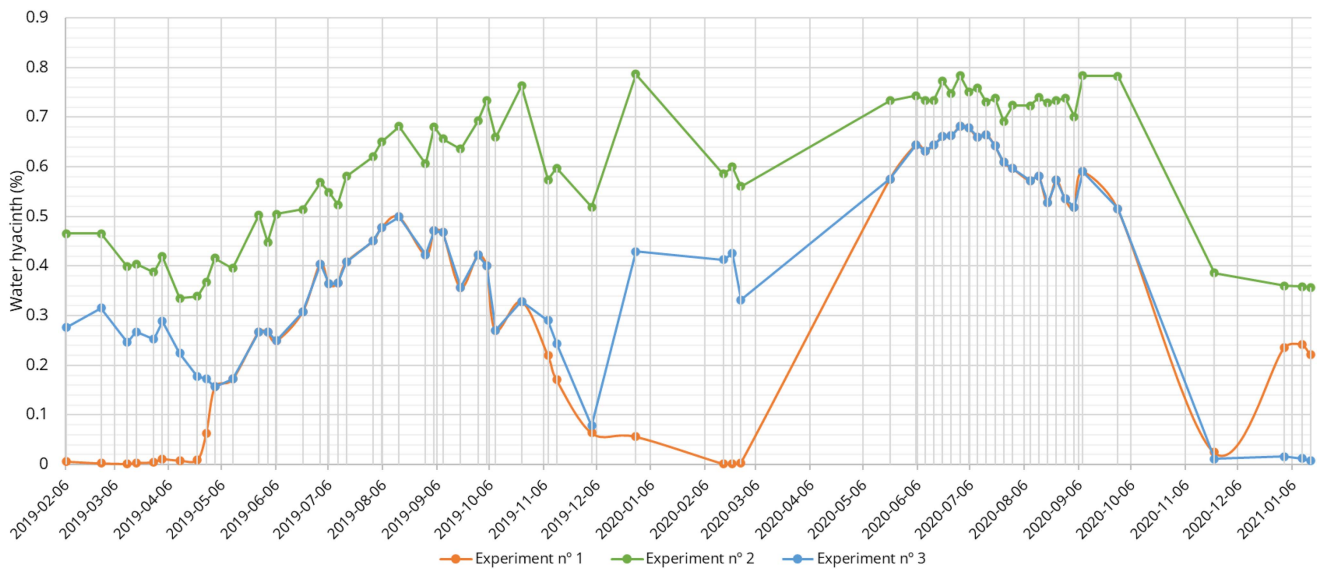


Fig. 11. Percentage of pixels of water hyacinth in the ROI (excluding no-data values) obtained for the full time series (2019–2021) in each considered experiment.

results over the complete time series for each considered experiment.

1) *Experiment 1*: The dynamics followed by the water hyacinth in the considered time series can be well-understood in the period from May to November. The plant first experiences a growth period, and then the percentage of pixels occupied by this invasive plant decreases. The increase is observed during the vegetative growth period of the plant, and the decrease happens when the vegetative rest period starts. On the contrary, little or no presence of water hyacinth was detected during the first months of the year (from January to May). Fewer invasive plants are also detected in December.

2) *Experiment 2*: This experiment also reveals an expected dynamic of increase and subsequent decrease of the number of pixels containing invasive plants in the input images collected along the year. Specifically, the percentage of pixels occupied by the invasive plant decreases until the vegetative growth period starts. When the change of vegetative growth phase happens, it increases until reaching a period of maximum occupancy, and then decreases again at the beginning of the vegetative dormancy phase.

3) *Experiment 3*: This experiment reveals a similar pattern as experiment 2. However, it is observed that the percentage of water hyacinth pixels decreases over the complete time series.

D. CNN Model Assessment

To assess that the considered CNN model can detect water hyacinth, this section conducts a more detailed assessment of such model. As shown in Fig. 8, the detection results obtained by the CNN can be assessed by comparisons with the PNOA high-resolution image. The S2 images allow identifying the masses of water hyacinth on the surface of the river (see Fig. 12). This visual verification has been complemented with reports provided from the CHG [30]. Moreover, the results are supported

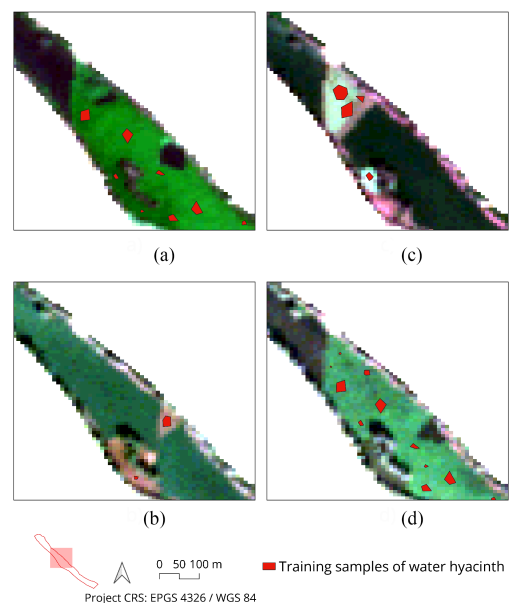


Fig. 12. Some training samples collected for water hyacinth in different training sets. (a) July 11, 2019 (set 1). (b) February 6, 2019 (set 2). (c) March 28, 2019 (set 3). (d) December 28, 2019 (set 4).

by the natural trend of the water hyacinth growth over the year, as shown in Fig. 2.

All the output images obtained by the CNN model in each experiment (a total of 186 images, 62 per experiment) have been carefully analyzed. However, we only display output images that exhibit important changes in the dynamics of the invasive plant for simplicity. These selected output images are shown in Fig. 13. Specifically, we show images from each experiment for different acquisition dates. Fig. 13 also includes a reproduction of Fig. 11 from the previous section to facilitate the evaluation of the results. Some considerations are given as follows for each individual experiment.

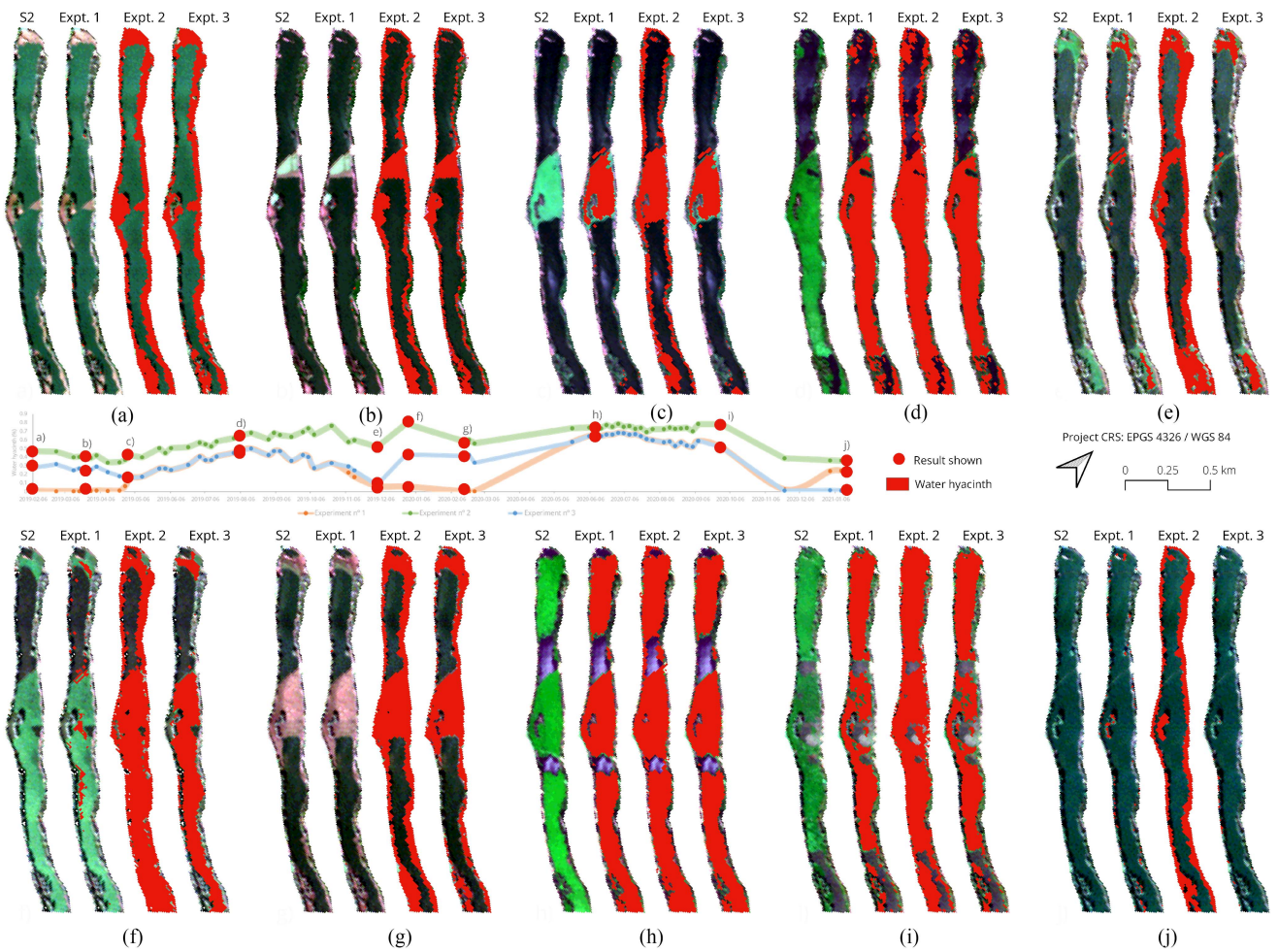


Fig. 13. Water hyacinth detection results on some acquisition dates included in the studied time series. (a) February 6, 2019. (b) March 28, 2019. (c) May 2, 2019. (d) August 5, 2019. (e) December 3, 2019. (f) December 28, 2019. (g) February 16, 2020. (h) June 10, 2020. (i) September 28, 2020. (j) January 16, 2020.

1) *Experiment 1*: It can be verified that with the set of training samples of experiment 1, no water hyacinth can be detected in the first months of the year (i.e., February and March) when it is present on the surface of the river. From May to October, the surface area detected by the CNN coincides with the one that can be seen in the satellite image. According to the CHG, the hyacinth reached its maximum occupation in the summer months [as shown in Fig. 13(d)]. In December, parts of the invasive plants that are present are actually detected [see Fig. 13(e) and (f)].

2) *Experiments 2 and 3*: In these two experiments, we detect all the water hyacinth that can be seen in the images acquired from S2 [as shown in Fig. 13(a)–(j)]. A sharp rise in the amount of hyacinth can be observed by the end of December, as it can be seen from the S2 image in Fig. 13(f). Far from being a prediction error, according to technical information from CHG technicians, on that date, the water hyacinth containment barrier was operating at full capacity, accumulating the invasive plants brought by the upstream current for its subsequent removal from the riverbed by mechanical means. Experiments 2 and 3 actually confirm this fact. In addition, according to the CHG reports, this study zone was considered to be free of invasive plants in December 2020, because they were removed with the change

of phase. Taking into account this situation, CHG changed the status to *pre-eradication* and *early warning*. When we use the training samples collected in December (experiment 3), the obtained results indicate that the water surface is free from these plants on those dates.

V. DISCUSSION

Results of experiment 1 reveal a successful monitoring of the study area affected by water hyacinth, because with only a few training samples (collected from a single S2 image), it was possible to detect the existing masses of invasive plants in the seasonal growth periods of the entire two-year period analyzed. The detection was not accurate on the periods of dormancy of these plants. However, if accurate detection of water hyacinth in all months of the year is necessary, experiments 2 and 3 are needed. As reported in [62], the temporal variations of the plant (due to its phenology) may limit the transferability of the predictive models through time. To avoid this, in this study, we collect training samples in specific months to consider multiple phenological phases of the plant. In other words, with a training set in which the water hyacinth samples come from the same date, it is not possible to detect water hyacinth in the

rest of the months of the year. As it was concluded in [43], the accuracy of aquatic weeds mapping by using remote sensing techniques can be improved by dividing the variability of species into phenological stages. Therefore, it is necessary to collect training samples in specific months in order to take into account the phenological behavior of the plant, which varies depending on the actual month being monitored.

In the analysis of S2 images from the time series considered in this study (2019–2021), checking the natural RGB color display (what the human eye perceives) can provide information about the state of the plant. During the months of January and February, when the plants are at the end of their phenological cycle, they appear in brown color. The plants become green in March and April. They remain green from May onwards, when they are in their vegetative growth stage, until the end of the year. It was therefore necessary to collect samples in July, December, February, and March to make sure that water hyacinth is properly detected throughout the year.

In order to choose the best training set for predicting the aquatic weeds in the time series, it was necessary to collect samples in December, February, and March. During these months, the aquatic weeds can be clearly seen, so it is easier to know where it is better to collect the training set from a specific date. This is particularly the case for February. In other dates, the detection results are not clear (e.g., with the March samples, we can obtain good detection results until the end of April).

Focusing on the color nature of the samples, our experiments reveal that samples with different colors are needed in order to obtain accurate detection results. This was suggested in [46]. It was also shown in [52] that the spectral signature of water hyacinth is clearly different in the wet and dry seasons. In our study, we found that samples from July allow for a correct identification of the plant when it appears in green color (from July to December). Quite opposite, when the plant appears in brown color, the detection results improve when we incorporate the training samples collected at the end of December, February, and March.

VI. CONCLUSION

In this work, we have modeled the spatiotemporal distribution of invasive plants (water hyacinth) in the Guadiana river (Spain) over the period 2019–2021. It has been shown that monitoring the distribution of hyacinth does not require field observations. In fact, the status of the plant can be monitored every five days using medium spatial resolution images, such as those collected by ESA's S2 satellite. We also demonstrated that it is only necessary to train the considered predictive model (CNN) once, using a high-resolution image (in our case, the PNOA image) to extract the most representative samples in the study area. This allows us to separate invasive plants from other land cover surfaces (such as water, soil, and other kinds of vegetation) for a period of at least two years. To detect the water hyacinth at different stages of its biological life cycle (considering that they exhibit different spectral signatures), a comprehensive training set was collected by visual interpretation of the S2 images. As a result, very few training samples are needed to make predictions in the subsequent year.

In future studies, we will consider other high spatial resolution images to quantitatively assess the obtained results via synthetic ground truth images.

ACKNOWLEDGMENT

The authors would like to thank CHG for providing monthly monitoring reports on the evolution of the water hyacinth, as well as information on the actions carried out in the study area, Tomás Rodríguez for providing photographs of the water hyacinth on the Guadiana river, and Associate Editor and the three Anonymous Reviewers for their outstanding comments and suggestions that greatly helped us to improve the technical presentation and content of our work.

REFERENCES

- [1] B. Gopal, *Water Hyacinth. (Aquatic Plant Studies 1)*. Cambridge, U.K.: Cambridge Univ. Press, 1987.
- [2] Y. Ghousein et al., "Multitemporal remote sensing based on an FVC reference period using Sentinel-2 for monitoring *Eichhornia crassipes* on a Mediterranean river," *Remote Sens.*, vol. 11, 2019, Art. no. 1856.
- [3] A. Malik, "Environmental challenge *vis a vis* opportunity: The case of water hyacinth," *Environ. Int.*, vol. 33, pp. 122–138, 2007.
- [4] N. Jafari, "Ecological and socio-economic utilization of water hyacinth (*Eichhornia crassipes* Mart Solms)," *J. Appl. Sci. Environ. Manage.*, vol. 14, 2010, Art. no. 57834.
- [5] Q. Mahmood et al., "Lab scale studies on water hyacinth (*Eichhornia crassipes* Mart Solms) for biotreatment of textile wastewater," *Caspian J. Environ. Sci.*, vol. 3, pp. 83–88, 2005.
- [6] A. M. Lissy and G. Madhu, "Removal of heavy metals from waste water using water hyacinth," *ACEEE Int. J. Transp. Urban Develop.*, vol. 1, 2011, Art. no. 48.
- [7] J. Lu, Z. Fu, and Z. Yin, "Performance of a water hyacinth (*Eichhornia crassipes*) system in the treatment of wastewater from a duck farm and the effects of using water hyacinth as duck feed," *J. Environ. Sci.*, vol. 20, pp. 513–519, 2008.
- [8] P. Saha, O. Shinde, and S. Sarkar, "Phytoremediation of industrial mines wastewater using water hyacinth," *Int. J. Phytoremediation*, vol. 19, pp. 87–96, Jan. 2017.
- [9] W. H. Ting, I. A. Tan, S. F. Salleh, and N. A. Wahab, "Application of water hyacinth (*Eichhornia crassipes*) for phytoremediation of ammoniacal nitrogen: A review," *J. Water Process Eng.*, vol. 22, pp. 239–249, Apr. 2018.
- [10] G. K. Gaurav, T. Mehmood, L. Cheng, J. J. Klemeš, and D. K. Shrivastava, "Water hyacinth as a biomass: A review," *J. Cleaner Prod.*, vol. 277, Dec. 2020, Art. no. 122214.
- [11] F. Li et al., "Water hyacinth for energy and environmental applications: A review," *Bioresour. Technol.*, vol. 327, May 2021, Art. no. 124809.
- [12] A. Salas-Ruiz and M. del Mar Barbero-Barrera, "Performance assessment of water hyacinth–cement composite," *Construction Building Mater.*, vol. 211, pp. 395–407, Jun. 2019.
- [13] N. Merry M. Mitán, *Water Hyacinth: Potential and Threat*, vol. 19. Amsterdam, The Netherlands: Elsevier, 2019, pp. 1408–1412.
- [14] A. A. Adelodun, U. O. Hassan, and V. O. Nwachuckwu, "Environmental, mechanical, and biochemical benefits of water hyacinth (*Eichhornia crassipes*)," *Environ. Sci. Pollut. Res.* vol. 27, pp. 30210–30221, May 2020.
- [15] Global Invasive Species Database. Accessed: Nov. 30, 2022. [Online]. Available: http://www.iucngisd.org/gisd/100_worst.php
- [16] Y. O. Ouma, A. Shalaby, and R. Tateishi, "Dynamism and abundance of water hyacinth in the Winam Gulf of Lake Victoria: Evidence from remote sensing and seasonal-climate data," *Int. J. Environ. Stud.*, vol. 62, pp. 449–465, Aug. 2005.
- [17] C. Perna and D. Burrows, "Improved dissolved oxygen status following removal of exotic weed mats in important fish habitat lagoons of the tropical Burdekin River floodplain, Australia," *Mar. Pollut. Bull.*, vol. 51, pp. 138–148, 2005.
- [18] V. D. Tobias, J. L. Conrad, B. Mahardja, and S. Khanna, "Impacts of water hyacinth treatment on water quality in a tidal estuarine environment," *Biol. Invasions*, vol. 21, pp. 3479–3490, Dec. 2019.

- [19] A. M. Villamagna and B. R. Murphy, "Ecological and socio-economic impacts of invasive water hyacinth (*Eichhornia crassipes*): A review," *Freshwater Biol.*, vol. 55, pp. 282–298, 2010.
- [20] V. Mozaffarian and B. Yaghoubi, "New record of *Eichhornia crassipes* (water hyacinth) from north of Iran," *Rostaniha*, vol. 16, pp. 208–2011, 2015.
- [21] J. Caudill, J. D. Madsen, W. Pratt, and C. Llp, "Operational aquatic weed management in the California Sacramento-San Joaquin River Delta," *J. Aquatic Plant Manage.*, vol. 59, pp. 112–122, 2021.
- [22] E. V. Wyk and B. W. V. Wilgen, "The cost of water hyacinth control in South Africa: A case study of three options," *Afr. J. Aquatic Sci.*, vol. 27, pp. 141–149, Jan. 2002.
- [23] B. Greenfield, M. Blankinship, and T. McNabb, "Control costs, operation, and permitting issues for non-chemical plant control: Case studies in the San Francisco bay-delta region, California," *J. Aquatic Plant Manage.*, vol. 44, pp. 40–49, 2006.
- [24] B. K. Greenfield, G. S. Siemering, J. C. Andrews, M. Rajan, S. P. Andrews, and D. F. Spencer, "Mechanical shredding of water hyacinth (*Eichhornia crassipes*): Effects on water quality in the Sacramento-San Joaquin River Delta, California," *Estuaries Coasts*, vol. 30, pp. 627–640, 2007.
- [25] M. P. Hill and J. A. Coetzee, "Integrated control of water hyacinth in Africa 1," *EPPO Bull.*, vol. 38, pp. 452–457, 2008.
- [26] J. jun Chu, Y. Ding, and Q. jia Zhuang, "Invasion and control of water hyacinth (*Eichhornia crassipes*) in China," *J. Zhejiang Univ. Sci. B*, vol. 7, pp. 623–626, 2006.
- [27] N. J. Waltham and S. Fixler, "Aerial herbicide spray to control invasive water hyacinth (*Eichhornia crassipes*): Water quality concerns fronting fish occupying a tropical floodplain wetland," *Trop. Conservation Sci.*, vol. 10, Dec. 2017. [Online]. Available: <https://journals.sagepub.com/doi/epub/10.1177/1940082917741592>
- [28] M. H. Julien, "Biological control of water hyacinth with arthropods: A review to 2000," in *Proc. ACIAR*, 2000, pp. 8–20.
- [29] J. A. Coetzee and M. P. Hill, "The role of eutrophication in the biological control of water hyacinth, *Eichhornia crassipes*, in South Africa," *BioControl*, vol. 57, no. 2, pp. 247–261, Apr. 2012.
- [30] Confederación Hidrográfica del Guadiana O. A. Ministerio para la transición ecológica y el reto demográfico. Gobierno de España. Accessed: Nov. 30, 2022. [Online]. Available: <https://www.chguadiana.es/cuenca-hidrografica/especies-exoticas-invasoras/actuaciones>
- [31] L. A. Wainger et al., "Evidence-based economic analysis demonstrates that ecosystem service benefits of water hyacinth management greatly exceed research and control costs," *PeerJ*, vol. 6, 2018, Art. no. e4824.
- [32] Z. H. Zhang and J. Y. Guo, "Biology of water hyacinth," *Water Hyacinth*, 1st Ed., 2017, pp. 1–29.
- [33] Centre for Agricultural Bioscience International– *Eichhornia Crassipes* (Water Hyacinth). Accessed: Nov. 30, 2022. [Online]. Available: <https://www.cabi.org/isc/datasheet/20544#tosummaryOfInvasiveness>
- [34] T. R. Téllez, E. M. de Rodrigo López, G. L. Granado, E. A. Pérez, R. M. López, and J. M. S. Guzmán, "The water hyacinth, *Eichhornia crassipes*: An invasive plant in the Guadiana river basin (Spain)," *Aquatic Invasions*, vol. 3, pp. 42–53, 2008.
- [35] E. P. Albano and D. T. R. Téllez, "Reproducción sexual del jacinto de agua (*Eichhornia crassipes*): Germinación, anatomía y banco de semillas," Ph.D. dissertation, Departamento de Biología Vegetal, Ecología y Ciencias de la Tierra. Grupo de Investigación en Biología de la Conservación, Universidad de Extremadura, Badajoz, Spain, 2012.
- [36] E. A. Pérez et al., "Seed germination and risks of using the invasive plant *Eichhornia crassipes* (Mart.) Solms-Laub. (water hyacinth) for composting, ovine feeding and biogas production," *Acta Botanica Gallica*, vol. 162, pp. 203–214, Jul. 2015.
- [37] J. D. Madsen, G. M. Morgan, and John Miskella, "Seasonal growth and phenology of water hyacinth, curlyleaf pondweed, and Brazilian egeria in the Sacramento-San Joaquin River Delta," *Article J. Aquatic Plant Manage.*, vol. 59, pp. 16–27, 2021.
- [38] T. D. Center and N. R. Spencer, "The phenology and growth of water hyacinth (*Eichhornia crassipes* (Mart.) Solms) in a eutrophic north-central Florida lake," *Aquatic Botany*, vol. 10, pp. 1–32, 1981.
- [39] E. A. Pérez, J. A. Coetzee, T. R. Téllez, and M. P. Hill, "A first report of water hyacinth (*Eichhornia crassipes*) soil seed banks in South Africa," *South Afr. J. Botany*, vol. 77, pp. 795–800, Aug. 2011.
- [40] D. Eva, A. Pérez, and D. T. R. Téllez, "Reproducción sexual del jacinto de agua (*Eichhornia crassipes*): Germinación, anatomía y banco de semillas," Ph.D. dissertation, Departamento de Biología Vegetal, Ecología y Ciencias de la Tierra. Grupo de Investigación en Biología de la Conservación, Universidad de Extremadura, Badajoz, Spain, 2012.
- [41] E. C. Rodríguez-Garlito, A. Paz-Gallardo, and A. Plaza, "Automatic detection of aquatic weeds: A case study in the Guadiana River, Spain," *IEEE J. Sel. Topics Appl. Earth Observ. Remote Sens.*, vol. 15, pp. 8567–8585, Sep. 2022.
- [42] K. H. Thamaga and T. Dube, "Remote sensing of invasive water hyacinth (*Eichhornia crassipes*): A review on applications and challenges," *Remote Sens. Appl.: Soc. Environ.*, vol. 10, pp. 36–46, 2018.
- [43] E. L. Hestir et al., "Identification of invasive vegetation using hyperspectral remote sensing in the California delta ecosystem," *Remote Sens. Environ.*, vol. 112, pp. 4034–4047, 2008.
- [44] A. Plaza, J. Plaza, A. Paz, and S. Sánchez, "Parallel hyperspectral image and signal processing [applications corner]," *IEEE Signal Process. Mag.*, vol. 28, no. 3, pp. 119–126, May 2011.
- [45] C. Joshi, J. D. Leeuw, and I. C. V. Duren, "Remote sensing and GIS applications for mapping and spatial modelling of invasive species," in *Proc. Int. Soc. Photogrammetry Remote Sens.*, 2004, pp. 669–677.
- [46] M. G. Dersseh et al., "Spatial and temporal dynamics of water hyacinth and its linkage with lake-level fluctuation: Lake Tana, a sub-humid region of the Ethiopian Highlands," *Water*, vol. 12, Jul. 2020, Art. no. 1435.
- [47] R. Gerardo and I. P. D. Lima, "Assessing the potential of Sentinel-2 data for tracking invasive water hyacinth in a river branch," *J. Appl. Remote Sens.*, vol. 16, 2022, Art. no. 014511.
- [48] P. Ghamisi, J. Plaza, Y. Chen, J. Li, and A. J. Plaza, "Advanced spectral classifiers for hyperspectral images: A review," *IEEE Geosci. Remote Sens. Mag.*, vol. 5, no. 1, pp. 8–32, Mar. 2017.
- [49] A. Datta et al., "Monitoring the spread of water hyacinth (*Pontederia crassipes*): Challenges and future developments," *Front. Ecol. Evol.*, vol. 9, Jan. 2021, Art. no. 631338.
- [50] N. Janssens, L. Schreyers, L. Biermann, M. V. D. Ploeg, T. K. L. Bui, and T. V. Emmerik, "Rivers running green: Water hyacinth invasion monitored from space," *Environ. Res. Lett.*, vol. 17, 2022, Art. no. 044069.
- [51] C. Ade, S. Khanna, M. Lay, S. L. Ustin, and E. L. Hestir, "Genus-level mapping of invasive floating aquatic vegetation using Sentinel-2 satellite remote sensing," *Remote Sens.*, vol. 14, Jun. 2022, Art. no. 3013.
- [52] K. H. Thamaga and T. Dube, "Understanding seasonal dynamics of invasive water hyacinth (*Eichhornia crassipes*) in the greater Letaba river system using Sentinel-2 satellite data," *GIScience Remote Sens.*, vol. 56, pp. 1355–1377, Nov. 2019.
- [53] G. Singh, C. Reynolds, M. Byrne, and B. Rosman, "A remote sensing method to monitor water, aquatic vegetation, and invasive water hyacinth at national extents," *Remote Sens.*, vol. 12, Dec. 2020, Art. no. 4021.
- [54] I. Goodfellow, Y. Bengio, and A. Courville, *Deep Learning*. Cambridge, MA, USA: MIT Press, 2016.
- [55] M. E. Paoletti, J. M. Haut, J. Plaza, and A. Plaza, "Deep learning classifiers for hyperspectral imaging: A review," *ISPRS J. Photogrammetry Remote Sens.*, vol. 158, pp. 279–317, 2019.
- [56] E. C. Rodríguez-Garlito and A. Paz-Gallardo, "Efficiently mapping large areas of olive trees using drones in Extremadura, Spain," *IEEE J. Miniaturization Air Space Syst.*, vol. 2, no. 3, pp. 148–156, Sep. 2021.
- [57] SentinelHub. Accessed: Nov. 30, 2022. [Online]. Available: <https://www.sentinel-hub.com>
- [58] S. M. Sharpe, A. W. Schumann, J. Yu, and N. S. Boyd, "Vegetation detection and discrimination within vegetable plasticulture row-middles using a convolutional neural network," *Precis. Agriculture*, vol. 21, pp. 264–277, Apr. 2020.
- [59] N. Flood, F. Watson, and L. Collett, "Using a U-Net convolutional neural network to map woody vegetation extent from high resolution satellite imagery across Queensland, Australia," *Int. J. Appl. Earth Observ. Geoinformation*, vol. 82, Oct. 2019, Art. no. 101897.
- [60] U. Bayr and O. Puschmann, "Automatic detection of woody vegetation in repeat landscape photographs using a convolutional neural network," *Ecological Inform.*, vol. 50, pp. 220–233, Mar. 2019.
- [61] Y. Jiang, S. M. Asce, Y. Bai, F. Asce, and S. Han, "Determining ground elevations covered by vegetation on construction sites using drone-based orthoimage and convolutional neural network," *J. Comput. Civil Eng.*, vol. 34, no. 6, 2020.
- [62] T. Kattenborn, J. Leitloff, F. Schiefer, and S. Hinz, "Review on convolutional neural networks (CNN) in vegetation remote sensing," *ISPRS J. Photogrammetry Remote Sens.*, vol. 173, pp. 24–49, Mar. 2021.
- [63] M. E. Paoletti, J. M. Haut, J. Plaza, and A. Plaza, "A new deep convolutional neural network for fast hyperspectral image classification," *ISPRS J. Photogrammetry Remote Sens.*, vol. 145, pp. 120–147, 2018.

- [64] Y. Lecun, Y. Bengio, and G. Hinton, "Deep learning," *Nature*, vol. 521, pp. 436–444, 2015.
- [65] Plan nacional de ortofotografía aérea. Accessed: Nov. 30, 2022. [Online]. Available: <https://pnoa.ign.es>
- [66] M. Govender, K. Chetty, and H. Bulcock, "A review of hyperspectral remote sensing and its application in vegetation and water resource studies," *Water SA*, vol. 33, pp. 145–151, 2007.



Elena C. Rodríguez-Garlito (Student Member, IEEE) received the B.Sc. degree in civil engineering and the M.Sc. degree in geographical information systems and RS, in 2013 and 2014, respectively, from the University of Extremadura, Cáceres, Spain, where she is currently working toward the Ph.D. degree with predoctoral contracts for the training of doctors in public RD centers belonging to the Extremadura System of Science, Technology, and Innovation and working on the development of machine/deep learning algorithms for invasive aquatic plants detection

and natural resources management, using remote sensing data from satellites and drones.

She is currently a Member of Hyperspectral Computing Laboratory, Department of Technology of Computers and Communications, University of Extremadura. Her research interests include GIS, remote sensing, and machine/deep learning.



Abel Paz-Gallardo received the B.S. degree in computer engineering and the M.Sc. and Ph.D. degrees in computer science from the University of Extremadura, Cáceres, Spain, in 2007, 2009, and 2011, respectively.

During 2006 and 2007, he was a Research Assistant with Computer Architecture Department, University of Extremadura, where he became an Associate Professor in 2008. At the same time, he started working with Minimally Invasive Surgery Center Jesús Usón, Cáceres. In 2010, he started working with Bull Spain

S.A., to deploy at CETA-Ciemat, Trujillo, Spain, the biggest GPGPU Cluster in Spain and one of the biggest ones in Europe. Since November 2010, he has been an Associate Professor with Computer Architecture Department. From October 2011 to July 2018, he was an IT Manager (CIO) of CETA-Ciemat, where he achieved the GPU Research Centre mention from NVIDIA as Principal Investigator. Since July 2018, he has been a Chief Information Officer of Greenfield Technologies, a precision agriculture company that provides recommendations to farmers, through the use of different innovative technologies (such as drones, satellites, sensors, and artificial intelligence) and applied research. He has participated in more than 40 international projects and has authored or coauthored more than 40 publications, including 16 journal citation report (JCR) papers (most of them published by IEEE journals) and more than 30 peer-reviewed international conference papers. His research interests include remotely sensed hyperspectral image analysis, signal processing, and efficient implementations of large-scale scientific problems on high-performance computing architectures, such as clusters and graphical processing units.

Prof. Paz-Gallardo was the recipient of the IEEE Signal Processing Magazine Best Column Award Paper from the IEEE Signal Processing Society in November 2015.



Antonio Plaza (Fellow, IEEE) received the M.Sc. and Ph.D. degrees in computer engineering from the University of Extremadura, Cáceres, Spain, in 1999 and 2002, respectively.

He is currently a Full Professor and the Head of Hyperspectral Computing Laboratory, Department of Technology of Computers and Communications, University of Extremadura. He has authored or coauthored more than 700 publications in the field of his research interests, including 381 JCR journal papers, 24 book chapters, and 330 peer-reviewed conference

proceeding papers, and also guest edited ten special issues on hyperspectral remote sensing for different journals. His research interests include hyperspectral data processing and parallel computing of remote sensing data.

Prof. Plaza was the recipient of the recognition of Best Reviewers of *IEEE Geoscience and Remote Sensing Letters* (in 2009), the recognition of Best Reviewers of the IEEE TRANSACTIONS ON GEOSCIENCE AND REMOTE SENSING (in 2010) for which he was an Associate Editor (in 2007–2012), the Best Column Award of the IEEE Signal Processing Magazine in 2015, the 2013 Best Paper Award of the JSTARS journal, the most highly cited paper (2005–2010) in the *Journal of Parallel and Distributed Computing*, and best paper awards at the IEEE Workshop on Hyperspectral Image and Signal Processing: Evolution in Remote Sensing, the IEEE International Conference on Space Technology, and the IEEE Symposium on Signal Processing and Information Technology. He is also an Associate Editor for IEEE ACCESS (receiving the recognition of Outstanding Associate Editor for the journal in 2017) and was also Member of the Editorial Board of the *IEEE Geoscience and Remote Sensing Newsletter* (2011–2012) and *IEEE Geoscience and Remote Sensing Magazine* (2013). He was a Member of the steering committee of the IEEE JOURNAL OF SELECTED TOPICS IN APPLIED EARTH OBSERVATIONS AND REMOTE SENSING (JSTARS). He was the Director of Education Activities for the IEEE Geoscience and Remote Sensing Society (GRSS) (in 2011–2012), and the President of the Spanish Chapter of IEEE GRSS (in 2012–2016). He is a Chair of the Publications Awards Committee of IEEE GRSS and a Vice-Chair of the Fellow Evaluations Committee of IEEE GRSS. He has reviewed more than 500 manuscripts for more than 50 different journals. He was the Editor-in-Chief for IEEE TRANSACTIONS ON GEOSCIENCE AND REMOTE SENSING for five years (2013–2017) and IEEE JOURNAL ON MINIATURIZATION FOR AIR AND SPACE SYSTEMS (2019–2020). He has been included in the 2018–2021 Highly Cited Researchers List (Clarivate Analytics). He is a Fellow of IEEE "for contributions to hyperspectral data processing and parallel computing of Earth observation data" and a Member of Academia Europaea, The Academy of Europe.

Mapping Invasive Aquatic Plants in Sentinel-2 Images Using Convolutional Neural Networks Trained With Spectral Indices

Escuela Politécnica
Av. de la Universidad, S/N, 10003
Teléfono: 0034927257000. Ext. 51662
correo electrónico: apazgal, aplaza @unex.es
Cáceres, España

Dr. Abel Francisco Paz Gallardo y Dr. Antonio Plaza Miguel, como directores de la Tesis Doctoral titulada “Desarrollo de nuevos métodos y algoritmos de análisis y clasificación de imágenes multiespectrales orientadas a la gestión y monitorización de plantas acuáticas invasoras”, certificamos el factor de impacto y la categorización de la siguiente publicación incluida en la Tesis Doctoral. Del mismo modo, se especifica la aportación de la doctoranda. Para cualquier otra información o aclaración, por favor, no duden en contactar con nosotros.

Titulo de la publicación: Mapping Invasive Aquatic Plants in Sentinel-2 Images Using Convolutional Neural Networks Trained With Spectral Indices

Autores: **Elena C. Rodríguez-Garlito**, Abel Paz-Gallardo y Antonio Plaza

Revista: IEEE Journal of Selected Topics in Applied Earth Observations and Remote Sensing

Otros datos: vol 16, págs 2889-2899, año 2023

DOI: 10.1109/JSTARS.2023.3257142

Factor de impacto 2022: 5.5

Abstract: Multispectral images collected by the European Space Agency’s Sentinel-2 satellite offer a powerful resource for accurately and efficiently mapping areas affected by the distribution of invasive aquatic plants. In this work, we use different spectral indices to detect invasive aquatic plants in the Guadiana river, Spain. Our methodology uses a convolutional neural network (CNN) as the baseline classifier and trains it using spectral indices calculated using different Sentinel-2 band combinations. Specifically, we consider the following spectral indices: With two bands, we calculate the normalized difference vegetation index, normalized difference water index, and normalized difference infrared index. With three bands, we calculate the red–green–blue composite and the floating algae index. Finally, we also use four bands to calculate the bare soil index. In our results, we observed that CNNs can better map invasive aquatic plants in the considered case study when trained intelligently (using spectral indices) as compared to using all spectral bands provided by the Sentinel-2 instrument.

Contribución de la doctoranda: Planteamiento de la hipótesis, conceptualización, búsqueda bibliográfica, metodología, análisis y discusión de resultados, elaboración de tablas y figuras, escritura del manuscrito borrador y redacción de la revisión.

Mapping Invasive Aquatic Plants in Sentinel-2 Images Using Convolutional Neural Networks Trained With Spectral Indices

Elena Cristina Rodríguez-Garlito ¹, Student Member, IEEE, Abel Paz-Gallardo ¹,
and Antonio Plaza ¹, Fellow, IEEE

Abstract—Multispectral images collected by the European Space Agency’s Sentinel-2 satellite offer a powerful resource for accurately and efficiently mapping areas affected by the distribution of invasive aquatic plants. In this work, we use different spectral indices to detect invasive aquatic plants in the Guadiana river, Spain. Our methodology uses a convolutional neural network (CNN) as the baseline classifier and trains it using spectral indices calculated using different Sentinel-2 band combinations. Specifically, we consider the following spectral indices: With two bands, we calculate the normalized difference vegetation index, normalized difference water index, and normalized difference infrared index. With three bands, we calculate the red–green–blue composite and the floating algae index. Finally, we also use four bands to calculate the bare soil index. In our results, we observed that CNNs can better map invasive aquatic plants in the considered case study when trained intelligently (using spectral indices) as compared to using all spectral bands provided by the Sentinel-2 instrument.

Index Terms—Convolutional neural networks (CNNs), invasive aquatic plants, remote sensing, Sentinel-2 (S2), spectral indices.

I. INTRODUCTION

REMOTE sensing has been widely used for water support management in recent years. For instance, the work developed in [1] supported water quality management, and monitored the spatial-temporal distribution of water turbidity. In [2], coastal ecosystem health status was evaluated. Other studies, such as [3] and [4], mapped flooded areas. In [5], polar sea ice leads in open

water were mapped. Water body extraction was carried out in [6], and permafrost areas were mapped in [7]. Many studies have been focused on mapping vegetation, i.e., estimating vegetation regions [8], monitoring vegetation growth [9] and vegetation changes [10], predicting the location of algal blooms [11], and discriminating between different macrophyte species [12], among other applications.

A. Using Spectral Indices to Detect Invasive Aquatic Plants

Spectral indices exhibit a great potential for effectively mapping ecosystems affected by invasive aquatic plants [13]. To detect *Spartina alterniflora* in Sentinel-2 images [14], several indices have been used, including the normalized difference vegetation index (NDVI), enhanced vegetation index (EVI), difference vegetation index (DVI), green difference vegetation index (gDVI), green NDVI (gNDVI), soil-adjusted vegetation index (SAVI), and a phenological vegetation index (PVI). The work in [15] combined vegetation indices (e.g., NDVI) and water indices such as the normalized difference water index (NDWI) to detect *Eichhornia crassipes* (water hyacinth) in Sentinel-2 images. The work in [16] also focused on the detection of water hyacinth by calculating fractional vegetation cover (FVC) in Sentinel-2 images using SAVI.

Multispectral images acquired by unmanned aerial vehicles were used in [17] to determine NDVI, enhanced normalized difference vegetation index (ENDVI), normalized difference red edge index (NDREI), normalized green-red difference index (NGRDI), and green normalized difference vegetation index (GNDVI). Landsat images were used in [18] to calculate NDVI for water hyacinth detection. Other works used spectral indices and spatial autocorrelation analysis to detect algal blooms in Sentinel-2 and Landsat images [19], and also used MODIS images to calculate the floating algae index (FAI).

In order to exploit the information provided by spectral indices and take advantage of state-of-the-art machine learning classifiers, several authors have combined both techniques in their studies. For instance, the authors in [20] used Landsat-8 and Sentinel-2 data to develop a hierarchical classifier based on three steps for water hyacinth detection. The steps can be summarized as follows: 1) water detection with a modified normalized difference water index (MNDWI); 2) vegetation detection with NDVI; and 3) detection of water hyacinth with a

Manuscript received 18 December 2022; revised 19 February 2023; accepted 9 March 2023. Date of publication 14 March 2023; date of current version 29 March 2023. This work was supported in part by the European Social Fund (Resolución de 10 de mayo de 2017, de la Secretaría General de Ciencia, Tecnología e Innovación, por la que se resuelve la convocatoria de ayudas para la financiación de contratos predoctorales para formación de Doctores en los centros públicos de I+D pertenecientes al Sistema Extremeño de Ciencia, Tecnología e Innovación en el ejercicio 2017; expediente PD16001); in part by the Consejería de Economía, Ciencia y Agenda Digital of the Junta de Extremadura and the European Regional Development Fund (ERDF) of the European Union under Grant GR21040; in part by ayuda PID2019-110315RB-I00 del proyecto “Desarrollo de técnicas de aprendizaje profundo para la optimización de la infraestructura de supercomputación y de aplicaciones de imagen hiperespectral” (APRISA), financed by MCIN/AEI/10.13039/501100011033; and in part by the European Union’s Horizon 2020 Research and Innovation Program under Grant 734541 (EOXPOSURE). (Corresponding author: Antonio Plaza.)

The authors are with the Hyperspectral Computing Laboratory, Department of Technology of Computers and Communications, Escuela Politécnica, University of Extremadura, 10003 Cáceres, Spain (e-mail: elenacristinarg@unex.es; apazgal@unex.es; aplaza@unex.es).

Digital Object Identifier 10.1109/JSTARS.2023.3257142

random forest (RF) classifier. The authors in [21] discriminated between water hyacinth and water primrose in Sentinel-2 images by using RF and nine spectral vegetation and water indices (NDVI, NDAVI, WAVI, SAVI, NDVIRE2, NDVIRE3, NDWI, NDII, and MNDWI). The authors in [22] mapped *Spartina alterniflora* using Sentinel-2 and Sentinel-1 data, SAR vegetation indices, and seven spectral indices: NDVI, EVI, NDWI, land surface water index, and automated water extraction index. To the best of our knowledge, no studies have combined deep learning classifiers and spectral indices for detection and mapping of aquatic invasive plants.

B. Mapping Invasive Aquatic Plants Using CNNs

One of the species that is considered to be most invasive is the water hyacinth. This plant tends to cover the river surface due to its tapestry-like distribution. Great efforts have been made to control the spread of this plant, with negative effects on biodiversity, the environment, and the economy [23]. In order to successfully manage these species, current strategies aim at their removal when present on the water surface to prevent their dispersal [24].

Our previous studies began a new line of research were invasive aquatic plants in the Guadiana river, the second longest river in Spain, were mapped by using remote sensing and deep learning techniques. In order to facilitate mapping, monitoring, and control of the invasive aquatic plant distribution in the Guadiana river, our previous work first focused on automatic detection of the plant using all the spectral bands provided by the Sentinel-2 satellite. In [23], a quantitative and qualitative comparison of different machine/deep learning algorithms was carried out, determining that convolutional neural networks (CNNs) were effective for mapping purposes. This conclusion is in agreement with other works, which concluded that CNNs are successful for mapping vegetation species in remotely sensed data [25], [26], [27], [28], [29], [30], [31], [32].

In a subsequent work [33], we used CNNs as a baseline to monitor the spatio-temporal distribution of water hyacinth using sparse training samples collected from only four images (out of a total of 62 images available in the analyzed two-year time series) independently of the phenological stage. To study the dynamics of the spread of invasive plants over a two-year period, a methodology for mapping the most frequent areas of water hyacinth accumulation was developed.

C. Motivation and Innovative Contributions of This Work

The goal of this article is to provide a better training mechanism for CNNs to identify invasive aquatic plants. In case of methods based on spectral indices to detect invasive aquatic plants, they use combinations of spectral bands to highlight pixels of the multispectral (MS) images with specific land-covers. However, when vegetation indices (such as NDVI) are used, invasive plants and other types of vegetation may coincide in the same thresholds (as it actually happens in the two test areas considered in our work). This requires manual segmentation to differentiate between invasive and noninvasive plants. Obviously, this entails a more costly and less automatic process.

Therefore, in this study, the invasive aquatic plant detection task consists of an automatic process by using deep learning techniques. Moreover, this work takes advantage of band combinations that are conducive to highlighting vegetation in the water. This is accomplished by extracting suitable training samples for the model. In summary, the main contributions of this work can be summarized as follows.

- 1) We introduce a new methodology for the automatic detection of invasive aquatic plants that simplifies the spectral complexity of the images acquired by the Sentinel-2 satellite. Specifically, we use spectral indices to improve the training process of CNNs and determine if the obtained results (calculated using a reduced set of carefully selected Sentinel-2 bands) can improve the results obtained using all available bands. Our approach uses remote sensing, geographical information systems (GIS) techniques, and a deep learning model. An additional advantage of using fewer spectral bands is to reduce the amount of data required for image downloading, preprocessing, and processing.
- 2) We test our new automatic detection strategy in two areas of the Guadiana river, Spain, which are heavily affected by the presence of invasive aquatic plants. Our methodology is tested in a quantitative and qualitative way. The first area is affected by Mexican water lily, while the second one is affected by water hyacinth.
- 3) We conduct a comprehensive comparison of the performance of the CNN model with other classical machine learning classifier, the RF, that was used as a standard in other studies.

II. METHODOLOGY

Fig. 1 graphically illustrates the workflow adopted in this work. First, multispectral images over the Guadiana river are collected by the Sentinel-2 satellite. Next, a preprocessing of these images is carried out where spectral indices are calculated. Region of interest (ROI) extraction and management of nodata values are also carried out as described in [23]. Then, automatic detection of invasive plants is carried out using CNNs trained with different spectral indices. Finally, the outputs are evaluated by comparing the results with a ground truth image, generated according to the procedure in [23], calculating different accuracy metrics.

A. Study Area

Two sections of the Guadiana river affected by invasive aquatic plants have been selected for experiments (see Fig. 2). The first ROI corresponds to an area affected by *Eichhornia crassipes*, also known as water hyacinth, close to the city of Mérida (ROI_ME). There, an invasive plant control barrier for mechanical removal of these plants has been installed. The second ROI (ROI_BA) is a section of the river affected by yellow water lily (also known as *Nymphaea mexicana*). This area crosses the city of Badajoz, in the SW of Extremadura region, Spain. The main characteristics of these ROIs are given in Table I.

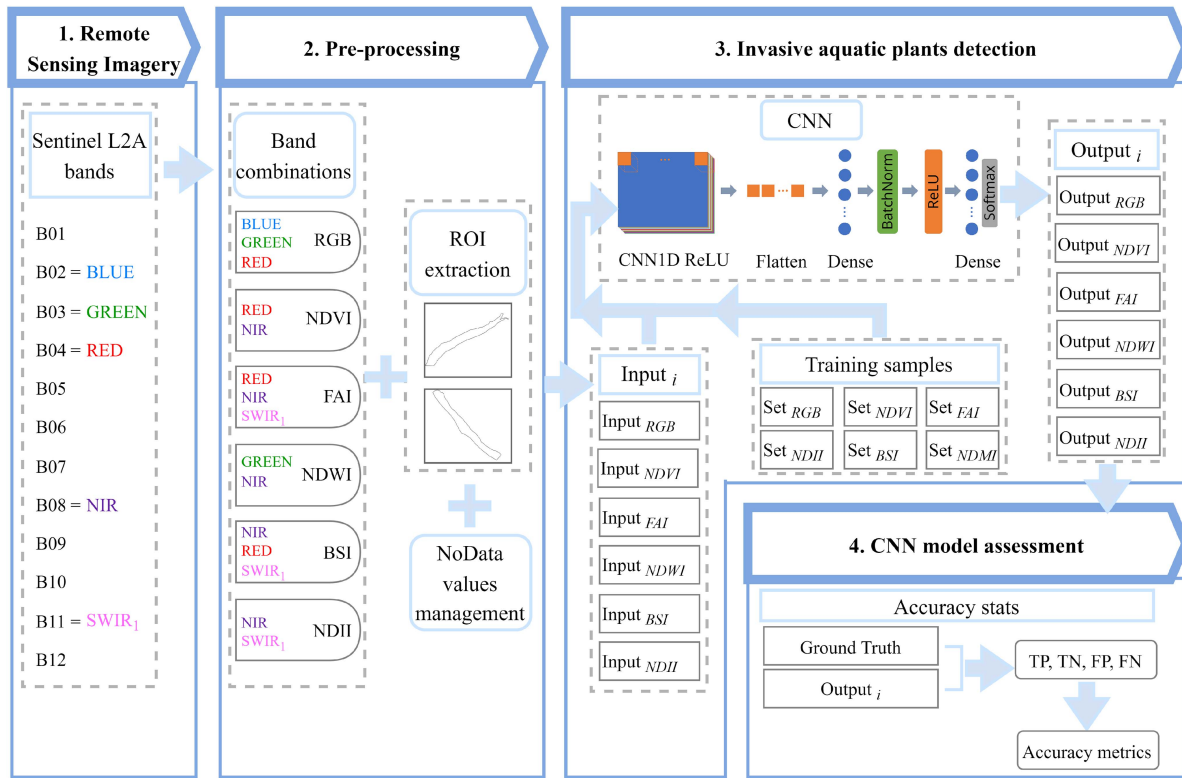


Fig. 1. Workflow of the procedure for mapping invasive aquatic plants in the Guadiana river. The CNN architecture used is also displayed.

TABLE I
CHARACTERISTICS OF THE TWO SELECTED ROIS AND THE CONSIDERED
MULTISPECTRAL DATASETS

	Mérida	Badajoz
Latitude	38° 50' - 38° 51'N	38° 51' - 38° 53'N
Longitude	6° 19' - 6° 18' W	7° 01' - 6° 58' W
Study area	45 ha	192 ha
Datasets dimensions	189 x 173 pixels	451 x 236 pixels
Type of RS images	Sentinel - 2 Level-2A (S2L2A) products	
Projection	UTM/WGS84	
Satellite revisit time	5 days	
Spectral resolution	12 bands (ranging from 442.7 nm to 2202.4 nm)	
Spatial resolution	10 m, 20 m or 60 m	
Format	8 bit	
Sentinel-2 datasets	14 images	

B. Remotely Sensed Imagery

Sentinel-2 images are open-access multispectral datasets provided by ESA's satellite, as part of the Copernicus programme. Level-1 C (S2L1C) and Level-2 A (S2L2A) products are offered. The data are collected in a discrete number of bands (13 or 12 spectral bands, respectively) with different levels of spatial resolution (from 10 to 60 m per pixel). Table II shows

the details of the 13 spectral bands available and their main applications. Sentinel-2 has successfully contributed to many studies for monitoring aquatic invasive plants, as indicated in Section I-A. In this work, S2L2A products with atmospheric correction are used. Moreover, the image datasets are acquired from SentinelHub [34]. Here, six different band combinations have been used as CNN inputs (details are given in Section II-C). In addition, to compare results, we also consider all Sentinel-2 bands as input to evaluate if the CNNs trained using only spectral indices (resulting from specific band combinations) can outperform the results obtained using all available bands. Table I describes the main characteristics of the considered multispectral datasets.

C. Band Compositions and Spectral Indices

In the following, we describe the spectral band combinations and the spectral indices used in this work. The Sentinel-2 band names (according to Table II) are also specified.

1) *RGB*: Composite of three bands: Red (B04), green (B03), and blue (B02), also called natural color band combination. It allows to display land covers in true color. The values range from 0 to 255 and they are normalized in this study to a range from 0 to 1.

2) *NDVI*: A well-known index [35] commonly used for green vegetation quantification. Equation (1) defines this index which is calculated by considering two bands: Red (B04) and near-infrared, hereinafter NIR (B08). The values are normalized

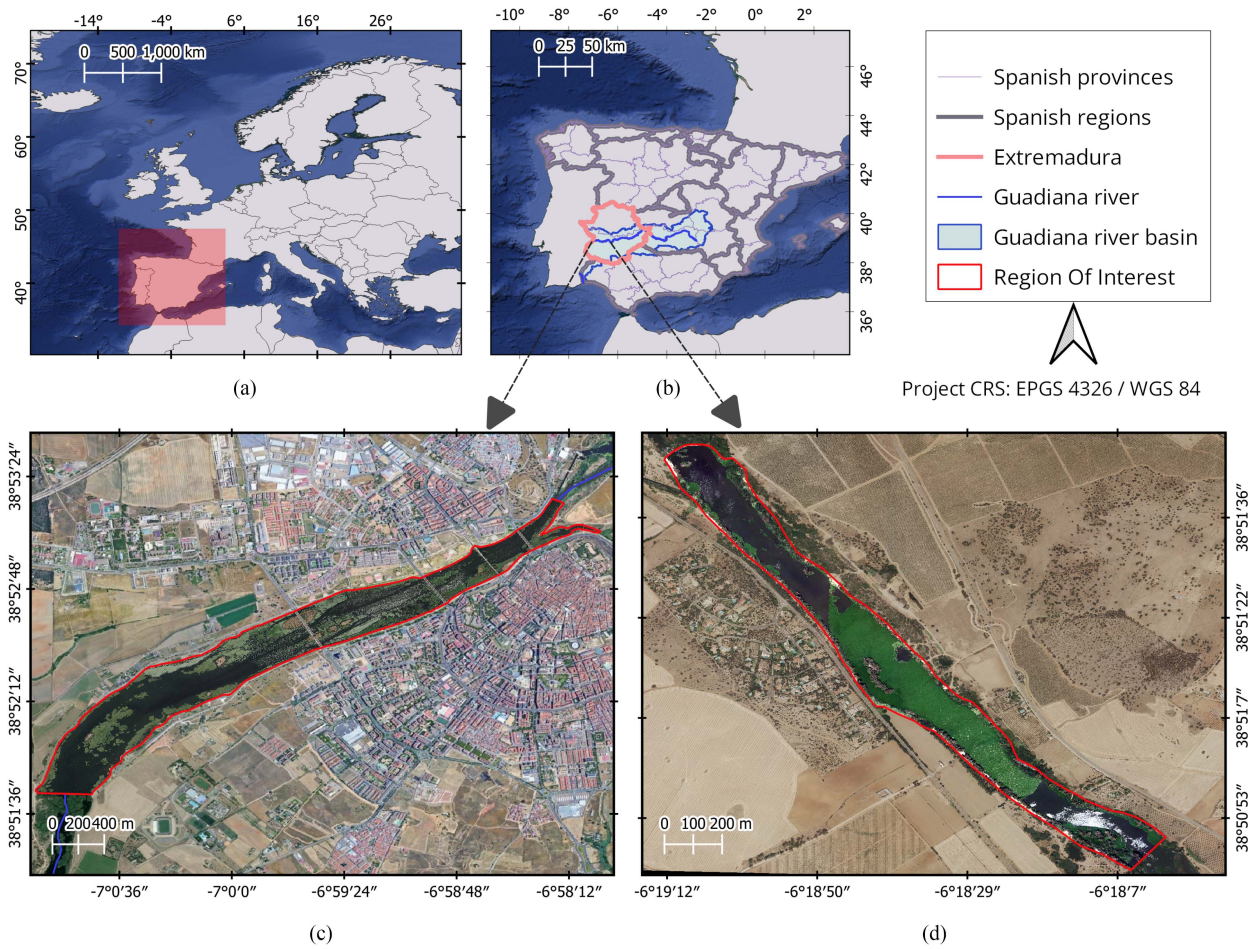


Fig. 2. (a) Geographical location of Spain. (b) Geographical location of the region of Extremadura, the Guadiana river and the Guadiana river basin. (c) Zoom of a high resolution image including an area affected by yellow water lily in the city of Badajoz. (d) Zoom of a high resolution image including an area affected by water hyacinth, close to the city of Mérida.

TABLE II
DESCRIPTION OF SENTINEL-2 BANDS

Band name	B01	B02	B03	B04	B05	B06	B07	B08	B8A	B09	B10	B11	B12
Resolution (meters)	60	10	10	10	20	20	20	10	20	60	60	20	20
Bandwidth (nanometers)	442.7	492.4	559.8	664.6	704.1	740.5	782.8	832.8	864.7	945.1	1373.5	1613.7	2202.4
Application	Coastal aerosol	Blue	Green	Red	Vegetation red edge ₁	Vegetation red edge ₂	Vegetation red edge ₃	NIR	Narrow NIR	Water vapour	Cirrus	SWIR ₁	SWIR ₂

to a range from -1 to 1 .

$$NDVI = \frac{NIR - Red}{NIR + Red}. \quad (1)$$

3) *FAI*: Introduced in [36] to detect vegetation on the surface of oceans. It is less sensitive to atmospheric effects than NDVI and EVI. Equation (2) shows the definition of the index for Sentinel-2 images, where three bands are considered: Red (B04), NIR (B08), and SWIR₁ (B11). Its values are normalized to a

range from 0 to 1 .

$$FAI = \left(NIR - \left(Red + (SWIR_1 - Red) \times \left(\frac{(\lambda_{NIR} - \lambda_{Red})}{(\lambda_{SWIR_1} - \lambda_{Red})} \right) \right) \right) \quad (2)$$

where $\lambda_{NIR} = 832.8$, $\lambda_{Red} = 664.6$, and $\lambda_{SWIR_1} = 1613.7$.

4) *NDWI*: It combines two bands: green (B03) and NIR (B08). It was proposed in [37] for determining vegetation water status. The index is defined in (3) and its values are normalized

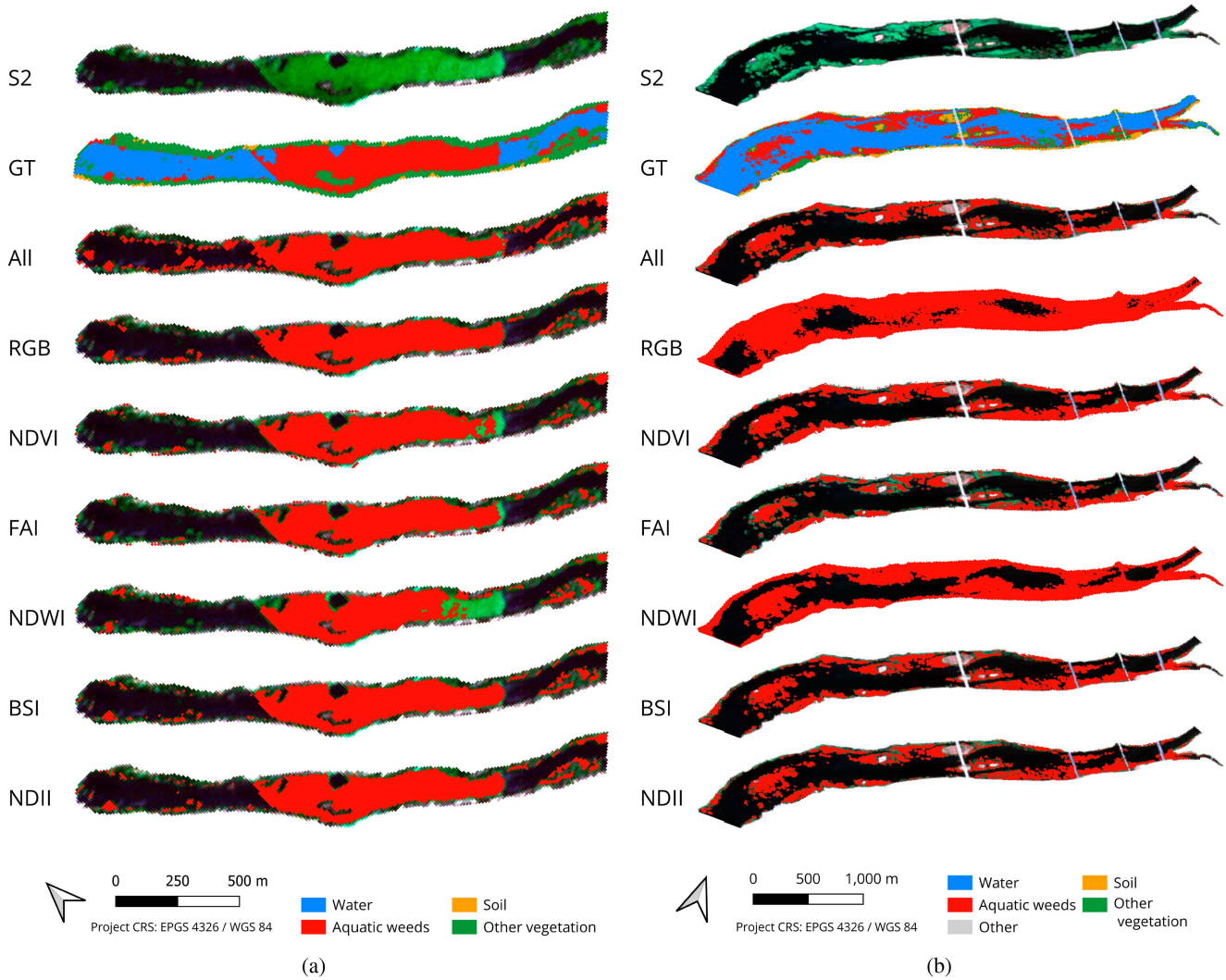


Fig. 3. Invasive aquatic plants detection results using different indices with the CNN: (a) Badajoz case. (b) Mérida case.

to a range from -1 to 1

$$NDWI = \frac{\text{Green} - \text{NIR}}{\text{Green} + \text{NIR}}. \quad (3)$$

5) *BSI*: Introduced in [38] to discriminate bare soil and fallow land from vegetation and other land cover classes by combining four bands: $SWIR_1$ (B11) and red (B04) bands (which determine the soil mineral composition), while NIR (B08) and blue (B02) determine the presence of vegetation. Their values are normalized to range from -1 to 1 . This index is defined as follows:

$$BSI = \frac{(\text{SWIR}_1 + \text{Red}) - (\text{NIR} + \text{Blue})}{(\text{SWIR}_1 + \text{Red}) + (\text{NIR} + \text{Blue})}. \quad (4)$$

6) *NDII*: Developed by [39] as infrared index and later used at [40] as NDII. It uses two spectral bands: NIR (B08) and $SWIR_1$ (B11). This index can also be seen as a normalized version of NDMI when using Sentinel-2 B08 (or B8A) and B11 bands [41]. NDII (or NDMI) gives information on the changes in vegetation water content. Leaf internal structure and leaf dry matter content

affect NIR reflectance, while the $SWIR_1$ band gives information on changes in the water content of the vegetation, as well as the structure of the spongy mesophyll in vegetation canopies. Its values are scaled to a range from -1 to 1 . The index is defined as follows:

$$NDII = \frac{\text{NIR} - \text{SWIR}_1}{\text{NIR} + \text{SWIR}_1}. \quad (5)$$

Table III summarizes the main characteristics of the set of images considered in this study, where spectral indices are used to train the CNN adopted in our work for mapping purposes. It should be noted that the resulting raster images after applying spectral indices have 10 m of spatial resolution. To deal with the different spatial resolutions between the spectral bands involved in the calculation of the indices, we sampled every band to a 10 m resolution. In this way, 20 -m resolution bands (60 m would be the same) are obtained by repeating their pixel values resampling them (without modifying their values) to 10 m resolution. Since there is at least one 10 -m band in every index, all the pixels offer

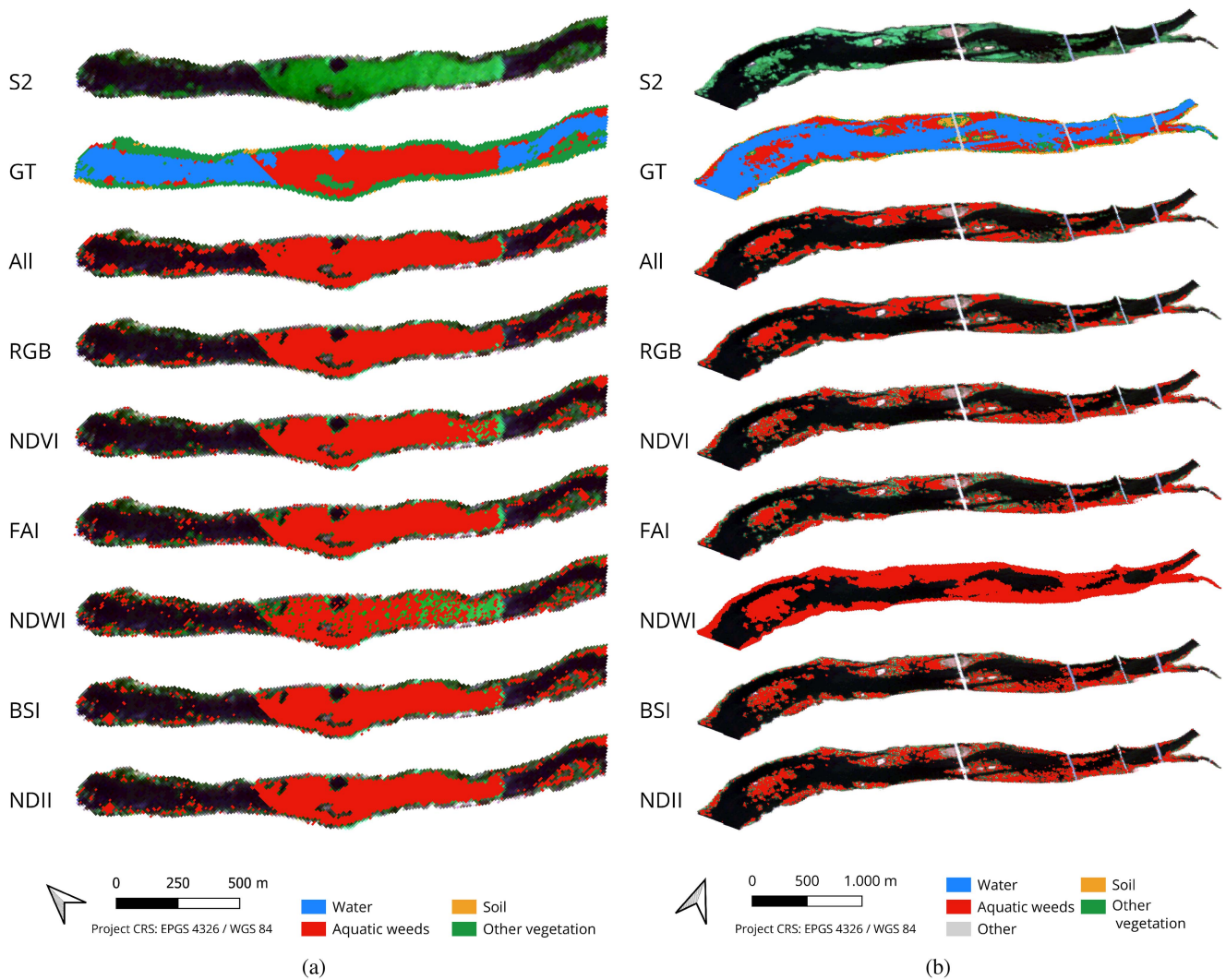


Fig. 4. Invasive aquatic plants detection results using different indices with the RF algorithm: (a) Badajoz case. (b) Mérida case.

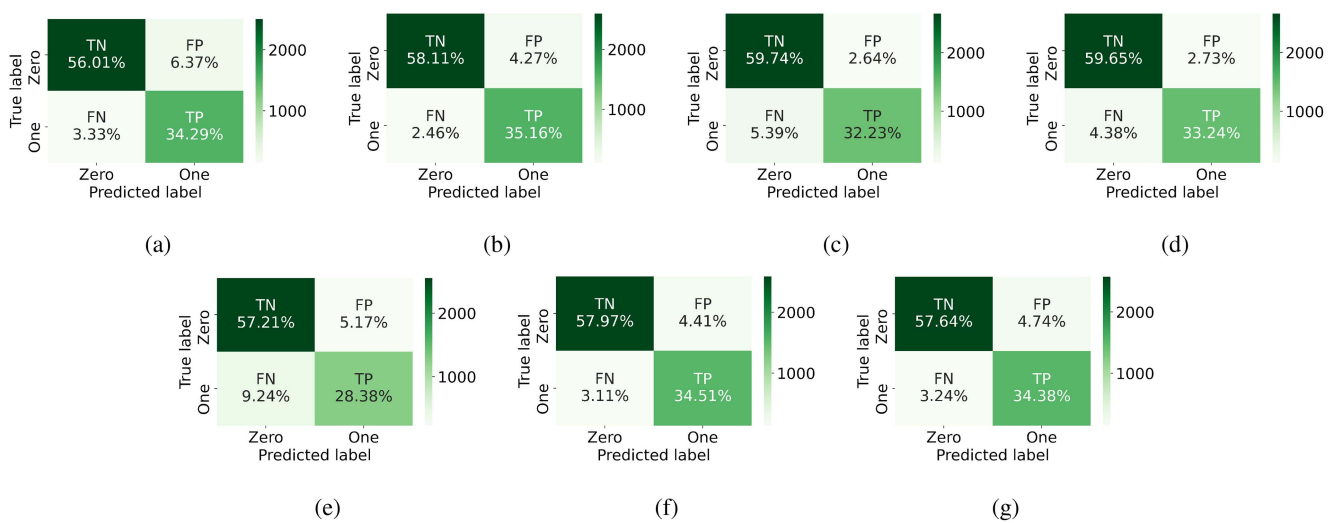


Fig. 5. Confusion matrices for ROI_ME. (a) All bands. (b) RGB. (c) NDVI. (d) FAI. (e) NDWI. (f) BSI. (g) NDII.

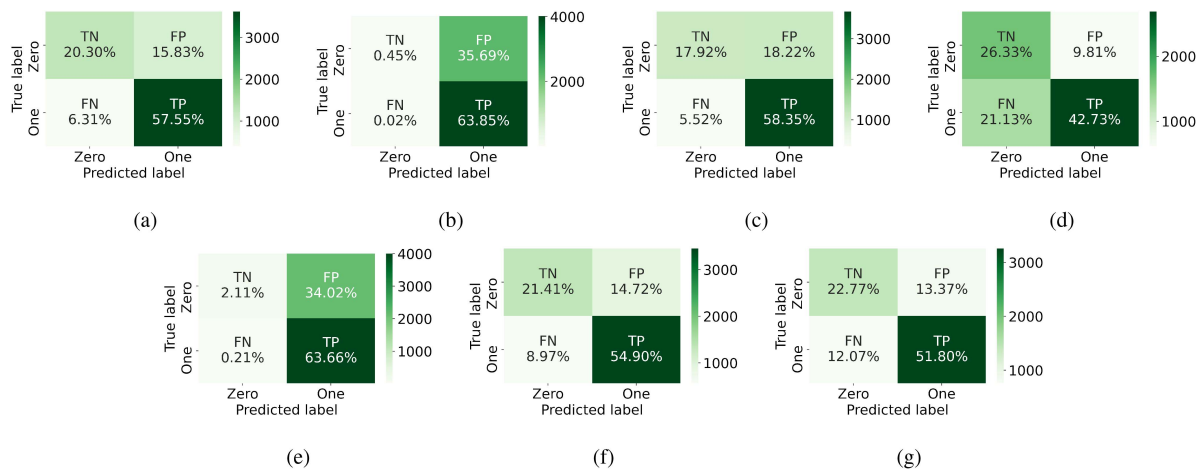


Fig. 6. Confusion matrices for ROI_BA. (a) All bands. (b) RGB. (c) NDVI. (d) FAI. (e) NDWI. (f) BSI. (g) NDII.

TABLE III
INPUTS TO THE CNN USED FOR MAPPING PURPOSES

Index	Number of spectral bands	Spatial resolution (m)
RGB	3 bands (Red, Green, Blue)	10
NDVI	2 bands (Green, NIR)	10
FAI	3 bands (Red, NIR, SWIR ₁)	10
NDWI	2 bands (Green, NIR)	10
BSI	4 bands (SWIR ₁ , Red, NIR, Blue)	10
NDII	2 bands (NIR, SWIR ₁)	10

different values when calculating the index, resulting in a final 10-m resolution raster image.

D. Preprocessing

After downloading the Sentinel-2 images, spectral indices are calculated for the pixels used for training as described in Section II-C, and the NoData values are managed as explained in [23], i.e., normalizing the pixel values between 0 and 1 and changing the format from 8 bits to 32 bits. The CNN architecture and the training process are explained in the following section.

E. Detection

As indicated above, the main novelty of our work is that the detection of aquatic plants is performed using a CNN trained using spectral indices. In the following, we describe the CNN architecture and the training process.

1) *CNN Architecture*: For aquatic weeds detection on pre-processed Sentinel-2 images, a CNN model was developed and trained with all Sentinel-2 spectral bands in [23], outperforming other traditional machine learning methods. The same CNN model was also used in our previous work [33], in which the training set was composed by samples collected from different Sentinel-2 images, acquired on different dates. In those works, the CNN model allowed us to detect water hyacinth at different phenological stages and also to analyze the spatio-temporal

dynamics in a time series, determining the areas where the invasive plants were most frequently accumulated in the period analyzed.

In this work, we adopt the same CNN architecture, but the CNN is trained using spectral indices instead of all the spectral bands from the Sentinel-2 satellite. A detailed scheme of the CNN architecture is shown in Fig. 1. Specifically, the CNN architecture has one convolutional 1-D layer with rectified linear unit (ReLU) activation function, 20 filters, and a kernel size of 12, together with a reshaping (flatten) layer, a fully connected (dense) layer (including 128 neurons), a batch normalization layer with ReLU activation, and a fully connected (dense) layer with 4 neurons and *Softmax* activation. The model is retrained in this work as indicated in the following section.

2) *Training Process*: As illustrated in Fig. 1, the CNN model has been trained with different sets. Specifically, six training sets (based on different spectral indices) have been used: Set_{RGB} , Set_{NDVI} , Set_{FAI} , Set_{NDWI} , Set_{BSI} , and Set_{NDII} . These sets have been generated as follows. First, a ROI is defined to label the pixels containing aquatic invasive plants in the image (here, two case studies are considered: Badajoz and Merida). As explained in [23], the ROI contours were carefully selected using high resolution imagery and ground knowledge, so that the ROI contours encompass only pixels that contain invasive aquatic plants in the image. Then, a percentage of the pixels in the ROI are selected for training the CNN architecture (while the remaining pixels in the ROI are used for testing). In the selected pixels, the per-pixel values of different indices are calculated, resulting in six different training sets. These training sets are used to train the CNN architecture. Table IV shows the total number of pixels used for training in each considered case study (Badajoz and Merida), resulting in two ROIs that are called ROI_BA and ROI_ME.

F. Hardware/software Environment

The hardware environment considered in our experiments comprises an Intel(R) Core(TM) i9-10900 k processor with 64-GB RAM memory and 2-TB SSD. Regarding the considered

TABLE IV
NUMBER OF TRAINING SAMPLES (PIXELS) USED FOR TRAINING THE CNN
ARCHITECTURE IN THE BADAJOZ CASE AND THE MÉRIDA CASE

Number of training samples (pixels)	ROI_BA	ROI_ME
Aquatic weeds	195	162
Other	224	288
Total number and percentage of training samples used	419 (2.58%)	450 (10.06%)
Total number of labeled pixels inside each ROI	16 240	4471

Note: The percentage of the total number of labeled samples used for training in each case are given in the parentheses. For testing, we used the rest of the available labeled samples in each ROI.

software environment, the implementation was developed in Python 3.10 by using TensorFlow and Keras framework. GIS techniques have been considered for preprocessing operations (raster clipping, image analysis, sample selection, etc.) by using Python scripts and QGIS software tools. These tools have also been used for the visualization of images and for the design of map layouts.

III. EXPERIMENTAL RESULTS

A. Metrics for Accuracy Assessment

In order to evaluate the CNN models, the prediction errors are calculated. For that purpose, ground truth data generated in our previous work [23] have been used in this study. A confusion matrix has been calculated for each CNN model. These are binary matrices that indicate whether a pixel of the image contains invasive plants or not (*zero* value if invasive plants are detected and *one* value if they are not). In the first column true negatives (TNs), false positives (FNs) are represented. In the second one, false positives (FPs) and true positives (TPs) are shown.

Moreover, different metrics have been implemented for evaluating the performance of the considered classification approaches. The different relationships between the model predictions and the real values (ground truth values) are defined in the following equations: Overall accuracy [(6)], user's accuracy [(7)], producer's accuracy [(8)]—also known as recall, sensitivity, or TP rate—and F_1 score [(9)].

$$\text{Overall accuracy} = \frac{\text{TP} + \text{TN}}{\text{TP} + \text{TN} + \text{FP} + \text{FN}} \quad (6)$$

$$\text{User's accuracy} = \frac{\text{TP}}{\text{TP} + \text{FP}} \quad (7)$$

$$\text{Producer's accuracy} = \frac{\text{TP}}{\text{TP} + \text{FN}} \quad (8)$$

$$F_1 \text{ score} = \frac{2 \times \text{TP}}{2 \times \text{TP} + \text{FP} + \text{FN}} \quad (9)$$

B. Assessment of Results

This section describes the results of invasive aquatic plants detection after applying the CNN model, using the different training sets considered in this study. Fig. 3 shows all the CNN

detection maps. In addition, the ground truth (GT) images and the Sentinel-2 (S2) images in true color are also shown, for better visual interpretation of the results. In the Mérida case [see Fig. 3(a)], by comparing the S2 and GT images with the CNN algorithm outputs, we can see that there is water hyacinth distributed in small masses on the river banks and in a large mass upstream of the containment barrier. In general terms, it can be seen from Table VI that better accuracies are obtained with spectral indices than with the total number of bands offered by the S2 satellite. In all cases, training with spectral indices results in high accuracies (from 0.856 to 0.933 in terms of overall accuracy, from 0.843 to 0.924 in terms of user's accuracy, from 0.754 to 0.935 in terms of producer's accuracy, and from 0.798 to 0.913 in terms of F_1 score). The index with the worst results is the NDWI.

In contrast, in the Badajoz case, the invasive plant (Mexican water lily) is distributed in several irregular masses over the entire surface and along the banks. As it can be seen in Fig. 3(b), very good accuracies (from 0.643 to 0.779 in terms of overall accuracy, from 0.641 to 0.813 in terms of user's accuracy, from 0.669 to 1.00 in terms of producer's accuracy, and from 0.734 to 0.839 in terms of F_1 score) are obtained with spectral indices. In two of the four accuracy metrics (user's accuracy and producer's accuracy), better results are obtained with spectral indices than with all the bands offered by the S2 satellite. In the cases in which the best scores are obtained using all bands (overall accuracy and F_1 score), the difference with the accuracy of the index offering the second best accuracy differs in less than 2% (in the case of overall accuracy) and less than 1% (in the case of F_1 score).

IV. DISCUSSION

The results in Table V reveal that the CNN model provides the best results when trained with spectral indices (RGB, FAI, BSI, NDVI, and NDII) instead of all spectral bands offered by S2L2A in the case of Mérida. We also generated the same results for the RF classifier and included them in Table VI to compare our CNN with a classical classifier, and we can see all results are improved by our method for both areas. However, as illustrated in Fig. 3(a), the results obtained with NDVI show that some of the accumulated water hyacinth is not detected upstream of the large mass in the containment barrier. Moreover, as can be seen in the confusion matrix in Fig. 5(c), the prediction success (i.e., the TPs and TNs) are higher and the prediction errors (i.e., the FPs and FNs) are lower with indices than with the all bands used as input. Therefore, the use of a large number of bands as input (instead of a specific index) introduces some confusion in the learning of the CNN. As it can be seen in Fig. 3(a), if we consider the NDWI as input, there is water hyacinth accumulated behind the barrier and on the banks that has not been correctly detected. This fact can also be appreciated in Fig. 5(e). In the same way, the results in Table VI (in terms of user's accuracy) show that, when the CNN is trained with spectral indices, better results are obtained than using all the bands as input. Regarding the producer's accuracy, as shown in Table VI, the spectral indices that do not exceed the accuracy provided by using all bands are NDVI, FAI and NDWI, because the percentage of TPs is lower and the percentage of FNs is higher (as is shown in Fig. 5).

TABLE V
PERFORMANCE EVALUATION FOR MÉRIDA CASE AND BADAJOZ CASE (BEST RESULTS IN BOLD) USING THE CNN ALGORITHM

		Overall accuracy	User's accuracy	Producer's accuracy	F_1 score
MÉRIDA Case	All bands	0.903	0.843	0.911	0.876
	RGB	0.933	0.892	0.935	0.913
	NDVI	0.920	0.924	0.857	0.889
	FAI	0.929	0.924	0.883	0.903
	NDWI	0.856	0.846	0.754	0.798
	BSI	0.925	0.887	0.917	0.902
	NDII	0.920	0.879	0.914	0.896
Badajoz Case	All bands	0.779	0.784	0.901	0.839
	RGB	0.643	0.641	1.000	0.781
	NDVI	0.763	0.762	0.914	0.831
	FAI	0.691	0.813	0.669	0.734
	NDWI	0.658	0.652	0.997	0.788
	BSI	0.763	0.789	0.860	0.823
	NDII	0.746	0.795	0.811	0.803

TABLE VI
PERFORMANCE EVALUATION FOR MÉRIDA CASE AND BADAJOZ CASE (BEST RESULTS IN BOLD) USING THE RF ALGORITHM

		Overall accuracy	User's accuracy	Producer's accuracy	F_1 score
MÉRIDA Case	All bands	0.892	0.800	0.952	0.869
	RGB	0.924	0.876	0.930	0.902
	NDVI	0.900	0.877	0.855	0.866
	FAI	0.897	0.852	0.880	0.866
	NDWI	0.783	0.727	0.676	0.701
	BSI	0.909	0.857	0.910	0.883
	NDII	0.906	0.847	0.916	0.880
Badajoz Case	All bands	0.766	0.832	0.794	0.813
	RGB	0.642	0.736	0.643	0.686
	NDVI	0.694	0.803	0.690	0.743
	FAI	0.662	0.805	0.621	0.701
	NDWI	0.658	0.652	0.997	0.788
	BSI	0.703	0.802	0.710	0.753
	NDII	0.702	0.791	0.724	0.756

Finally, considering the F_1 score metric, the worst accuracy is obtained with NDWI index.

In the Badajoz case study, it can be observed in Fig. 3(b) that the worst results are obtained when training the CNN with RGB, NDWI, and FAI, due to over-detection in RGB and NDWI and under-detection in FAI. On the other hand, as shown in Table VI, training with BSI, NDII, and NDVI provides similar results to using all bands in terms of overall accuracy. It can also be seen in Fig. 6 that there are higher FP values in RGB

and NDWI and lower TP values in the case of FAI. However, when analyzing the user's accuracy metric, it can be appreciated that the worst results are obtained with RGB and NDWI and the best ones with BSI and NDII. In the case of producer accuracy, RGB and NDWI obtain very high results because they result in a high percentage of TPs and a very low percentage of FNs and, on the contrary, lower results are obtained in cases where the percentage of FNs is higher (as with the BSI and NDII inputs). Finally, analyzing F_1 score, the highest values in terms of FPs

do have a negative effect, penalizing the RGB, NDWI, and FAI indices, while favoring other indices such as NDVI, BSI, and NDII. To visually compare the results, Fig. 4(a) and (b) were generated with the same conditions but using the RF algorithm.

Our results also reveal that the accuracies vary if we consider the case of Mérida or Badajoz. In the case of Mérida, higher accuracies are obtained than in Badajoz. As it can be seen in Fig. 3(b), the distribution of invasive plants on the surface of the river in the area of Badajoz is presented in masses with more irregular shapes than the masses of invasive plants present in the area of Mérida. These masses are also responsible for the higher percentage of FP detections.

Another significant benefit of using spectral indices (instead of all bands) for training the CNN is computational efficiency. Not only because fewer bands need to be downloaded from the S2 satellite, but also because of the higher throughput resulting from the fact that less information has to be processed. Moreover, since the results provided by all indices resulted in better accuracies, a more efficient training of the CNN architecture can be performed. If we compare the training times needed for the RF and CNN algorithms, the mean time (after 10 runs) for training the RF algorithm is about 0.3 s using indices or the whole set of bands. Regarding the CNN training time, it is higher (about 11 s).

V. CONCLUSION

In this work, we have developed a new method for invasive aquatic plant detection in Sentinel-2 images that relies on a CNN architecture trained with different spectral indices. This represents a significant advantage over previous works, in which the CNN was trained with all the spectral bands available (which generally resulted in lower quality results despite using a higher number of spectral bands). The index with better detection accuracy depends on the evaluation metric that is considered, but in general it can be concluded that the information provided by spectral indices is more useful for training than the raw multispectral data provided by the Sentinel-2 satellite. This opens new perspectives in terms of more efficient and effective data processing. In future studies, we will perform a more detailed assessment of computational performance and consider other deep learning models.

ACKNOWLEDGMENT

The authors would like to thank the Confederación Hidrográfica del Guadiana (CHG) for providing reference information about the presence of aquatic invasive plants and about the actions carried out in the study area.

REFERENCES

- [1] Y. Ma et al., "Remote sensing of turbidity for lakes in Northeast China using Sentinel-2 images with machine learning algorithms," *IEEE J. Sel. Topics Appl. Earth Observ. Remote Sens.*, vol. 14, pp. 9132–9146, 2021.
- [2] F. S. Marzano, M. Iacobelli, M. Orlandi, and D. Cimini, "Coastal water remote sensing from Sentinel-2 satellite data using physical, statistical, and neural network retrieval approach," *IEEE Trans. Geosci. Remote Sens.*, vol. 59, pp. 915–928, 2021.
- [3] G. I. Drakonakis, G. Tsagkatakis, K. Fotiadou, and P. Tsakalides, "OmbriaNet-supervised flood mapping via convolutional neural networks using multitemporal Sentinel-1 and Sentinel-2 data fusion," *IEEE J. Sel. Topics Appl. Earth Observ. Remote Sens.*, vol. 15, pp. 2341–2356, 2022.
- [4] H. Feng et al., "Mapping the 2021 October flood event in the Subsiding Taiyuan Basin by multi-temporal SAR data," *IEEE J. Sel. Topics Appl. Earth Observ. Remote Sens.*, vol. 15, pp. 7515–7524, 2022.
- [5] Z. Liang, X. Pang, Q. Ji, X. Zhao, G. Li, and Y. Chen, "An entropy-weighted network for polar sea ice open lead detection from Sentinel-1 SAR images," *IEEE Trans. Geosci. Remote Sens.*, vol. 60, pp. 1–14, 2022.
- [6] M. Li, P. Wu, B. Wang, H. Park, Y. Hui, and W. Yanlan, "A deep learning method of water body extraction from high resolution remote sensing images with multisensors," *IEEE J. Sel. Topics Appl. Earth Observ. Remote Sens.*, vol. 14, pp. 3120–3132, 2021.
- [7] Z. Zhang, M. Wang, X. Liu, C. Wang, and H. Zhang, "Map and quantify the ground deformation around salt lake in Hoh Xil, Qinghai-Tibet plateau using time-series InSAR from 2006 to 2018," *IEEE J. Sel. Topics Appl. Earth Observ. Remote Sens.*, vol. 14, pp. 858–869, 2021.
- [8] M. A. Ghazal et al., "Vegetation cover estimation using convolutional neural networks," *IEEE Access*, vol. 7, pp. 132563–132576, 2019.
- [9] J. Zhan, R. Zhang, L. Xie, S. Li, J. Lv, and J. Tu, "Vegetation growth monitoring based on BDS interferometry reflectometry with triple-frequency SNR data," *IEEE Geosci. Remote Sens. Lett.*, vol. 19, pp. 1–5, 2022.
- [10] S. Zhu et al., "Multidimensional response evaluation of remote-sensing vegetation change to drought stress in the Three-River Headwaters, China," *IEEE J. Sel. Topics Appl. Earth Observ. Remote Sens.*, vol. 13, pp. 6249–6259, 2020.
- [11] Y. Tang et al., "Spatio-temporal deep learning-based algal bloom prediction for Lake Okeechobee using multi-source data fusion," *IEEE J. Sel. Topics Appl. Earth Observ. Remote Sens.*, vol. 15, pp. 8318–8331, 2022.
- [12] L. R. Sartori, N. N. Imai, J. C. Mura, E. M. L. D. M. Novo, and T. S. F. Silva, "Mapping macrophyte species in the Amazon floodplain wetlands using fully polarimetric ALOS/PALSAR data," *IEEE Trans. Geosci. Remote Sens.*, vol. 49, no. 12, pp. 4717–4728, Dec. 2011.
- [13] K. H. Thamaga and T. Dube, "Remote sensing of invasive water hyacinth (Eichhornia crassipes): A review on applications and challenges," *Remote Sens. Appl.: Soc. Environ.*, vol. 10, pp. 36–46, 2018.
- [14] R. Xu, S. Zhao, and Y. Ke, "A simple phenology-based vegetation index for mapping invasive *Spartina alterniflora* using Google Earth Engine," *IEEE J. Sel. Topics Appl. Earth Observ. Remote Sens.*, vol. 14, pp. 190–201, 2021.
- [15] R. Gerardo and I. P. D. Lima, "Assessing the potential of Sentinel-2 data for tracking invasive water hyacinth in a river branch," *J. Appl. Remote Sens.*, vol. 16, 2022, Art. no. 014511.
- [16] Y. Ghousssein et al., "Multitemporal remote sensing based on an FVC reference period using Sentinel-2 for monitoring *Eichhornia crassipes* on a Mediterranean river," *Remote Sens.*, vol. 11, 2019, Art. no. 1856.
- [17] B. Song and K. Park, "Detection of aquatic plants using multispectral UAV imagery and vegetation index," *Remote Sens.*, vol. 12, p. 387, 2020.
- [18] D. Bubenheim, V. Genovese, J. D. Madsen, and E. Hard, "Remote sensing and mapping of floating aquatic vegetation in the Sacramento–San Joaquin River Delta," *J. Aquat. Plant Manage.*, vol. 59, pp. 46–54, 2021.
- [19] D. Xu, Y. Pu, M. Zhu, Z. Luan, and K. Shi, "Automatic detection of algal blooms using Sentinel-2 MSI and Landsat OLI images," *IEEE J. Sel. Topics Appl. Earth Observ. Remote Sens.*, vol. 14, pp. 8497–8511, 2021.
- [20] G. Singh, C. Reynolds, M. Byrne, and B. Rosman, "A remote sensing method to monitor water, aquatic vegetation, and invasive water hyacinth at national extents," *Remote Sens.*, vol. 12, pp. 1–24, 12 2020.
- [21] C. Ade, S. Khanna, M. Lay, S. L. Ustin, and E. L. Hestir, "Genus-level mapping of invasive floating aquatic vegetation using Sentinel-2 satellite remote sensing," *Remote Sens.*, vol. 14, 2022, Art. no. 3013.
- [22] Z. Qiu, D. Mao, K. Feng, M. Wang, H. Xiang, and Z. Wang, "High-resolution mapping changes in the invasion of *Spartina alterniflora* in the Yellow River Delta," *IEEE J. Sel. Topics Appl. Earth Observ. Remote Sens.*, vol. 15, pp. 6445–6455, 2022.
- [23] E. C. Rodríguez-Garrito, A. Paz-Gallardo, and A. Plaza, "Automatic detection of aquatic weeds: A case study in the Guadiana River, Spain," *IEEE J. Sel. Topics Appl. Earth Observ. Remote Sens.*, vol. 15, pp. 8567–8585, 2022.
- [24] "Confederación Hidrográfica del Guadiana O. A.," Accessed: Mar. 23, 2023. [Online]. Available: <https://www.chguadiana.es/cuenca-hidrografica/especies-exoticas-invasoras>
- [25] S. Zorzi, E. Maset, A. Fusiello, and F. Crosilla, "Full-waveform airborne LiDAR data classification using convolutional neural networks," *IEEE Trans. Geosci. Remote Sens.*, vol. 57, no. 20, pp. 8255–8261, Oct. 2019.

- [26] Y. J. E. Gbdjo, O. Montet, D. Ienco, R. Gaetano, and S. Dupuy, "Multisensor land cover classification with sparsely annotated data based on convolutional neural networks and self-distillation," *IEEE J. Sel. Topics Appl. Earth Observ. Remote Sens.*, vol. 14, pp. 11485–11499, 2021.
- [27] M. E. Paoletti, J. M. Haut, J. Plaza, and A. Plaza, "Deep learning classifiers for hyperspectral imaging: A review," *ISPRS J. Photogrammetry Remote Sens.*, vol. 158, pp. 279–317, 2019.
- [28] T. Kattenborn, J. Leitloff, F. Schiefer, and S. Hinz, "Review on convolutional neural networks (CNN) in vegetation remote sensing," *ISPRS J. Photogrammetry Remote Sens.*, vol. 173, pp. 24–49, 2021.
- [29] D. Marinelli, C. Paris, and L. Bruzzone, "An approach based on deep learning for tree species classification in LiDAR data acquired in mixed forest," *IEEE Geosci. Remote Sens. Lett.*, vol. 19, pp. 1–5, 2022.
- [30] N. Flood, F. Watson, and L. Collett, "Using a U-net convolutional neural network to map woody vegetation extent from high resolution satellite imagery across Queensland, Australia," *Int. J. Appl. Earth Observation Geoinformation*, vol. 82, 2019, Art. no. 101897.
- [31] Y. Jiang, Y. Bai, and S. Han, "Determining ground elevations covered by vegetation on construction sites using drone-based orthoimage and convolutional neural network," *J. Comput. Civil Eng.*, vol. 34, 2020, Art. no. 04020049.
- [32] U. Bayr and O. Puschmann, "Automatic detection of woody vegetation in repeat landscape photographs using a convolutional neural network," *Ecological Informat.*, vol. 50, pp. 220–233, 2019.
- [33] E. C. Rodríguez-Garlito, A. Paz-Gallardo, and A. Plaza, "Monitoring the spatiotemporal distribution of invasive aquatic plants in the Guadiana river, Spain," *IEEE J. Sel. Topics Appl. Earth Observ. Remote Sens.*, vol. 16, pp. 228–241, 2022.
- [34] "SentinelHub," Accessed: Mar. 23, 2023. [Online]. Available: <https://www.sentinel-hub.com>
- [35] J. J. W. Rouse, R. H. Haas, J. A. Schell, and D. W. Deering, "Monitoring vegetation systems in the great plains with ERTS," in *Proc. NASA. Goddard Space Flight Center 3rd ERTS-1 Symp.*, vol. 1, 1974. [Online]. Available: <https://ntrs.nasa.gov/citations/19740022614>
- [36] C. Hu, "A novel ocean color index to detect floating algae in the global oceans," *Remote Sens. Environ.*, vol. 113, pp. 2118–2129, 2009.
- [37] B.-C. Gao, "NDWI—A normalized difference water index for remote sensing of vegetation liquid water from space," *Remote Sens. Environ.*, vol. 58, pp. 257–266, 1996.
- [38] S. Miyatake and A. Rikimaru, "Development of forest canopy density mapping and monitoring model using indices of vegetation, bare soil and shadow," in *Proc. 18th Asian Conf. Remote Sens.*, 1997.
- [39] M. A. Hardisky, V. Klemas, and R. M. Smart, "The influence of soil salinity, growth form, and leaf moisture on the spectral radiance of *Spartina Alterniflora* Canopies," *Photogrammetric Eng. Remote Sens.*, vol. 49, pp. 77–83, 1983.
- [40] E. R. Hunt and B. N. Rock, "Detection of changes in leaf water content using near-and middle-infrared reflectances," *Remote Sens. Environ.*, vol. 30, pp. 43–54, 1989.
- [41] O. Strashok, M. Ziemiańska, and V. Strashok, "Evaluation and correlation of Sentinel-2 NDVI and NDMI in Kyiv (2017–2021)," *J. Ecological Eng.*, vol. 23, pp. 212–218, 2022.



Elena Cristina Rodríguez-Garlito (Student Member, IEEE) received the B.Sc. degree in civil engineering, the M.Sc. degree in GIS (geographical information systems) and RS from the University of Extremadura, Cáceres, Spain, in 2013 and 2014, respectively, where she is currently working toward the Ph.D. degree in predoctoral contracts for the training of doctors in public RD centers belonging to the Extremadura System of Science, Technology and Innovation.

She is currently a Member of the Hyperspectral Computing Laboratory, Department of Computers and Communications, University of Extremadura. She is working on the development of machine/deep learning algorithms for invasive aquatic plants detection and natural resources management, using RS data from satellites and drones. Her research interests include GIS, RS, and machine/deep learning.



Abel Paz-Gallardo received the B.S. degree in computer engineering from the University of Extremadura, Cáceres, Spain, in 2007, and the M.Sc. and Ph.D. degrees in computer science from the University of Extremadura, in 2009 and 2011, respectively.

From 2006 to 2007, he was a Research Assistant with the Department of Computer Architecture with the University of Extremadura, where he became Associate Professor in 2008. At the same time he started with the Minimally Invasive Surgery Center Jesús Usón, Cáceres, Spain. In 2010 he started working with Bull Spain S.A. to deploy at CETA-Ciemat (Trujillo, Spain) the biggest GPGPU Cluster in Spain and one of the biggest ones in Europe. From October 2011 to July 2018, he was the IT Manager (CIO) of CETA-Ciemat, where he achieved the GPU Research Centre mention from NVIDIA as Principal Investigator. Finally, from July 2018, he is the Chief Information Officer of Greenfield Technologies, Badajoz, Spain, a precision agriculture company that provides recommendations to farmers, through the use of different innovative technologies (such as drones, satellites, sensors, and artificial intelligence) and applied research. He has participated in more than 40 international projects and has authored or coauthored more than 40 publications, including 16 journal citation report (JCR) papers (most of them published by IEEE journals), and over 30 peer-reviewed international conference papers. His main research interests include remotely sensed hyperspectral image analysis, signal processing, and efficient implementations of large-scale scientific problems on high performance computing architectures such as clusters and graphical processing units (GPUs).

Dr. Paz-Gallardo was the recipient of the IEEE Signal Processing Magazine Best Column Award Paper from the IEEE Signal Processing Society in November 2015.



Antonio Plaza (Fellow, IEEE) received the M.Sc. degree in 1999 and the Ph.D. degree in 2002, both in computer engineering, from the University of Extremadura, Cáceres, Spain.

He is a Full Professor and the Head of the Hyperspectral Computing Laboratory, Department of Technology of Computers and Communications, University of Extremadura. He has authored or coauthored more than 800 publications in this field, including 400 JCR journal papers, 25 book chapters, and 330 peer-reviewed conference proceeding papers. His main

research interests include hyperspectral data processing and parallel computing of RS data.

Dr. Plaza was the recipient of the recognition of Best Reviewers of the IEEE Geoscience and Remote Sensing Letters (in 2009) and the recognition of Best Reviewers of IEEE TRANSACTIONS ON GEOSCIENCE AND REMOTE SENSING (in 2010), for which he served as Associate Editor in 2007–2012, the Best Column Award of the *IEEE Signal Processing* magazine in 2015, the 2013 Best Paper Award of the JSTARS journal, and the Most Highly Cited Paper (2005–2010) in the *Journal of Parallel and Distributed Computing*, and Best Paper Awards at the IEEE Workshop on Hyperspectral Image and Signal Processing: Evolution in Remote Sensing, the IEEE International Conference on Space Technology, and the IEEE Symposium on Signal Processing and Information Technology. He is a Fellow of IEEE "For contributions to hyperspectral data processing and parallel computing of Earth observation data," and a Member of Academia Europaea, The Academy of Europe. He is also an Associate Editor for *IEEE Access* (receiving the recognition of Outstanding Associate Editor for the journal in 2017), and was also Member of the Editorial Board of the *IEEE Geoscience and Remote Sensing Newsletter* (2011–2012) and the *IEEE Geoscience and Remote Sensing Magazine* (2013). He has guest edited 17 special issues on hyperspectral imaging for different journals. He was also a member of the steering committee of the IEEE JOURNAL OF SELECTED TOPICS IN APPLIED EARTH OBSERVATIONS AND REMOTE SENSING (JSTARS). He served as the Director of Education Activities for the IEEE Geoscience and Remote Sensing Society (GRSS) from 2011 to 2012, and as President of the Spanish Chapter of IEEE GRSS in 2012–2016. He is currently serving as Chair of the Publications Awards Committee of IEEE GRSS and as a Vice-Chair of the Fellow Evaluations Committee of IEEE GRSS. He has reviewed more than 500 manuscripts for over 50 different journals. He served as the Editor-in-Chief of IEEE TRANSACTIONS ON GEOSCIENCE AND REMOTE SENSING for five years (2013–2017) and as the Editor-in-Chief of the IEEE JOURNAL ON MINIATURIZATION FOR AIR AND SPACE SYSTEMS (2019–2020). He has been included in the 2018, 2019, 2020, 2021, and 2022 Highly Cited Researchers List (Clarivate Analytics). Additional information: <http://sites.google.com/view/antonioplaza>.

Mapping the Accumulation of Invasive Aquatic Plants in the Guadiana River, Spain, Using Multitemporal Remote Sensing

Escuela Politécnica
Av. de la Universidad, S/N, 10003
Teléfono: 0034927257000. Ext. 51662
correo electrónico: apazgal, aplaza @unex.es
Cáceres, España

Dr. Abel Francisco Paz Gallardo y Dr. Antonio Plaza Miguel, como directores de la Tesis Doctoral titulada "Desarrollo de nuevos métodos y algoritmos de análisis y clasificación de imágenes multiespectrales orientadas a la gestión y monitorización de plantas acuáticas invasoras", certificamos el factor de impacto y la categorización de la siguiente publicación incluida en la Tesis Doctoral. Del mismo modo, se especifica la aportación de la doctoranda. Para cualquier otra información o aclaración, por favor, no duden en contactar con nosotros.

Titulo de la publicación: Mapping the Accumulation of Invasive Aquatic Plants in the Guadiana River, Spain, Using Multitemporal Remote Sensing

Autores: **Elena C. Rodríguez-Garlito**, Abel Paz-Gallardo y Antonio Plaza

Revista: IEEE Geoscience and Remote Sensing Letters

Otros datos: vol 20, págs 1-5, año 2023

DOI: 10.1109/LGRS.2023.3277366

Factor de impacto 2022: 4.8

Abstract: Multispectral remote sensing is very effective for the detection of different types of land cover. Satisfactory results have been obtained in the task of monitoring different types of vegetation covers using satellite images, including areas conquered by invasive aquatic plants such as water hyacinth. Several countries around the world are suffering from negative effects caused by the quick spread of these plants. For instance, several strategies have been carried out for their control and elimination in the Guadiana River, Spain. In this letter, we develop a new methodology capable of automatically finding the geolocation of the most frequent areas of accumulation of invasive aquatic plants in the Guadiana River. Our strategy exploits multispectral time series acquired by European Space Agency (ESA) Sentinel-2 satellite. Once the invasive plants have been detected using deep learning [a convolutional neural network (CNN)], a subsequent analysis is carried out using geographic information systems (GIS) to map the areas where water hyacinth patches are most frequently found. In this way, we demonstrate that the management of invasive aquatic plants in the Guadiana River can be successfully carried out.

Contribución de la doctoranda: Planteamiento de la hipótesis, conceptualización, búsqueda bibliográfica, metodología, análisis y discusión de resultados, elaboración de tablas y figuras, escritura del manuscrito borrador y redacción de la revisión.

Mapping the Accumulation of Invasive Aquatic Plants in the Guadiana River, Spain, Using Multitemporal Remote Sensing

Elena C. Rodríguez-Garlito^{1b}, Graduate Student Member, IEEE, Abel Paz-Gallardo^{1b},
and Antonio J. Plaza^{1b}, Fellow, IEEE

Abstract—Multispectral remote sensing is very effective for the detection of different types of land cover. Satisfactory results have been obtained in the task of monitoring different types of vegetation covers using satellite images, including areas conquered by invasive aquatic plants such as water hyacinth. Several countries around the world are suffering from negative effects caused by the quick spread of these plants. For instance, several strategies have been carried out for their control and elimination in the Guadiana River, Spain. In this letter, we develop a new methodology capable of automatically finding the geolocation of the most frequent areas of accumulation of invasive aquatic plants in the Guadiana River. Our strategy exploits multispectral time series acquired by European Space Agency (ESA) Sentinel-2 satellite. Once the invasive plants have been detected using deep learning [a convolutional neural network (CNN)], a subsequent analysis is carried out using geographic information systems (GIS) to map the areas where water hyacinth patches are most frequently found. In this way, we demonstrate that the management of invasive aquatic plants in the Guadiana River can be successfully carried out.

Index Terms—Deep learning, mapping invasive species, multitemporal remote sensing, Sentinel-2, water hyacinth.

I. INTRODUCTION

IN RECENT decades, remote-sensing products have been used to manage natural resources such as water bodies affected by invasive plants. Studies aimed at mapping the spatial distribution of invasive aquatic plants (like water hyacinth) have undergone an exponential increase [1]. In recent works, several studies have been conducted to demonstrate the ability of remotely sensed imagery to improve the effectiveness and

efficiency of aquatic weed monitoring and management in different parts of the world [2], such as Lake Victoria (Kenya) [3], Al Kabir River (Lebanon) [4], or Lake Tana (Ethiopia) [5]. Different remote-sensing methodologies have been applied to detect and map invasive plants using images acquired by different sensors (Landsat-8, Sentinel-2, MODIS, and drones) using vegetation indices and machine-learning techniques [6], [7], [8]. Geographic information systems (GIS) have also been proven to be effective tools to map water hyacinth coverage [9]. The application of deep-learning techniques, such as convolutional neural networks (CNNs), to remote sensing of vegetation has also been explored in this context [10]. In our previous works [11] and [12], other methods for invasive plant detection were briefly reviewed (most studies were focused on the use of spectral indices).

The *Eichhornia crassipes* (also known as water hyacinth) is a plant native to the Amazon River that has spread as an invasive species to all continents. In the summer of 2004, the first patches of this plant appeared on the Spanish stretch of the Guadiana River [13]. Its presence causes environmental and economic damages such as loss of water quality or damage to irrigation and hydraulic infrastructures and recreational areas. Large economic investments have been made to implement projects aimed at controlling its expansion and eliminating the plant from the river. The strategies followed in the so-called “*shock plan*” against water hyacinth reveal how budget availability influences the continuity of control tasks. Therefore, successful invasion control has varied according to financial efforts. Removal mechanisms (without using chemical or biological substances) have mainly consisted of cleaning the affected sections (i.e., removing them from the surface) by mechanical and manual procedures, assisted by floating barriers. Current efforts are focused on the development of a sustained monitoring plan.

Our previous work [11] revealed that invasive plants (like water hyacinth) can be automatically detected by applying machine/deep-learning classification algorithms to satellite images collected over affected areas. Our results indicated that CNNs offer better accuracy compared to other traditional machine-learning methods (such as *k*-means or random forests) in the detection of water hyacinth in the Guadiana River. In a subsequent work [12], a custom-designed CNN model was developed to detect these invasive aquatic plants in a time series of satellite images collected over the same

Manuscript received 18 October 2022; revised 24 February 2023 and 12 April 2023; accepted 10 May 2023. Date of publication 17 May 2023; date of current version 1 June 2023. This work was supported in part by the European Social Fund Resolución de 10 de mayo de 2017, de la Secretaría General de Ciencia, Tecnología e Innovación, por la que se resuelve la convocatoria de ayudas para la financiación de contratos predoctorales para formación de Doctores en los centros públicos de I+D pertenecientes al Sistema Extremeño de Ciencia, Tecnología e Innovación en el ejercicio 2017 under Grant PD16001; in part by the Consejería de Economía, Ciencia y Agenda Digital of the Junta de Extremadura and the European Regional Development Fund (ERDF) through the European Union under Grant GR21040; in part by the Spanish Ministerio de Ciencia e Innovación (APRISA) under Project PID2019-110315RB-I00; and in part by the European Union’s Horizon 2020 Research and Innovation Program (EOXPOSURE) under Grant 734541. (Corresponding author: Antonio J. Plaza.)

The authors are with the Hyperspectral Computing Laboratory, Department of Technology of Computers and Communications, Escuela Politécnica, University of Extremadura, 10003 Cáceres, Spain (e-mail: elenacristinarg@unex.es; apazgal@unex.es; aplaza@unex.es).

Digital Object Identifier 10.1109/LGRS.2023.3277366

1558-0571 © 2023 IEEE. Personal use is permitted, but republication/redistribution requires IEEE permission.
See <https://www.ieee.org/publications/rights/index.html> for more information.

area, using sparse training samples from a few satellite images to represent the phenological cycle of these invasive plants in the Guadiana River. These previous studies are focused on the detection of invasive plants, separating them from the rest of the classes present in the image. In this ROI, there is also soil, water, and different types of vegetation (apart from water and invasive plants). Detailed information about the classification of invasive plants is available in [11], while the use of the adopted classification system to extract information from time series is given in [12]. In this letter, we focus on the problem of how to map the distribution of invasive plants in different areas of the river.

As stated in reports by the *Confederación Hidrográfica del Guadiana* (CHG) (a Spanish organization), each reduction in funding has led to further spread and growth of invasive plants in the river. Any knowledge about the behavior and distribution of the plants helps to make informed decisions on how to act in the face of the problems generated by the expansion of such plants.

The main contribution of this letter is the development of a new methodology for detecting the areas where invasive plants tend to be present or accumulated over time in the Guadiana River. For that purpose, a full methodology is established, based on analyzing a time series of satellite images collected by European Space Agency (ESA) Sentinel-2. Thus, the methodology includes preprocessing and processing of time series of Sentinel-2 images using a deep-learning model (the custom-designed CNN in [11] and [12]) for monitoring the spatiotemporal distribution of invasive aquatic plants. The result of our method is an indication of the accumulation of water hyacinth in the period under consideration. Knowing the areas with a large accumulation of invasive plants provides information of great interest in monitoring and control tasks and represents an innovative contribution of this letter.

II. METHODOLOGY

In this section, we describe the processes involved in the generation of maps showing the accumulation areas of invasive aquatic plants in the considered time series.

A. Remote-Sensing Time-Series Image Preprocessing

Given a time series of remote-sensing images, an ROI is first extracted (see Fig. 1). The pixel values outside the contour will be considered as NoData values. To exclude the NoData values from subsequent training, prediction, and classification processes, the procedure described in our previous work [11] is adopted. First of all, normalization of all pixel values of each image between 0 and 1 is performed. Then, the data format is changed and a reassignment of the NoData values is performed.

B. Automatic Detection of Invasive Aquatic Plants

Based on the time series that contain the ROI, invasive aquatic plants are automatically detected by using machine/deep-learning classification algorithms. In our previous study [11], several supervised and unsupervised classification algorithms were tested. Among them, CNNs obtained

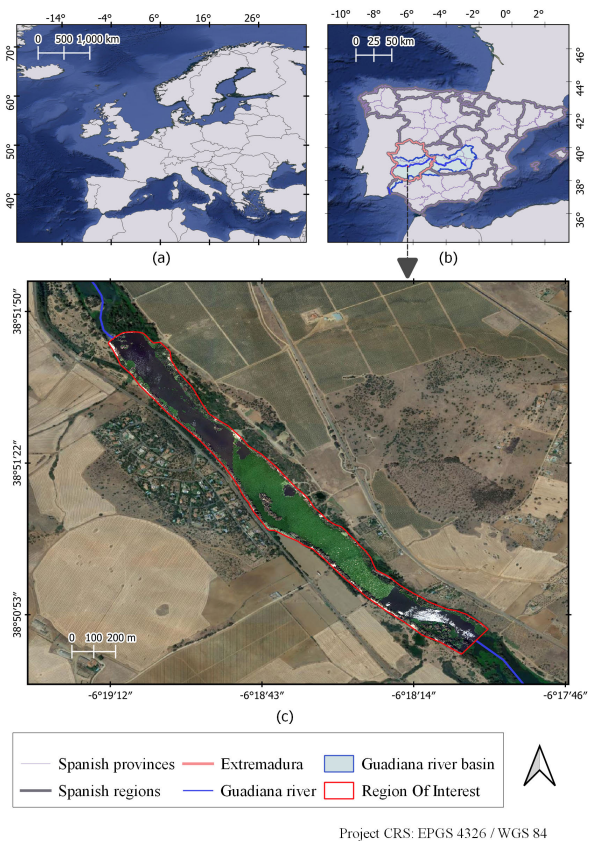


Fig. 1. (a) Geographical location of Spain. (b) Geographical location of Extremadura region, the Guadiana River, and the Guadiana River basin. (c) Geolocation of the ROI affected by water hyacinth.

better accuracies in detecting invasive aquatic plants in the ROI considered in our study, displayed in Fig. 1(c).

1) *Training Set Selection*: The samples of the ROI containing water hyacinth have been extracted using the methodology in [14].

2) *Image Processing*: A CNN is trained with the aforementioned training samples so that it can predict the pixels in the input image where invasive aquatic plants are present. The output images will contain the pixels where invasive plants have been detected.

C. Mapping the Accumulation Areas of Invasive Aquatic Plants in a Time Series

This step consists of the generation of a heat map from images containing the geolocation of pixels where aquatic invasive plants have been detected (hereinafter referred to as outputs). The main steps of this procedure are shown in Fig. 2. The involved processes are described as follows (see part 4 of Fig. 2).

1) *Creation of a Vector Layer of Points*: The process starts with an output image from the classification algorithm. This image contains the pixels where invasive plants have been detected. In this step, the output image (a raster layer) is converted to a vector layer of points, where each point corresponds to the centroid of the analyzed pixel. Next, NoData values are removed. For the next step, it is required that the attribute table of these geolocated point layers is empty.

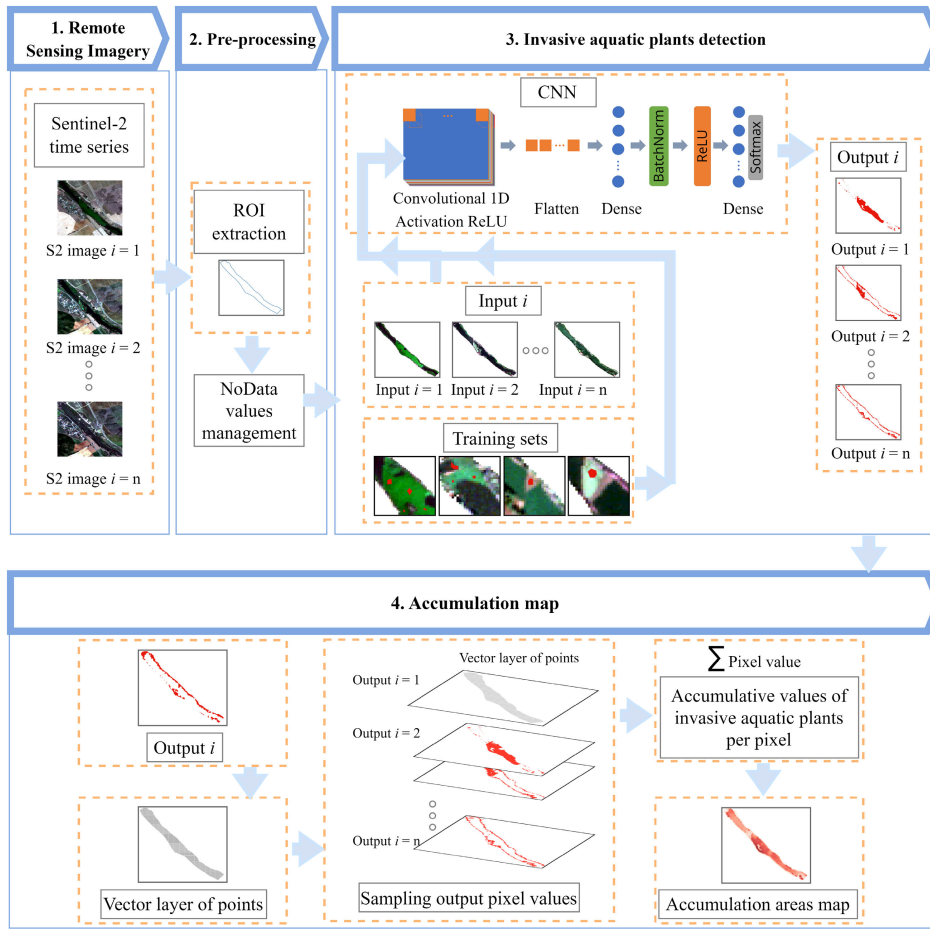


Fig. 2. Workflow of the procedure for generating accumulation maps of water hyacinth in the Guadiana River.

2) *Sampling Output Pixel Values to the Vector Layer of Points*: The pixel values from the output images are collected by the points of the vector layer of points, generated in the previous step. In other words, by using GIS tools, a stack of outputs is created. Next, the vector layer of points is situated over this stack. In this way, a new vector layer of points is created given by the sampling points and the values taken from all the underlying pixels (with the same geolocation). The obtained vector file of points has an attribute table where the pixel values of all the outputs are labeled with their collection date. The attribute table associated with the new vector layer of points has as many rows as pixels present in the analyzed ROI. In addition, this table has as many columns as the number of output images of the time series.

3) *Column Addition With Cumulative Values of Water Hyacinth Detection Results (Per Pixel) in the Analyzed Time Series*: The cells of the attribute table of the vector file from the previous step contain a value of 1 when invasive aquatic plants are present in that pixel, and a value of 0 otherwise. In this step, a new column with the sum value is added. Thus, the new column contains a cumulative value indicating the presence of aquatic plants in each pixel of the time series being analyzed.

The accumulation (A) of values between two output dates, t_1 and t_2 , can be calculated by the formula: $A(t_1, t_2) =$

$\sum_{t=t_1}^{t_2} v(t)$, where $v(t)$ is a function that returns either 0 or 1 for each time point t in the interval $[t_1, t_2]$.

4) *Graphical Representation of Results*: Finally, a graphical representation of the obtained results is made in the form of a heat map generated using GIS tools. Here, we start from the vector layer of points from the previous step, which has an associated attribute table that contains the cumulative values per pixel in the analyzed time series. To make the map more visually comprehensive, a triangulated irregular network (TIN) interpolation is conducted. In this way, each pixel shows the number of times that water hyacinth has been detected in the time period analyzed, being able to indicate the areas where it has mostly accumulated over time.

III. EXPERIMENTS

Fig. 2 shows the main steps of the approach followed in the experiments reported below. In the following, we provide a comprehensive description of such experiments.

A. Remote-Sensing Datasets

Our experiments have been carried out using satellite remote-sensing images collected over the Guadiana River in Spain. The study area is a stretch affected by water hyacinth [(see Fig. 1(c)), which is a high-resolution image acquired

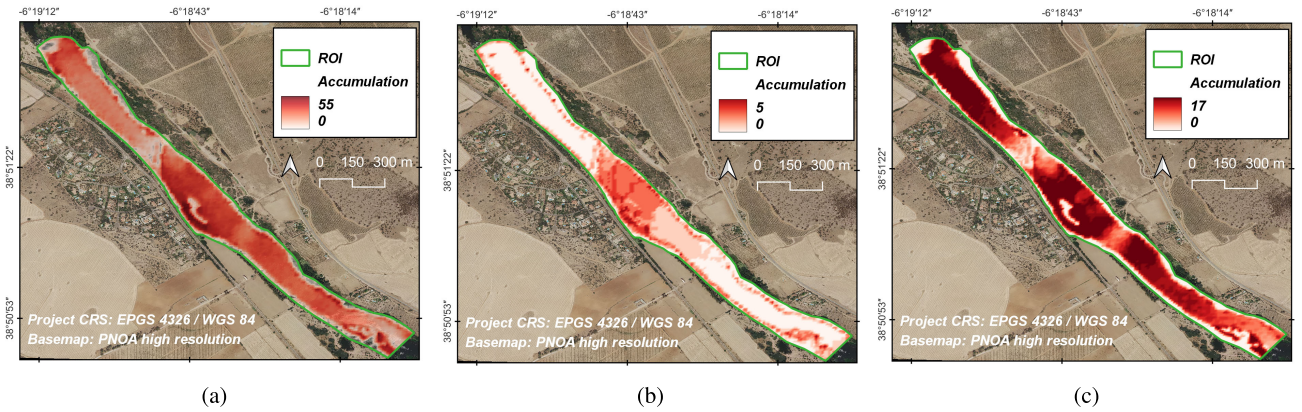


Fig. 3. Water hyacinth accumulation maps for different periods: (a) Complete time series. (b) From 2019-04-12 to 2019-05-27. (c) From 2020-06-05 to 2020-08-29.

TABLE I
REMOTE-SENSING DATASETS USED IN OUR STUDY

Latitude / Longitude	38° 50' - 38° 51'N / 6° 19' - 6° 18' W
Study area	45 ha
Remote sensing images	Sentinel - 2 Level-2A (S2L2A) products
Projection	UTM/WGS84
Satellite revisit time	5 days
Spectral resolution	12 bands (442.7-2202.4 nm)
Spatial resolution	10 m, 20 m or 60 m
Datasets dimensions	189 x 173 pixels
Format	8 bit
Number of Sentinel-2 datasets	62
Years covered	2019-2020

by the Spanish National Plan of Aerial Orthophotography (PNOA)]. A satellite time series acquired by Sentinel-2 has been used. These images are freely available from ESA as part of the Copernicus program. Images covered by clouds have been discarded. The main characteristics of the datasets used in this work are described in Table I.

B. Image Analysis

1) *Preprocessing*: First, the 62 Sentinel-2 images of the time series were preprocessed using the procedure described in Section II-A. The ROI (with 4471 pixels) was extracted, and NoData values were managed. For this purpose, a normalization of the pixel values between 0 and 1 and a change of format of the datasets (from 8 to 32 bits) was carried out. The replacement of NoData values with values that were not in the pixel value histogram of the datasets was also conducted.

2) *Training Sets*: In our previous work [12], a methodology was proposed to collect sparse samples of water hyacinth in a reduced number of Sentinel-2 satellite images of the analyzed time series, to train a prediction model. The supervised deep-learning model (a CNN) was capable of automatically detecting aquatic invasive plants in the time series analyzed. These training sets took into account the annual dynamics that considers the different phenological stages of the plant (dormancy, vegetative growth, flowering, and fruiting). In this work, training samples have been collected from only four

TABLE II
NUMBER OF TRAINING SAMPLES (PIXELS) USED

	February	March-April	May-October	November-January
Water hyacinth	30	57	162	178
Other land cover types	288	288	288	288

images of the whole time series. Fig. 2 illustrates the third step by providing a zoom of some of the water hyacinth training samples collected in the four images of the time series. For more information on the complete process, we refer to experiment 3 in [12]. In this way, four different training sets were considered in four different periods of the year. The characteristics of these training sets are given in Table II.

3) *CNN Model*: In this work, the CNN model developed in [11] and applied in [12] has been used due to the good water hyacinth detection accuracies obtained (more than 90% overall accuracy). As it can be seen in Fig. 2, the CNN design comprises the following layers: convolutional, reshaping, fully connected, normalization, and activation. It is a CNN1-D [15] where only the spectral information contained by each pixel is considered.

C. Software Environment

The CNN has been implemented using the Python 3.8 programming language and the TensorFlow and Keras libraries. GIS techniques have been used through tools from QGIS software and Python scripts.

D. Accumulation Map

Fig. 3(a) shows the final accumulation map generated from the output images of the CNN algorithm for the complete time series of 62 images. This map reveals the geolocation of the areas where the invasive aquatic plants accumulate most frequently. We can see that there are many areas where water hyacinth has been repeatedly detected in almost all the Sentinel-2 images of the time series analyzed (about 55 images). These areas (displayed in dark red color) are

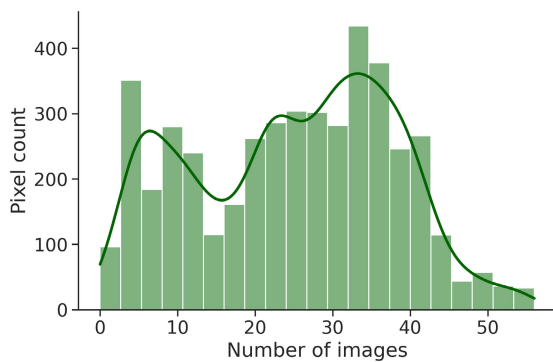


Fig. 4. Histogram showing the number of pixels detected as water hyacinth for the complete time series.

mostly concentrated on the river banks, on small islands, and in the areas close to a water hyacinth containment barrier (installed during the studied period). On the contrary, the areas where water hyacinth has been detected in few images of the complete time series are displayed in a lighter red color.

Fig. 4 shows the histogram of the pixel accumulation results. Each histogram bar (also known as bin or bucket) represents ranges of the number of images (X -axis). Then, the number of pixels containing invasive species is displayed for every bin in the Y -axis. The line plot over the bins represents kernel density estimation (KDE), a known method for kernel smoothing to show the shape of the statistical distribution. This plot reveals that, in the considered two-year period, there is a large number of pixels with invasive aquatic plants in more than half of the images analyzed, reaching a maximum of about 400 pixels (10% of the total) in around 30–40 images, and a minimum of around 50 pixels in 55 images. The histogram also shows a mean value of about 200 pixels with invasive plants in the studied period.

This methodology was repeated for monitoring specific time periods. For example, by analyzing the Sentinel-2 images acquired from April to May 2019 (six images), the map in Fig. 3(b) shows that the greatest accumulation of water hyacinth has occurred on the vicinity of the containment barrier (as expected). On the other hand, Fig. 3(c) shows the map generated for the June–August (summer) period in 2020 (17 images). Here, the water hyacinth accumulation is more evenly distributed throughout the ROI. This is due to the fact that invasive aquatic plants are in vegetative growth, and the large amount of biomass present on the surface of the river has passed through the barrier. This last map reveals a need to remove the accumulated plants to prevent them from invading the river channel downstream.

IV. CONCLUSION

In this letter, a methodology for mapping the accumulation of invasive plants in the Guadiana River has been developed. The proposed approach provides valuable knowledge in

monitoring and control of invasive aquatic plants and the following advantages. In our specific case study, the geolocation of the most frequent areas of accumulation of water hyacinth is relevant for the subsequent removal of the plant from the river surface. It can also be used to predict the location of new water hyacinth retention barriers. The availability of free Sentinel-2 satellite images and the knowledge provided by this study will greatly simplify the control of the spread of invasive aquatic plants in the Guadiana River.

REFERENCES

- [1] K. H. Thamaga and T. Dube, "Remote sensing of invasive water hyacinth (*Eichhornia crassipes*): A review on applications and challenges," *Remote Sens. Appl., Soc. Environ.*, vol. 10, pp. 36–46, Apr. 2018.
- [2] L. Royimani, O. Mutanga, J. Odindi, T. Dube, and T. N. Matongera, "Advancements in satellite remote sensing for mapping and monitoring of alien invasive plant species (AIPs)," *Phys. Chem. Earth*, vol. 112, pp. 237–245, Aug. 2019.
- [3] C. O. Ongore, C. M. Aura, Z. Ogari, J. M. Njiru, and C. S. Nyamweya, "Spatial-temporal dynamics of water hyacinth, *Eichhornia crassipes* (Mart.) and other macrophytes and their impact on fisheries in Lake Victoria, Kenya," *J. Great Lakes Res.*, vol. 44, no. 6, pp. 1273–1280, Dec. 2018.
- [4] Y. Ghousssein et al., "Multitemporal remote sensing based on an FVC reference period using Sentinel-2 for monitoring *Eichhornia crassipes* on a Mediterranean river," *Remote Sens.*, vol. 11, no. 16, p. 1856, 2019.
- [5] M. G. Dersseh et al., "Spatial and temporal dynamics of water hyacinth and its linkage with lake-level fluctuation: Lake Tana, a sub-humid region of the Ethiopian highlands," *Water*, vol. 12, no. 5, p. 1435, May 2020.
- [6] G. Singh, C. Reynolds, M. Byrne, and B. Rosman, "A remote sensing method to monitor water, aquatic vegetation, and invasive water hyacinth at national extents," *Remote Sens.*, vol. 12, no. 24, p. 4021, Dec. 2020.
- [7] L. Pádua et al., "Water hyacinth (*Eichhornia crassipes*) detection using coarse and high resolution multispectral data," *Drones*, vol. 6, no. 2, p. 47, 2022.
- [8] J. A. Mukarugwiro, S. W. Newete, E. Adam, F. Nsanganwimana, K. Abutaleb, and M. J. Byrne, "Mapping spatio-temporal variations in water hyacinth (*Eichhornia crassipes*) coverage on Rwandan water bodies using multispectral imageries," *Int. J. Environ. Sci. Technol.*, vol. 18, no. 2, pp. 275–286, 2021.
- [9] L. Duarte, J. P. Castro, J. J. Sousa, and L. Padua, "GIS application to detect invasive species in aquatic ecosystems," in *Proc. IEEE Int. Geosci. Remote Sens. Symp. (IGARSS)*. Piscataway, NJ, USA: Institute of Electrical and Electronics Engineers, Jul. 2022, pp. 6013–6018.
- [10] T. Kattenborn, J. Leitloff, F. Schiefer, and S. Hinz, "Review on convolutional neural networks (CNN) in vegetation remote sensing," *ISPRS J. Photogramm. Remote Sens.*, vol. 173, pp. 24–49, Mar. 2021.
- [11] E. C. Rodríguez-Garlito, A. Paz-Gallardo, and A. Plaza, "Automatic detection of aquatic weeds: A case study in the Guadiana river, Spain," *IEEE J. Sel. Topics Appl. Earth Observ. Remote Sens.*, vol. 15, pp. 8567–8585, 2022.
- [12] E. C. Rodríguez-Garlito, A. Paz-Gallardo, and A. Plaza, "Monitoring the spatiotemporal distribution of invasive aquatic plants in the Guadiana river, Spain," *IEEE J. Sel. Topics Appl. Earth Observ. Remote Sens.*, vol. 16, pp. 228–241, 2022.
- [13] T. R. Téllez, E. M. R. López, G. L. Granado, E. A. Pérez, R. M. López, and J. M. S. Guzmán, "The water hyacinth, *Eichhornia crassipes*: An invasive plant in the Guadiana river basin (Spain)," *Aquatic Invasions*, vol. 3, no. 1, pp. 42–53, Mar. 2008.
- [14] E. C. Rodríguez-Garlito and A. Paz-Gallardo, "Efficiently mapping large areas of olive trees using drones in Extremadura, Spain," *IEEE J. Miniaturization Air Space Syst.*, vol. 2, no. 3, pp. 148–156, Sep. 2021.
- [15] M. E. Paoletti, J. M. Haut, J. Plaza, and A. Plaza, "Deep learning classifiers for hyperspectral imaging: A review," *ISPRS J. Photogramm. Remote Sens.*, vol. 158, pp. 279–317, Dec. 2019.